frontiers | Research Topics

Small non-coding RNAs in diseases

Edited by
Xiaoyong Bao, Yong Sun Lee and Inhan Lee

Published in
Frontiers in Molecular Biosciences

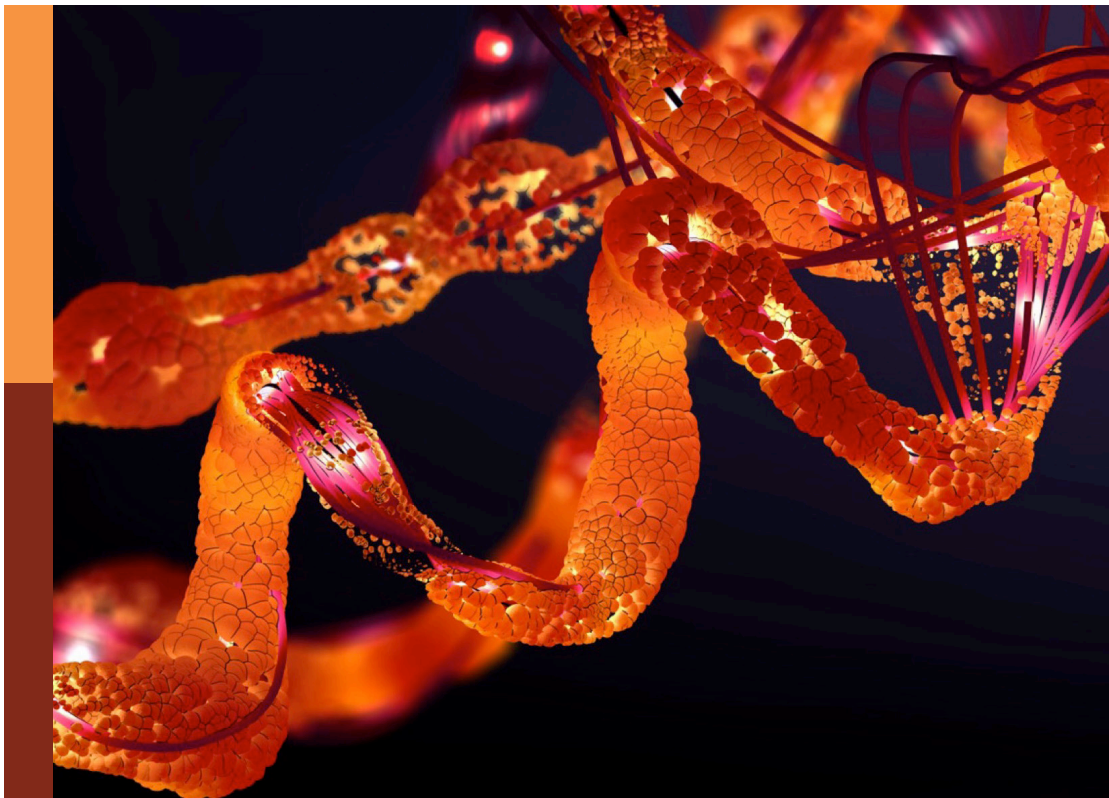

ISSN 1664-8714
ISBN 978-2-83251-341-5
DOI 10.3389/978-2-83251-341-5

About Frontiers

Frontiers is more than just an open access publisher of scholarly articles: it is a pioneering approach to the world of academia, radically improving the way scholarly research is managed. The grand vision of Frontiers is a world where all people have an equal opportunity to seek, share and generate knowledge. Frontiers provides immediate and permanent online open access to all its publications, but this alone is not enough to realize our grand goals.

Frontiers journal series

The Frontiers journal series is a multi-tier and interdisciplinary set of open-access, online journals, promising a paradigm shift from the current review, selection and dissemination processes in academic publishing. All Frontiers journals are driven by researchers for researchers; therefore, they constitute a service to the scholarly community. At the same time, the *Frontiers journal series* operates on a revolutionary invention, the tiered publishing system, initially addressing specific communities of scholars, and gradually climbing up to broader public understanding, thus serving the interests of the lay society, too.

Dedication to quality

Each Frontiers article is a landmark of the highest quality, thanks to genuinely collaborative interactions between authors and review editors, who include some of the world's best academicians. Research must be certified by peers before entering a stream of knowledge that may eventually reach the public - and shape society; therefore, Frontiers only applies the most rigorous and unbiased reviews. Frontiers revolutionizes research publishing by freely delivering the most outstanding research, evaluated with no bias from both the academic and social point of view. By applying the most advanced information technologies, Frontiers is catapulting scholarly publishing into a new generation.

What are Frontiers Research Topics?

Frontiers Research Topics are very popular trademarks of the *Frontiers journals series*: they are collections of at least ten articles, all centered on a particular subject. With their unique mix of varied contributions from Original Research to Review Articles, Frontiers Research Topics unify the most influential researchers, the latest key findings and historical advances in a hot research area.

Find out more on how to host your own Frontiers Research Topic or contribute to one as an author by contacting the Frontiers editorial office: frontiersin.org/about/contact

Small non-coding RNAs in diseases

Topic editors

Xiaoyong Bao — University of Texas Medical Branch at Galveston, United States
Yong Sun Lee — National Cancer Center, Republic of Korea
Inhan Lee — Other, United States

Citation

Bao, X., Lee, Y. S., Lee, I., eds. (2023). *Small non-coding RNAs in diseases*. Lausanne: Frontiers Media SA. doi: 10.3389/978-2-83251-341-5

Table of contents

frontiers | Frontiers in Molecular Biosciences

TYPE Editorial
PUBLISHED 04 January 2023
DOI 10.3389/fmolb.2022.1086768

OPEN ACCESS

EDITED BY
William C. Cho,
QEH, Hong Kong, SAR China

REVIEWED BY
Yao Xiao,
Illumina, United States

*CORRESPONDENCE
Xiaoyong Bao,
xibao@utmb.edu

SPECIALTY SECTION
This article was submitted to Molecular Diagnostics and Therapeutics, a section of the journal Frontiers in Molecular Biosciences

RECEIVED 01 November 2022
ACCEPTED 30 November 2022
PUBLISHED 04 January 2023

CITATION
Zhang K, Lee YS, Lee I and Bao X (2023), Editorial: Small non-coding RNAs in diseases.
Front. Mol. Biosci. 9:1086768.
doi: 10.3389/fmolb.2022.1086768

Editorial: Small non-coding RNAs in diseases

Ke Zhang[1], Yong Sun Lee[2], Inhan Lee[3] and Xiaoyong Bao[1,4,5]*

[1]Department of Pediatrics, University of Texas Medical Branch, Galveston, TX, United States, [2]Department of Cancer Biomedical Science, Graduate School of Cancer Science and Policy, National Cancer Center, Goyang-si, South Korea, [3]miRcore, Ann Arbor, MI, United States, [4]Institute for Translational Science, University of Texas Medical Branch, Galveston, TX, United States, [5]Institute for Human Infections and Immunity, University of Texas Medical Branch, Galveston, TX, United States

KEYWORDS

small non-coding RNA, viral infections, RNA sequencing, inflammatory diseases, tRNA-derived RNA fragment

Editorial on the Research Topic
Small non-coding RNAs in diseases

Small non-coding RNAs in diseases

Non-coding RNAs (ncRNAs) are RNA molecules that are not translated into proteins. They show great potential to serve as novel biomarkers and prophylactic/therapeutic targets of human diseases, including cancer, neurodegenerative disease, viral infection, and inflammatory diseases (Skalsky and Cullen, 2010; Carpenter et al., 2013; Maoz et al., 2017; Damas et al., 2019; Wang et al., 2019). Based on their size, ncRNAs are generally grouped into long ncRNAs (lncRNAs, >200 nt) and small ncRNAs (sncRNAs, <200 nt). Major sncRNA classes include microRNAs (miRNAs), small nucleolar RNAs (snoRNAs), small nuclear RNAs (snRNAs), piwi-interacting RNA (piRNA), and tRNA-derived RNA Fragment (tRFs) (Liao et al., 2010; Fu et al., 2015; Hombach and Kretz, 2016; Haack et al., 2019). This special issue focused on the sncRNAs and their essential roles in physiological and pathological conditions to explore the mechanisms of sncRNA-mediated human diseases.

miRNAs-regulated gastrointestinal inflammation

In addition to the roles of lncRNAs and circular RNAs in human inflammatory bowel diseases (Lin et al., 2020), miRNAs were also reported to regulate intestinal epithelial integrity in mice recently (Wang et al., 2017). In this Research Topic, an original research paper from Dr. Haque's group found increased expression of miR-122 and miR-21 in stool in children with increased intestinal permeability (IIP) (Rashid et al.). The finding was from a large sample (n = 442) and through integrative analysis of miRNA profiling,

mucosal inflammation, and intestinal permeability. The association of enhanced miR-122 and miR-21 expression with international permeability suggests that assessing these miRNAs may serve as a new diagnosis method of IIP in children who suffer diseases associated with intestinal barrier dysfunction.

This topic also reviewed miRNA-regulated primary biliary cholangitis (PBC) (Zhang et al.), with highlighted functions of miRNAs participating in PBC inflammation and related pathogenesis pathways, supporting ncRNAs being potential diagnostic biomarkers and/or therapeutic targets.

sncRNAs and infectious diseases

This Research Topic includes three original research manuscripts about ncRNAs in viral infections. Two are related to severe acute respiratory syndrome coronavirus 2 (SARS-CoV-2) infection with high volumes of views (Zhang et al.; Wu et al.). The results from Dr. Bao's group demonstrated that tRFs are the most impacted sncRNAs in the nasopharyngeal swab specimens of SARS-CoV-2-positive patients and SARS-CoV-2-infected airway epithelial cells. The group also revealed several SARS-CoV-2-derived sncRNAs with a predicted structure similar to tRFs (Wu et al.). The study also established physiologically relevant cell models for tRF functional studies and a new sequencing (seq) method, called T4 PNK (polynucleotide kinase)-RNA-seq, to accurately quantify the tRFs. These tools will benefit future sncRNA studies. Changes in a tRF profile have been demonstrated in other viral infections, with some being virus-specific and functionally crucial in viral replication (Wang et al., 2013; Ruggero et al., 2014; Selitsky et al., 2015). Therefore, rather than simply serving as biomarkers, any mechanisms associated with tRF biogenesis and function would also reveal potential targets to control viral replication. In addition to tRFs, four SARS-CoV-2-impacted lncRNAs were discovered by applying microarrays to peripheral blood mononuclear cells from healthy donors and COVID-19 patients (Zhang et al.). Although the lncRNA research is a bit off the topic scope, the urgent need to configure disease mechanisms of SARS-CoV-2 and the finding on the correlation between lncRNA expression in T cells and monocytes and the disease severity made us include this into the topic.

Respiratory syncytial virus (RSV) is the leading cause of acute lower respiratory tract infections in children worldwide. For the first time, Dr. Casola's group showed a time-dependent increase in piRNAs in RSV-infected small airway epithelial (SAE) cells (Corsello et al.). Her group also identified genes related to cytoskeletal or Golgi organization and nucleic acid/nucleotide binding to be the most significantly altered by RSV-induced piRNAs, increasing the knowledge of the piRNA in viral infection and the potential of novel therapeutic targets for viral-mediated lung diseases.

We also included an original manuscript studying the roles of nematode miRNAs in T cell differentiation and cytokine production in macrophages (Soichot et al.), providing a new mechanism on how parasite miRNAs shape host gene expression.

miRNA and intervertebral disc degeneration (IDD)

IDD is one of the main causes of lower back pain, but its pathogenesis mechanism remains unclear. An original research manuscript from Dr. Zhang's group highlighted the importance of let-7b-5p plays a critical role in the maintenance of intervertebral disc structure and function (Zhuang et al.). The group showed that let-7b-5p in the exosome, secreted by nucleus pulposus stem cells derived from the degenerative intervertebral disc, can exacerbate annulus firbosus cell degeneration *via* inhibiting IGF1R expression and subsequently blocking the activation of the PI3K-Akt pathway.

sncRNAs and their future directions

A review from Dr. Dutta's group reviewed the functions and therapeutic implications of tRNA-derived small RNAs (Wilson and Dutta), which were found to be a dominant sncRNA group using Thermostable Group II Intron Reverse Transcriptase (TGIRT)-seq in bladder cancer samples (Su et al.). Their biogenesis mechanisms and functions in posttranscriptional gene silencing, regulating nascent RNA expression, altering protein translation, and affecting protein function were comprehensively discussed (Wilson and Dutta). The group also discussed the challenge when using tRFs as therapeutic targets, which is applicable to all sncRNA-based therapeutic development. Among them, the effectiveness of oligonucleotide delivery is a major issue. To overcome this, several tissue-specific delivery methods, including using lipid nanoparticles, N-acetylgalactosamine conjugation, and encapsulation of oligonucleotide in extracellular vesicles, were recently developed and showed the promise. In addition to the delivery issue, the oligonucleotide stability in circulation is another concern. tRFs/tRNAs are full of modifications, which may be functionally important including stabilizing sncRNAs. How to determine the modification location and their functions is challenging and raising difficulties of therapeutic oligo design. Overall, sncRNA-based therapeutic development is a challenging task. However, with more accumulating data revealing their biogenesis and function mechanisms, we may have the chance to target the pathways involved in biogenesis and functions,

not necessarily direct oligo-based therapy, to prevent and treat the diseases.

Author contributions

KZ and XB drafted the editorial. IL and YSL commended and revised the editorial.

Funding

This work was supported by NIH grants R21 AG069226 and R21 AI166543 to XB; grants from the National Cancer Center, Korea (NCC- 2210320 and NCC-2110191) to YL.

Conflict of interest

The authors declare that the research was conducted in the absence of any commercial or financial relationships that could be construed as a potential conflict of interest.

Publisher's note

References

Carpenter, S., Aiello, D., Atianand, M. K., Ricci, E. P., Gandhi, P., Hall, L. L., et al. (2013). A long noncoding RNA mediates both activation and repression of immune response genes. *Science* 341 (6147), 789–792. doi:10.1126/science.1240925

Damas, N. D., Fossat, N., and Scheel, T. K. H. (2019). Functional interplay between RNA viruses and non-coding RNA in mammals. *Noncoding. RNA* 5 (1), 7. doi:10.3390/ncrna5010007

Fu, Y., Lee, I., Lee, Y. S., and Bao, X. (2015). Small non-coding transfer RNA-derived RNA fragments (tRFs): Their biogenesis, function and implication in human diseases. *Genomics Inf.* 13 (4), 94–101. doi:10.5808/GI.2015.13.4.94

Haack, F., Trakooljul, N., Gley, K., Murani, E., Hadlich, F., Wimmers, K., et al. (2019). Deep sequencing of small non-coding RNA highlights brain-specific expression patterns and RNA cleavage. *RNA Biol.* 16, 1764–1774. doi:10.1080/15476286.2019.1657743

Hombach, S., and Kretz, M. (2016). Non-coding RNAs: Classification, biology and functioning. *Adv. Exp. Med. Biol.* 937, 3–17. doi:10.1007/978-3-319-42059-2_1

Liao, J. Y., Ma, L. M., Guo, Y. H., Zhang, Y. C., Zhou, H., Shao, P., et al. (2010). Deep sequencing of human nuclear and cytoplasmic small RNAs reveals an unexpectedly complex subcellular distribution of miRNAs and tRNA 3' trailers. *PLoS ONE* 5 (5), e10563. doi:10.1371/journal.pone.0010563

Lin, L., Zhou, G., Chen, P., Wang, Y., Han, J., Chen, M., et al. (2020). Which long noncoding RNAs and circular RNAs contribute to inflammatory bowel disease? *Cell Death Dis.* 11 (6), 456. doi:10.1038/s41419-020-2657-z

Maoz, R., Garfinkel, B. P., and Soreq, H. (2017). Alzheimer's Disease and ncRNAs. *Adv. Exp. Med. Biol.* 978, 337–361. doi:10.1007/978-3-319-53889-1_18

Ruggero, K., Guffanti, A., Corradin, A., Sharma, V. K., De Bellis, G., Corti, G., et al. (2014). Small noncoding RNAs in cells transformed by human T-cell leukemia virus type 1: A role for a tRNA fragment as a primer for reverse transcriptase. *J. Virol.* 88 (7), 3612–3622. doi:10.1128/JVI.02823-13

Selitsky, S. R., Baran-Gale, J., Honda, M., Yamane, D., Masaki, T., Fannin, E. E., et al. (2015). Small tRNA-derived RNAs are increased and more abundant than microRNAs in chronic Hepatitis B and C. *Sci. Rep.* 5, 7675. doi:10.1038/srep07675

Skalsky, R. L., and Cullen, B. R. (2010). Viruses, microRNAs, and host interactions. *Annu. Rev. Microbiol.* 64, 123–141. doi:10.1146/annurev.micro.112408.134243

Wang, J. Y., Xiao, L., and Wang, J. Y. (2017). Posttranscriptional regulation of intestinal epithelial integrity by noncoding RNAs. *WIREs. RNA* 8 (2), e1399. doi:10.1002/wrna.1399

Wang, Q., Lee, I., Ren, J., Ajay, S. S., Lee, Y. S., and Bao, X. (2013). Identification and functional characterization of tRNA-derived RNA fragments (tRFs) in respiratory syncytial virus infection. *Mol. Ther.* 21 (2), 368–379. doi:10.1038/mt.2012.237

Wang, W. T., Han, C., Sun, Y. M., Chen, T. Q., and Chen, Y. Q. (2019). Noncoding RNAs in cancer therapy resistance and targeted drug development. *J. Hematol. Oncol.* 12 (1), 55. doi:10.1186/s13045-019-0748-z

frontiers in Molecular Biosciences

ORIGINAL RESEARCH
published: 08 December 2021
doi: 10.3389/fmolb.2021.765301

MicroRNA Expression and Intestinal Permeability in Children Living in a Slum Area of Bangladesh

Humaira Rashid[1]*, *Towfida J. Siddiqua*[2], *Biplob Hossain*[1], *Abdullah Siddique*[1], *Mamun Kabir*[1], *Zannatun Noor*[1], *Masud Alam*[1], *Mamun Ahmed*[3] and *Rashidul Haque*[1]

[1]Emerging Infections and Parasitology Laboratory, International Centre for Diarrheal Disease Research, Dhaka, Bangladesh, [2]Nutrition and Clinical Service Division (NCSD), International Centre for Diarrheal Disease Research, Dhaka, Bangladesh, [3]Department of Biochemistry and Molecular Biology, University of Dhaka, Dhaka, Bangladesh

OPEN ACCESS

Edited by:
Inhan Lee,
miRcore, Ann Arbor, MI, United States

Reviewed by:
Amit Kumar Pandey,
Amity University Gurgaon, India
Giuseppe Losurdo,
University of Bari Medical School, Italy
Chengyuan Lin,
Hong Kong Baptist University, Hong Kong SAR, China

***Correspondence:**
Humaira Rashid
humairarashid777@gmail.com
humaira.rashid@icddrb.org

Specialty section:
This article was submitted to Molecular Diagnostics and Therapeutics, a section of the journal Frontiers in Molecular Biosciences

Received: 26 August 2021
Accepted: 22 November 2021
Published: 08 December 2021

Citation:
Rashid H, Siddiqua TJ, Hossain B, Siddique A, Kabir M, Noor Z, Alam M, Ahmed M and Haque R (2021) MicroRNA Expression and Intestinal Permeability in Children Living in a Slum Area of Bangladesh. Front. Mol. Biosci. 8:765301. doi: 10.3389/fmolb.2021.765301

Introduction: MicroRNAs (miRNAs) are small, non-coding RNAs that post-transcriptionally regulate gene expression. Changes in miRNA expression have been reported in a number of intestinal diseases, in both tissue samples and readily accessible specimens like stools. Pathogenic infections, diet, toxins, and other environmental factors are believed to influence miRNA expression. However, modulation of miRNAs in humans is yet to be thoroughly investigated. In this study, we examined the expression levels of two human miRNAs (miRNA-122 and miRNA-21) in stool samples of a group of Bangladeshi children who had an altered/increased intestinal permeability (IIP).

Methods: Stool samples were collected from children with IIP (L:M > 0.09) and normal intestinal permeability (NIP) (L:M ≤ 0.09). Quantitative PCR was performed to quantify the levels of miRNA-122 and miR-21 in stools. Commercial ELISA kits were used to measure gut inflammatory markers Calprotectin and REG1B. Serum samples were tested using Human Bio-Plex Pro Assays to quantify IL-1β, IL-2, IL-5, IL-10, IL-13, IFN-γ, and TNF-α. Total nucleic acid extracted from stool specimens were used to determine gut pathogens using TaqMan Array Card (TAC) system real-time polymerase chain reaction.

Results: The expression levels of miRNA-122 (fold change 11.6; $p < 0.001$, 95% CI: 6.14–11.01) and miR-21 (fold change 10; $p < 0.001$, 95% CI: 5.05–10.78) in stool were upregulated in children with IIP than in children with normal intestinal permeability (NIP). Significant correlations were observed between stool levels of miR-122 and miR-21 and the inflammatory cytokines IL-1β, IL-2, IFN-γ, and TNF-α ($p < 0.05$). Children with IIP were frequently infected with rotavirus, *Campylobacter jejuni*, *Bacteroides fragilis*, adenovirus, norovirus, astrovirus, and various *Escherichia coli* strains (ETEC_STh, ETEC_STp, EAEC_aaiC, EAEC_aatA) ($p < 0.001$). miR-122 significantly correlated with the fecal inflammatory biomarkers REG1B ($p = 0.015$) and Calprotectin ($p = 0.030$), however miR-21 did not show any correlation with these fecal biomarkers.

Keywords: intestinal permeability, intestinal barrier dysfunction, qPCR, cytokines, fecal miRNA

Conclusion: miR-122 and miR-21 may be associated with intestinal permeability. Assessment of these miRNAs may provide new tools for diagnosis of IIP in children from developing countries suffering diseases associated with intestinal barrier dysfunction.

INTRODUCTION

The fundamental function of the intestinal tract is to absorb and digest nutrients. Additionally, apart from being the largest immune organ, the intestinal tract is also the largest reservoir of endotoxins and bacteria. The intestinal epithelium functions as a barrier that separates the body from the outside environment (Vancamelbeke and Vermeire, 2017). The most essential function of intestinal epithelial cells is maintenance of the intestinal epithelial barrier (Ulluwishewa et al., 2011). Disruption of the intestinal epithelial barrier is associated with inflammation and disturbance of the immune system. Earlier research indicated that toxins, pro-inflammatory cytokines, *in vitro* mild irritants and pathogens open the tight junctions and increase paracellular permeability (Fukui, 2016). Enteric pathogens also play a significant role in disruption of the epithelial barrier. Pathogens may stimulate immune and intestinal epithelial cells to secrete pro-inflammatory cytokines, including interleukin-1β (IL-1β), tumor necrosis factor-α (TNF-α), and interferon-γ (IFN-γ). These pro-inflammatory cytokines can induce intestinal barrier dysfunction and increase intestinal permeability (Bruewer et al., 2003). Intestinal epithelial barrier dysfunction has been documented to affect the children of low- and middle-income countries (LMIC), such as Bangladesh. Repeated chronic exposure to fecal pathogens and toxins can induce intestinal inflammation, which allows inflammatory molecules such as unwanted toxins, colonic bacteria and bacterial antigens to cross the barrier and intensify the immune response (Bischoff et al., 2014; Martinez-Medina and Garcia-Gil, 2014; Nishida et al., 2018). In Bangladesh, children who suffer persistent infections caused by astrovirus, adenovirus, rotavirus, norovirus, enterotoxigenic *Escherichia coli*, enteric protozoa (amebiasis, cryptosporidiosis, giardiasis), *Campylobacter jejuni* or *Bacteroides fragilis* are at risk of a sharp decline in growth and impaired nutritional status (Mondal et al., 2012; König et al., 2016; Prendergast and Kelly, 2016; George et al., 2018; Bray et al., 2019). These findings suggest that pathogen colonization may induce chronic inflammation and trigger changes in the intestinal microbiota that lead to disruption of the intestinal barrier (Buret et al., 2002; De Magistris et al., 2003; Mondal et al., 2012; Bischoff et al., 2014).

MicroRNAs (miRNAs) are short, highly conserved, non-coding 18–23 nucleotide RNA molecules that bind to the untranslated regions (UTRs) of mRNAs to control gene expression at the post-transcriptional level (Ha and Kim, 2014). The miRNAs function as post-transcriptional regulators by binding to their complementary sequences, which results in translational repression or degradation of specific mRNAs (O'Brien et al., 2018). As miRNAs regulate many important physiological processes in eukaryotic cells, their altered expression has been linked to a variety of diseases. This can lead to remarkable alterations to gene expression, and thus induce inflammatory conditions (Cichon et al., 2014). Intense exposure to enteric pathogens during infection induces inflammation, which allows pathogens to directly adhere to and invade the intestinal epithelial barrier, which in turn disrupt the tight junctional protein complexes composed of proteins such as occludin and claudins, leading to the onset and progression of intestinal diseases (Lee, 2015). MiRNAs have been shown to play crucial roles during infection with viruses such as the adenovirus, enterovirus, rotavirus, which are mainly responsible for gastroenteritis as well as changes in enterocyte and bacterial microflora (Maudet et al., 2014; Das et al., 2016; Huang et al., 2018; Mukhopadhyay et al., 2021).

In addition, a recent study reported that miRNAs are relevant to intestinal-associated disorders induced by infection and impact the regulation of inflammatory and immune responses (Sheedy and O'Neill, 2008; Bi et al., 2009). For instance, miRNAs, such as miR-21 and miR-122 target negative regulators of the immune response to promote inflammation. Expression of miR-122 and miR-21 have been reported to be dysregulated in patients with increased intestinal permeability (IIP) induced by various inflammatory stimuli (Zhang et al., 2015; Zhang et al., 2017). miR-21 is a ubiquitously expressed miRNA that is, traditionally considered as oncogenic (Li et al., 2012). However numerous miRNAs are commonly altered during pathogen infection and also induced by TNF-α and other cytokine molecules (Staedel and Darfeuille, 2013; Zhang et al., 2014; Drury et al., 2017). Persistent exposure to multiple enteropathogens induces a rapid change in miR-122 and miR-21 expression in enterocytes. Previous research indicates that children with enteric dysfunction caused by pathogen-induced inflammation have altered intestinal permeability, implying that inflammatory bowel syndrome (IBS) and other inflammatory-related gut pathologies may be exacerbated through such barrier dysfunction (Shulman et al., 2008).

The present study aimed to evaluate whether persistent exposure to multiple fecal pathogens leads to IIP and decreased barrier function that cause aberrant expression of miRNA-21 and miRNA-122. We also investigated whether aberrant levels of miRNA-122 and miRNA-21 can also influence the risk of intestinal inflammation. We assessed children living in communities where sanitation is often poor and hygiene practices are sub-optimal. IBS-like symptoms are widely accepted to persist in a small percentage of patients after a documented episode of intestinal viral or bacterial infection. Also, dysregulation of miRNAs has been implicated in several pediatric non-neoplastic diseases (Omran et al., 2013). Therefore, from our study we can determine that aberrant expression of microRNAs in children with an IIP can play a pathogenic role in diseases, including those primarily affecting the gut (Hollander et al., 1986; Distrutti et al., 2016).

MATERIALS AND METHODS

Study Area and Human Subjects

This study was performed as a nested observational study (2016–2019) within a longitudinal birth cohort study in

Mirpur slum areas of Dhaka city, Bangladesh (Kirkpatrick et al., 2015). A total of 442 children aged 2-years-old were selected for this study. Inclusion criteria for the current study were: mothers willing to sign informed consent form, no obvious congenital abnormalities or birth defects. The exclusion criteria were children aged below or above 2 years-of-age, children who do not have any major congenital anomalies and parents who are not willing to have child's blood drawn.

Sample and Data Collection

Urine samples were collected from the children (n = 442) over 5 h after ingestion of lactulose and mannitol solution. The selection of children for miRNA expression analysis was based on the availability of fecal samples from a previously conducted larger study. We assessed approximately 120 mg stool samples from 85 randomly selected children. From IIP group we selected 43 children and from NIP group we selected 42 children for miRNA-122 gene expression analysis and identical stool samples from 36 children (16 children with IIP and 20 children with NIP) for miRNA-21 gene expression analysis. However, remaining 49 children were not included for the miRNA-21 gene expression analysis because they did not have adequate stool volume to perform qPCR. The fecal biomarkers REG1B and Calprotectin were also assessed in the same stool samples used to determine miRNA-122 and miRNA-21. From the same children we also analyzed 3-ml blood samples to quantify inflammatory cytokines and correlate with miRNA-122 and miRNA-21. Diarrheal stools were assessed to detect enteropathogens. The urine, blood and stool samples were transported from the field clinic to the Parasitology Lab, Icddr,b in a cold box and samples were stored at −70°C prior to analysis.

Anthropometry

Anthropometric measurements were taken at the time of enrolment using a calibrated digital baby scale (UC-321; A & D Co., Tokyo, Japan) and standardized supine length measurement equipment (TALC, St Albans, Herts, UK) to determine height-for-age (HAZ) z-score and weight-for-age (WAZ) z-scores, measures of stunting and underweight, respectively (World Health Organization, 1995). A HAZ less than −2 SD is defined as stunting and a WAZ less than −2 SD is defined as underweight.

Measures of Intestinal Permeability

The L/M ratio is a test of intestinal permeability. Individuals with intestinal barrier dysfunction exhibit increased absorption of lactulose due to increased mucosal permeability and decreased absorption of mannitol due to a decrease in the intestinal surface area (Zhang et al., 2000). The lactulose and mannitol was given to the children at a dose of 2 ml/kg of body weight. The solution in water included 250 mg/ml of lactulose and 50 mg/ml of mannitol. Urine was collected upto 2 h after lactulose and mannitol ingestion. The assay was conducted using high-performance anion exchange chromatography (HPAEC-PAD). Children with a lactulose to mannitol ratio (L:M > 0.09) were considered to have increased IIP and children with a (L:M ≤ 0.09), NIP (Musa et al., 2019).

MicroRNA Extraction in Stool Specimens

Given that miRNAs have previously been detected in other body fluids (Cortez et al., 2011), we compared the presence of miRNAs in the fecal samples of children with IIP and NIP.

Total RNA was extracted from the stool samples using miRNAeasy Mini Kits (Qiagen). Stool (120 mg) was mixed with RNAse free water and homogenized using a vortex mixer in Qiazol lysis reagent for 30 s. RNA was precipitated by adding chloroform into a 2 ml RNAse-free tube, vortexed for 15 s, incubated at room temperature for 2–3 min, centrifuged at 12,000 g for 15 min at 4°C and total stool RNA was eluted in RNase free water. Finally, the RNA concentration was measured using a Nanodrop 2000 (Thermo Fisher Scientific, Wilmington, DE, United States).

Reverse Transcription and Real-Time PCR

The Revert Aid First Strand cDNA Synthesis Kit (Thermo Scientific, United States) was used to perform reverse transcription (RT) according to the manufacturer's instructions. A RT universal stemloop primer and total treated RNA was used to perform the RT reaction (Raymond et al., 2005). Each 20 μL RT reaction mixture contained 0.1–5 μg/1 μL treated total RNA, 1 μL of stem-loop RT primer (5 μM), 1 μL of 10 mM dNTP blend, 4 μL of reaction buffer, 1 μL of Ribolock RNase inhibitor (20 U/μL), and 1 μL of Revert Aid MMuLV Reverse Transcriptase (200 U/μL). The mixtures were incubated at 65°C for 5 min, then at 42°C for 60 min, and stopped by heating to 70°C for 5 min. The cDNA was stored at −20°C until further use.

SYBR Green [EXPRESS SYBR® GreenER™ qPCR SuperMix Universal (Invitrogen)] was used to quantify the miRNAs in the stool nucleic acid samples. Reverse-transcribed RNA was quantified using a Bio-Rad CFX96 real-time PCR detection system. A 12 μL PCR reaction volume included 5 μL of SYBR green super mix, 1 μL of RT product and 0.4 μL of primer (forward and reverse, 1 μM each). The reactions were incubated at 50°C for 2 min, 95°C for 2 min, followed by 40 cycles of 95°C for 15 s, 60°C for 60 s. The expression levels of miRNA were measured using the quantification cycle values (Cq values). U6 RNA was used as an endogenous control/housekeeping gene for data normalization and the assay was quantified by the $2^{-\Delta\Delta Cq}$ method (Livak and Schmittgen, 2001; Bustin et al., 2009; Jacobsen et al., 2011). The $2^{-\Delta\Delta CT}$ method [ΔΔCT = ΔCT (a miRNA of interest)-ΔCT (U6 RNA as a normalizer accounting for sample-to-sample variation)] was used to analyze the relative expression of miRNA-122 and miRNA-21.

TaqMan Array Card for the Detection of Enteric Pathogens

Total nucleic acid extracted from stool samples was used to detect multiple enteropathogens using The TaqMan Array Card system real-time polymerase chain reaction format by Applied Biosystems ViiA7 Real-Time PCR system (Life Technologies,

TABLE 1 | Clinical and demographic features of children in Mirpur slum area, Dhaka, Bangladesh. Moderate underweight −3 ≤WAZ < −2, severely underweight WAZ < −3.

Characteristics (442 children)	Number	Percentage
Age in years	2	—
Female	209	47.2
Moderate underweight	111	25.1
Severely underweight	23	5.2
Moderate stunted	102	23
Severely stunted	41	9.2

Moderate stunted −3 ≤HAZ < −2, severely stunted HAZ < −3.

Foster City, CA, United States), which can rapidly detect and quantify 27 enteropathogens, including helminths and viruses. TAC enables the identification of a wide range of enteropathogens in a fast and precise manner with a quantitative detection.

Stool Enzyme-Linked Immunosorbent Assay

Fecal Calprotectin a gut inflammatory biomarker for intestinal mucosal inflammation and gut damage (Harper et al., 2018) was measured following the manufacturer's instructions by using commercially available ELISA kits (Calprotectin ELISA, BÜHLMANN Laboratories AG, Basel, Switzerland) (Jensen et al., 2011). Fecal Calprotectin was quantified using a standard curve generated using the kit standards and expressed as μg/g stool.

Another inflammatory biomarker fecal REG1B which is a potential indicator of intestinal injury and repair (Peterson et al., 2013) was also measured using ELISA technique (TECHLAB, Inc., Blacksburg, VA, United States) to quantify REG1B concentration (μg/g) in stool samples to evaluate epithelial health.

Cytokine Measurements

The serum samples were tested for IL-1β, IL-2, IL-5, IL-10, IL-13, IFN-γ, and TNF-α using Human Bio-Plex Pro Assays (Bio-Rad, Hercules, CA) (Jiang et al., 2014) on a Bio-Plex 200 platform (Bio-Rad, Hercules, CA, United States). Bio-Plex Manager software version 6.0 was used for data analysis.

Statistical Analysis

Statistical analyses were conducted using SPSS (version 17.0) or GraphPad prism 8.0 software (San Diego, CA, United States). Results were expressed as mean ± standard deviation (SD). Differences were considered significant if $p \leq 0.05$. Data were compared using Mann–Whitney *U* tests and *t*-test was applied to test the association of miRNAs and pathogenic infections with intestinal permeability. Bivariate correlations between variables, including miRNA levels, cytokines and fecal inflammatory biomarkers, were examined using Pearson's correlation coefficient (r). The sensitivity and specificity of miRNAs for identifying children with IIP (L:M > 0.09) were calculated by receiver operating characteristic (ROC) curve analysis.

RESULTS

Nutritional Status of Children

A total of 442 children were available for this study; 47.2% of the children were female (**Table 1**) and 37.5% (166/442) had elevated L:M ratio (> 0·09) suggestive of increased intestinal permeability (IIP). Of these 442 children, 30.3% of the children were less than −2 WAZ and 32.3% were less than −2 HAZ.

42% (69/166) of children with IIP were less than −2 WAZ while only 23.5% (65/276) with normal intestinal permeability (NIP) children were less than −2 WAZ which is statistically significant ($p = 0.0001$). Similarly, 40% (66/166) of children with IIP were less than −2 HAZ whereas, 27.8% (77/276) children with NIP were less than −2 HAZ which is also statistically significant ($p = 0.012$). We also checked for the nutritional status of the selected 85 children for miRNA-122 expression analysis; 27% children were less than −2WAZ and 28.2% children were less than −2HAZ.

miR-122 and miR-21 Expression Levels in Stool

miR-122 and miR-21 expression analyzed from the fecal RNA where the total RNA concentration was from 661 to 2,298 ng/μL. Data derived from RT-qPCR are presented as normalized ΔCT values. A significant differential expression was determined in stool samples of children with IIP compared to NIP children for miR-122 ($p < 0.001$). Similarly, fecal samples of children with IIP showed significant differential expression of miR-21 compared to children with NIP ($p < 0.001$). The mean ± standard deviation (SD) normalized ct values for miR-122 and miR-21 were significantly different in children with IIP compared to children with NIP (miR-122: 6.99 ± 2.75 vs. 10.53 ± 1.51; miR-21: 6.78 ± 3.24 vs. 10.12 ± 1.40). miR-122 and miR-21 expression levels of stool were upregulated 11.6; ($p < 0.001$, 95% CI: 6.146–11.01) and 10; ($p < 0.001$, 95% CI:5.055–10.78) times respectively in children with an increased intestinal permeability when compared to children with a normal intestinal permeability. These results are graphically presented in **Figure 1**.

Receiver Operating Characteristic Curve Analysis for miRNA-122 and miRNA-21

Biomarkers are important for early disease identification, as early diagnosis can help to avoid and improve prognosis. Stool-based miRNA detection has high sensitivity and specificity (Yau et al., 2019). To investigate the possibility that these miRNAs may serve as new and potential biomarkers for increased intestinal permeability, receiver operating characteristic (ROC) curve analysis was carried out to evaluate the diagnostic potential of stool miRNA-122 and miRNA-21 levels. As shown in **Figure 2**, the AUC values for miR-122 and miR-21 were 0.893 [95% confidence interval (CI) 0.822–0.964, $p = 0.0001$] and 0.850 [95% confidence interval (CI) 0.706–0.94, $p = 0.0001$], respectively. This result demonstrated that miR-122 and miR-21 have potentials for detection of IIP. Thus, the stool miRNA-

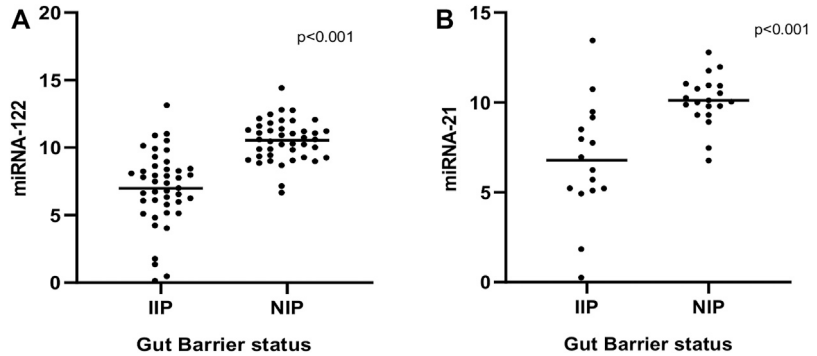

FIGURE 1 | Comparison of expression levels of miRNA-122 **(A)** and miRNA-21 **(B)** between normal and increased intestinal permeability respectively. Statistical analysis was carried out by the Mann-Whitney *U* test.

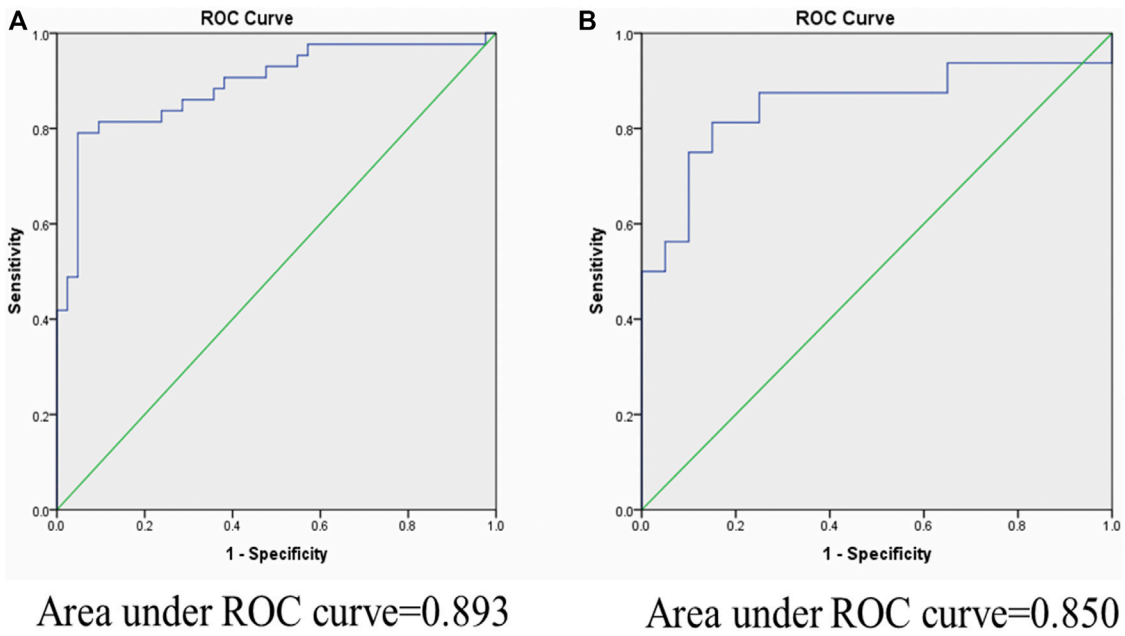

FIGURE 2 | Area under curve (AUC) of receiver operating characteristic (ROC) analysis for miR-122 and miR-21 relative expression in fecal samples for discriminating increased and normal intestinal permeability. ROC curve analysis revealed that fecal miR-122 and miR-21 relative expression has significant specificity and sensitivity to distinguish between children with IIP and NIP. **(A)**: miR-122 yield an area under the curve (AUC) value of 0.893 (*p*-value = 0.0001). **(B)**: miR-21 yield an area under the curve (AUC) value of 0.850 (*p*-value = 0.0001).

122 and miRNA-21 levels could be considered as promising biomarkers for the diagnosis of IIP in children.

We also compared the stool miRNA expression levels with the L:M ratios of the children to identify cut-off values of miR-122 and miR-21 that indicate IIP. A L:M ratio >0.09 is regarded as increased intestinal permeability and a L:M ratio ≤0.09 is regarded as normal intestinal permeability. Using a cut-off of 9.8 for miR-122 (normalized ct value) 84% (36/43) of children with IIP were below this cut-off. Thus, at this cut-off value miRNA-122 had a sensitivity of 84% and specificity of 71.4% to detect IIP. Using the same cut-off value for miR-21, 88% (14/16) children with IIP were below this cut-off, with a sensitivity of 88% and specificity of 75% (**Tables 2A,B**).

Association of Enteric Pathogens With Intestinal Permeability

We compared the presence of enteric pathogens in children with IIP and children with NIP. Rotavirus, *Campylobacter jejuni, Bacteroides fragilis*, adenovirus, norovirus, astrovirus, and *Escherichia coli* strains (*Enterotoxigenic Escherichia coli*-STh, Enterotoxigenic *Escherichia coli*-STp, Enteroaggregative *Escherichia coli*-_aaiC, Enteroaggregative *Escherichia coli*-aatA) were significantly more frequent in children with IIP compared to children with NIP (*p*-value < 0.001) (**Supplementary Figure**).

TABLE 2 | (A) Normalized miR-122 ct value (DCT) *Lactulose: Mannitol ratio (L:M) Status Crosstabulation. L:M status 1 indicates children with (L:M > 0.09) considered to have increased IIP and L:M status 0 indicates children with (L:M ≤ 0.09), considered to have NIP. DCT 1 indicates normalized miR-122 ct value ≤9.8 and DCT 2 indicates normalized miR-122 ct value >9.8. **(B)** Normalized miR-21 ct value (DCT)*Lactulose: Mannitol ratio (L:M) status crosstabulation. L:M status 1 indicates children with (L:M > 0.09) were considered to have increased IIP and 0 indicates children with (L:M ≤ 0.09), were considered to have NIP. DCT 1 indicates normalized miR-21 ct value ≤9.8 and DCT 2 indicates normalized miR-21 ct value >9.8.

Count

		L:M status (Lactulose: Mannitol status)		Total
		0	1	
DCT (normalized miR-122 ct value)	1	12	36	48
	2	30	07	37
Total		42	43	85

Count

		L:M status (Lactulose: Mannitol status)		Total
		0	1	
DCT (normalized miR-21 ct value)	1	05	14	19
	2	15	02	17
Total		20	16	36

Correlation of Inflammatory Cytokines With miRNAs

We assessed the correlations between the inflammatory cytokines (IL-1β, IL-2, IL-5, IL-10, IL-13, IFN-γ, and TNF-α), with the levels of miRNAs (miR-122 and miRNA-21). The cytokines IL-1β, IL-2, IFN-γ, and TNF-α levels were correlated significantly with the levels of the miRNAs. The expression level of miRNA-122 correlated with the levels of IL-1β ($r = -0.3939$, $p = 0.007$), IL-2 ($r = -0.385$, $p = 0.008$), IFN-γ ($r = -0.2683$, $p = 0.05$), and TNF-α ($r = -0.3222$, $p = 0.030$) The expression level of miRNA-21 correlated with the levels of IL-1β ($r = -0.390$, $p = 0.018$), IL-2 ($r = -0.441$, $p = 0.007$), IFN-γ ($r = -0.466$, $p = 0.004$) and TNF-α ($r = -0.495$, $p = 0.002$) (**Figures 3A,B**). No significant correlations were observed between miRNA levels (miR-122 and miRNA-21) with inflammatory cytokines IL-5, IL-10, or IL-13.

Correlations Between miRNA-122 and miRNA-21 and Fecal Inflammatory Biomarkers

Significant correlations were observed between miR-122 and REG1B. The stools of children with a high concentration of REG1B contained higher expression levels of miRNA-122 ($r = -0.259$, $p < 0.015$) compared to children with low concentration of REG1B. Calprotectin, the most common inflammatory biomarker observed during disease progression, correlated significantly with miRNA-122 ($r = -0.278$, $p < 0.030$). However, both REG1B and Calprotectin fecal biomarkers were not correlated significantly with miR-21 (**Figure 4**).

DISCUSSION

Exposure to various enteric pathogens causes extensive mucosal disruption (Kosek et al., 2017) and intestinal inflammation leading to IIP and microbial translocation. We assessed intestinal permeability among 442 children using the lactulose/mannitol assay of urine samples; 166 children had a L:M ratio >0.09, indicative of altered/increased intestinal permeability. Previous studies associated IIP with the presence of enteric pathogens, suggesting a mechanism of intestinal and systemic inflammation (Amour et al., 2016; Rogawski et al., 2017). In our study, we demonstrated that the expression levels of miR-122 and miR-21 were significantly upregulated in children with IIP compared to children with normal intestinal permeability.

Compared to children with normal intestinal permeability, miRNA-122 (fold change 11.6; $p < 0.001$) and miR-21 (fold change 10; $p < 0.001$) were significantly upregulated in children with IIP. Similarly, previous research identified that unique miRNA expression profile signatures in intestinal-related diseases and persistent exposure to multiple fecal pathogens lead to IIP and decreased barrier function, which may cause aberrant expression of miRNA-122 and miRNA-21 (Ye et al., 2011; Zhang et al., 2015; Johnston et al., 2018; Al-Sadi et al., 2020; Rashid et al., 2020). Zhang et al. (2015) observed significant overexpression of miRNA-21 was associated with increased tight junction permeability *in vitro*. Another study showed the levels of several miRNAs, including miR-21, miR-122, miR-155, miR-146a, miR-429, and miR-874, were altered in small intestinal epithelial cells isolated from patients in a burns unit with IIP (Morris, 2018; Zhang et al., 2018) found that miRNA-21 is upregulated during intestinal barrier dysfunction (Ye et al., 2011; Liu et al., 2019). Reported that miRNA-122 and miRNA-21 may also play an important role in the maintenance of intestinal barrier function, thus dysregulation of miRNA-122 and miRNA-21 can lead to altered intestinal barrier function.

The levels of specific miRNAs have also been reported to be modulated in the feces of patients affected by enteric pathogens (Liu et al., 2016; Liu and Weiner, 2016; Sarshar et al., 2020), suggesting these miRNAs may be involved in the pathogenesis of intestinal barrier dysfunction and could potentially represent diagnostic or prognostic tools for altered intestinal permeability/intestinal barrier dysfunction (Zhou et al., 2010; Zhang et al., 2015; Zhang et al., 2017). In our study, a number of pathogens were detected in children with altered intestinal permeability. Adenovirus, rotavirus, different strains of *Escherichia coli* (ETEC_STh, ETEC_STp, EAEC_aaiC, EAEC_aatA), *Campylobacter. jejuni*, *Bacteroides. fragilis*, norovirus, and astrovirus were frequently detected in the stool samples of children with IIP. The presence of pathogens can affect miRNA expression, which in turn may disrupt the intestinal barrier. This suggestion is in line with a growing body of evidence that indicates enteric pathogens can induce intestinal inflammation by modifying the intestinal microbiota, weakening the intestinal barrier, and priming the intestine for chronic inflammatory responses (Amour et al., 2016; Kosek et al., 2017; Fahim et al., 2018; Fahim et al., 2020). Moreover, the

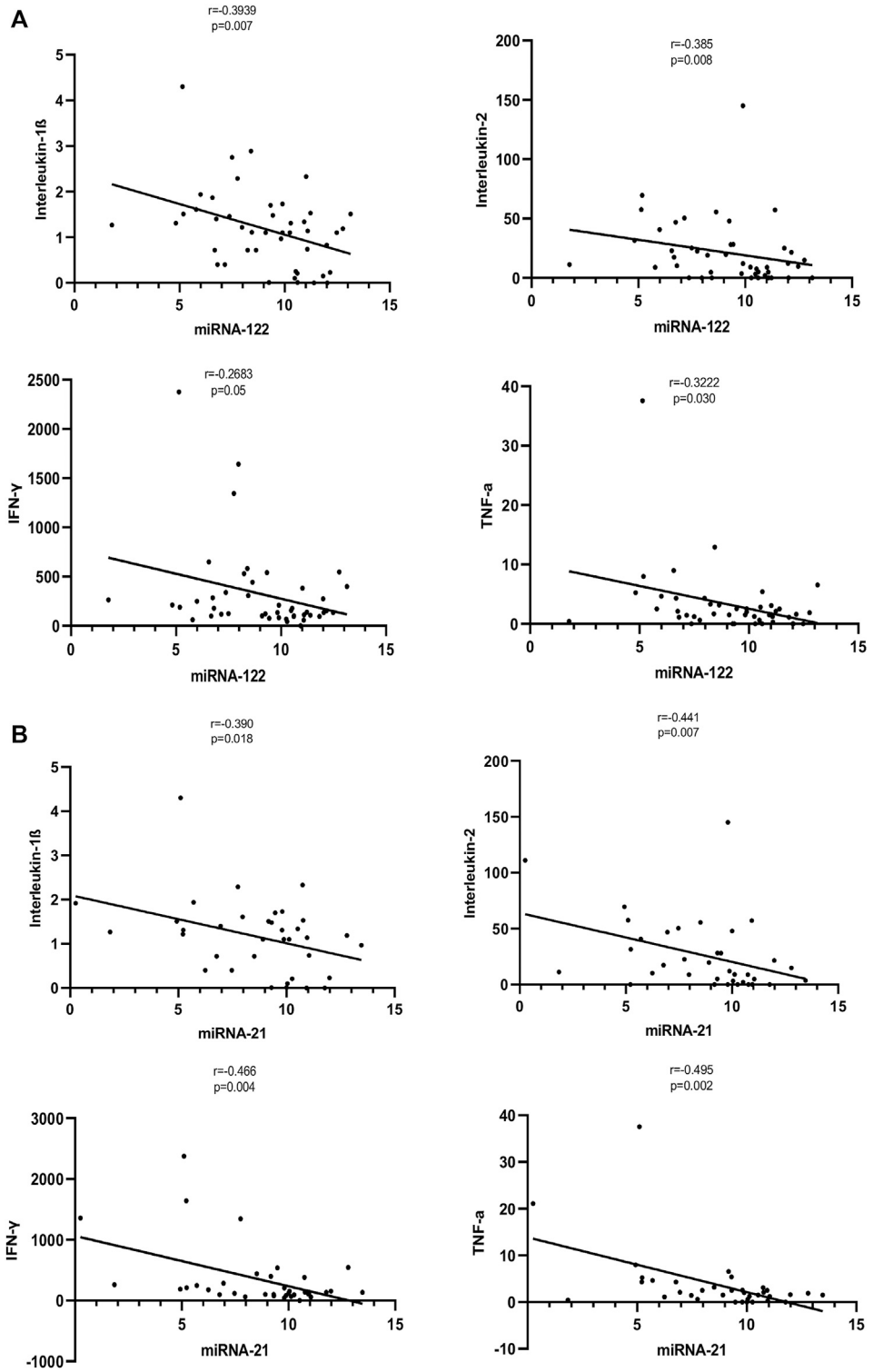

FIGURE 3 | (A): Correlation of expression levels of miRNA-122 with inflammatory cytokines. The *X*-axis indicates the miR-122 relative expression, while the *Y*-axis denotes cytokines. We performed the Pearson's correlation test for statistical evaluation. **(B)**: Correlation of expression levels of miRNA-21 with inflammatory cytokines. The *X*-axis indicates the miR-21 relative expression, while the *Y*-axis denotes cytokines. We performed the Pearson's correlation test for statistical evaluation.

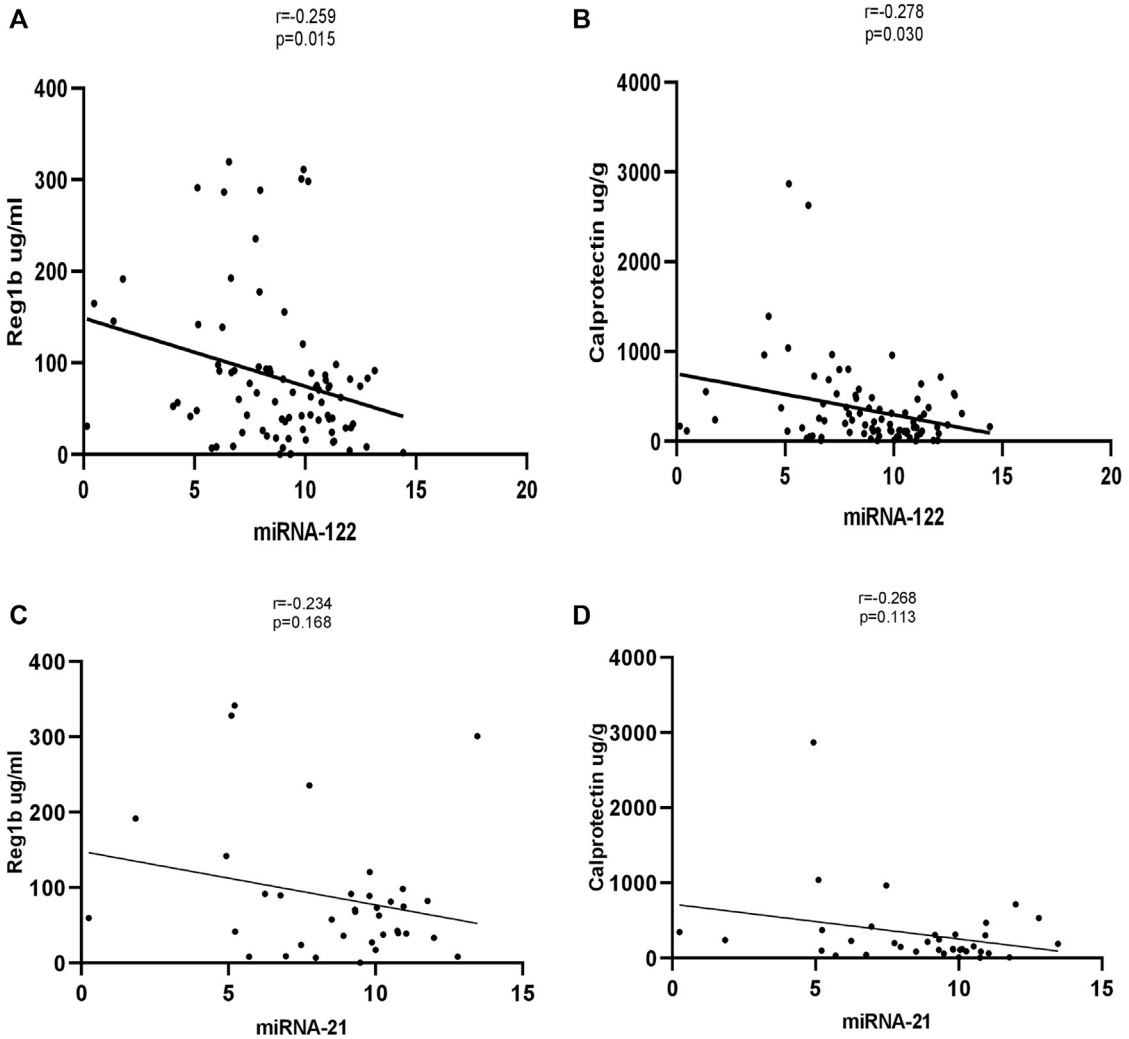

FIGURE 4 | Correlation of expression levels of miRNA-122 and miRNA-21 values with fecal biomarkers (with Reg1b and Calprotectin). The *X*-axis indicates the relative expression of miR-122, while the *Y*-axis denotes fecal biomarkers. We performed Pearson's correlation test for statistical evaluation which showed a significant association between miRNA-122 **(A, B)** and fecal biomarkers, but no significant association was seen between miRNA-21 and fecal biomarkers **(C, D)**.

expression of miRNAs can change dramatically during the course of infection with pathogens (Zhao et al., 2015; Drury et al., 2017). Infections with viruses such as rotavirus are one of the most common causes of diarrhoea in children <5 years, and no effective drug is available to treat these viruses. One study showed that oral administration of a mimic miRNA-7 agomir inhibited the replication of rotavirus in mice, indicating miR-7 may suppress the replication of rotavirus (Zhou et al., 2020). In another study, compared to controls children infected with adenovirus showed altered microRNA expression profiles (Huang et al., 2018). Similarly, as notable findings of this study, infections caused by enteric pathogens were associated with aberrant levels of miRNA-122 and miRNA-21, which could have a profound impact on the development and growth of children. These fecal miRNAs are related to the dysbiosis and inflammation of the host. Dysbiosis of the normal intestinal microbiota can lead to a number of diseases including inflammatory bowel diseases (Tlaskalová-Hogenová et al., 2011). In addition, miRNAs have been found to play a vital role in modulating pathogenic infections, and are primarily responsible for alterations to the bacterial microflora (Schönauen et al., 2018). Thus, the potential of miRNAs as tools for genetic research, diagnosis and treatment of pathogenic infections caused by bacteria, viruses, parasites, and fungi in human merits further investigation.

Expression of REG1B and Calprotectin are elevated in tissue samples from patients with benign diseases, such as acute amoebic colitis (Peterson et al., 2011), Crohn's disease and ulcerative colitis (Lawrance et al., 2001; Bjarnason, 2017). In one study, the levels of fecal miRNAs correlated with fecal Calprotectin levels (Schönauen et al., 2018). Interestingly, in this study, the fecal biomarker REG1B—a putative measure of intestinal injury and repair—correlated significantly with the levels of miRNA-122 in stool samples. Also, Calprotectin—the most commonly assessed

inflammatory biomarker of disease progression—significantly correlated with miRNA-122. However, both REG1B and Calprotectin fecal biomarkers was not statistically significant with miR-21, most likely due to low subject numbers.

This study examined a population in which undernutrition, as well as pathogen exposure, are prevalent. One study showed that Escherichia *coli* is characterized by destruction of epithelial cells and are associated with an upregulation of cytokines such as TNF-α and IFN-γ (Shea-Donohue et al., 2010). Our results indicate that although the prevalence of IBD is lower in Bangladesh than among children in western countries, the high infection burden induces increased expression of inflammatory cytokines, which leads to aberrant miR-21 and miR-122 expression among children with IIP. Furthermore, numerous published studies suggest a significant link between miRNAs and cytokine activities, since miRNA expression is regulated in response to cytokine stimulation. Furthermore, our analysis suggests that the C_t values of miR-122 and miR-21 in stools negatively correlate with the serum levels of the inflammatory cytokines TNF-α, INF-γ, IL-1β, and IL-2 ($r < 0$) where low C_t values indicates higher expression of miRNA-122 and miRNA-21. These findings are in line with (Chen et al., 2014; Yan et al., 2020) who found that miR-21 and miR-122 can promote the production of inflammatory cytokines that are closely related to the pathogenesis of IBD, such as TNF-α, IFN-γ, and IL-1β. In general, miRNA-122 and miRNA-21 target negative regulators of the immune response to promote inflammation. Several studies found that miRNA-21 and miRNA-122 exerted inflammatory roles in intestinal barrier dysfunction that leads to impaired barrier function (Ye et al., 2011; Zhang et al., 2015; Zhang et al., 2017). Showed that TNF-α can abruptly upregulate miRNA-122 and miRNA-21 in enterocytes and intestinal tissues, and consequently lead to barrier disruption and IIP.

To our knowledge, no previous studies have examined the expression levels of miRNA-122 and miRNA-21 in the fecal samples of Bangladeshi children or explored the association of these miRNAs with IIP and the presence of enteric pathogens. The findings of this study provide critical evidence that dysregulation of miRNAs during inflammation could be potentially involved in the pathogenesis of intestinal-related diseases. Furthermore, the correlations between these miRNAs and other inflammatory biomarkers offers new possibilities to use miRNAs as disease biomarkers.

However, this study has limitations. Firstly, correlation between fecal inflammatory biomarkers REG1B and Calprotectin and miRNA-21 did not show a statistical significance. However, the correlation was seen to be significant with miRNA-122. We also did not see any correlation between fecal pathogens and miRNA-122 and miRNA-21. This could be due to small sample size that limits statistical power to detect differences. Secondly, this study was conducted in children residing in the slum areas of Mirpur, Bangladesh. To validate these findings, large clinical studies in different geographical regions are needed. Our findings suggest fecal miRNA-21 and miRNA-122 may have potential as clinically useful, non-invasive prognostic and diagnostic biomarkers for pediatric patients, though this suggestion requires confirmation in large validation groups. Additional studies with larger sample sizes are required to reliably validate our findings. Also, our data point towards a molecular mechanism by which dysregulation of miRNAs due to altered intestinal permeability can lead to impaired growth/malnutrition, and correction of the levels of miRNAs using therapeutics could potentially help to manage environmental enteric dysfunction.

In conclusion, we show that Bangladeshi children with IIP have substantially altered levels of miRNAs in their stools. Two fecal miRNAs were closely linked to disease activity and easily accessible surrogate biomarkers, such as REG1B, fecal Calprotectin, and the serum levels of inflammatory cytokines. Furthermore, this study demonstrates that the levels of miRNAs in feces are very stable and can be reproducibly detected, even after long term storage. Overall, in conjunction with previous findings the levels of miRNAs in feces correlate with disease activity, our results indicate miRNAs merit further research as potential biomarkers of gut barrier diseases.

DATA AVAILABILITY STATEMENT

The original contributions presented in the study are included in the article/**Supplementary Material**, further inquiries can be directed to the corresponding author.

ETHICS STATEMENT

The studies involving human participants were reviewed and approved by the institutional review board Icddr,b. Written informed consent to participate in this study was provided by the participants' legal guardian/next of kin.

AUTHOR CONTRIBUTIONS

HR conceived the study and carried out the experiments. HR drafted the manuscript. HR, TS, BH, and RH analyzed the data. HR, TS, BH, ZN, RH, and MA reviewed the first draft of the manuscript and suggested additional analysis. BH, AS contributed to the experimental work. HR, TS, BH, AS, ZN, MK, MAl, MA, and RH revised the final draft manuscript and provided critical comments. All authors read and approved the final version of the manuscript.

ACKNOWLEDGMENTS

We are grateful to all of the participants for their valuable participation in this study. Icddr,b is grateful to the governments of Bangladesh, Canada, Sweden, and the UK for providing core/unrestricted support.

SUPPLEMENTARY MATERIAL

The Supplementary Material for this article can be found online at: https://www.frontiersin.org/articles/10.3389/fmolb.2021.765301/full#supplementary-material

REFERENCES

Al-Sadi, R., Engers, J., and Abdulqadir, R. (2020). Talk about Micromanaging! Role of microRNAs in Intestinal Barrier Function. *Am. J. Physiol.-Gastrointest. Liver Physiol.* 319 (2), G170–G174. doi:10.1152/ajpgi.00214.2020

Amour, C., Gratz, J., Mduma, E., Svensen, E., Rogawski, E. T., McGrath, M., et al. (2016). Epidemiology and Impact of Campylobacter Infection in Children in 8 Low-Resource Settings: Results from the MAL-ED Study. *Clin. Infect. Dis.* 63 (9), ciw542–1179. doi:10.1093/cid/ciw542

Bi, Y., Liu, G., and Yang, R. (2009). MicroRNAs: Novel Regulators during the Immune Response. *J. Cel. Physiol.* 218 (3), 467–472. doi:10.1002/jcp.21639

Bischoff, S. C., Barbara, G., Buurman, W., Ockhuizen, T., Schulzke, J.-D., Serino, M., et al. (2014). Intestinal Permeability - a New Target for Disease Prevention and Therapy. *BMC Gastroenterol.* 14 (1), 1–25. doi:10.1186/s12876-014-0189-7

Bjarnason, I. (2017). The Use of Fecal Calprotectin in Inflammatory Bowel Disease. *Gastroenterol. Hepatol.* 13 (1), 53.

Bray, A. E., Ahmed, S., Das, S. K., Khan, S. H., Chisti, M. J., Ahmed, T., et al. (2019). Viral Pathogen-Specific Clinical and Demographic Characteristics of Children with Moderate-To-Severe Diarrhea in Rural Bangladesh. *Am. J. Trop. Med. Hyg.* 101 (2), 304–309. doi:10.4269/ajtmh.19-0152

Bruewer, M., Luegering, A., Kucharzik, T., Parkos, C. A., Madara, J. L., Hopkins, A. M., et al. (2003). Proinflammatory Cytokines Disrupt Epithelial Barrier Function by Apoptosis-independent Mechanisms. *J. Immunol.* 171 (11), 6164–6172. doi:10.4049/jimmunol.171.11.6164

Buret, A. G., Mitchell, K., Muench, D. G., and Scott, K. G. E. (2002). Giardia Lamblia Disrupts Tight Junctional ZO-1 and Increases Permeability in Non-transformed Human Small Intestinal Epithelial Monolayers: Effects of Epidermal Growth Factor. *Parasitology* 125 (1), 11–19. doi:10.1017/s0031182002001853

Bustin, S. A., Benes, V., Garson, J. A., Hellemans, J., Huggett, J., Kubista, M., et al. (2009). The MIQE Guidelines: Minimum Information for Publication of Quantitative Real-Time PCR Experiments. *Clin. Chem.* 55, 611–622. doi:10.1373/clinchem.2008.112797

Chen, W.-X., Ren, L.-H., and Shi, R.-H. (2014). Implication of miRNAs for Inflammatory Bowel Disease Treatment: Systematic Review. *World J. Gastrointest. Pathophysiol.* 5 (2), 63. doi:10.4291/wjgp.v5.i2.63

Cichon, C., Sabharwal, H., Rüter, C., and Schmidt, M. A. (2014). MicroRNAs Regulate Tight junction Proteins and Modulate Epithelial/endothelial Barrier Functions. *Tissue barriers* 2 (4), e944446. doi:10.4161/21688362.2014.944446

Cortez, M. A., Bueso-Ramos, C., Ferdin, J., Lopez-Berestein, G., Sood, A. K., and Calin, G. A. (2011). MicroRNAs in Body Fluids-The Mix of Hormones and Biomarkers. *Nat. Rev. Clin. Oncol.* 8 (8), 467–477. doi:10.1038/nrclinonc.2011.76

Das, K., Garnica, O., and Dhandayuthapani, S. (2016). Modulation of Host miRNAs by Intracellular Bacterial Pathogens. *Front. Cel. Infect. Microbiol.* 6, 79. doi:10.3389/fcimb.2016.00079

De Magistris, L., Secondulfo, M., Sapone, A., Carratù, R., Iafusco, D., Prisco, F., et al. (2003). Infection with Giardia and Intestinal Permeability in Humans. *Gastroenterology* 125 (1), 277–279. doi:10.1016/s0016-5085(03)00822-9

Distrutti, E., Monaldi, L., Ricci, P., and Fiorucci, S. (2016). Gut Microbiota Role in Irritable Bowel Syndrome: New Therapeutic Strategies. *World J. Gastroenterol.* 22 (7), 2219–2241. doi:10.3748/wjg.v22.i7.2219

Drury, R. E., O'Connor, D., and Pollard, A. J. (2017). The Clinical Application of microRNAs in Infectious Disease. *Front. Immunol.* 8, 1182. doi:10.3389/fimmu.2017.01182

Fahim, S. M., Das, S., Gazi, M. A., Mahfuz, M., and Ahmed, T. (2018). Association of Intestinal Pathogens with Faecal Markers of Environmental Enteric Dysfunction Among Slum-Dwelling Children in the First 2 Years of Life in Bangladesh. *Trop. Med. Int. Health* 23 (11), 1242–1250. doi:10.1111/tmi.13141

Fahim, S. M., Das, S., Gazi, M. A., Alam, M. A., Hasan, M. M., Hossain, M. S., et al. (2020). *Helicobacter pylori* Infection Is Associated with Fecal Biomarkers of Environmental Enteric Dysfunction but Not with the Nutritional Status of Children Living in Bangladesh. *Plos Negl. Trop. Dis.* 14 (4), e0008243. doi:10.1371/journal.pntd.0008243

Fukui, H. (2016). Increased Intestinal Permeability and Decreased Barrier Function: Does it Really Influence the Risk of Inflammation? *Inflamm. Intest Dis.* 1 (3), 135–145. doi:10.1159/000447252

George, C. M., Burrowes, V., Perin, J., Oldja, L., Biswas, S., Sack, D., et al. (2018). Enteric Infections in Young Children Are Associated with Environmental Enteropathy and Impaired Growth. *Trop. Med. Int. Health* 23 (1), 26–33. doi:10.1111/tmi.13002

Ha, M., and Kim, V. N. (2014). Regulation of microRNA Biogenesis. *Nat. Rev. Mol. Cel Biol* 15 (8), 509–524. doi:10.1038/nrm3838

Harper, K. M., Mutasa, M., Prendergast, A. J., Humphrey, J., and Manges, A. R. (2018). Environmental Enteric Dysfunction Pathways and Child Stunting: A Systematic Review. *Plos Negl. Trop. Dis.* 12 (1), e0006205. doi:10.1371/journal.pntd.0006205

Hollander, D., Vadheim, C. M., Brettholz, E., Petersen, G. M., Delahunty, T., and Rotter, J. I. (1986). Increased Intestinal Permeability in Patients with Crohn's Disease and Their Relatives. *Ann. Intern. Med.* 105 (6), 883–885. doi:10.7326/0003-4819-105-6-883

Huang, F., Zhang, J., Yang, D., Zhang, Y., Huang, J., Yuan, Y., et al. (2018). MicroRNA Expression Profile of Whole Blood Is Altered in Adenovirus-Infected Pneumonia Children. *Mediators Inflamm.* 2018, 1–11. doi:10.1155/2018/2320640

Jacobsen, N., Andreasen, D., and Mouritzen, P. (2011). "Profiling microRNAs by Real-Time PCR," in *MicroRNAs in Development* (Springer), 39–54. doi:10.1007/978-1-61779-083-6_4

Jensen, M. D., Kjeldsen, J., and Nathan, T. (2011). Fecal Calprotectin Is Equally Sensitive in Crohn's Disease Affecting the Small Bowel and colon. *Scand. J. Gastroenterol.* 46 (6), 694–700. doi:10.3109/00365521.2011.560680

Jiang, N. M., Tofail, F., Moonah, S. N., Scharf, R. J., Taniuchi, M., Ma, J. Z., et al. (2014). Febrile Illness and Pro-Inflammatory Cytokines Are Associated with Lower Neurodevelopmental Scores in Bangladeshi Infants Living in Poverty. *BMC Pediatr.* 14 (1), 1–9. doi:10.1186/1471-2431-14-50

Johnston, D. G. W., Williams, M. A., Thaiss, C. A., Cabrera-Rubio, R., Raverdeau, M., McEntee, C., et al. (2018). Loss of microRNA-21 Influences the Gut Microbiota, Causing Reduced Susceptibility in a Murine Model of Colitis. *J. Crohn's Colitis* 12 (7), 835–848. doi:10.1093/ecco-jcc/jjy038

Kirkpatrick, B. D., Carmolli, M. P., Taniuchi, M., Haque, R., Mychaleckyj, J. C., Petri, W. A., et al. (2015). The "Performance of Rotavirus and Oral Polio Vaccines in Developing Countries" (PROVIDE) Study: Description of Methods of an Interventional Study Designed to Explore Complex Biologic Problems. *Am. J. Trop. Med. Hyg.* 92 (4), 744–751. doi:10.4269/ajtmh.14-0518

König, J., Wells, J., Cani, P. D., García-Ródenas, C. L., MacDonald, T., Mercenier, A., et al. (2016). Human Intestinal Barrier Function in Health and Disease. *Clin. translational Gastroenterol.* 7 (10), e196. doi:10.1038/ctg.2016.54

Kosek, M. N., Ahmed, T., Bhutta, Z., Caulfield, L., Guerrant, R., Houpt, E., et al. (2017). Causal Pathways from Enteropathogens to Environmental Enteropathy: Findings from the MAL-ED Birth Cohort Study. *EBioMedicine* 18, 109–117. doi:10.1016/j.ebiom.2017.02.024

Lawrance, I. C., Fiocchi, C., and Chakravarti, S. (2001). Ulcerative Colitis and Crohn's Disease: Distinctive Gene Expression Profiles and Novel Susceptibility Candidate Genes. *Hum. Mol. Genet.* 10 (5), 445–456. doi:10.1093/hmg/10.5.445

Lee, S. H. (2015). Intestinal Permeability Regulation by Tight junction: Implication on Inflammatory Bowel Diseases. *Intest Res.* 13 (1), 11–18. doi:10.5217/ir.2015.13.1.11

Li, S., Liang, Z., Xu, L., and Zou, F. (2012). MicroRNA-21: a Ubiquitously Expressed Pro-Survival Factor in Cancer and Other Diseases. *Mol. Cel. Biochem.* 360 (1-2), 147–158. doi:10.1007/s11010-011-1052-6

Liu, S., and Weiner, H. L. (2016). Control of the Gut Microbiome by Fecal microRNA. *Microb. Cel.* 3 (4), 176–177. doi:10.15698/mic2016.04.492

Liu, S., da Cunha, A. P., Rezende, R. M., Cialic, R., Wei, Z., Bry, L., et al. (2016). The Host Shapes the Gut Microbiota via Fecal microRNA. *Cell Host & Microbe* 19 (1), 32–43. doi:10.1016/j.chom.2015.12.005

Liu, Z., Li, C., Chen, S., Lin, H., Zhao, H., Liu, M., et al. (2019). MicroRNA-21 Increases the Expression Level of Occludin through Regulating ROCK1 in Prevention of Intestinal Barrier Dysfunction. *J. Cel. Biochem.* 120 (3), 4545–4554. doi:10.1002/jcb.27742

Livak, K. J., and Schmittgen, T. D. (2001). Analysis of Relative Gene Expression Data Using Real-Time Quantitative PCR and the 2−ΔΔCT Method. *methods* 25 (4), 402–408. doi:10.1006/meth.2001.1262

Martinez-Medina, M., and Garcia-Gil, L. J. (2014). *Escherichia coli* in Chronic Inflammatory Bowel Diseases: An Update on Adherent Invasive *Escherichia coli* Pathogenicity. *World J. Gastrointest. Pathophysiol.* 5 (3), 213. doi:10.4291/wjgp.v5.i3.213

Maudet, C., Mano, M., and Eulalio, A. (2014). MicroRNAs in the Interaction between Host and Bacterial Pathogens. *FEBS Lett.* 588 (22), 4140–4147. doi:10.1006/meth.2001.126210.1016/j.febslet.2014.08.002

Mondal, D., Minak, J., Alam, M., Liu, Y., Dai, J., Korpe, P., et al. (2012). Contribution of Enteric Infection, Altered Intestinal Barrier Function, and Maternal Malnutrition to Infant Malnutrition in Bangladesh. *Clin. Infect. Dis.* 54 (2), 185–192. doi:10.1093/cid/cir807

Morris, N. L. (2018). *Role of Micrornas in Impaired Gut Permeability Following Ethanol and Burn Injury*. Chicago: Loyola University.

Mukhopadhyay, U., Banerjee, A., Chawla-Sarkar, M., and Mukherjee, A. (2021). Rotavirus Induces Epithelial-Mesenchymal Transition Markers by Transcriptional Suppression of miRNA-29b. *Front. Microbiol.* 12 (170), 631183. doi:10.3389/fmicb.2021.631183

Musa, M. A., Kabir, M., Hossain, M. I., Ahmed, E., Siddique, A., Rashid, H., et al. (2019). Measurement of Intestinal Permeability Using Lactulose and Mannitol with Conventional Five Hours and Shortened Two Hours Urine Collection by Two Different Methods: HPAE-PAD and LC-MSMS. *PloS one* 14 (8), e0220397. doi:10.1371/journal.pone.0220397

Nishida, A., Inoue, R., Inatomi, O., Bamba, S., Naito, Y., and Andoh, A. (2018). Gut Microbiota in the Pathogenesis of Inflammatory Bowel Disease. *Clin. J. Gastroenterol.* 11 (1), 1–10. doi:10.1007/s12328-017-0813-5

O'Brien, J., Hayder, H., Zayed, Y., and Peng, C. (2018). Overview of MicroRNA Biogenesis, Mechanisms of Actions, and Circulation. *Front. Endocrinol.* 9, 402. doi:10.3389/fendo.2018.00402

Omran, A., Elimam, D., and Yin, F. (2013). MicroRNAs: New Insights into Chronic Childhood Diseases. *Biomed. Research International* 2013, 1–13. doi:10.1155/2013/291826

Peterson, K. M., Guo, X., Elkahloun, A. G., Mondal, D., Bardhan, P. K., Sugawara, A., et al. (2011). The Expression of REG 1A and REG 1B Is Increased during Acute Amebic Colitis. *Parasitol. Int.* 60 (3), 296–300. doi:10.1016/j.parint.2011.04.005

Peterson, K. M., Buss, J., Easley, R., Yang, Z., Korpe, P. S., Niu, F., et al. (2013). REG1B as a Predictor of Childhood Stunting in Bangladesh and Peru. *Am. Clin. Nutr.* 97 (5), 1129–1133. doi:10.3945/ajcn.112.048306

Prendergast, A. J., and Kelly, P. (2016). Interactions between Intestinal Pathogens, Enteropathy and Malnutrition in Developing Countries. *Curr. Opin. Infect. Dis.* 29 (3), 229–236. doi:10.1097/QCO.0000000000000261

Rashid, H., Hossain, B., Siddiqua, T., Kabir, M., Noor, Z., Ahmed, M., et al. (2020). Fecal MicroRNAs as Potential Biomarkers for Screening and Diagnosis of Intestinal Diseases. *Front. Mol. Biosci.* 7, 181. doi:10.3389/fmolb.2020.00181

Raymond, C. K., Roberts, B. S., Garrett-Engele, P., Lim, L. P., and Johnson, J. M. (2005). Simple, Quantitative Primer-Extension PCR Assay for Direct Monitoring of microRNAs and Short-Interfering RNAs. *Rna* 11 (11), 1737–1744. doi:10.1261/rna.2148705

Rogawski, E. T., Bartelt, L. A., Platts-Mills, J. A., Seidman, J. C., Samie, A., Havt, A., et al.MAL-ED Network Investigators(2017). Determinants and Impact of Giardia Infection in the First 2 Years of Life in the MAL-ED Birth Cohort. *J. Pediatr. Infect. Dis. Soc.* 6 (2), 153–160. doi:10.1093/jpids/piw082

Sarshar, M., Scribano, D., Ambrosi, C., Palamara, A. T., and Masotti, A. (2020). Fecal microRNAs as Innovative Biomarkers of Intestinal Diseases and Effective Players in Host-Microbiome Interactions. *Cancers* 12 (8), 2174. doi:10.3390/cancers12082174

Schönauen, K., Le, N., von Arnim, U., Schulz, C., Malfertheiner, P., and Link, A. (2018). Circulating and Fecal microRNAs as Biomarkers for Inflammatory Bowel Diseases. *Inflamm. Bowel Dis.* 24 (7), 1547–1557. doi:10.1093/ibd/izy046

Shea-Donohue, T., Fasano, A., Smith, A., and Zhao, A. (2010). Enteric Pathogens and Gut Function: Role of Cytokines and STATs. *Gut Microbes* 1 (5), 316–324. doi:10.4161/gmic.1.5.13329

Sheedy, F. J., and O'Neill, L. A. (2008). Adding Fuel to Fire: microRNAs as a New Class of Mediators of Inflammation. *Ann. Rheum. Dis.* 67 (Suppl. 3), iii50–iii55. doi:10.1136/ard.2008.100289

Shulman, R. J., Eakin, M. N., Czyzewski, D. I., Jarrett, M., and Ou, C.-N. (2008). Increased Gastrointestinal Permeability and Gut Inflammation in Children with Functional Abdominal Pain and Irritable Bowel Syndrome. *J. Pediatr.* 153 (5), 646–650. doi:10.1016/j.jpeds.2008.04.062

Staedel, C., and Darfeuille, F. (2013). MicroRNAs and Bacterial Infection. *Cell Microbiol.* 15 (9), 1496–1507. doi:10.1111/cmi.12159

Tlaskalová-Hogenová, H., Štěpánková, R., Kozáková, H., Hudcovic, T., Vannucci, L., Tučková, L., et al. (2011). The Role of Gut Microbiota (Commensal Bacteria) and the Mucosal Barrier in the Pathogenesis of Inflammatory and Autoimmune Diseases and Cancer: Contribution of Germ-free and Gnotobiotic Animal Models of Human Diseases. *Cell Mol Immunol* 8 (2), 110–120. doi:10.1038/cmi.2010.67

Ulluwishewa, D., Anderson, R. C., McNabb, W. C., Moughan, P. J., Wells, J. M., and Roy, N. C. (2011). Regulation of Tight junction Permeability by Intestinal Bacteria and Dietary Components. *J. Nutr.* 141 (5), 769–776. doi:10.3945/jn.110.135657

Vancamelbeke, M., and Vermeire, S. (2017). The Intestinal Barrier: a Fundamental Role in Health and Disease. *Expert Rev. Gastroenterol. Hepatol.* 11 (9), 821–834. doi:10.1080/17474124.2017.1343143

World Health Organization (1995). *Physical Status: The Use of and Interpretation of Anthropometry*. Geneva: Report of a WHO Expert Committee.

Yan, H., Zhang, X., and Xu, Y. (2020). Aberrant Expression of miR-21 in Patients with Inflammatory Bowel Disease. *Medicine* 99 (17), e19693. doi:10.1097/MD.0000000000019693

Yau, T. O., Tang, C.-M., Harriss, E. K., Dickins, B., and Polytarchou, C. (2019). Faecal microRNAs as a Non-invasive Tool in the Diagnosis of Colonic Adenomas and Colorectal Cancer: A Meta-Analysis. *Sci. Rep.* 9 (1), 1–13. doi:10.1038/s41598-019-45570-9

Ye, D., Guo, S., Al–Sadi, R., and Ma, T. Y. (2011). MicroRNA Regulation of Intestinal Epithelial Tight Junction Permeability. *Gastroenterology* 141 (4), 1323–1333. doi:10.1053/j.gastro.2011.07.005

Zhang, Y., Lee, B., Thompson, M., Glass, R., Lee, R. C., Figueroa, D., et al. (2000). Lactulose–mannitol Intestinal Permeability Test in Children with Diarrhea Caused by Rotavirus and Cryptosporidium. *J. Pediatr. Gastroenterol. Nutr.* 31 (1), 16–21. doi:10.1097/00005176-200007000-00006

Zhang, L., Cheng, J., and Fan, X. M. (2014). MicroRNAs: New Therapeutic Targets for Intestinal Barrier Dysfunction. *World J. Gastroenterol. WJG* 20 (19), 5818. doi:10.3748/wjg.v20.i19.5818

Zhang, L., Shen, J., Cheng, J., and Fan, X. (2015). MicroRNA-21 Regulates Intestinal Epithelial Tight junction Permeability. *Cel Biochem. Funct.* 33 (4), 235–240. doi:10.1002/cbf.3109

Zhang, B., Tian, Y., Jiang, P., Jiang, Y., Li, C., Liu, T., et al. (2017). MicroRNA-122a Regulates Zonulin by Targeting EGFR in Intestinal Epithelial Dysfunction. *Cell Physiol. Biochem.* 42 (2), 848–858. doi:10.1159/000478629

Zhang, L., Zhang, F., He, D. K., Fan, X. M., and Shen, J. (2018). MicroRNA-21 Is Upregulated during Intestinal Barrier Dysfunction Induced by Ischemia Reperfusion. *Kaohsiung J. Med. Sci.* 34 (10), 556–563. doi:10.1016/j.kjms.2018.05.006

Zhao, H., Chen, M., Tellgren-Roth, C., and Pettersson, U. (2015). Fluctuating Expression of microRNAs in Adenovirus Infected Cells. *Virology* 478, 99–111. doi:10.1016/j.virol.2015.01.033

Zhou, Q., Souba, W. W., Croce, C. M., and Verne, G. N. (2010). MicroRNA-29a Regulates Intestinal Membrane Permeability in Patients with Irritable Bowel Syndrome. *Gut* 59 (6), 775–784. doi:10.1136/gut.2009.181834

Zhou, Y., Chen, L., Du, J., Hu, X., Xie, Y., Wu, J., et al. (2020). MicroRNA-7 Inhibits Rotavirus Replication by Targeting Viral NSP5 *In Vivo* and *In Vitro*. *Viruses* 12 (2), 209. doi:10.3390/v12020209

Author Disclaimer: The authors alone are responsible for the views expressed in this manuscript.

Conflict of Interest: The authors declare that the research was conducted in the absence of any commercial or financial relationships that could be construed as a potential conflict of interest.

Publisher's Note: All claims expressed in this article are solely those of the authors and do not necessarily represent those of their affiliated organizations, or those of the publisher, the editors and the reviewers. Any product that may be evaluated in this article, or claim that may be made by its manufacturer, is not guaranteed or endorsed by the publisher.

frontiers in Molecular Biosciences

ORIGINAL RESEARCH
published: 17 January 2022
doi: 10.3389/fmolb.2021.766115

Exosomes Secreted by Nucleus Pulposus Stem Cells Derived From Degenerative Intervertebral Disc Exacerbate Annulus Fibrosus Cell Degradation *via* Let-7b-5p

Yin Zhuang[1†], *Sheng Song*[1†], *Dan Xiao*[2], *Xueguang Liu*[1], *Xiaofei Han*[1], *Shihao Du*[1], *Yuan Li*[1], *Yanming He*[1] *and Shujun Zhang*[1*]

[1]*Department of Spine Surgery, Wuxi 9th Affiliated Hospital of Soochow University, Wuxi, China,* [2]*Department of Spine Surgery, Orthopedics Center, Guangdong Provincial People's Hospital, Guangdong Academy of Medical Sciences, Guangzhou, China*

OPEN ACCESS

Edited by:
Inhan Lee,
miRcore, United States

Reviewed by:
Saroj Kumari,
Nation institute of immunology, India
Kangcheng Zhao,
Huazhong University of Science and Technology, China

***Correspondence:**
Shujun Zhang
spine_zhang@vip.163.com

[†]*These authors contributed equally to this work*

Specialty section:
This article was submitted to Molecular Diagnostics and Therapeutics, a section of the journal Frontiers in Molecular Biosciences

Received: *28 August 2021*
Accepted: *30 November 2021*
Published: *17 January 2022*

Citation:
Zhuang Y, Song S, Xiao D, Liu X, Han X, Du S, Li Y, He Y and Zhang S (2022) Exosomes Secreted by Nucleus Pulposus Stem Cells Derived From Degenerative Intervertebral Disc Exacerbate Annulus Fibrosus Cell Degradation via Let-7b-5p. Front. Mol. Biosci. 8:766115. doi: 10.3389/fmolb.2021.766115

The pathogenesis of intervertebral disc degeneration (IDD) is complex and remains unclear. Nucleus pulposus stem cells (NPSCs) and annulus fibrosus cells (AFCs) play a critical role in the maintenance of intervertebral disc structure and function. Exosome-mediated miRNAs regulate cell proliferation, differentiation, apoptosis, and degradation. However, it is not clear whether the degenerative intervertebral disc-derived nucleus pulposus stem cells (D-NPSCs) can regulate the function of AFCs by delivering exosomes. Here, we show that exosomes secreted by nucleus pulposus stem cells derived from degenerative intervertebral disc (D-DPSC-exo) can exacerbate AFC degeneration via inhibiting cell proliferation, migration, matrix synthesis, and promoting apoptosis. Specifically, let-7b-5p was highly expressed in D-DPSC-exo. Transfection of let-7b-5p mimic was found to promote apoptosis and inhibit proliferation migration and matrix synthesis of AFCs. In addition, transfection with let-7b-5p inhibitor caused the effect of D-DPSC-exo on AFCs to be reversed. Furthermore, we found that D-DPSC-exo and let-7b-5p inhibited IGF1R expression and blocked the activation of the PI3K–Akt pathway. Results suggested that NPSC-exo exacerbated cell degeneration of AFCs via let-7b-5p, accompanied by inhibition of IGF1R expression, and PI3K–Akt pathway activation. Therefore, insights from this work may provide a clue for targeted molecular therapy of intervertebral disc degeneration.

Keywords: intervertebral disc degeneration, nucleus pulposus stem cells, annulus fibrosus cell, proliferation, apoptosis, miRNA

INTRODUCTION

Intervertebral disc degeneration (IDD) is one of the main causes of lower back pain, but its specific pathogenesis remains unclear (Nakashima et al., 2020). Surgical treatment can relieve symptoms and alleviate pain, but it has no effect on the underlying disease itself (Dowdell et al., 2017). The intervertebral disc is mainly composed of nucleus pulposus cells and annulus fibrosus cells (AFCs), and the senescence and degeneration of these cells are the basis of IDD (Zhang et al., 2019b). Recent advances in strategies to engage stem cell transplantation for IDD therapy have established as a new

avenue for the treatment of IDD and achieved many encouraging results (Urits et al., 2019; Vadala et al., 2019), However, there are still many challenges and limitations that need to be further improved, such as short survival time, poor cell activity, and difficulty in differentiation, and the most important issue is that exogenous stem cells cannot tolerate the adverse microenvironment of local hypoxia, hyperosmolarity, low pH, and nutrient deficiency that develops after intervertebral disc degeneration (Wang et al., 2015; Hang et al., 2017; Ma et al., 2019). It may be possible to render the use of stem cells more practical using endogenous nucleus pulposus stem cells (NPSCs) to repair and reconstruct intervertebral disc function, taking advantage of the fact that most adult tissues have their own stem cell niche (Vickers et al., 2019).

NPSCs are mesenchymal stem cells (MSCs) derived from the endogenous nucleus pulposus tissues (Ying et al., 2019). They have the characteristics of self-renewal and differentiation into intervertebral disc cells (Lazzarini et al., 2019). NPSCs can better tolerate the local acidic microenvironment of degenerated disc than other tissue-derived mesenchymal stem cells, and they play an important role in the biological treatment of IDD (Choi et al., 2015). Research has shown that the characteristics of nucleus pulposus stem cells derived from degenerative intervertebral disc (D-DPSCs) and derived from normal intervertebral disc (N-DPSCs) are not exactly the same (Liu et al., 2019). With patient aging and aggravation of intervertebral disc degeneration, the proliferation and stemness of NPSCs decreased, which was not conducive to self-repair of the intervertebral disc (Sakai et al., 2012; Wu et al., 2018). Rather, it was more likely to aggravate the degeneration of the intervertebral disc tissue (Vergroesen et al., 2015).

In addition to direct differentiation into nucleus pulposus cells, the regulation of NPSCs on damaged tissues can also be realized through the paracrine pathway of their secretions (such as exosomes and cytokines) (Schneider and Simons, 2013). Exosomes are lipid bilayer membrane vesicles with diameters of approximately 30–150 nm, which can be secreted by most cell types. Exosomes have the ability to carry proteins, lipids, RNA, and a variety of other biological macromolecules that play an important role in cell-to-cell transfer of materials and information (Du et al., 2017; Liu et al., 2017). Moreover, some studies indicated that MSC-derived exosomes can promote angiogenesis (Aziz et al., 2020) and wound healing (An et al., 2021), as well as regulate immunity (Whiteside, 2018), while aging MSC-derived exosomes do not have this ability. Other studies have shown that aging bone-derived extracellular vesicles inhibited the proliferation of bone marrow stem cells and induced stem cell senescence (Davis et al., 2017).

The effect of NPSCs-derived exosomes on the surrounding tissue cells in the microenvironment of intervertebral disc degeneration is still unknown. In this study, we explored the differential effect of exosomes secreted by nucleus pulposus stem cells derived from degenerative intervertebral disc (D-DPSC-exo) and exosomes secreted by nucleus pulposus stem cells derived from normal intervertebral disc (N-DPSC-exo) on annulus fibrosus cells. Results showed that D-DPSC-exo exacerbated AFCs degradation through let-7b-5p by inhibiting the PI3K/AKT signaling pathway.

MATERIALS AND METHODS

Cell isolation and culture

All the experimental protocols were approved by the Ethics Committee of Wuxi 9th Affiliated Hospital of Soochow University and were obtained with the informed consent of the patients. Normal nucleus pulposus tissues were obtained from five patients (2 females and 3 males, aged 18–49 years) who underwent spine surgery of burst thoracolumbar fracture and degenerative nucleus pulposus, and the annular fibers tissues were gently obtained from 11 patients (4 females and 7 males, aged 37–61 years) who underwent surgery of disc excision for lumbar degenerative disease. Nucleus pulposus tissues were washed three times with PBS, then cut into pieces, and digested with 1 mg/ml of type II collagenase (Solarbio, China) for 4 h at 37°C. After being filtered through a 70-μm filter, the suspension was centrifuged at $300 \times g$ for 5 min, and the isolated cells were cultured in Complete Culture Medium of Mesenchymal Stem Cell (Cyagen, China) containing 88% basal medium, 10% MSC cell-qualified fetal bovine, 1% penicillin-streptomycin, and 1% glutamine. Annular fibers tissues were washed three times with PBS, then cut into pieces, and digested with 1 mg/ml of type I collagenase (Solarbio, China) for 2 h at 37°C. After being filtered through a 70-μm filter, the suspension was centrifuged at $300 \times g$ for 5 min, and the isolated cells were cultured in Dulbecco's Modified Eagle Medium/Nutrient Mixture F-12 (DMEM/F12) (Gibco, United States) containing 10% fetal bovine serum (FBS) (Gemini, China) and 1% penicillin–streptomycin (Gibco, USA). Finally, all the isolated NPSCs and AFCs were incubated at 37°C in a humidified atmosphere of 5% CO_2 with the culture medium replaced every 3 days.

Cell identification

The NPSCs were identified by flow cytometry analysis and multipotential differentiation. The multipotential differentiation of NPSCs was determined using an MSCs Adipogenic Differentiation Kit (Cyagen, China) and an MSCs Osteogenic Differentiation Kit (Cyagen, China), respectively. Oil red O staining and Alizarin red staining were used to assess adipogenic and osteogenic differentiation. For the detection of surface markers by flow cytometry, NPSCs were stained for 30 min with fluorescein isothiocyanate (FITC)-conjugated or phycoerythrin (PE)-conjugated anti-human CD29, CD34, CD44, CD45, CD73, CD90, CD105, and HLA-DR monoclonal antibodies, and characterized using flow cytometry (BD Biosciences, USA). The monoclonal antibodies were all purchased from BioLegend, Inc.

The AFCs were identified by immunofluorescence analysis and toluidine blue staining. For the detection of type II collagen immunohistochemical staining, AFCs were incubated with primary antibody type II collagen (1:200, Abcam, USA) at 4°C overnight. After PBS washing three times, cells were incubated with FITC-conjugated goat-anti-rabbit secondary antibody (1: 1,000, Beyotime, China) at room temperature for 1 h before

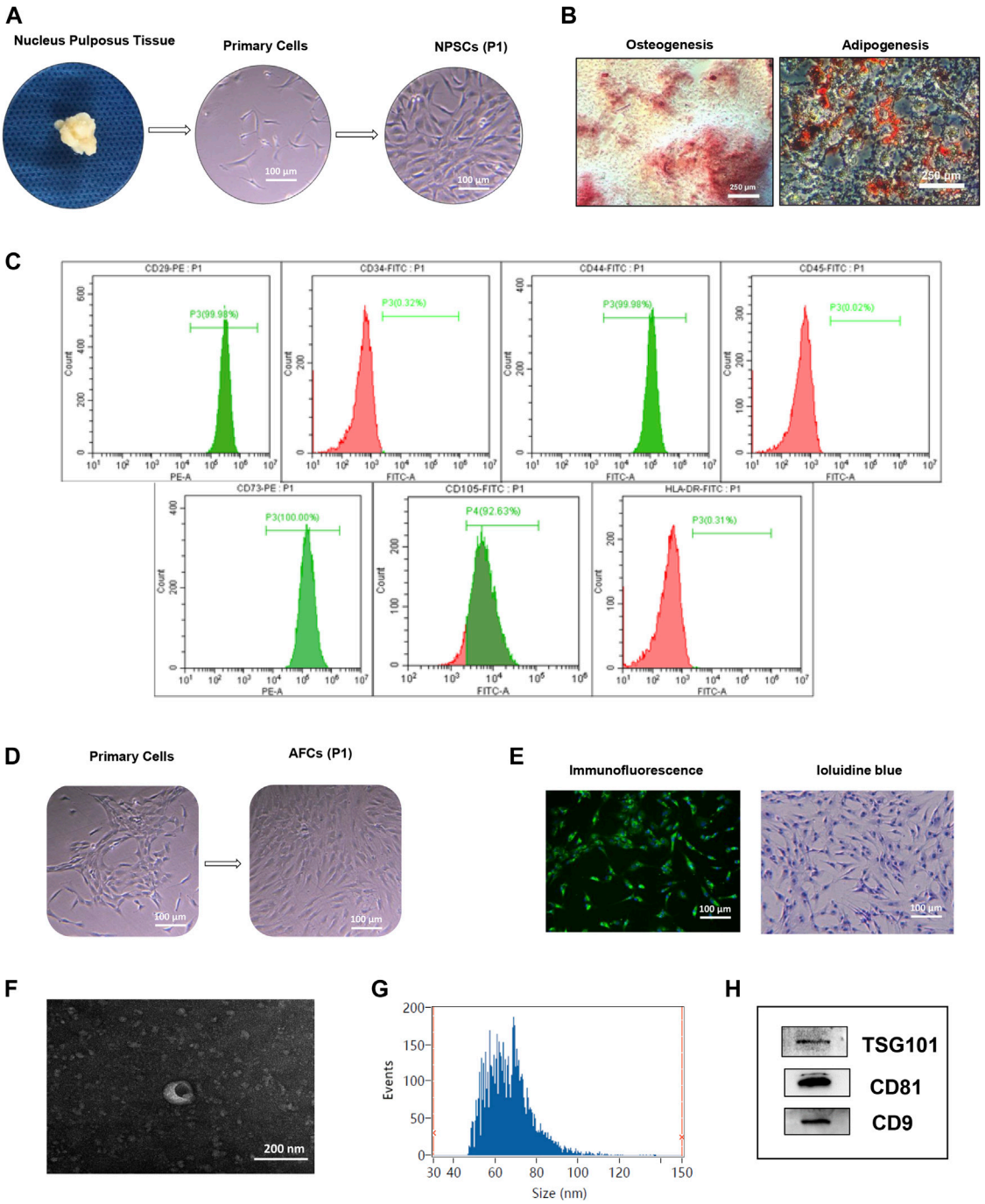

FIGURE 1 | Identification of nucleus pulposus stem cells (NPSCs), annulus fibrosus cells (AFCs), and NPSC-exo. **(A)** Process of isolation and culture of NPSCs from nucleus pulposus tissue. Cultured NPSCs at passage 1 (P1) were spindle shaped. **(B)** Differentiation potential of osteogenesis and adipogenesis of NPSCs was confirmed by Alizarin red staining and Oil red O staining after 2 weeks after *in vitro* induction, respectively. **(C)** Identification of surface makers of NPSCs indicated that the harvested NPSCs were positive expressions for CD29, CD44, CD73, and CD105 makers, and were negative expressions for CD34, CD45, and HLA-DR makers. **(D)** The cell morphology of cultured AFCs at passage 1 (P1) displayed long fusiform or polygonal shaped. **(E)** Immunofluorescence staining indicated that AFCs expressed type II collagen and toluidine blue staining showed AFCs were purple and exhibited metachromatic granules. **(F)** The typical saucer-like morphology of NPSC-exo was captured by transmission electron microscopy. **(G)** Particle size of NPSC-exo was characterized by flow nano analysis. **(H)** NPSC-exo were positive expressions for exosomal surface markers TSG101, CD81, and CD9 by Western blotting.

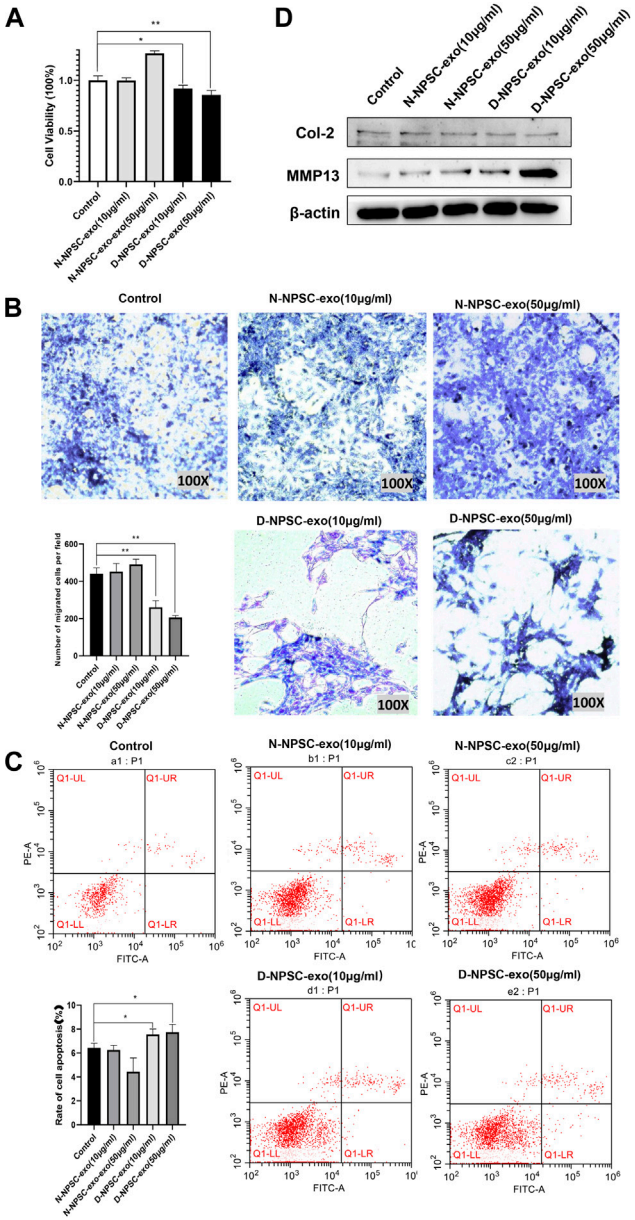

FIGURE 2 | Degenerative intervertebral disc-derived nucleus pulposus stem cells secreted exosomes (D-NPSC-exo) inhibited proliferation, migration, and extracellular matrix synthesis, and promoted apoptosis of AFCs. **(A)** Proliferation of AFCs treated with D-NPSC-exo, normal intervertebral disc-derived nucleus pulposus stem cells secreted exosomes (N-NPSC-exo), or PBS (control group) was evaluated by cell counting kit 8 (CCK-8) assay. D-NPSC-exo in both low (10 μg/ml) and high (50 μg/ml) concentrations significantly inhibited cell proliferation, and N-NPSC-exo in high (50 μg/ml) concentrations promoted cell proliferation, oppositely. **(B)** Migration of AFCs was evaluated by Transwell assay. D-NPSC-exo in both low (10 μg/ml) and high (50 μg/ml) concentrations significantly inhibited cell migration, and N-NPSC-exo promoted cell migration, oppositely. **(C)** Apoptosis of AFCs was evaluated by Annexin V/PI apoptosis detection kit. D-NPSC-exo in both low (10 μg/ml) and high (50 μg/ml) concentrations significantly promoted cell apoptosis. However, N-NPSC-exo in high (50 μg/ml) concentrations reduced the apoptotic rate of AFCs. **(D)** Protein expression levels of Col II, and MMP13 were detected by Western blotting. D-NPSC-exo in high (50 μg/ml) concentrations significantly promoted the expression of MMP13 and inhibits the expression of Col II. $^{*}p < 0.05$; $^{**}p < 0.01$.

counterstaining with DAPI (Solarbio, China). Images were obtained using a fluorescence microscopy (Olympus, Japan). For toluidine blue staining, AFCs stained with 1% toluidine blue for 30 min at room temperature before fixing in 4% paraformaldehyde for 30 min, then briefly rinsed in ethanol and observed using an inverted biological microscope (Olympus, Japan).

Exosome isolation, purification, and identification

N-NPSCs and D-NPSCs were cultured in exosome-free medium for 2 days. NPSC-exo was isolated from supernatant by ultracentrifugation. The culture medium was centrifuged at $1,000 \times g$ for 10 min at 4°C to remove dead cells and centrifuged at $10,000 \times g$ for 30 min at 4°C to remove cell debris. Next, exosomes were centrifuged by ultracentrifugation at $100,000 \times g$ for 70 min after filtering through 0.22-μm membrane filters. Moreover, exosomes were purified by a commercial kit using ExoJuice (WeinaBio, China) according to the instruction of the manufacturer. Briefly, exosome samples were transferred to 5-ml ultracentrifuge tubes and 500 μl of Exojuice was added to the bottom. The tube was then centrifuged at $100,000 \times g$ for 70 min at 4°C, carefully recovered, and fractionated from the bottom. The first 200 μl of the liquid from the bottom of the tube was discarded, then the next 200 μl fraction of solution from the bottom was collected, which contained the purified exosomes.

After purification, morphology was observed by transmission electron microscopy, particle diameter and concentration were analyzed by flow nano analysis, and the exosomal markers, such as CD9, CD81, and TSG101 (Affinity, USA) were detected by Western blotting assay.

Cell counting kit-8 assay

Cell counting kit-8 (CCK-8) assay was used to value the proliferation capacity of AFCs. Briefly, AFCs were plated in 96-well plates at a density of 5×10^3 cells per well with 100 μl of complete culture medium. After 24 h, cells were treated with exosomes (or miRNA mimic/inhibitor) and incubated for 48 h, respectively. Finally, 10 μl of CCK-8 reagents (APExBIO, USA) was added to each well and then incubated for another 2 h at 37°C. The absorbance value at 450 nm was detected by a microplate reader (Biorad imark, USA).

Transwell assay

Transwell assay was used to value the migration capacity of AFCs. Briefly, AFCs (5×10^4 cells per well) in 100 μl of serum-free medium was transferred to the upper chambers of the Transwell, then 600 μl of medium treated with exosomes (or miRNA mimic/inhibitor) was added to the bottom chambers, as previously described, respectively. After 24 h, cells were fixed in 4% paraformaldehyde and stained with 0.1% crystal violet. Then the cells were observed and the stained migrated cells were counted by using a microscope.

Western blotting

Exosomes or cells were lysed with RIPA buffer, then the protein concentration was measured using the BCA protein detection kit (Beyotime, China). Each sample was mixed with protein loading buffer (5×) and heated at 95°C for 10 min to denature. Then

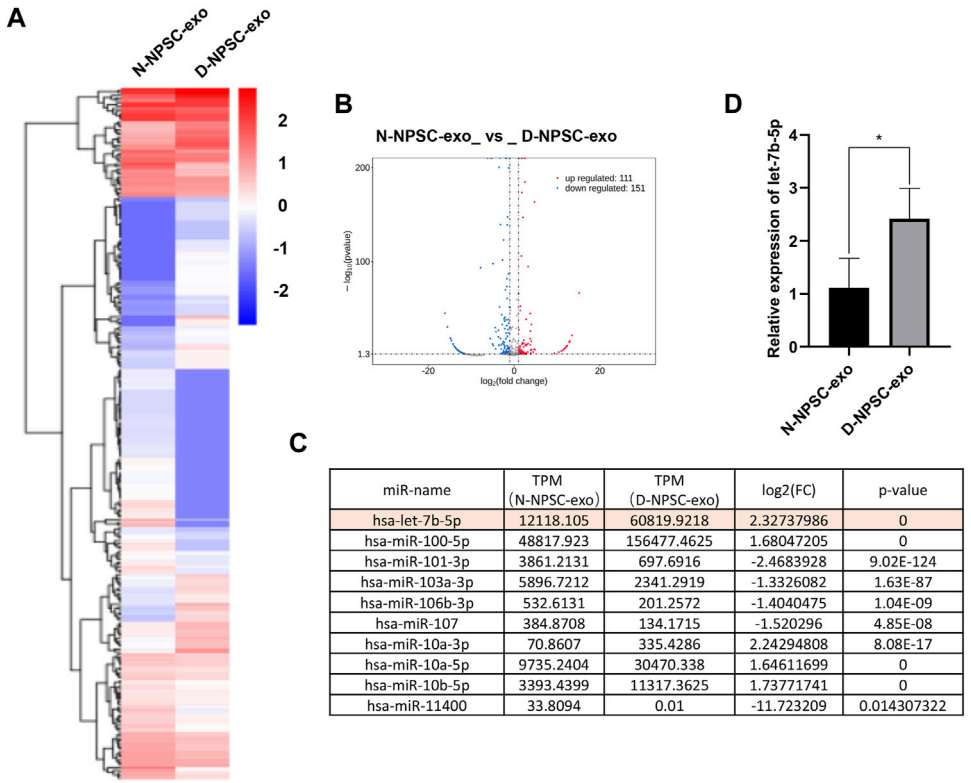

C

miR-name	TPM (N-NPSC-exo)	TPM (D-NPSC-exo)	log2(FC)	p-value
hsa-let-7b-5p	12118.105	60819.9218	2.32737986	0
hsa-miR-100-5p	48817.923	156477.4625	1.68047205	0
hsa-miR-101-3p	3861.2131	697.6916	-2.4683928	9.02E-124
hsa-miR-103a-3p	5896.7212	2341.2919	-1.3326082	1.63E-87
hsa-miR-106b-3p	532.6131	201.2572	-1.4040475	1.04E-09
hsa-miR-107	384.8708	134.1715	-1.520296	4.85E-08
hsa-miR-10a-3p	70.8607	335.4286	2.24294808	8.08E-17
hsa-miR-10a-5p	9735.2404	30470.338	1.64611699	0
hsa-miR-10b-5p	3393.4399	11317.3625	1.73771741	0
hsa-miR-11400	33.8094	0.01	-11.723209	0.014307322

FIGURE 3 | Profiling of the expression of miRNA in N-NPSC-exo and D-NPSC-exo. **(A)** The miRNA profiles of N-NPSC-exo and D-NPSC-exo are represented in the heat map and hierarchical clustering-based dendrograms. **(B)** Volcano plot showing up- and downregulated miRNAs in N-NPSC-exo compared with D-NPSC-exo. **(C)** Fold changes observed in miRNA expression in N-NPSC-exo compared with D-NPSC-exo on microarray data. **(D)** Real-time PCR of hsa-let-7b-5p in N-NPSC-exo compared with D-NPSC-exo. $^{*}p < 0.05$; $^{**}p < 0.01$.

protein samples were separated by 10% SDS–polyacrylamide gel electrophoresis and transferred to polyvinylidene fluoride membranes (PVDF) (Millipore, Germany). PVDF membranes were blocked with 5% skim milk for 1 h, and primary antibody (MMP-13, collagenase II, IGFR1, p-PI3K, *p*-AKT, GAPDH, and β-ACTIN) (Bioss, China) was added in for incubating overnight at 4°C, then the secondary antibody conjugated with horseradish peroxidase was incubated for 2 h at room temperature. Fluorescence was analyzed using the enhanced chemiluminescence kit (Tanon, China) and imaged by the luminescent image analyzer (Tanon, China), and the absorbance value of each band was calculated using the ImageJ software.

Flow cytometry analysis

Apoptosis rates were evaluated using an Annexin V/PI apoptosis detection kit (BD Biosciences, USA) according to the instruction of the manufacturer. Annexin V-FITC (5 μl) and PI (5 μl) solutions were added into 100 μl of cell suspension, respectively. The cells were incubated at room temperature for 15 min in the dark, cells were detected, and analyzed by flow cytometry (Beckman, USA).

miRNA sequencing

Exosomal miRNAs were sequenced in N-NPSC-exo and D-NPSC-exo. The total RNA was isolated from the exosomes using TRIzol reagent (Life Technologies, United States) according to the instructions of the manufacturer. The extracted RNA was then quantified using the OneDrop (WuYi, China). The sample quality control, library preparation, and sequencing were performed by HuaYing, China.

Analysis of the effects of miRNA mimics and inhibitors

According to the results of the miRNA sequencing of exosomes, the mimics and inhibitors of let-7b-5p and the control were synthesized by WeinaBio (Foshan, China).

AFCs were transfected with miRNA mimics or control at 100 nM with Lipofectamine 3,000 reagent (Invitrogen, USA) and then cultured for 48 h. To further confirm the effects of miRNAs in exosomes, AFCs were cultured in medium with D-NPSC-exo (50 μg/ml) and then were transfected with miRNA inhibitors (100 nM) or control for 48 h. Cell proliferation, migration, and apoptosis was detected by CCK-8 assay, Transwell assay, and flow cytometry analysis, and the relative proteins were detected by Western blotting.

qRT-PCR assay

The total RNA was isolated from the exosomes and cells by using TRIzol reagent (Life Technologies, USA). For miRNA,

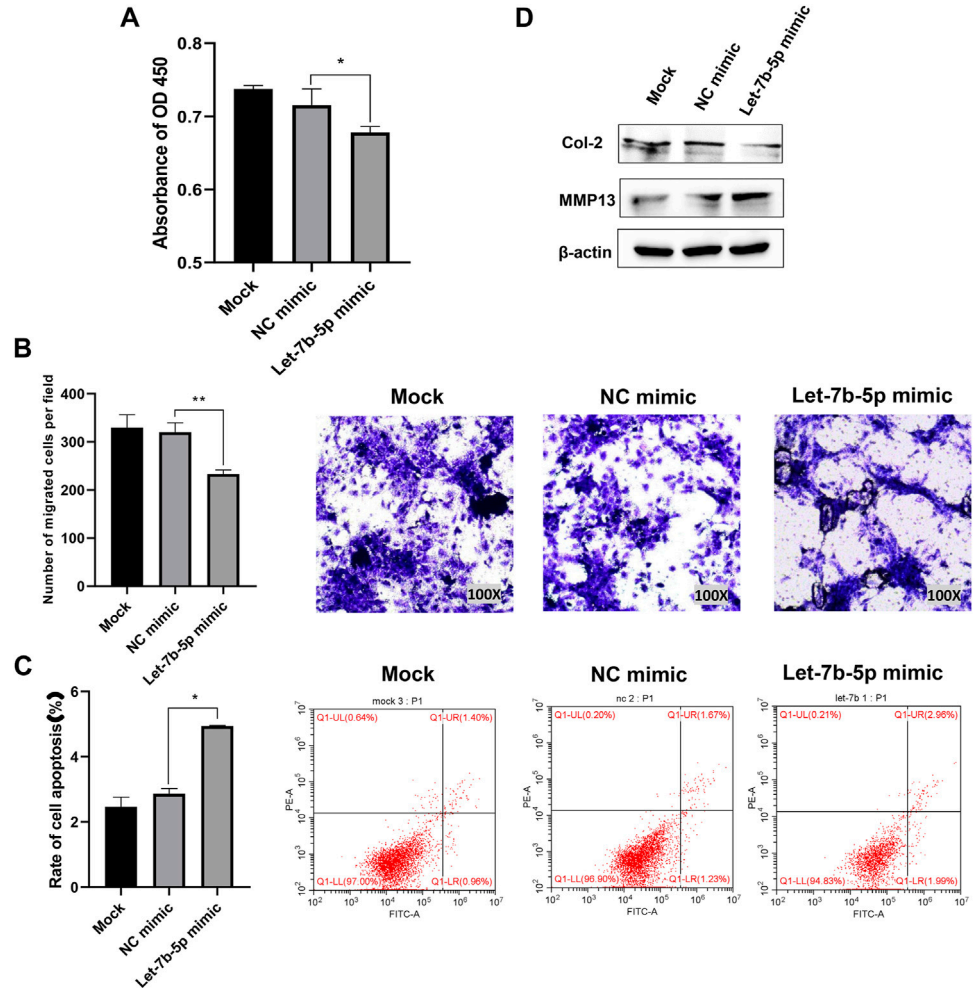

FIGURE 4 | Overexpression of let-7b-5p inhibited proliferation, migration, and extracellular matrix synthesis, and promoted apoptosis of AFCs. AFCs were transfected with let-7b-5p mimic, NC mimic, or PBS (mock group). **(A)** Let-7b-5p mimic inhibited cell proliferation of AFCs by CCK-8 assay. **(B)** Let-7b-5p mimic inhibited cell migration of AFCs by Transwell assay. **(C)** Let-7b-5p mimic promoted cell apoptosis of AFCs by Annexin V/PI apoptosis detection kit. **(D)** Let-7b-5p mimic promoted the expression of MMP13 and inhibits the expression of Col II by Western blotting. $^{*}p < 0.05$; $^{**}p < 0.01$.

the first-strand cDNA was synthesized by using miRNA 1st Strand cDNA Synthesis Kit (Vazyme, China), then real-time PCR was performed by miRNA Universal SYBR qPCR Master Mix (Vazyme, China) under LightCycler480 Real-Time PCR Detection System (Roche, Switzerland). For mRNA, the first-strand cDNA was synthesized by using HiScript III 1st Strand cDNA Synthesis Kit (Vazyme, China), then real-time PCR was performed by Universal SYBR qPCR Master Mix (Vazyme, China). U6 was used as an internal reference for miRNAs, and beta-actin was for mRNAs. Comparative quantification was determined using the $2^{-\Delta\Delta Ct}$ method. The primer sequences used are summarized in **Supplementary Table S1**.

Statistical analysis

GraphPad Prism 8 software was used for statistical analysis. Data are expressed as mean ± standard deviation. The differences between the two groups were analyzed with the unpaired *t*-test. A p-value < 0.05 was considered statistically significant.

RESULTS

Cell identification

Isolated NPSCs displayed fibroblast-like morphology and vortex-styled adherent growth in culture (**Figure 1A**). The results of induced differentiation *in vitro* showed visible calcium deposits formed and stained bright red by Alizarin red staining after osteogenic differentiation, and lipid droplets appeared and stained red by Oil red O staining after adipogenic differentiation (**Figure 1B**). Based on the flow cytometry analysis, NPSCs were positive for surface markers CD29, CD44, CD73, and CD105 (>90%), and negative for surface markers CD34, CD45, and HLA-DR (<2%) (**Figure 1C**). AFCs displayed a long spindle or

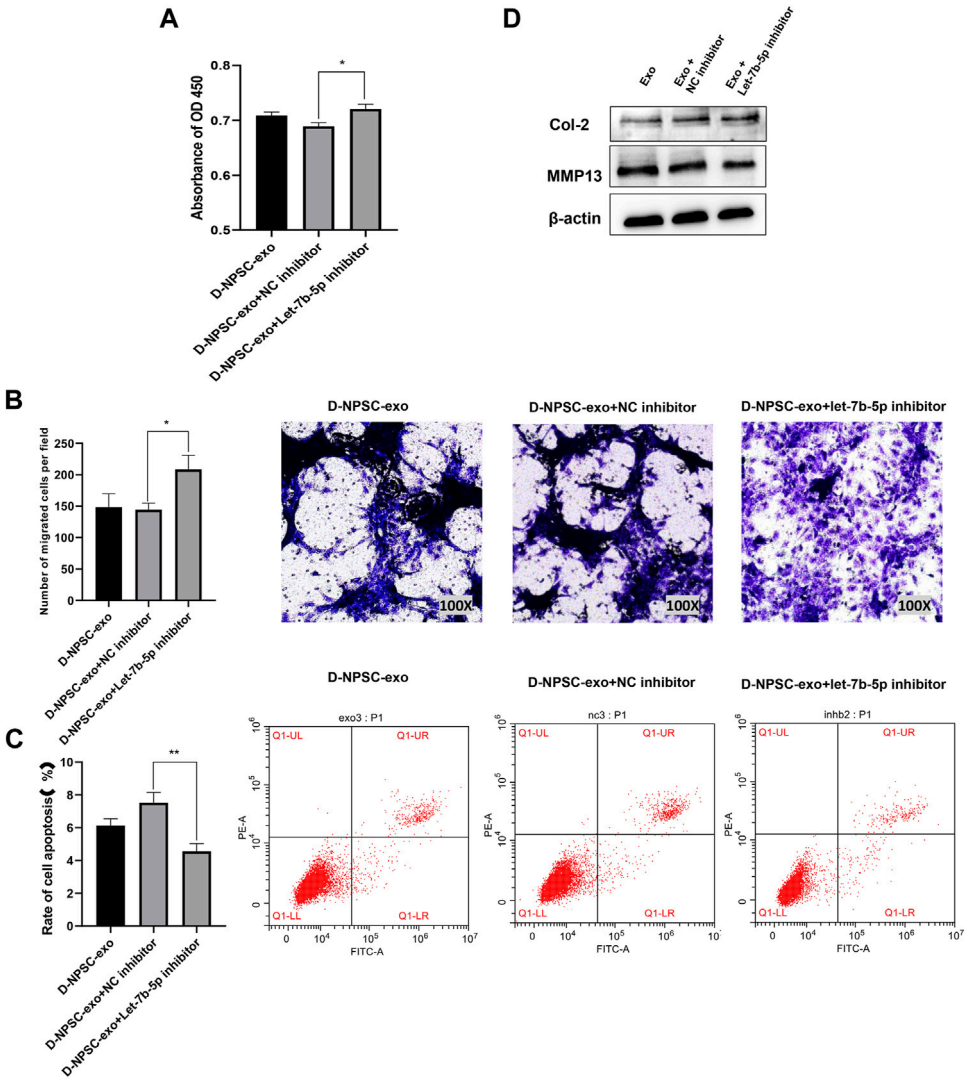

FIGURE 5 | Inhibition of let-7b-5p in D-NPSC-exo alleviated cell degeneration of AFCs. AFCs were treated with D-NPSC-exo, then transfected with let-7b-5p inhibitor or NC inhibitor. **(A)** Inhibition of exosomal let-7b-5p promoted cell proliferation of AFCs by CCK-8 assay. **(B)** Inhibition of exosomal let-7b-5p promoted cell migration of AFCs by Transwell assay. **(C)** Inhibition of exosomal let-7b-5p inhibited cell apoptosis of AFCs by Annexin V/PI apoptosis detection kit. **(D)** Inhibition of exosomal let-7b-5p inhibits the expression of MMP13 and promoted the expression of Col II by Western blotting. $^{*}p < 0.05$; $^{**}p < 0.01$.

polygon shape (**Figure 1D**), and expressed type II collagen by immunofluorescence staining (**Figure 1E** left panel). The toluidine blue staining showed AFCs were purple and exhibited metachromatic granules (**Figure 1E** right panel).

Exosome identification

Morphology, diameter, and surface markers of NPSC-exo were characterized by transmission electron microscopy, flow nano analysis, and Western blotting, respectively. NPSC-exo was displayed as cup-shaped vesicles using transmission electron microscopy (**Figure 1F**). The mean diameter of the exosomes was 66.64 nm, and the concentration of exosomes was 8.8×10^9 particles/ml using flow nano analysis (**Figure 1G**). Western blotting results showed that NPSC-exo were positive for exosomal surface markers TSG101, CD81, and CD9 (**Figure 1H**).

Effect of N-NPSC-Exo and D-NPSC-Exo on cell proliferation, migration, apoptosis, and extracellular matrix metabolism

To explore the effect of the NPSC-exo in AFCs, N-NPSC-exo and D-NPSC-exo in concentrations of 10 and 50 μg/ml were incubated with AFCs, respectively. Then cell proliferation, migration, apoptosis, and extracellular matrix metabolism were analyzed using CCK-8 assay, Transwell migration assay, flow cytometry, and Western blotting, respectively. Our results showed that D-NPSC-exo in low and high concentrations also significantly inhibited cell proliferation

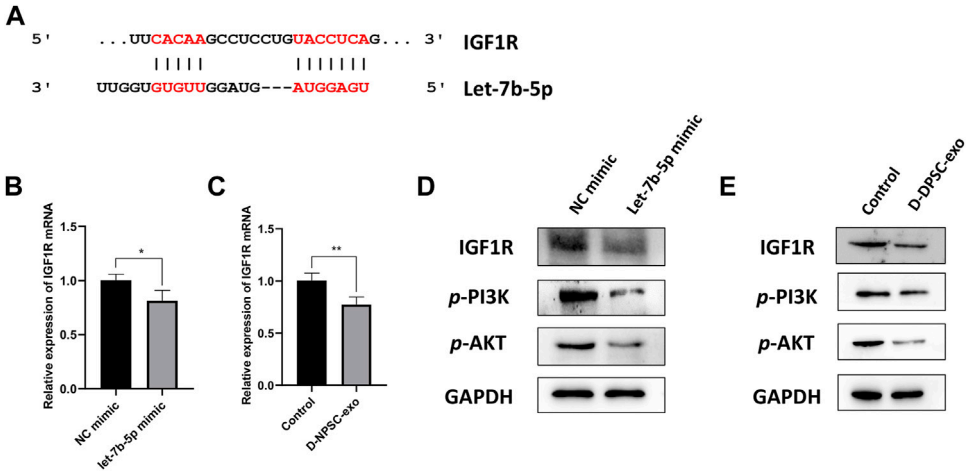

FIGURE 6 | D-NPSC-exo aggravated cell degeneration of AFCs by inhibiting the activation of the IGF1R/PI3K/Akt pathway. **(A)** Shown are let-7b-5p binding sites in the IGF1R 3′ UTR as predicted in TargetScan. **(B)** mRNA expression level of IGF1R in AFCs transfected with let-7b-5p mimic was detected by real-time PCR. **(C)** mRNA expression level of IGF1R in AFCs treated with D-NPSC-exo was detected by real-time PCR. **(D)** Protein expression levels of IGF1R, *p*-PI3K, and *p*-AKT in AFCs transfected with let-7b-5p mimic were detected by Western blotting. **(E)** Protein expression levels of IGF1R, *p*-PI3K, and *p*-AKT in AFCs treated with D-NPSC-exo were detected by Western blotting. $^{*}p < 0.05$; $^{**}p < 0.01$.

(**Figure 2A**), suppressed cell migration (**Figure 2B**), and promoted the apoptosis of AFCs (**Figure 2C**). On the contrary, N-NPSC-exo on high concentration tended to promote cell proliferation and migration, and inhibit cell apoptosis. In order to detect the effect of NPSC-exo on extracellular matrix metabolism in AFCs, protein expression levels of Col II, and MMP13 were detected by Western blotting. D-NPSC-exo in high (50 μg/ml) concentrations significantly promoted the expression of MMP13 and inhibits the expression of Col II. However, the N-NPSC-exo had no effect on extracellular matrix secretion in AFCs (**Figure 2D**).

Differentially expressed miRNAs in N-NPSC-Exo and D-NPSC-Exo

To detect the different miRNA constituents of N-NPSC-exo and D-NPSC-exo, miRNA sequencing was conducted. A clustered heat map (**Figure 3A**) shows the upregulated and downregulated miRNA expressions, and a volcano plot (**Figure 3B**) shows log 2 (fold change) (N-NPSC-exo vs. D-NPSC-exo) on the *x*-axis and −log 10 (*p*-value) on the *y*-axis. Ten significantly up-/downregulated miRNAs in N-NPSC-exo compared with D-NPSC-exo were listed (**Figure 3C**), and let-7b-5p was upregulated in D-NPSC-exo on the microarray data. Consistent with the sequencing results, the expression of let-7b-5p was upregulated in D-NPSC-exo compared with N-NPSC-exo by real-time PCR analysis (**Figure 3D**).

Overexpression of let-7b-5p inhibited proliferation, migration, and extracellular matrix synthesis, and promoted apoptosis of annulus fibrosus cells

The results of CCK-8 assay and transwell assay showed that overexpression of let-7b-5p by transfecting with let-7b-5p mimic significantly inhibited proliferation (**Figure 4A**) and migration (**Figure 4B**) of AFCs. The transfection of let-7b-5p mimic significantly promoted the apoptotic ratio compared with the NC mimic by Annexin V/PI apoptosis detection kit (**Figure 4C**). Moreover, the decreased protein level of Col II and elevated MMP13 expression demonstrated that overexpression of let-7b-5p mimic affected the synthesis of the extracellular matrix (**Figure 4D**).

Inhibition of let-7b-5p in D-NPSC-Exo alleviated cell degeneration of annulus fibrosus cells

To further confirm that D-NPSC-exo inhibited proliferation, migration, and extracellular matrix synthesis, and promoted apoptosis of AFCs by delivering let-7b-5p, the let-7b-5p inhibitor was applied to transfect with D-NPSC-exo-treated AFCs. The overall effects of D-NPSC-exo on AFCs were abolished by the let-7b-5p inhibitor. Compared with the NC inhibitor groups, the cell proliferation (**Figure 5A**) and migration (**Figure 5B**) of AFCs were promoted, and cell apoptosis (**Figure 5C**) of AFCs was reduced. Meanwhile, the protein expression of MMP13 was reduced, and the protein expression of Col II was promoted (**Figure 5D**). Collectively, exosomal let-7b-5p plays important roles in cell degeneration of AFCs.

Exosomal let-7b-5p leads to targeted inhibition of IGF1R followed by inhibiting the activation of the PI3K/Akt pathway in annulus fibrosus cells

Finally, we explored the mechanism by which exosomal let-7b-5p aggravated cell degeneration of AFCs. A binding site at 3′-UTR of

IGF1R was predicted on let-7b-5p by TargetScan (**Figure 6A**). The result of real-time PCR confirmed that the mRNA expression of IGF1R was significantly decreased in AFCs by transfecting with let-7b-5p (**Figure 6B**). Similarly, this decrease in the mRNA expression of IGF1R appeared in D-NPSC-exo-treated AFCs (**Figure 6C**). To test whether exosomal let-7b-5p modulates IGF1R and the PI3K/Akt signal pathway, protein expression levels of IGF1R, *p*-PI3K, and *p*-AKT in AFCs transfected with let-7b-5p mimic were detected by Western blotting. The result of Western blotting confirmed that the protein expressions of IGF1R, *p*-PI3K, and *p*-AKT were decreased in AFCs by transfecting with let-7b-5p (**Figure 6D**). Similarly, this decrease in the protein expressions of IGF1R, p-PI3K, and *p*-AKT appeared in D-NPSC-exo-treated AFCs (**Figure 6E**). Collectively, exosomal let-7b-5p leads to targeted inhibition of IGF1R followed by inhibiting the activation of the PI3K/Akt pathway in AFCs.

DISCUSSION

In recent years, stem cell transplantation has become a research hotspot for biological treatment of IDD (Xia et al., 2019). Some studies found that transplantation of autologous NPSCs into degenerative intervertebral disc tissues can significantly delay the development of IDD (Chen et al., 2016). NPSCs are progenitors of nucleus pulposus cells, and they have considerable potential for proliferation and differentiation, and some results have been observed in both normal and degenerative intervertebral disc tissues. Endogenous NPSCs can better tolerate the local acidic and hypertonic microenvironment and play a key role in stem cell biological treatment of IDD (Tao et al., 2013; Han et al., 2014). However, Sakai found that the number of NPSCs in the nucleus pulposus gradually decreased with aging and the degree of intervertebral disc degeneration in rats and humans. Sakai also pointed out that the intervertebral disc degeneration may be caused by the depletion of NPSC apoptosis (Sakai et al., 2012). A study by Liu showed that the biological characteristics of NPSCs derived from normal and degenerative intervertebral discs were different (Liu et al., 2019).

Currently, researchers believe that secreting exosomes is one of the important ways in which stem cells perform biological functions (Phinney and Pittenger, 2017; Mendt et al., 2019). To determine whether there are functional differences between N-NPSC-exo and D-NPSC-exo, we studied the effects of N-NPSC-exo and D-NPSC-exo on the proliferation, migration, apoptosis, and extracellular matrix synthesis of degenerated AFCs. The results showed that N-NPSC-exo was beneficial to AFCs. However, D-NPSC-exo inhibited AFC proliferation, migration, and matrix synthesis, and promoted apoptosis.

miRNAs, important intermediaries of the exosome function, play an important role in maintaining normal homeostasis (Shan et al., 2019). Exosomes transport miRNAs to recipient cells and participate in such physiological processes as cell proliferation, differentiation, migration, and apoptosis (Zhang et al., 2020). To further explore how D-NPSC-exo affects AFCs, N-NPSC-exo and D-NPSC-exo were sequenced and found to be discrepant in some miRNAs. This difference may regulate the cellular function of AFCs. We found that let-7b-5p was upregulated in D-NPSC-exo, and was confirmed by real-time PCR, which suggested a possible connection between the increase of miRNA and the AFCs degeneration. The mimic and inhibitor of let-7b-5p were used to establish the effects of miRNA in D-DPSC-exo. After transfection with the let-7b-5p mimic, the proliferation, migration, and extracellular matrix synthesis were reduced, and the rate of apoptosis among AFCs increased significantly. After transfection with the let-7b-5p inhibitor, the effect of D-DPSC-exo on AFCs was reversed. This indicated that D-DPSC-exo may exacerbate AFC degeneration by delivering let-7b-5p.

Let-7b-5p is a miRNA with a wide range of biological functions (Mandolesi et al., 2021). It plays a very important role in cell migration and proliferation and in antitumor processes (Babapoor et al., 2017; Wu et al., 2020). Let-7b-5p has been shown to regulate proliferation and apoptosis in multiple myeloma by targeting IGF1R (Xu et al., 2014). The results of the study of Zhang indicated that let-7b suppressed proliferation and invasion of osteosarcoma cells via targeting IGF1R (Zhang et al., 2019a). In this present work, real-time PCR and Western blotting analysis confirmed that the mRNA and protein expression of IGF1R were significantly decreased in AFCs by transfecting with let-7b-5p.

Many studies confirmed that IGF1R is one of the upstream regulatory molecules of the PI3K-Akt pathway, involved in cell proliferation, apoptosis, and metabolism (Park et al., 2018). Here, we confirmed that the activation of the PI3K/Akt pathway could be blocked by the let-7b-5p mimic targeting IGF1R. Our results also suggested that D-NPSC-exo exacerbated cell degeneration of AFCs *via* let-7b-5p, possibly by blocking the IGF1R/PI3K/Akt pathway.

CONCLUSION

In summary, let-7b-5p carried by D-NPSC-exo was found to regulate the function of AFCs by downregulating IGF1R and blocking the PI3K/Akt pathway, thus, ultimately exacerbating cell degeneration of AFCs. These results suggest the clinical application prospect of D-NPSC-exo-derived let-7b-5p, possibly as a molecular target in the treatment of IDD.

DATA AVAILABILITY STATEMENT

The data and materials used to support the findings of this experiment are available from the corresponding author upon reasonable request. The raw data has been deposited at: https://www.aliyundrive.com/s/nnbQQNG2ZQm.

ETHICS STATEMENT

All the experimental protocols were approved by the Ethics Committee of Wuxi 9th Affiliated Hospital of Soochow University and obtained the informed consent of patients.

AUTHOR CONTRIBUTIONS

SZ, YZ, and SS designed the study. XL, XH, SD, YL, and YH performed the experiments and analyzed the data. DX and XL collected the samples. YZ and SS wrote the. and SZ wrote the final manuscript. All authors read and approved the final manuscript.

FUNDING

This study was supported by grants from the General Project of Wuxi Municipal Health Commission in 2020 (grant number M202002).

ACKNOWLEDGMENTS

We thank LetPub (www.letpub.com) for its linguistic assistance during the preparation of this manuscript.

SUPPLEMENTARY MATERIAL

The Supplementary Material for this article can be found online at: https://www.frontiersin.org/articles/10.3389/fmolb.2021.766115/full#supplementary-material

REFERENCES

An, Y., Lin, S., Tan, X., Zhu, S., Nie, F., Zhen, Y., et al. (2021). Exosomes from Adipose-derived Stem Cells and Application to Skin Wound Healing. *Cell Prolif* 54 (3), e12993. doi:10.1111/cpr.12993

Aziz, N. S., Yusop, N., and Ahmad, A. (2020). Importance of Stem Cell Migration and Angiogenesis Study for Regenerative Cell-Based Therapy: A Review. *Cscr* 15 (3), 284–299. doi:10.2174/1574888X15666200127145923

Babapoor, S., Wu, R., Kozubek, J., Auidi, D., Grant-Kels, J. M., and Dadras, S. S. (2017). Identification of microRNAs Associated with Invasive and Aggressive Phenotype in Cutaneous Melanoma by Next-Generation Sequencing. *Lab. Invest.* 97 (6), 636–648. doi:10.1038/labinvest.2017.5

Chen, X., Zhu, L., Wu, G., Liang, Z., Yang, L., and Du, Z. (2016). A Comparison between Nucleus Pulposus-Derived Stem Cell Transplantation and Nucleus Pulposus Cell Transplantation for the Treatment of Intervertebral Disc Degeneration in a Rabbit Model. *Int. J. Surg.* 28, 77–82. doi:10.1016/j.ijsu.2016.02.045

Choi, H., Johnson, Z., and Risbud, M. (2015). Understanding Nucleus Pulposus Cell Phenotype: A Prerequisite for Stem Cell Based Therapies to Treat Intervertebral Disc Degeneration. *Cscr* 10 (4), 307–316. doi:10.2174/1574888x10666150113112149

Davis, C., Dukes, A., Drewry, M., Helwa, I., Johnson, M. H., Isales, C. M., et al. (2017). MicroRNA-183-5p Increases with Age in Bone-Derived Extracellular Vesicles, Suppresses Bone Marrow Stromal (Stem) Cell Proliferation, and Induces Stem Cell Senescence. *Tissue Eng. A* 23 (21-22), 1231–1240. doi:10.1089/ten.TEA.2016.0525

Dowdell, J., Erwin, M., Choma, T., Vaccaro, A., Iatridis, J., and Cho, S. K. (2017). Intervertebral Disk Degeneration and Repair. *Neurosurgery* 80 (3S), S46–S54. doi:10.1093/neuros/nyw078

Du, Y., Li, D., Han, C., Wu, H., Xu, L., Zhang, M., et al. (2017). Exosomes from Human-Induced Pluripotent Stem Cell-Derived Mesenchymal Stromal Cells (hiPSC-MSCs) Protect Liver against Hepatic Ischemia/Reperfusion Injury via Activating Sphingosine Kinase and Sphingosine-1-Phosphate Signaling Pathway. *Cell. Physiol. Biochem.* 43 (2), 611–625. doi:10.1159/000480533

Han, B., Wang, H.-c., Li, H., Tao, Y.-q., Liang, C.-z., Li, F.-c., et al. (2014). Nucleus Pulposus Mesenchymal Stem Cells in Acidic Conditions Mimicking Degenerative Intervertebral Discs Give Better Performance Than Adipose Tissue-Derived Mesenchymal Stem Cells. *Cells Tissues Organs* 199 (5-6), 342–352. doi:10.1159/000369452

Hang, D., Li, F., Che, W., Wu, X., Wan, Y., Wang, J., et al. (2017). One-Stage Positron Emission Tomography and Magnetic Resonance Imaging to Assess Mesenchymal Stem Cell Survival in a Canine Model of Intervertebral Disc Degeneration. *Stem Cell Dev.* 26 (18), 1334–1343. doi:10.1089/scd.2017.0103

Lazzarini, R., Guarnieri, S., Fulgenzi, G., Mariggiò, M. A., Graciotti, L., Martiniani, M., et al. (2019). Mesenchymal Stem Cells from Nucleus Pulposus and Neural Differentiation Potential: A Continuous challenge. *J. Mol. Neurosci.* 67 (1), 111–124. doi:10.1007/s12031-018-1216-x

Liu, L., Jin, X., Hu, C.-F., Li, R., Zhou, Z. e., and Shen, C.-X. (2017). Exosomes Derived from Mesenchymal Stem Cells rescue Myocardial Ischaemia/Reperfusion Injury by Inducing Cardiomyocyte Autophagy via AMPK and Akt Pathways. *Cel. Physiol. Biochem.* 43 (1), 52–68. doi:10.1159/000480317

Liu, Y., Li, Y., Huang, Z.-N., Wang, Z.-Y., Nan, L.-P., Wang, F., et al. (2019). The Effect of Intervertebral Disc Degenerative Change on Biological Characteristics of Nucleus Pulposus Mesenchymal Stem Cell: An *In Vitro* Study in Rats. *Connect. Tissue Res.* 60 (4), 376–388. doi:10.1080/03008207.2019.1570168

Ma, K., Chen, S., Li, Z., Deng, X., Huang, D., Xiong, L., et al. (2019). Mechanisms of Endogenous Repair Failure during Intervertebral Disc Degeneration. *Osteoarthritis and Cartilage* 27 (1), 41–48. doi:10.1016/j.joca.2018.08.021

Mandolesi, G., Rizzo, F. R., Balletta, S., Stampanoni Bassi, M., Gilio, L., Guadalupi, L., et al. (2021). The microRNA Let-7b-5p Is Negatively Associated with Inflammation and Disease Severity in Multiple Sclerosis. *Cells* 10 (2), 330. doi:10.3390/cells10020330

Mendt, M., Rezvani, K., and Shpall, E. (2019). Mesenchymal Stem Cell-Derived Exosomes for Clinical Use. *Bone Marrow Transpl.* 54 (Suppl. 2), 789–792. doi:10.1038/s41409-019-0616-z

Nakashima, D., Fujita, N., Hata, J., Komaki, Y., Suzuki, S., Nagura, T., et al. (2020). Quantitative Analysis of Intervertebral Disc Degeneration Using Q-space Imaging in a Rat Model. *J. Orthop. Res.* 38 (10), 2220–2229. doi:10.1002/jor.24757

Park, B. R., Lee, S. A., Moon, S. M., and Kim, C. S. (2018). Anthricin-induced C-aspase-dependent A-poptosis through IGF1R/PI3K/AKT P-athway I-nhibition in A549 H-uman N-on-small L-ung C-ancer C-ells. *Oncol. Rep.* 39 (6), 2769–2776. doi:10.3892/or.2018.6333

Phinney, D. G., and Pittenger, M. F. (2017). Concise Review: MSC-Derived Exosomes for Cell-Free Therapy. *Stem Cells* 35 (4), 851–858. doi:10.1002/stem.2575

Sakai, D., Nakamura, Y., Nakai, T., Mishima, T., Kato, S., Grad, S., et al. (2012). Exhaustion of Nucleus Pulposus Progenitor Cells with Ageing and Degeneration of the Intervertebral Disc. *Nat. Commun.* 3, 1264. doi:10.1038/ncomms2226

Schneider, A., and Simons, M. (2013). Exosomes: Vesicular Carriers for Intercellular Communication in Neurodegenerative Disorders. *Cell Tissue Res* 352 (1), 33–47. doi:10.1007/s00441-012-1428-2

Shan, S.-K., Lin, X., Li, F., Xu, F., Zhong, J.-Y., Guo, B., et al. (2020). Exosomes and Bone Disease. *Cpd* 25 (42), 4536–4549. doi:10.2174/1381612825666191127114054

Tao, Y.-Q., Liang, C.-Z., Li, H., Zhang, Y.-J., Li, F.-C., Chen, G., et al. (2013). Potential of Co-culture of Nucleus Pulposus Mesenchymal Stem Cells and Nucleus Pulposus Cells in Hyperosmotic Microenvironment for Intervertebral Disc Regeneration. *Cell Biol. Int.* 37 (8), 826–834. doi:10.1002/cbin.10110

Urits, I., Capuco, A., Sharma, M., Kaye, A. D., Viswanath, O., Cornett, E. M., et al. (2019). Stem Cell Therapies for Treatment of Discogenic Low Back Pain: A Comprehensive Review. *Curr. Pain Headache Rep.* 23 (9), 65. doi:10.1007/s11916-019-0804-y

Vadalà, G., Ambrosio, L., Russo, F., Papalia, R., and Denaro, V. (2019). Interaction between Mesenchymal Stem Cells and Intervertebral Disc Microenvironment: From Cell Therapy to Tissue Engineering. *Stem Cell Int.* 2019, 1–15. doi:10.1155/2019/2376172

Vergroesen, P.-P. A., Kingma, I., Emanuel, K. S., Hoogendoorn, R. J. W., Welting, T. J., van Royen, B. J., et al. (2015). Mechanics and Biology in Intervertebral Disc Degeneration: A Vicious circle. *Osteoarthritis and Cartilage* 23 (7), 1057–1070. doi:10.1016/j.joca.2015.03.028

Vickers, L., Thorpe, A. A., Snuggs, J., Sammon, C., and Le Maitre, C. L. (2019). Mesenchymal Stem Cell Therapies for Intervertebral Disc Degeneration: Consideration of the Degenerate Niche. *JOR Spine* 2 (2), e1055. doi:10.1002/jsp2.1055

Wang, F., Shi, R., Cai, F., Wang, Y.-T., and Wu, X.-T. (2015). Stem Cell Approaches to Intervertebral Disc Regeneration: Obstacles from the Disc Microenvironment. *Stem Cell Dev.* 24 (21), 2479–2495. doi:10.1089/scd.2015.0158

Whiteside, T. L. (2018). Exosome and Mesenchymal Stem Cell Cross-Talk in the Tumor Microenvironment. *Semin. Immunol.* 35, 69–79. doi:10.1016/j.smim.2017.12.003

Wu, D. S., Zheng, C. F., Zeng, Y. P., Lin, J., Chen, J. L., and Shi, S. J. (2020). Hsa-let-7b-5p Inhibits Proliferation of Human Leukemia THP-1 Cells via FTO/m6A/MYC Signaling Pathway. *Zhongguo Shi Yan Xue Ye Xue Za Zhi* 28 (6), 1873–1879. doi:10.19746/j.cnki.issn.1009-2137.2020.06.014

Wu, H., Shang, Y., Yu, J., Zeng, X., Lin, J., Tu, M., et al. (2018). Regenerative Potential of Human Nucleus Pulposus Resident Stem/progenitor Cells Declines with Ageing and Intervertebral Disc Degeneration. *Int. J. Mol. Med.* 42 (4), 2193–2202. doi:10.3892/ijmm.2018.3766

Xia, K., Zhu, J., Hua, J., Gong, Z., Yu, C., Zhou, X., et al. (2019). Intradiscal Injection of Induced Pluripotent Stem Cell-Derived Nucleus Pulposus-like Cell-Seeded Polymeric Microspheres Promotes Rat Disc Regeneration. *Stem Cell Int.* 2019, 1–14. doi:10.1155/2019/6806540

Xu, H., Liu, C., Zhang, Y., Guo, X., Liu, Z., Luo, Z., et al. (2014). Let-7b-5p Regulates Proliferation and Apoptosis in Multiple Myeloma by Targeting IGF1R. *Acta Biochim. Biophys. Sin (Shanghai).* 46 (11), 965–972. doi:10.1093/abbs/gmu089

Ying, J.-W., Wen, T.-Y., Pei, S.-S., Su, L.-H., and Ruan, D.-K. (2019). Stromal Cell-Derived Factor-1α Promotes Recruitment and Differentiation of Nucleus Pulposus-Derived Stem Cells. *Wjsc* 11 (3), 196–211. doi:10.4252/wjsc.v11.i3.196

Zhang, K., Wang, W., Liu, Y., Guo, A., and Yang, D. (2019a). Let-7b A-cts as a T-umor S-uppressor in O-steosarcoma via T-argeting IGF1R. *Oncol. Lett.* 17 (2), 1646–1654. doi:10.3892/ol.2018.9793

Zhang, N., Zhu, J., Ma, Q., Zhao, Y., Wang, Y., Hu, X., et al. (2020). Exosomes Derived from Human Umbilical Cord MSCs Rejuvenate Aged MSCs and Enhance Their Functions for Myocardial Repair. *Stem Cel Res. Ther.* 11 (1), 273. doi:10.1186/s13287-020-01782-9

Zhang, Y., He, F., Chen, Z., Su, Q., Yan, M., Zhang, Q., et al. (2019b). Melatonin Modulates IL-1β-induced Extracellular Matrix Remodeling in Human Nucleus Pulposus Cells and Attenuates Rat Intervertebral Disc Degeneration and Inflammation. *Aging* 11 (22), 10499–10512. doi:10.18632/aging.102472

Conflict of Interest: The authors declare that the research was conducted in the absence of any commercial or financial relationships that could be construed as a potential conflict of interest.

Publisher's Note: All claims expressed in this article are solely those of the authors and do not necessarily represent those of their affiliated organizations, or those of the publisher, the editors, and the reviewers. Any product that may be evaluated in this article, or claim that may be made by its manufacturer, is not guaranteed or endorsed by the publisher.

frontiers in Molecular Biosciences

ORIGINAL RESEARCH
published: 23 February 2022
doi: 10.3389/fmolb.2022.821137

Changes of Small Non-coding RNAs by Severe Acute Respiratory Syndrome Coronavirus 2 Infection

*Wenzhe Wu[1], Eun-Jin Choi[1], Binbin Wang[2], Ke Zhang[1], Awadalkareem Adam[2], Gengming Huang[3], Leo Tunkle[4,5,6], Philip Huang[4,7], Rohit Goru[4,7], Isabella Imirowicz[4,7], Leanne Henry[4,6], Inhan Lee[4], Jianli Dong[3,8], Tian Wang[2,3,8] and Xiaoyong Bao[1,8,9]**

[1]Department of Pediatrics, The University of Texas Medical Branch, Galveston, TX, United States, [2]Department of Microbiology and Immunology, The University of Texas Medical Branch, Galveston, TX, United States, [3]Department of Pathology, The University of Texas Medical Branch, Galveston, TX, United States, [4]miRcore, Ann Arbor, MI, United States, [5]Department of Nuclear Engineering and Radiological Sience, University of Michigan, Ann Arbor, MI, United States, [6]Department of Computer Science, University of Michigan, Ann Arbor, MI, United States, [7]Department of Molecular, Cellular and Developmental Biology, University of Michigan, Ann Arbor, MI, United States, [8]The Institute for Human Infections and Immunity, The University of Texas Medical Branch, Galveston, TX, United States, [9]The Institute of Translational Sciences, The University of Texas Medical Branch, Galveston, TX, United States

OPEN ACCESS

Edited by:
Hem Chandra Jha,
Indian Institute of Technology Indore, India

Reviewed by:
Fumiaki Uchiumi,
Tokyo University of Science, Japan
Valeria Micheli,
ASST Fatebenefratelli Sacco, Italy

***Correspondence:**
Xiaoyong Bao
xibao@utmb.edu

Specialty section:
This article was submitted to Molecular Diagnostics and Therapeutics, a section of the journal Frontiers in Molecular Biosciences

Received: *23 November 2021*
Accepted: *19 January 2022*
Published: *23 February 2022*

Citation:
Wu W, Choi E-J Wang B, Zhang K, Adam A, Huang G, Tunkle L, Huang P, Goru R, Imirowicz I, Henry L, Lee I, Dong J, Wang T and Bao X (2022) Changes of Small Non-coding RNAs by Severe Acute Respiratory Syndrome Coronavirus 2 Infection. Front. Mol. Biosci. 9:821137. doi: 10.3389/fmolb.2022.821137

The ongoing pandemic of coronavirus disease 2019 (COVID-19), which results from the rapid spread of the severe acute respiratory syndrome coronavirus 2 (SARS-CoV-2), is a significant global public health threat, with molecular mechanisms underlying its pathogenesis largely unknown. In the context of viral infections, small non-coding RNAs (sncRNAs) are known to play important roles in regulating the host responses, viral replication, and host-virus interaction. Compared with other subfamilies of sncRNAs, including microRNAs (miRNAs) and Piwi-interacting RNAs (piRNAs), tRNA-derived RNA fragments (tRFs) are relatively new and emerge as a significant regulator of host-virus interactions. Using T4 PNK-RNA-seq, a modified next-generation sequencing (NGS), we found that sncRNA profiles in human nasopharyngeal swabs (NPS) samples are significantly impacted by SARS-CoV-2. Among impacted sncRNAs, tRFs are the most significantly affected and most of them are derived from the 5′-end of tRNAs (tRF5). Such a change was also observed in SARS-CoV-2-infected airway epithelial cells. In addition to host-derived ncRNAs, we also identified several small virus-derived ncRNAs (svRNAs), among which a svRNA derived from CoV2 genomic site 346 to 382 (sv-CoV2-346) has the highest expression. The induction of both tRFs and sv-CoV2-346 has not been reported previously, as the lack of the 3′-OH ends of these sncRNAs prevents them to be detected by routine NGS. In summary, our studies demonstrated the involvement of tRFs in COVID-19 and revealed new CoV2 svRNAs.

Keywords: SARS-CoV-2, TRF, SARS-CoV-2-derived sncRNAs, tRF5DC, viral replication and SARS-CoV-2-derived sncRNAs

INTRODUCTION

Severe acute respiratory syndrome coronavirus 2 (SARS-CoV-2) is a beta coronavirus belonging to the sarbecovirus subgenus of Coronaviridae family (Zhu et al., 2020). It is a positive-sense single-stranded RNA virus with a genome length of ~30 kb. By the middle of January 2022, the ongoing coronavirus disease 2019 (COVID-19) pandemic, caused by SARS-CoV-2, has respectively caused more than 320 million infectious cases and over five million deaths globally (World Health, 2021).

Small non-coding RNAs (sncRNAs) have diverse functions through various regulatory mechanisms. They virtually participate in all biological pathways, including cell proliferation, differentiation, apoptosis, autophagy, and tissue remodeling. sncRNAs are also essential to regulate host responses to viral infections (Choudhuri, 2010; Beermann et al., 2016; Romano et al., 2017; Rajput et al., 2020; Wu et al., 2020). Among sncRNAs, the most widely studied sncRNAs are microRNAs (miRNAs), which are 18–24 nt in length, carry 5′ monophosphate and 3′ hydroxyl (3′-OH) ends, and generally regulate genes *via* the argonaute (AGO) platform (Schwarz et al., 2004; Fabian and Sonenberg, 2012).

Other than miRNAs, piwi-interacting RNAs (piRNAs), small nucleolar RNAs (snoRNAs), and tRNA-derived RNA fragments (tRFs) are also important members of sncRNAs (Dozmorov et al., 2013). Currently, there is very limited information on whether or how SARS-CoV-2 regulates the sncRNA expression, except the reports on SARS-CoV-2-impacted miRNAs (Mallick et al., 2009; Hasan et al., 2014; Khan et al., 2020).

Using T4 polynucleotide kinase (T4 PNK)-RNA-seq, a modified next-generation sequencing (NGS), we found that tRFs and piRNAs were the two most abundant sncRNAs in nasopharyngeal swabs (NPS) samples of the SARS-CoV-2-positive group. However, only tRFs were significantly enhanced in SARS-CoV positive samples. Generally, tRFs are generated by specific cleavages within pre-tRNAs or mature tRNAs (Lee et al., 2009). Compared with other sncRNAs, tRFs are relatively new members. However, their importance in diseases, such as cancer, infectious diseases, neurodegenerative diseases, and metabolic diseases, was quickly acknowledged after the discovery (Wang et al., 2013; Selitsky et al., 2015; Shen et al., 2018; Sun et al., 2018; Zhu et al., 2018; Choi et al., 2020; Qin et al., 2020; Wu et al., 2021). tRFs are classified mainly into tRF-1 series, tRF-3 series, and tRF-5 series (Fu et al., 2009). tRF-1 series are usually those from the 3′-trailer sequences of pre-tRNA, while tRF-3 and tRF-5 series are aligned to the 3′- and 5′- end of the mature tRNAs respectively. Among SARS-CoV-2-impacted tRFs, the most impacted tRFs belonged to tRF5s. In addition, the impacted tRF profile seemed to be SARS-CoV-2 specific, which is consistent with what we and others found previously on the changes in tRF signatures being virus-dependent (Wang et al., 2013; Selitsky et al., 2015), implicating tRFs as potential prognosis and diagnosis biomarkers. The impacted tRFs were also observed in SARS-CoV-2 infected human alveolar type II-like epithelial cells expressing human angiotensin-converting enzyme 2 (A549-ACE2) and human small airway epithelial cells (SAECs) in the air-liquid interface (ALI) culture.

In addition to host-derived ncRNAs, viral genomes can also encode ncRNAs. These viral ncRNAs vary in length and have diverse biological functions, including the regulation of viral replication, viral persistence, host immune evasion, host inflammatory response, and cell transformation (Tycowski et al., 2015). For example, SARS-CoV-encoded small RNAs contribute to SARS-CoV-induced lung injury (Morales et al., 2017), and SARS-CoV-2-encoded miRNAs enhance inflammation (Cheng et al., 2021). In this study, we revealed several new small viral RNA (svRNA) fragments, with the length of 25 nt, 33 nt, and 36 nt, by T4 PNK-RNA-seq. Among svRNAs derived from CoV-2 (sv-CoV2), a svRNA spanning from site 346 to site 382 of nsp1(sv-CoV2-346) had the highest expression.

In summary, this is the first report demonstrating the altered tRFs by SARS-CoV-2. T4 PNK pretreatment also enabled small RNA seq to reveal additional new sv-CoV2. In the future, we will characterize the biogenesis and function mechanisms of these new sncRNAs associated with SARS-CoV-2 infection.

MATERIALS AND METHODS

Nasopharyngeal Swab Specimens

NPS were collected from patients who visited outpatient clinics of the University of Texas Medical Branch (UTMB) for SARS-CoV-2 screening in April 2020. NPS samples in universal viral transport media were transported to the Molecular Pathology laboratory, directed by Dr. Jianli Dong, and subjected to SARS-CoV-2 test using Abbott m2000 SARS-CoV-2 RT-PCR assay. The limit of detection (LOD) of detection assays is 100 viral genome copies/ml.

Thirteen anonymous NPS samples were used in this study, including seven SARS-CoV-2 negative (51.7 ± 13.7 years old) and six SARS-CoV-2 positive (49.2 ± 10.5 years old) samples. The protocol was approved by the Institutional Review Boards (IRB) of UTMB at Galveston, under the IRB protocol # 02-089 and 03-385.

RNA Isolation

After the SARS-CoV-2 validation, 1 ml of NPS sample from each individual was subjected to RNA extraction using the mirVana PARIS kit (Invitrogen, MA, United States) according to the manufacturer's protocol. At the elution step, samples were incubated on the column for 5 min at 65°C, and the RNA was eluted with 45 μL nuclease-free water. To extract RNAs from cells, TRIzol reagents (Thermo Fisher Scientific, MA, United States) were used for total RNA preparation, as described (Choi et al., 2020), followed by qRT-PCR.

T4 PNK-RNA-seq and Data Analyses

To study whether other sncRNAs than miRNAs are impacted by SARS-CoV-2, we used T4 PNK-RNA-seq, a modified NGS, to get sncRNA profiles for samples derived from NSP or cultured cells, similarly as described in (Honda et al., 2015; Giraldez et al., 2019). A flowchart of the T4 PNK-RNA-seq is shown in **Supplementary Figure S1A** and data have been deposited in GEO (GSE193555). Basically, we treated sample RNAs with T4 PNK before the

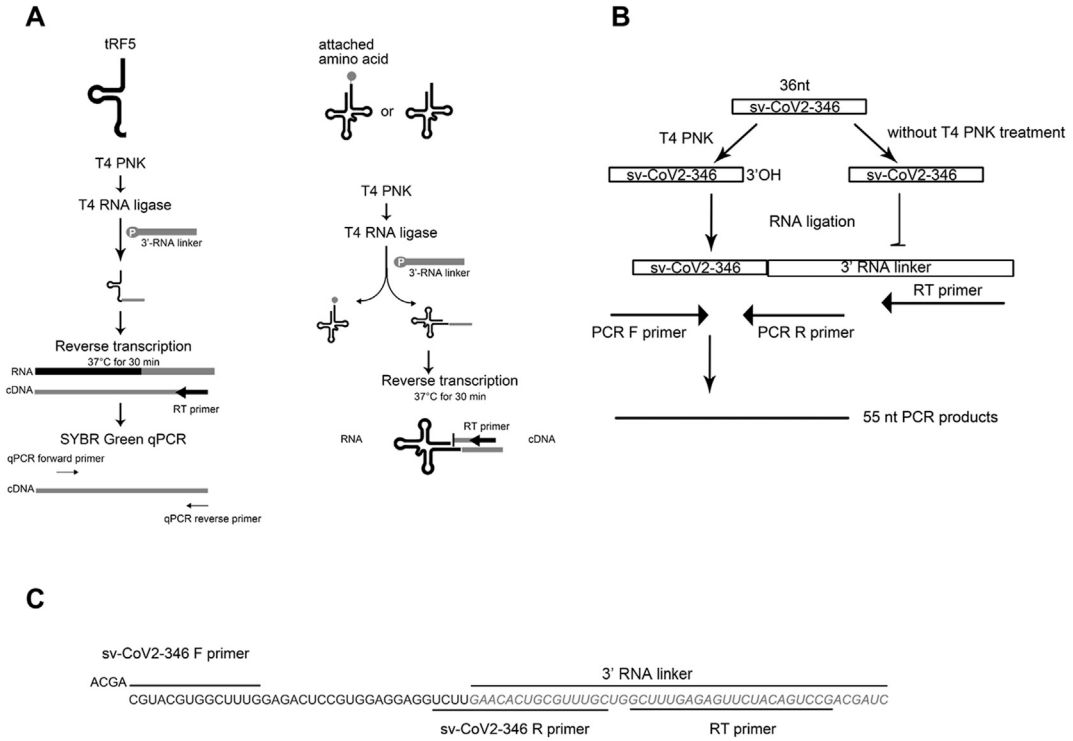

FIGURE 1 | The schematic summaries on tRF quantification by qRT-PCR **(A)** and the detection of sv-CoV2-346 by RT-PCR **(B)**. **(C)** The sequence information on sv-CoV2-346 and associated primers and the 3′ RNA linker for its detection.

library construction and small RNA-seq to make the 3′-end of RNAs homogenous with -OH, as the ligation of the 3′-end of sncRNAs with sequencing barcodes requires the presence of 3′-OH and not all sncRNAs have 3-OH ends. The seq was done in the NGS Core of UTMB. In brief, the RNA samples were pretreated with 10 units of T4 PNK using 14 μL extracted RNAs in a final reaction volume of 50 μL and incubated at 37°C for 30 min, and then were heat-inactivated at 65°C for 20 min. The RNA was purified and concentrated within 6 μL nuclease-free water using Zymo RNA Clean and Concentrator kit (Irvine, CA, United States). Ligation-based small RNA libraries were prepared with an RNA input of 6 μL using NEB Next Multiplex Small RNA Library Prep Set for Illumina (Ipswich, MA, United States). Libraries were sequenced using the Illumina NextSeq 550 Mid-Output sequencing run. About 7,680 Mb of sequence data was generated.

To analyze the seq data, adaptor sequences were first removed using Cutadpat and reads with a length of more than 15 bp were extracted. We further filtered out RNAs with counts of less than 10 and all rRNA sequences, using the remainders as cleaned input reads. In terms of the mapping databases, we prepared tRF5 and tRF3 databases using the same sequences derived from different tRNAs [sequences downloaded from tRNA genes using the Table Browser of the UCSC genome browser (Karolchik et al., 2004)]. We also prepared tRF1 sequences using genome locations of tRNAs. Our in-house small RNA database includes 1) these tRFs, 2) miR/snoR sequences downloaded from the UCSC genome browser, and 3) piRNA sequences downloaded from piRBase (http://www.regulatoryrna.org/database/piRNA/). The cleaned input reads were mapped to our inhouse small RNA database using bowtie2 (v2.4.1) allowing two mismatches (option N -1). After we mapped the cleaned input reads to the small RNA database, the unmapped sequences were then mapped to the hg38 genome using the bowtie2 pre-built index (GRCh38_noalt_as) to detect all human sequences. The unmapped sequences to the human genome were then mapped to the SARS-CoV-2 reference genome (NC_045512) using the same parameters.

Raw read counts were normalized with the DEseq2 median of ratios method. Differentially expressed genes were determined by p-value < 0.05, fold change >2, and mean of normalized counts >10 in either Control (CN) or SARS-CoV-2 group. Unsupervised hierarchical clustering was performed using the Pearson correlation coefficient. A flowchart of the sequencing data analyses is summarized in **Supplementary Figure S1B**.

Cell Culture and Viruses

African green monkey kidney epithelial cells (Vero E6) were obtained from ATCC (Manassas, VA, United States) and maintained in a high-glucose DMEM (Gibco, MA, United States) supplemented with 10% fetal bovine serum (FBS), 10 units/ml penicillin, and 10 μg/ml streptomycin. The human alveolar type II-like epithelial cells expressing human angiotensin-converting enzyme 2 (A549-ACE2) cells were a kind gift from Dr. Shinji Makino and were cultured in DMEM (Gibco,

TABLE 1 | Sequence information for tRF5s, RNA linker, RT primer, qPCR primers and PCR primers.

tRFs		Sequence (5'-3')
tRF5-GlyGCC	tRFs	GCAUUGGUGGUUCAGUGGUAGAAUUCUCGCC
	Forward primer	GCATGGGTGGTTCAGTG
	Reverse primer	CGTCGGACTGTAGAACTCTCAAAGC
tRF5-GluCTC	tRFs	UCCCUGGUGGUCUAGUGGUUAGGAUUCGGCGCU
	Forward primer	TCCCTGGTGGTCTAGTG
	Reverse primer	CGTCGGACTGTAGAACTCTCAAAGC
tRF5-LysCTT	tRFs	GCCCGGCUAGCUCAGUCGGUAGAGCAUGAGACU
	Forward primer	GCCCGGCTAGCTCAGTCGGTAG
	Reverse primer	CGTCGGACTGTAGAACTCTCAAAGC
tRF5-ValCAC	tRFs	GUUUCCGUAGUGUAGUGGUUAUCACGUUCGCU
	Forward primer	GTTTCCGTAGTGTAGTGGTTATC
	Reverse primer	CGTCGGACTGTAGAACTCTCAAAGC
tRF5-CysGCA	tRFs	GGGUAUAGCUCAGUGGUAGAGCAUUUGACUGC
	Forward primer	AGTGGTAGAGCATTTGACTGC
	Reverse primer	CGTCGGACTGTAGAACTCTCAAAGC
tRF5-GlnCTG	tRFs	UGGUGUAAUAGGUAGCACAGAGAAUUCUGG
	Forward primer	GGTGTAATAGGTAGCACAGAG
	Reverse primer	CGTCGGACTGTAGAACTCTCAAAGC
5sRNA	Forward primer	GGGAATACCGGGTGCTGTAGG
	Reverse primer	CGTCGGACTGTAGAACTCTCAAAGC
U6	Forward primer	GATGACACGCAAATTCGTGAAGCG
	Reverse primer	CGTCGGACTGTAGAACTCTCAAAGC
3'RNA linker		/5Phos/GAACACUGCGUUUGCUGGCUUUGAGAGUUCUACAGUCCGACGAUC/3ddC/
RT primer		CGTCGGACTGTAGAACTCTCAAAGC
CoV2-346	CoV2-346	CGUACGUGGCUUUGGAGACUCCGUGGAGGAGGUCUU
	RT primer	CGTCGGACTGTAGAACTCTCAAAGC
	Forward primer	ACGACGTACGTGGCTTTG
	Reverse primer	GCAAACGCAGTGTTCAAGA

MA, United States) containing 10% FBS, 10 units/ml penicillin, and 10 μg/ml streptomycin.

Small airway epithelial cells (SAECs), isolated from the normal distal portion of the lung in the 1 mm bronchiole area, were purchased from Lonza (Basel, Switzerland) to generate cells in the air-liquid interface (ALI) culture. The cells were cultured and differentiated using Complete PneumaCult™-Ex plus medium and PneumaCult™-ALI-S Maintenance medium (Stemcell Technologies, Vancouver, Canada), respectively, according to the manufacturer's instructions.

Briefly, the cells at passage two (P2) were expanded in the T-25 flask using the complete PneumaCultTM-Ex plus medium, with a medium change every other day. For ALI cultures, the cells (P3) were seeded into Corning Costar 12 mm transwell inserts (Corning, NY, United States) at a concentration of 11×10^4 cells/insert in 0.5 ml medium/insert, and another 1 ml/well medium was added to the basal chamber. Cells were submerged cultured in Complete PneumaCultTM-Ex plus medium, with a medium change every other day. After reaching ~100% confluency, ALI was initiated by removing the apical medium and replacing the PneumaCultTM-Ex plus medium in the basal compartment with PneumaCult™-ALI-S Maintenance medium. The basal compartment medium was changed every other day. It took about 21 days to complete cell differentiation.

SARS-CoV-2 (USA-WA1/2020 strain) was obtained from the World Reference Center for Emerging Viruses and Arboviruses (WRCEVA) at the UTMB. Viral stocks were prepared by propagation in Vero E6 cells. Viral titers were determined by plaque assay as described (Blanco-Melo et al., 2020). All experiments using live SARS-CoV-2 were performed in a biosafety level 3 (BSL-3) laboratory with redundant fans in the biosafety cabinets. All personnel wore powered air-purifying respirators (Breathe Easy, 3M) with Tyvek suits, aprons, booties, and double gloves. All cell cultures, cell lines or primary cultured cells, and viruses have been approved for use by the Institutional Biosafety Committee of UTMB (NOU# 2018056 and NOU# 2020043).

Viral Infection

To infect A549-ACE2 cells in monolayer culture, the cells were seeded into the 24-well plate 24 h prior to the infection to allow the cells to reach 80–90% confluence in the following day. For infection, the cells were incubated with viruses in DMEM media with 10% FBS at a multiplicity of infection of 0.1 (MOI = 0.1). After 1 h incubation, cells were washed with PBS three times to remove the remaining viruses and cultured in fresh media containing 10% FBS. The cells were collected on day 4 post-infection.

Regarding the infection of SAECs in ALI culture, the infection was performed when hallmarks of excellent differentiation were evident, such as extensive apical coverage with cilia. Prior to infection, the apical side of the cells was washed five times with PBS, and the basal surface was washed once with PBS. Viruses were diluted to the specified MOI in 200 μL MEM medium and inoculated onto the apical surface of the ALI cultures. After a 2-h

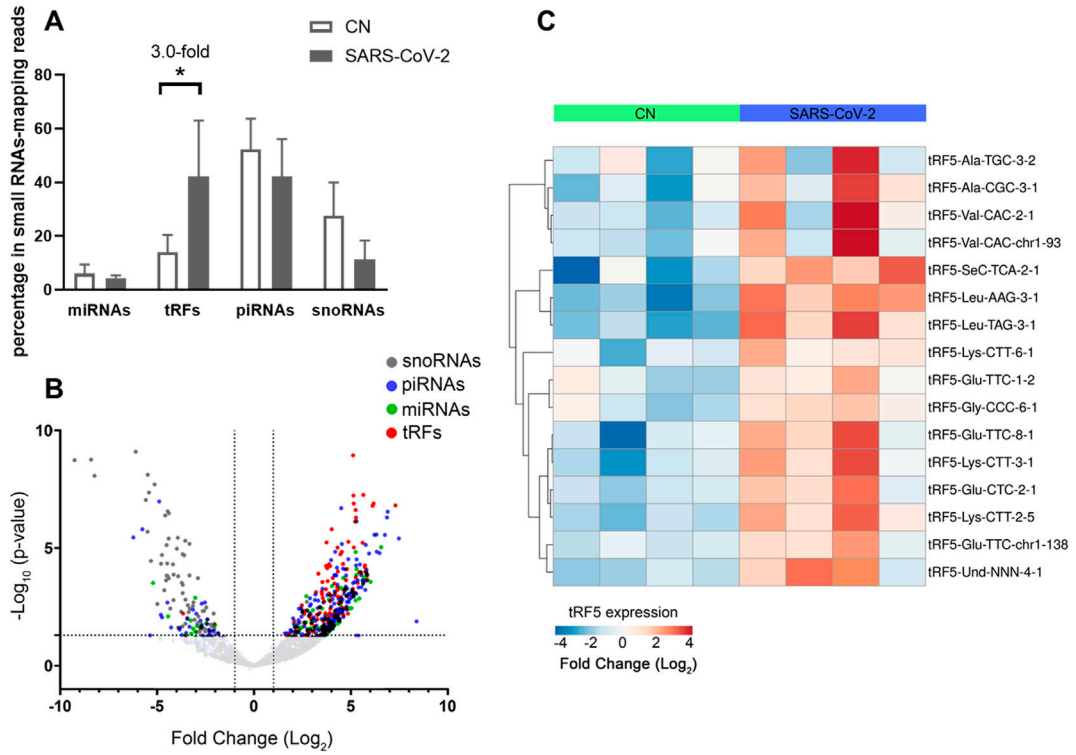

FIGURE 2 | Impacted sncRNAs by SARS-CoV-2 infection in patients. **(A)** The relative sequencing frequency of miRNAs, tRFs, piRNAs, and snoRNAs was calculated by normalizing their raw reads with the DEseq2 median ratio method. **(B)** The volcano plot showed that sncRNAs were differentially expressed between and control group (CN) and SARS-CoV-2 patient group (SARS-COV-2). **(C)** Heatmap for unsupervised clustering of the differently expressed tRFs with >20 mean of normalized counts in any groups according to Pearson correlation. Data are shown as means ± standard error (SE). The single asterisk represents *p* values of <0.05.

incubation at 37°C with 5% CO_2, unbound viruses were removed by washing the surface with PBS three times. The cells were collected on day 1 or 3 post-infection. The SARS-CoV-2 S gene was detected using qRT-PCR with primers as follows: S forward primer, 5′ CCTACTAAATTAAATGATCTCTGCTTTACT; reverse primer, 5′′ CAAGCTATAACGCAGCCTGTA.

qRT-PCR and RT-PCR

To evaluate sncRNAs expression, qRT-PCR was performed, as described previously (Choi et al., 2020; Wu et al., 2021). A schematic summary of tRF quantification by qRT-PCR is shown in the left panel of **Figure 1A**. Briefly, the total RNA was treated with T4 PNK, and then ligated to a 3′-RNA linker using T4 RNA ligase from Thermo Fisher Scientific (Waltham, MA, United States). The product was used as a template for reverse transcription (RT) with a linker-specific reverse primer using TaqMan Reverse Transcription Reagents from Thermo Fisher Scientific. The cDNA was subjected to SYBR Green qPCR using iTaq™ Universal SYBR Green Supermix kit from Bio-Rad (Hercules, CA, United States) and primers specific to the 5′-end of tRFs and RNA linker. U6 was used for normalization. The addition of a 3′-RNA linker enables the detection of tRF5s without the signal interference from its corresponding parent tRNAs, possibly because 1) the 3-end of tRNA is usually attached with an amino acid, preventing RNA linker attachment, and 2) reverse transcription annealing temperature sets tRFs, not tRNAs, to be annealed by the primer, as tRNA cloverleaf structure requires a specific denaturing temperature before annealing (right panel of **Figure 1A**) (Choi et al., 2020; Wu et al., 2021). The primers and 3′-RNA linker sequences are listed in **Table 1**.

To validate the seq data of CoV2-encoded small RNAs (CoV2-346), RT-PCR was performed, using RT and PCR primers listed in **Table 1**. The overall experimental design to detect CoV2-346 by RT-PCR is illustrated in **Figure 1B**, with detailed seq information of primers and the RNA linker shown in **Figure 1C**. In brief, RNAs, pretreated with or without T4 PNK, were ligated to a 3′-RNA linker. The RT was done using primers complementary to the RNA linker, followed by PCR using forward primers annealing to 5′-end of CoV2-346 and reverse primers annealing to the last 4 nt of CoV2-346 and the first 15 nt of RNA linker.

Northern Blot

Northern hybridization for tRF5-GluCTC was performed as described (Wang et al., 2013). Briefly, 3 μg RNA was loaded on 15% denaturing polyacrylamide gel with 7 M ureas and then transferred to a positively charged nylon membrane (Amersham Biosciences, NJ, United States). The membrane was hybridized with a ^{32}P-labeled DNA probe in ULTRAhyb-Oligo solution (Life Technologies, Grand Island, NY, United States), followed by

TABLE 2 | Changes in tRFs by SARS-CoV-2.

	Mean		Log2FC	Fold Change (FC)	*p*-value	Padj
	CN	COVID-19				
Down-regulated						
tRF1_chr5_24_Lys_CTT_26198538	19.94	1.62	−3.65	12.54	0.00607	0.02862
Up-regulated						
tRF5-Val-TAC-1-2	1.43	32.82	4.31	19.79	0.00047	0.00439
tRF5-Val-CAC-chr1-93	65.75	869.52	3.72	13.20	0.00056	0.00498
tRF5-Val-CAC-3-1	3.38	27.07	2.86	7.26	0.00781	0.03457
tRF5-Val-CAC-2-1	6.11	120.86	4.34	20.25	0.00010	0.00151
tRF5-Und-NNN-4-1	9.13	128.84	3.79	13.85	0.00007	0.00117
tRF5-Thr-CGT-6-1	5.28	95.45	4.08	16.86	0.00019	0.00220
tRF5-Ser-CGA-2-1	0.92	10.74	4.81	28.14	0.00112	0.00798
tRF5-SeC-TCA-2-1	41.06	609.64	3.94	15.34	0.00006	0.00099
tRF5-nmt-Gln-TTG-6-1	0.39	21.22	5.23	37.52	0.00079	0.00632
tRF5-Lys-CTT-chr15-5	0.45	14.56	4.60	24.24	0.00389	0.02083
tRF5-Lys-CTT-6-1	27.07	118.09	2.09	4.27	0.01283	0.04915
tRF5-Lys-CTT-3-1	13.01	199.40	3.89	14.80	0.00005	0.00089
tRF5-Lys-CTT-2-5	40.64	667.89	4.03	16.29	0.00000	0.00006
tRF5-Leu-TAG-3-1	2.23	73.96	5.23	37.54	0.00000	0.00003
tRF5-Leu-CAG-2-1	2.55	32.99	3.57	11.84	0.00132	0.00913
tRF5-Leu-AAG-3-1	7.52	247.62	5.12	34.87	0.00000	0.00000
tRF5-iMet-CAT-1-8	3.33	109.22	4.89	29.56	0.00001	0.00017
tRF5-His-GTG-2-1	3.93	34.02	3.00	8.03	0.01555	0.05736
tRF5-Gly-CCC-6-1	4.71	20.69	2.14	4.39	0.02402	0.07725
tRF5-Glu-TTC-chr1-138	82.66	458.76	2.48	5.59	0.00270	0.01595
tRF5-Glu-TTC-8-1	140.13	1637.50	3.54	11.63	0.00028	0.00287
tRF5-Glu-TTC-1-2	13.42	47.61	1.85	3.60	0.04498	0.12120
tRF5-Glu-CTC-3-1	1.18	12.02	4.17	18.05	0.00619	0.02892
tRF5-Glu-CTC-2-1	8234.45	83040.94	3.33	10.08	0.00012	0.00173
tRF5-Ala-TGC-3-2	3.89	27.72	2.98	7.89	0.01629	0.05924
tRF5-Ala-CGC-3-1	2.93	29.71	3.41	10.60	0.00335	0.01915
tRF5-Ala-CGC-2-1	1.59	27.28	3.95	15.42	0.00182	0.01173
tRF5-Ala-AGC-4-1	2.44	27.91	3.41	10.62	0.00566	0.02723
tRF3-Val-TAC-3-1	1.08	49.08	5.17	35.90	0.00001	0.00024
tRF3-Val-TAC-1-2	3.11	79.25	4.47	22.16	0.00002	0.00040
tRF3-Val-CAC-chr1-93	0.72	47.24	5.62	49.09	0.00001	0.00018
tRF3-Val-AAC-4-1	1.25	43.10	4.81	28.06	0.00008	0.00122
tRF3-Trp-CCA-5-1	0.16	16.24	5.45	43.78	0.00011	0.00156
tRF3-Trp-CCA-4-1	2.46	112.29	5.26	38.29	0.00000	0.00001
tRF3-Thr-TGT-5-1	7.34	36.03	2.62	6.14	0.01642	0.05924
tRF3-Thr-CGT-4-1	1.83	14.12	2.86	7.24	0.03537	0.09972
tRF3-Thr-CGT-3-1	0.59	10.11	3.69	12.94	0.00596	0.02835
tRF3-Thr-CGT-1-1	0.00	12.25	5.76	54.09	0.00010	0.00151
tRF3-Thr-AGT-5-1	0.49	12.34	4.34	20.24	0.00116	0.00823
tRF3-Thr-AGT-4-1	0.16	12.77	5.11	34.64	0.00054	0.00485
tRF3-Thr-AGT-3-1	0.33	12.24	4.50	22.66	0.00120	0.00843
tRF3-SeC-TCA-2-1	2.95	128.28	5.28	38.72	0.00000	0.00002
tRF3-Pro-TGG-3-5	38.00	215.39	2.53	5.77	0.00515	0.02533
tRF3-Phe-GAA-10-1	4.75	119.56	4.54	23.34	0.00001	0.00033
tRF3-nm-Tyr-GTA-chr21-2	2.28	12.21	2.29	4.90	0.03717	0.10322
tRF3-nmt-Gln-TTG-9-1	7.30	276.42	5.16	35.76	0.00000	0.00001
tRF3-nmt-Gln-TTG-7-1	7.17	278.12	5.15	35.42	0.00000	0.00001
tRF3-Lys-TTT-14-1	4.97	73.70	3.84	14.29	0.00686	0.03108
tRF3-Lys-CTT-9-1	0.00	10.54	5.54	46.55	0.00011	0.00163
tRF3-Leu-TAG-3-1	6.59	143.71	4.32	20.02	0.00001	0.00024
tRF3-Leu-TAG-2-1	15.06	196.02	3.74	13.35	0.00006	0.00099
tRF3-Leu-TAG-1-1	3.46	72.59	4.61	24.39	0.00005	0.00089
tRF3-Leu-CAG-chr9-7	6.77	50.14	2.95	7.74	0.01033	0.04250
tRF3-Leu-CAG-1-6	7.52	51.42	2.93	7.64	0.00670	0.03063
tRF3-Leu-AAG-7-1	2.89	45.39	3.81	14.06	0.00025	0.00271
tRF3-Leu-AAG-2-4	14.00	184.25	3.75	13.46	0.00001	0.00017
tRF3-iMet-CAT-1-6	0.52	15.97	4.67	25.41	0.00067	0.00567
tRF3-Gly-TCC-2-5	1.86	201.79	6.53	92.33	0.00000	0.00000
tRF3-Gly-CCC-7-1	14.44	134.89	3.22	9.29	0.00075	0.00611
tRF3-Gln-TTG-3-3	1.08	12.93	3.26	9.57	0.00691	0.03113

(Continued on following page)

TABLE 2 | (*Continued*) Changes in tRFs by SARS-CoV-2.

	Mean		Log2FC	Fold Change (FC)	*p*-value	Padj
	CN	COVID-19				
tRF3-Gln-CTG-5-1	0.82	12.55	3.63	12.37	0.00186	0.01193
tRF3-Gln-CTG-1-5	0.23	19.81	5.73	53.01	0.00007	0.00108
tRF3-Cys-GCA-9-4	0.33	14.30	4.70	26.06	0.00061	0.00525
tRF3-Cys-GCA-5-1	0.82	15.93	3.98	15.77	0.00106	0.00777
tRF3-Cys-GCA-4-1	0.69	16.86	4.33	20.09	0.00059	0.00514
tRF3-Cys-GCA-24-1	0.71	15.60	4.20	18.42	0.00082	0.00645
tRF3-Cys-GCA-23-1	0.62	21.73	4.77	27.20	0.00023	0.00257
tRF3-Cys-GCA-21-1	0.16	19.72	5.74	53.58	0.00006	0.00095
tRF3-Cys-GCA-17-1	1.10	19.03	3.89	14.79	0.00084	0.00657
tRF3-Cys-GCA-10-1	0.26	14.50	5.26	38.21	0.00018	0.00211
tRF3-Arg-TCT-1-1	2.49	118.78	5.66	50.51	0.00000	0.00001
tRF3-Arg-CCT-5-1	1.58	12.23	2.77	6.84	0.03258	0.09412
tRF3-Arg-CCT-4-1	2.60	13.48	2.19	4.57	0.03323	0.09521
tRF3-Arg-CCG-2-1	4.96	61.43	3.51	11.36	0.00072	0.00595
tRF3-Ala-TGC-4-1	1.46	30.32	4.16	17.91	0.00033	0.00320
tRF3-Ala-TGC-3-1	3.57	44.92	3.53	11.52	0.00091	0.00693
tRF3-Ala-TGC-2-1	0.91	75.23	6.13	70.14	0.00000	0.00001
tRF3-Ala-TGC-1-1	0.16	58.71	7.31	159.08	0.00000	0.00001
tRF3-Ala-CGC-4-1	14.18	93.77	2.66	6.30	0.00456	0.02318
tRF3-Ala-AGC-4-1	0.98	80.87	6.19	72.78	0.00000	0.00001
tRF3-Ala-AGC-2-2	14.67	92.70	2.60	6.07	0.00638	0.02969
tRF1_chr2_6_Glu_TTC_75124115	0.00	13.35	5.86	58.15	0.00022	0.00249

membrane washing and image development. The ^{32}P-labeled DNA probe for tRF5-GluCTC was 5′-CGCCGAATCCTAACC ACTAGACCACCA-3′.

Statistical Analysis

The experimental results were analyzed using Graphpad Prism 5 software. To compare the sncRNAs expression of NPS between SARS-CoV-2 negative and positive groups, an unpaired two-tailed Mann-Whitney *U* test was used. To compare the sncRNAs expression in SARS-CoV-2 infected cells and mock-infected cells, an unpaired two-tailed *t*-test was employed. A p-value < 0.05 was considered to indicate a statistically significant difference. Single and two asterisks represent a p-value of <0.05 and <0.01, respectively. Means ± standard errors (SE) are shown.

RESULTS

T4 PNK-RNA-seq Revealed SARS-CoV-2-Impacted sncRNAs in NPS Samples.

To identify SARS-CoV-2-impacted sncRNAs, we initialized T4 PNK-RNA-seq for the NPS samples from four SARS-CoV-2 positive patients with their ages at 54.3 ± 4.0 years old and four SARS-CoV-2 negative subjects, with matched age at 50.5 ± 10.2 years old. The seq data were analyzed similarly as described in (Wang et al., 2013; Liu et al., 2018). In brief, the sequences with length >15 bp and reads >10 were mapped to the in-house small RNA database containing tRFs, miR/snoRs, and piRs to address redundant tRNA sequences across the genome after removing rRNAs. Unmapped sequences were then mapped to the hg38 human genome to identify other human-derived sequences and their composition. We found that piRNAs and tRFs were the two most abundant sncRNAs in SARS-CoV-2 positive samples. The top-10 ranked piRNAs and tRFs in the SARS-CoV-2 positive group are listed in **Supplementary Tables S1, S2**, respectively. As shown in **Supplementary Table S2**, all tRFs were derived from the 5′-ends of tRNAs, therefore tRF5s. Compared with the tRFs and piRNAs, the overall reads of miRNAs were much less (**Figure 2A**). We also compared the sncRNA profiles between SARS-CoV-2 positive and negative samples. As shown in **Figure 2A**, while the tRFs consisted of about 14% of all sncRNA counts in the control group, tRFs counts became 42% in the COVID-19 group, demonstrating a significant increase by COVID-19. In contrast, the overall expression of miRNAs and piRNAs was not impacted by COVID-19 (**Figure 2A**).

Differential expression analysis for individual sncRNAs was also performed for SARS-CoV-2 negative and positive groups. As shown in **Figure 2B**, there were more up-regulated tRFs than down-regulated tRFs, while SARS-CoV-2 down-regulated snoRNAs were more than up-regulated ones. We also listed sncRNAs, which were significantly altered by SARS-CoV-2 in **Tables 2–4**. The cutoff was set as a fold change >2, with the significance of $p < 0.05$ in changes by SARS-CoV-2, and the mean of normalized counts >10 in the negative or positive group. The differentially expressed tRFs, miRNAs, and snoRNAs were listed in **Tables 2–4**, respectively.

As shown in **Table 2**, tRFs were significantly impacted by SARS-CoV-2 in NPS. Among those, 2 tRFs belong to the tRF1 series, 28 tRFs were tRF5s, and 53 tRFs were tRF3s. However, top-ranked SARS-CoV-2-impacted tRFs all belong to the tRF5. In **Figure 2C**, the mean of normalized counts >20 in the control (CN) or SARS-CoV-2 positive (SARS-CoV-2) group were

TABLE 3 | Changes in miRNAs by SARS-CoV-2.

	Mean		Log2FC	Fold Change (FC)	*p*-value	Padj
	CN	COVID-19				
Up-regulated						
hsa-miR-4443	1.99	497.56	8.16	286.11	3.6E-11	1.5E-08
hsa-miR-12116	0.23	36.13	6.57	95.26	9.1E-06	0.00024
hsa-miR-765	0.00	14.76	6.02	65.02	0.00027	0.00282
hsa-miR-1224-3p	0.00	13.04	5.84	57.20	0.00014	0.00181
hsa-miR-6880-3p	0.00	12.98	5.83	56.87	0.00012	0.00165
hsa-miR-6886-3p	0.00	11.95	5.71	52.37	0.00017	0.00202
hsa-miR-6758-5p	0.16	19.09	5.68	51.37	0.00019	0.0022
hsa-miR-4716-5p	0.00	11.28	5.64	49.85	0.00032	0.00317
hsa-miR-1281	0.00	10.01	5.45	43.62	0.00137	0.0093
hsa-miR-6741-3p	0.45	23.94	5.31	39.69	7.7E-05	0.00122
hsa-miR-769-5p	0.26	14.85	5.31	39.64	0.00013	0.00181
hsa-miR-877-3p	1.17	54.42	5.26	38.26	1.5E-05	0.00033
hsa-miR-1469	0.16	13.97	5.26	38.23	0.00164	0.01068
hsa-miR-10401-5p	1.58	59.29	5.07	33.70	0.00067	0.00567
hsa-miR-7111-3p	0.23	12.72	5.07	33.59	0.00073	0.00597
hsa-miR-4646-3p	0.23	10.42	4.78	27.49	0.00106	0.00777
hsa-miR-204-3p	0.66	24.52	4.73	26.59	0.0005	0.00463
hsa-miR-7107-5p	2.14	59.30	4.62	24.67	0.00018	0.00215
hsa-miR-6510-5p	0.49	17.34	4.55	23.44	0.00052	0.00473
hsa-miR-6823-3p	0.85	23.17	4.48	22.27	0.00048	0.00441
hsa-miR-3196	8.17	141.16	4.04	16.41	0.0004	0.00389
hsa-miR-665	0.78	14.73	3.89	14.79	0.00153	0.0102
hsa-miR-7847-3p	2.36	30.55	3.53	11.52	0.00358	0.01993
hsa-miR-1268b	3.52	32.94	3.05	8.30	0.00432	0.02222
hsa-miR-139-3p	1.28	12.34	3.00	7.98	0.01266	0.04865
hsa-miR-4728-5p	1.10	10.31	2.98	7.89	0.01414	0.05307
hsa-miR-320c	8.22	62.47	2.85	7.20	0.00743	0.03314
hsa-miR-92b-5p	87.47	600.46	2.77	6.80	0.00429	0.02216
hsa-miR-320b	13.69	93.88	2.71	6.56	0.00109	0.00783
hsa-miR-140-3p	1.48	11.69	2.70	6.49	0.01402	0.05278
hsa-miR-186-5p	6.64	39.95	2.46	5.50	0.02296	0.07477
hsa-miR-378a-3p	9.29	50.19	2.34	5.07	0.02429	0.07761
hsa-miR-1268a	5.61	27.61	2.15	4.43	0.02005	0.06879
hsa-miR-762	5.81	27.57	2.13	4.38	0.03574	0.09995
hsa-miR-2110	8.28	38.68	2.12	4.35	0.02247	0.07433
Down-regulated						
hsa-miR-34b-3p	43.92	1.10	−5.20	36.68	0.0003	0.00306
hsa-miR-328-3p	26.78	3.38	−2.93	7.60	0.02036	0.06968
hsa-miR-6510-3p	15.86	1.64	−3.25	9.54	0.01166	0.04608
hsa-miR-26a-5p	143.78	25.93	−2.45	5.48	0.01568	0.05743
hsa-miR-99a-5p	657.50	163.26	−2.01	4.03	0.01872	0.06548
hsa-miR-92b-3p	346.22	42.48	−3.02	8.12	0.00127	0.0089

selected to plot the heatmap and their sequences were listed in **Table 5**.

Experimental Validation of SARS-CoV-2-Impacted tRFs

To validate the seq data, we used modified qRT-PCR to detect the expression of tRF5-GluCTC, tRF5-LysCTT, and tRF5-ValCAC, three top-ranked tRF5s in SARS-CoV-2-positive patients according to the seq data, as we previously described (Choi et al., 2020; Wu et al., 2021). Compared with Northern blot validation, the modified qRT-PCR with T4 PNK pretreatment and 3′-end RNA linker ligation provides the possibility to validate as many tRFs as possible for NPS samples, which usually have a limited yield of RNAs. Our results demonstrated that tRF5-GluCTC, tRF5-LysCTT, and tRF5-ValCA were significantly increased in the SARS-CoV-2 group (**Figures 3A–C**). Unlike SARS-CoV-2, which could induce tRF5-ValCAC, respiratory syncytial virus (RSV), a negative-sense RNA virus, does not induce tRF5-ValCAC infected cells (Wang et al., 2013), suggesting the change in tRF profile in response to viral infections is virus-specific.

Other than the three tRF5s mentioned above, tRF5-CysGCA, tRF5-GlnCTG and tRF5-GlyGCC were also chosen for the validation, as these three tRFs are highly inducible by RSV with the function tRF5-GlyGCC and tRF5-GlnCTG being vital in promoting RSV replication (Choi et al., 2020; Zhou et al., 2017). Although the function of tRF5-CysGCA in RSV is not clear in viral infection, it is important in regulating stress responses and neuroprotection (Ivanov et al., 2014). We validated that tRF5-

TABLE 4 | Changes in snoRNAs by SARS-CoV-2.

	Mean		Log2FC	Fold Change (FC)	*p*-value	Padj
	CN	COVID-19				
Down-regulated						
hg38_wgRna_ACA49	227.26	0.27	–9.25	609.86	1.9E-09	3.4E-07
hg38_wgRna_ACA40	180.98	0.53	–8.40	338.05	1.7E-09	3.4E-07
hg38_wgRna_ACA28	219.23	0.72	–8.22	299.21	8.6E-09	1.1E-06
hg38_wgRna_ACA8	409.75	8.53	–5.57	47.58	9.1E-08	7.7E-06
hg38_wgRna_U92	79.97	1.72	–5.49	44.82	2.1E-06	8E-05
hg38_wgRna_E3	162.73	3.73	–5.41	42.66	4.4E-08	4.7E-06
hg38_wgRna_ACA25	38.67	0.92	–5.31	39.75	3.6E-05	0.00069
hg38_wgRna_ACA16	158.54	4.34	–5.13	34.92	2E-08	2.3E-06
hg38_wgRna_ACA3	206.55	7.70	–4.74	26.71	2E-05	0.00042
hg38_wgRna_U73a	25.28	1.01	–4.62	24.63	0.00062	0.00531
hg38_wgRna_U35A	99.03	4.05	–4.58	23.87	4.2E-07	2.1E-05
hg38_wgRna_ACA38	35.59	1.45	–4.53	23.09	0.00024	0.00258
hg38_wgRna_mgU6-77	93.30	4.01	–4.50	22.65	7.6E-06	0.0002
hg38_wgRna_HBII-82B	36.20	1.76	–4.50	22.57	0.00015	0.00187
hg38_wgRna_E2	88.91	4.05	–4.48	22.26	4.5E-05	0.00087
hg38_wgRna_ACA63	122.12	5.51	–4.45	21.84	0.00016	0.00192
hg38_wgRna_HBII-180A	157.02	7.50	–4.39	21.04	4E-06	0.00013
hg38_wgRna_U71a	38.72	1.83	–4.39	20.95	0.00019	0.00221
hg38_wgRna_ACA41	21.63	1.00	–4.31	19.86	0.00372	0.02024
hg38_wgRna_U90	86.50	4.66	–4.18	18.07	5E-05	0.00089
hg38_wgRna_ACA10	38.56	2.01	–4.15	17.73	0.00162	0.0106
hg38_wgRna_U97	89.21	4.93	–4.14	17.68	0.00013	0.00181
hg38_wgRna_ACA44	114.67	7.12	–3.97	15.72	1.1E-05	0.00027
hg38_wgRna_ACA9	13.58	1.00	–3.75	13.48	0.00509	0.02516
hg38_wgRna_ACA51	85.91	6.42	–3.72	13.16	0.0003	0.00306
hg38_wgRna_ACA3-2	124.34	9.63	–3.68	12.78	0.00082	0.00645
hg38_wgRna_U15A	87.31	6.73	–3.67	12.73	0.00036	0.00352
hg38_wgRna_U15B	37.76	3.37	–3.53	11.57	0.00156	0.01027
hg38_wgRna_ACA1	28.02	2.69	–3.43	10.81	0.00929	0.0395
hg38_wgRna_ACA53	62.15	5.85	–3.41	10.60	0.0027	0.01595
hg38_wgRna_SNORD123	21.14	2.10	–3.36	10.30	0.00525	0.02556
hg38_wgRna_U17b	86.15	8.67	–3.32	10.02	0.00015	0.00184
hg38_wgRna_ACA6	31.12	3.13	–3.31	9.89	0.00373	0.02024
hg38_wgRna_U34	33.68	3.92	–3.15	8.87	0.00286	0.01669
hg38_wgRna_U18B	16.65	1.90	–3.07	8.38	0.01113	0.04479
hg38_wgRna_SNORA38B	13.91	1.82	–2.91	7.49	0.01566	0.05743
hg38_wgRna_U32A	70.17	9.50	–2.86	7.27	0.00813	0.03551
hg38_wgRna_U52	41.92	6.17	–2.79	6.92	0.03576	0.09995
hg38_wgRna_U51	26.73	4.02	–2.75	6.73	0.02161	0.07241
hg38_wgRna_U17a	28.75	4.49	–2.64	6.21	0.00479	0.02396
hg38_wgRna_HBII-85-18	38.90	6.61	–2.53	5.76	0.02759	0.08448
hg38_wgRna_U19-2	18.33	4.68	–2.00	4.00	0.04758	0.12608

CysGCA and tRF5-GlnCTG were also significantly enhanced in the SARS-CoV-2 group, compared with the control (CN) group (**Figures 3D,E**). However, SARS-CoV-2 did not affect tRF5-GlyGCC expression (**Figure 3F**). Given the fact that RSV induces significantly tRF5-GlyGCC (Wang et al., 2013), the result of **Figure 3F** supported virus-specific induction of tRFs and tRFs as potential biomarkers of viral infection.

Impacted tRFs in SARS-CoV-2-Infected Cells

A549-ACE2 is a common cell model to study coronaviruses, such as SARS-CoV and SARS-CoV-2 (Mossel et al., 2005; Blanco-Melo et al., 2020; Weston et al., 2020; Buchrieser et al., 2021). Herein, we studied whether the induction of tRFs can be recapitulated in SARS-CoV-2-infected A549-ACE2. As shown in **Figures 4A–E**, A549-ACE2 cells, at day 4 post-infection (p.i.) of SARS-CoV-2, had dramatically induction of tRF5-GluCTC, tRF5-LysCTT, tRF5-ValCAC, tRF5-CysGCA, and tRF5-GlnCTG. The northern blot also confirmed the induction of tRF5-GluCTC (**Figure 4F**), which was the most abundant tRF5 among the tested four tRF5s, confirming the liability of our newly developed qRT-PCR.

We also used primary SAECs in ALI culture, a commonly acknowledged physiology airway infection model (Bhowmick and Gappa-Fahlenkamp, 2016; Chandorkar et al., 2017), to confirm SARS-CoV-2-affected tRFs. SAECs, after a few weeks of ALI culture, have been shown to establish a pseudostratified cell layer that resembles the small airway epithelium as found *in vivo* (Hiemstra et al., 2018). Moreover, SAECs in ALI cultures

TABLE 5 | tRF5s with mean of normalized counts > 20 in Control (CN) or COVID-19 groups.

	Mean		Log2FC	Fold Change (FC)	*p*-value	Padj	Sequence	Length (nt)
	CN	COVID-19						
Up-regulated								
tRF5-Ala-TGC-3-2	3.89	27.72	2.98	7.89	0.01629	0.05924	GGGGAUGUAGCUCAGUGGC	19
tRF5-Ala-CGC-3-1	2.93	29.71	3.41	10.60	0.00335	0.01915	GGGGAUGUAGCUCAGUGG	18
tRF5-Val-CAC-2-1	6.11	120.86	4.34	20.25	0.00010	0.00151	GCUUCUGUAGUGUAGUGGUUAUCACGUUCG CCUC	34
tRF5-Val-CAC-chr1-93	65.75	869.52	3.72	13.20	0.00056	0.00498	GUUUCCGUAGUGUAGUGGUUAUCACGU UCGCC	32
tRF5-SeC-TCA-2-1	41.06	609.64	3.94	15.34	0.00006	0.00099	AGUGGUCUGGGGUGC	15
tRF5-Leu-AAG-3-1	7.52	247.62	5.12	34.87	0.00000	0.00000	GGUAGCGUGGCCGAGC	16
tRF5-Leu-TAG-3-1	2.23	73.96	5.23	37.54	0.00000	0.00003	GGUAGCGUGGCCGAGU	16
tRF5-Lys-CTT-6-1	27.07	118.09	2.09	4.27	0.01283	0.04915	AGCUCAGUCGGUAGAGCAUGGGACA	25
tRF5-Glu-TTC-1-2	13.42	47.61	1.85	3.60	0.04498	0.12120	AUGGUCUAGCGGUUAGGAUUCCUGGU	26
tRF5-Gly-CCC-6-1	4.71	20.69	2.14	4.39	0.02402	0.07725	AGUGGUAGAAUUCUCGCC	18
tRF5-Glu-TTC-8-1	140.13	1637.50	3.54	11.63	0.00028	0.00287	UCCCCUGUGGUCUAGUGGUUAGGAUUC GGCGCU	33
tRF5-Lys-CTT-3-1	13.01	199.40	3.89	14.80	0.00005	0.00089	GCCCGGCUAGCUCAGUCGGUAGAGCAU GAGACC	33
tRF5-Glu-CTC-2-1	8234.45	83040.94	3.33	10.08	0.00012	0.00173	UCCCUGGUGGUCUAGUGGUUAGGAUUC GGCGCU	33
tRF5-Lys-CTT-2-5	40.64	667.89	4.03	16.29	0.00000	0.00006	GCCCGGCUAGCUCAGUCGGUAGAGCAU GAGACU	33
tRF5-Glu-TTC-chr1-138	82.66	458.76	2.48	5.59	0.00270	0.01595	UCCCUGGUGGUCUAGUGGCUAGGAUUC GGCGCU	33
tRF5-Und-NNN-4-1	9.13	128.84	3.79	13.85	0.00007	0.00117	UCCCUGUAGUCUAGUGGUUAGGAUUCG GCGCU	32

have been found to express the receptor for SARS-CoV-2, therefore, a physiologically relevant cell model to study SARS-CoV-2 (Zhang et al., 2020; Zhu et al., 2020; Schweitzer et al., 2021). Therefore, we also studied tRF5s expression in SAECs in ALI culture. As shown in **Figures 5A,B**, the cilia were oriented towards the upper transwell compartment, after the cells were in ALI culture for 21 days. The differentiated cultures were infected with SARS-CoV-2 at an MOI of 0.1 for 1 or 3 days, followed by viral S gene quantification using qRT-PCR (**Figure 5C**). Our qRT-PCR confirmed the expression change in tRF5-GlnCTG and tRF5-ValCAC, two tRFs with relatively low abundance in SARS-CoV-2 positive NPS samples and infected A549-ACE2 cells, can also be detected in SAECs in ALI culture (**Figures 5D, E**). Since the cleaved tRNAs account for a very tiny portion of parent tRNAs, the difference in the induction folds of tRF5-GlnCTG and tRF5-ValCAC should not be determined by the abundance of their parent tRNAs, but possibly resulted from the distinct sensitivities of their parent tRNAs to the cleavage during the infection. Overall, in this study, we established two cell models, A549-AEC2 cells in monolayer culture and SAECs in ALI culture, to characterize SARS-CoV-2-induced tRFs in the future.

Identification of SARS-CoV-2-Encoded svRNAs

Viral-derived sncRNAs are also an important family of sncRNAs (Tycowski et al., 2015). To investigate whether SARS-CoV-2-encoded svRNAs are produced in the context of SARS-CoV-2 infection, the seq data were also aligned to the complete genome sequence of SARS-CoV-2 isolate Wuhan-Hu-1 (NC_045512.2). Several SARS-CoV-2-derived svRNAs were identified in SARS-CoV-2 positive samples. The eight most abundant SARS-CoV-2-encoded svRNAs are listed in **Table 6**.

We further analyzed the sequences of svRNAs. Since only RNA <200 bp were selected for the cDNA library, our results should not give svRNAs larger than 200 bp. We found that the length of mapped svRNAs ranged from 17 to 75 nt. Interestingly, svRNAs with the length of 25 nt, 33 nt, and 36 nt were enriched (**Figure 6A**, two representatives are shown). In **Figure 6B**, the locations of the top 8 svRNAs along the SARS-CoV-2 genome are shown.

Experimental Validation of SARS-CoV-2-Encoded svRNAs

Among CoV-2-derived svRNAs (sv-CoV2), a 36 nt sv-CoV2, derived from genomic site 346 to site 382 of nsp1 (sv-CoV2-346) had the highest expression. To further validate the presence of sv-CoV2-346, NPS RNAs from two control samples and two COVID-19 samples were treated with T4 PNK and linked to a 3′ RNA linker, and then the RT-PCR was performed. The RT-PCR was also performed without the T4 PNK treatment and RNA linker addition so that the importance of such treatments can be demonstrated. The overall workflow is illustrated in **Figures 1B,C**. The specific 55 nt RT-PCR products of sv-CoV2-346 were observed in SARS-CoV-2 samples, but not in the control samples, when samples were pretreated with T4 PNK and ligated with an RNA linker (**Figure 7A**). The length reflected the 36 nt

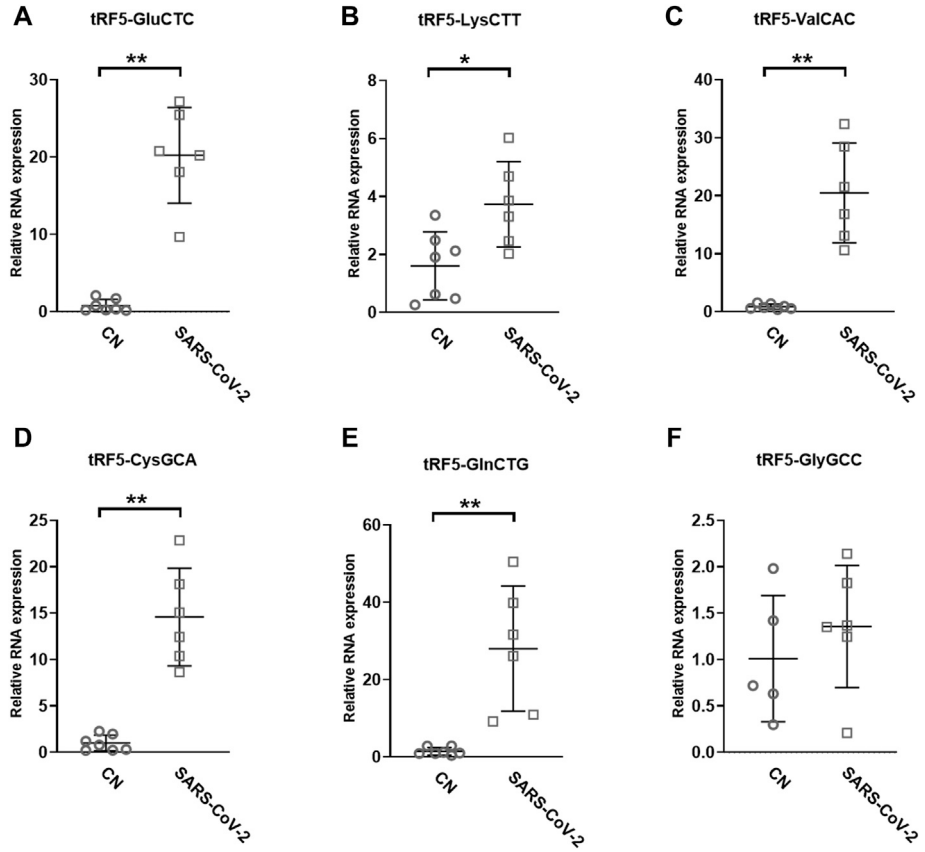

FIGURE 3 | Changes in the expression of tRF5s in NPS samples by SRAS-CoV-2. qRT-PCR was performed to detect tRF5-GluCTC **(A)**, tRF5-LysCTT **(B)**, tRF5-ValCAC **(C)**, tRF5-CysGCA **(D)**, tRF5-GlnCTG **(E)**, and tRF5-GlyGCC **(F)** in the NPS from SARS-COV-2 and control (CN) patients. U6 was used as an internal control. Unpaired two-tailed Mann-Whitney U tests were performed for statistical comparisons. Single and double asterisks represent *p* values of <0.05 and <0.01, respectively. Data are shown as means ± SE.

sv-CoV2-346 along with the 3′ RNA linker. In addition, we found that the RT-PCR product of one SARS-CoV-2 sample was more than another one, which was consistent with their read frequency in Seq-data. The presence of sv-CoV2-346 was confirmed in SARS-CoV-2-infected A549-ACE2 cells using RT-PCR (**Figure 7B**).

Coronavirus-encoded svRNAs have been previously reported to be 18–22 nt long and therefore, share similar lengths with miRNAs (Morales et al., 2017; Cheng et al., 20212021). Coronavirus-encoded svRNAs with lengths longer than 30 nt have not been identified. Herein, we think that the identification of additional SARS-CoV-2-derived svRNAs was benefited from the treatment of T4 PNK and RNA linker ligation at their 3′-end. As shown in **Figure 7C**, both patient or infected cell samples, without such treatments, did not result in the band presence, supporting the lack of 3′-OH end of sv-CoV2-346 and the necessity of specific T4 PNK treatment for sv-CoV2-346 detection.

Herein, we also initialed to characterize sv-CoV2-346 by predicting the secondary RNA structure of svRNAs. Besides sv-CoV2-346, there were two other svRNAs, sv-CoV2-299 and svCoV2-404, near the region where sv-CoV-346 was derived (**Table 7**). sv-CoV2-299, sv-CoV2-346, and sv-CoV2-404 were derived from nucleotide 299 to 328, 346 to 382, and 400 to 443, respectively. Therefore, we took the viral genome spanning from 289 to 485, which covers all these three regions with some nt extension on both ends and predicted its RNA secondary structure using RNAfold web server based on minimum free energy to have a clue of biogenesis mechanisms (Hofacker, 2003) (**Figure 8A**). We found that nucleotides 299, 328, 400, 443, and 382 are all located on loops, implying the cleavage at these five sites along with the single-stranded RNA by ribonuclease (**Figure 8A**). Only nucleotide 346 was in the middle of the stem (**Figure 8A**). Interestingly, we found that 68 nt long svRNAs (sv-CoV2-314) overlapped with sv-CoV2-346 (**Table 7**). We, therefore, took the genome section spanning from 314 to 382 and run the secondary and tertiary structures of sv-CoV2-314 using RNAfold web server and RNAComposer, respectively (Hofacker, 2003; Popenda et al., 2012) (**Figures 8B,C**). This 68 nt fragment contained three hairpin loops and was folded into an L-shaped-like tertiary structure, and nucleotide 346 was located within the bottom loop (**Figures 8B,C**). The secondary and tertiary structures of sv-CoV2-314 were similar to tRNA, and nucleotide 346 location was similar to

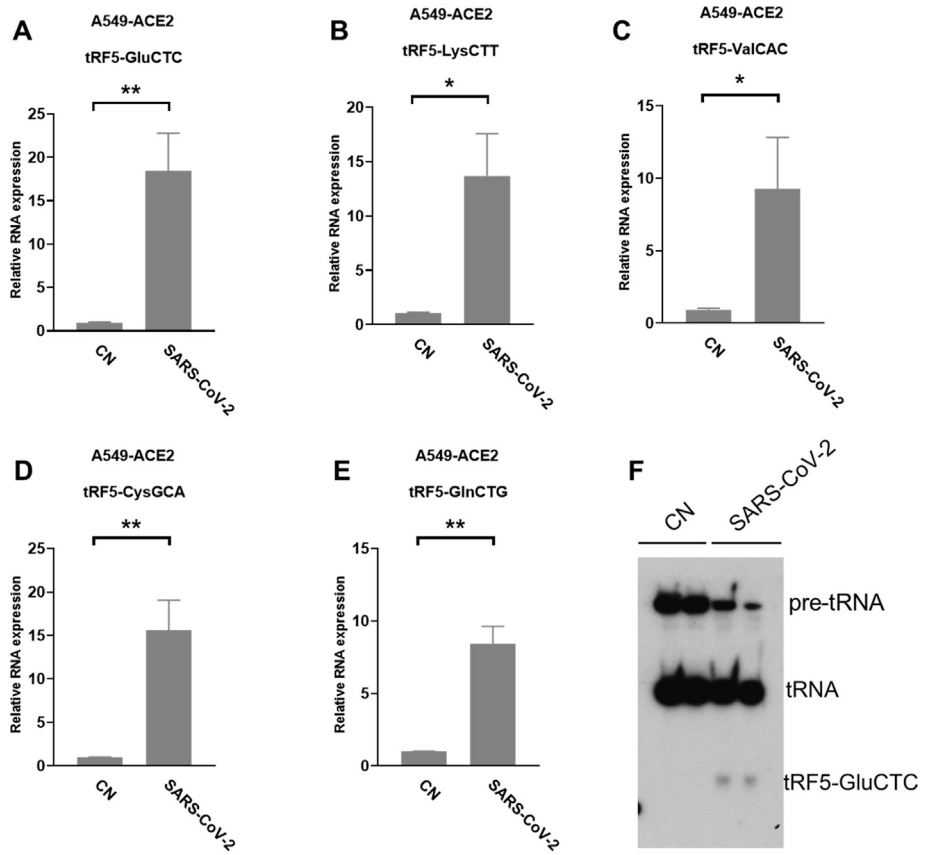

FIGURE 4 | SARS-CoV-2-impacted tRF5s in A549-ACE2 cells. **(A–E)** A549-ACE2 cells were infected with SARS-CoV-2 at an MOI of 0.1 for 4 days, qRT-PCR was performed to detect tRF5-GluCTC **(A)**, tRF5-LysCTT **(B)**, tRF5-ValCAC **(C)**, tRF5-CysGCA **(D)**, and tRF5-GlnCTG **(E)**. A northern blot was performed to detect tRF5-GluCTC **(F)**. Mock-infected cells (those without SARS-CoV-2 infection) were used as control (CN). Unpaired two-tailed t-tests were performed for statistical comparisons. Single and double asterisks represent *p* values of <0.05 and <0.01, respectively. Data, shown as means ± SE, are representative of three independent experiments.

the cleavage site of tRFs (**Figures 8D,E**). Thus, we speculated that 68 nt sv-CoV2-314 may be the precursor of 36 nt sv-CoV2-346 and the virus may use endonuclease involved in tRF biogenesis to generate viral small RNAs fragments.

DISCUSSION

In this study, we identified the change in sncRNA expression by SARS-CoV-2. Among sncRNAs, miRNAs have been getting lots of attention in the studies (Vaz et al., 2010; Plieskatt et al., 2014; Max et al., 2018; Hou and Yao, 2021). Standard barcode-ligation-based small RNA-seq are usually designed to capture miRNAs, which usually have 3′-OH ends (Hafner et al., 2008). It is increasingly acknowledged that the 3′-ends of other types of sncRNAs are heterogeneous (Honda et al., 2015), resulting in unsuccessful sequencing barcode ligation in the standard small RNA-seq. In our study, T4 PNK-RNA-seq was employed to profile sncRNAs with heterogeneous ends. Sequencing data revealed that piRNAs and tRFs had higher global expression than miRNAs in NPS (**Figure 2A**). sncRNAs may carry various unidentified modifications, which are insensitive to T4 PNK treatment. Therefore, T4 PNK-RNA-seq may leave some SARS-CoV-2-impacted sncRNAs unidentified. Herein, the consistency among the seq data, qRT-PCR result, and NB data of tRF5-GluCTC suggested the reliability of T4 PNK-RNA-seq for tRF5 detection.

Notable, among differently expressed tRF5s with mean of normalized counts >20 in control (CN) or SARS-CoV-2 groups (**Table 5**), we found four tRF5s: tRF5-GluTTC-1-2, tRF5-GlyCCC-6-1, tRF5-LysCTT61 and tRF5-SecTCA-2-1, were not classic tRF5s. While their 3′-ends commonly stop around the anticodon region like classical tRF5s, they lack the first 10-15 nt of the tRNA 5′end. Since they span the complete region of the D loop and the first half of the anticodon loop, we subgrouped and named them as tRF5DC (**Supplementary Figure S2**). Interestingly, tRF5DC and classic tRF5s were derived from the different tRNA isoacceptors tRNA, suggesting different biogenesis mechanisms of these two type tRFs.

This study further supported that tRFs induction is virus-specific. Previously, we and others have shown that RSV, hepatitis B virus (HBV), and hepatitis C virus (HCV) infections lead to

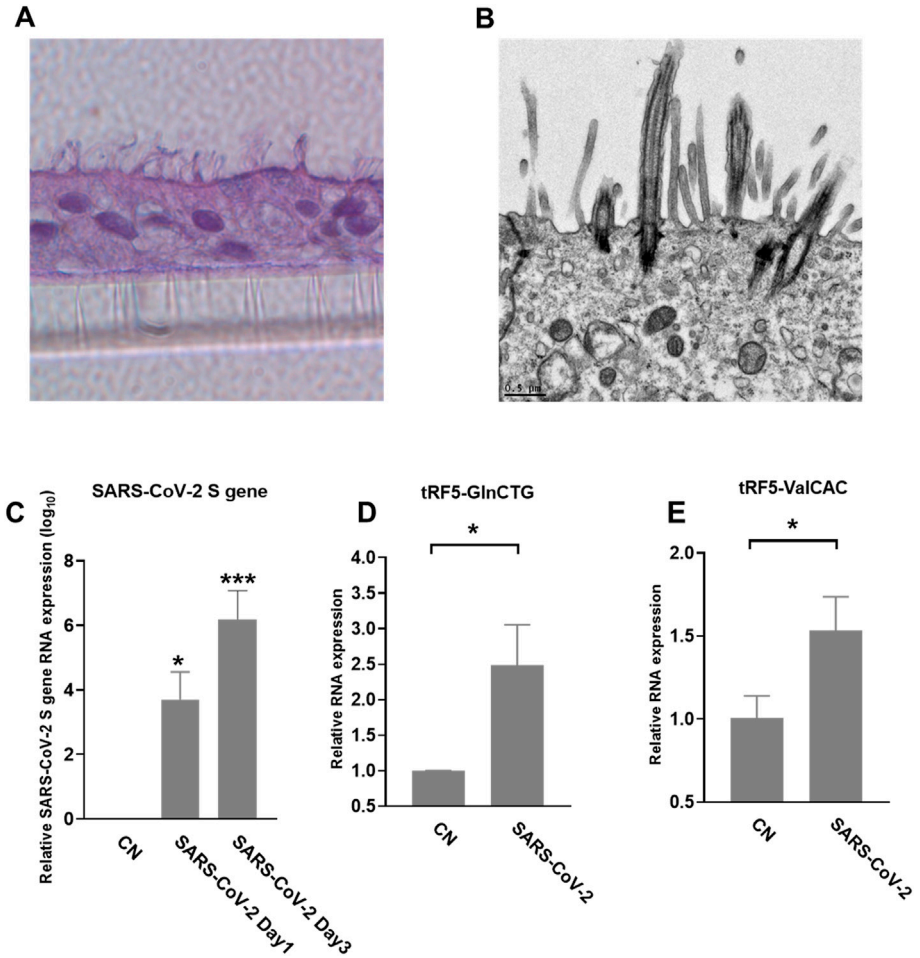

FIGURE 5 | SARS-CoV-2-affected tRF5s in ALI-cultured SAECs. **(A)** Histological examination SAECs in ALI culture. After SAECs were in ALI culture for 21 days, the insert was fixed with 4% polyoxymethylene, followed by tissue processing, sectioning, and H&E staining. **(B)** Transmission electron microscopy (TEM) of SAECs in ALI culture. **(C)** ALI-cultured SEACs were apically infected with SARS-CoV-2 at an MOI of 0.1 for 1 or 3 days, qRT-PCR was performed to detect SARS-CoV-2 S gene expression. GAPDH was used as an internal control. **(D,E)** On day 3 postinfection, tRF5-GlnCTG **(D)** and tRF5-ValCAC **(E)** expressions were measured using qRT-PCR. Mock-infected cells were used as control (CN). Unpaired two-tailed t-tests were performed for statistical comparisons. Single asterisks represent *p* values of <0.05. Data are shown as means ± SE and are representative of three independent experiments.

TABLE 6 | SARS-CoV-2-encoded svRNAs.

sv-CoV2 small RNAs	G enome position	Sequence	Length (nt)	Derived ORFs of SARS CoV-2	Raw reads	
					Sample 1	Sample 2
sv-CoV2-346	346–382	CGUACGUGGCUUUGGAGACUCCGUGGAGGA GGUCUU	36	nsp1	43071	3258
sv-CoV2-2825	2,825–2,861	AAUGAGAAGUGCUCUGCCUAUACAGUUGAACUCGGU	36	nsp3	13535	4426
sv-CoV2-6286	6,286–6,311	CUGGUGUAUACGUUGUCUUUGGAGC	25	nsp3	11743	2939
sv-CoV2-14728	14,728–14,751	AAGGAAGGAAGUUCUGUUGAAUU	23	nsp12	2026	2188
sv-CoV2-15954	15,954–15,979	AGGGGCCGGCUGUUUUGUAGAUGAU	25	nsp12	10998	1846
sv-CoV2-20364	20,364–20,415	ACAUCUACUGAUUGGACUAGCUAAACGUUUUAAGGA AUCACCUUUUGAAUU	51	nsp15	10510	3422
sv-CoV2-21145	21,145–21,171	CUUGGAGGUUCCGUGGCUAUAAAGAU	26	nsp16	3134	1394
sv-CoV2-26183	26,183–26,216	AUGAUGAACCGACGACGACUACUAGCGUGCCUU	33	3a	15134	4925

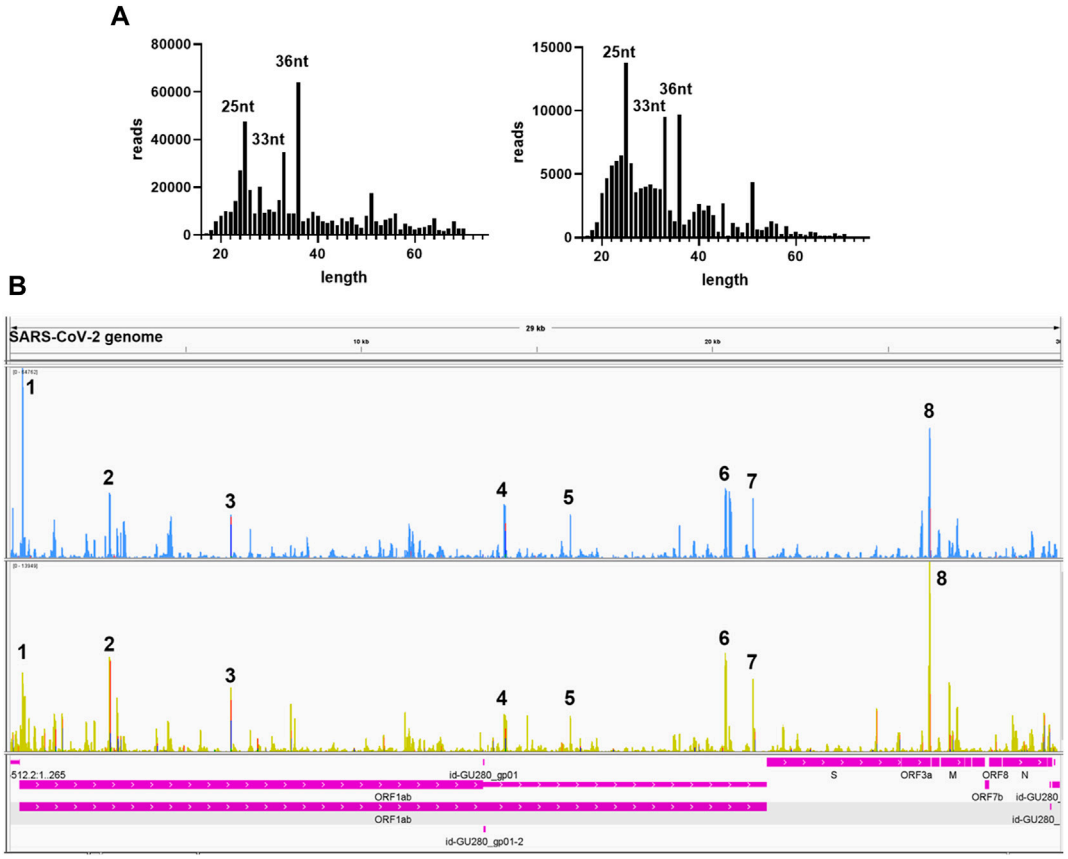

FIGURE 6 | Sequence information of virus-derived sncRNAsA. **(A)** Length distribution of viral small RNAs from two representative patient samples. **(B)** Two representative visual inspections of the small RNA sequences aligning with the SARS-CoV-2 genome. The names of viral genes and the genome positions (nt) are indicated.

different tRF profile changes (Wang et al., 2013; Selitsky et al., 2015; Zhou et al., 2017; Choi et al., 2020). Compared with tRF induction by RSV, we found that SARS-CoV-2 could induce tRF5-ValCAC, while RSV cannot. On the other hand, we found that tRF5-GlyGCC, which is significantly inducible by RSV, was not induced by SARS-CoV-2. The virus-specific changes in tRFs suggest them to be promising biomarkers for viral infections.

Other than host-derived sncRNAs, sncRNAs can also be derived from viruses. svRNAs have been reported to be involved in the regulation of viral replication, viral persistence, host immune evasion, and cellular transformation (Tycowski et al., 2015). SARS-CoV-2-encoded sncRNAs have been demonstrated by two independent groups (Cheng et al., 20212021; Fu et al., 2021). Using T4-PNK-RNA-seq, several novel svRNAs in SARS-CoV-2 NPS samples were identified. One of them, sv-CoV2-346, was verified to be present in SARS-CoV-2-infected A549-ACE2 cells as well. Due to the limited NPS RNA samples, the leftover RNAs after sequencing were not enough for stem-loop qRT-PCR to validate svRNAs. Thus, we detected sv-CoV2-346 by RT-PCR using the same cDNA generated by the RT step for the qRT-PCR assays for tRF5s. Our RT-PCR revealed a sv-CoV2-346 specific band around 55 nt and a non-specific band. In the future, we will study the relationship between SARS-CoV-2 svRNAs and viral loads/disease severity.

The most widely studied viral sncRNAs are miRNAs-like svRNAs. Both DNA and RNA viruses could encode miRNAs-like svRNAs *via* Dicer-dependent miRNAs biogenesis pathways (Tycowski et al., 2015; Grundhoff and Sullivan, 2011). Among RNA viruses, cytoplasmic restricted RNA viruses were thought incapable of producing miRNA-like svRNAs. However, accumulating evidence indicates cytoplasmic RNA viruses, such as H5N1 influenza virus, enterovirus 71(EV71), West Nile virus (WNV), SARS-CoV, and SARS-CoV-2, also encode viral miRNAs (Morales et al., 2017; Cheng et al., 20212021; Fu et al., 2021; Perez et al., 2010; Li et al., 2018; Weng et al., 2014; Hussain et al., 2012). These cytoplasmic RNA viruses generate viral miRNAs *via* multiple non-canonical miRNAs biogenesis mechanisms. Dicer, not Drosha, is involved in WNV and EV71 viral miRNAs generation (Weng et al., 2014; Hussain et al., 2012). H5N1 influenza virus and SARS-CoV encode viral miRNAs in a Dicer-and Drosha-independent way (Morales et al., 2017; Li et al., 2018). Besides viral miRNAs, the induction of functional svRNAs, which do not look like miRNAs, was reported for cytoplasmic RNA viruses (Perez et al., 2010). However, the knowledge on how cytoplasmic RNA viruses produce svRNAs is limited. One of the

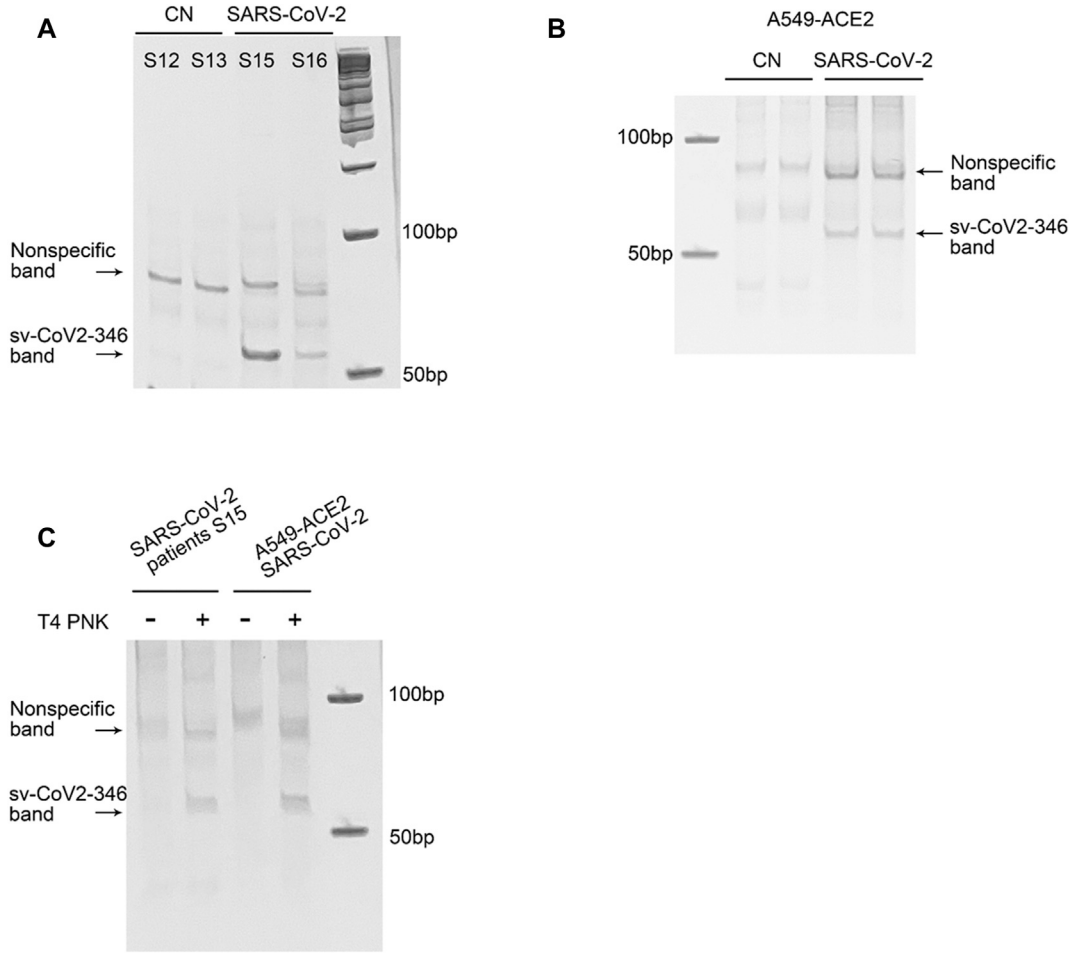

FIGURE 7 | Experimental validation of sv-CoV2-346. **(A)** RT-PCR was performed to detect sv-CoV2-346 in NPS samples of two control (CN, SARS-CoV-2 negative) and two SARS-CoV-2 patients. **(B)** The presence of svCoV2-346 in SARS-CoV-2-infected A549-ACE2 cells. **(C)** Detection of sv-CoV2-346 needs the pretreatment of T4 PNK. The 3′-end of sv-CoV2-346 does not have –OH, as samples without pretreatment of T4 PNK did not result in sv-CoV2-346 bands. All experiments were independently repeated twice.

TABLE 7 | RNA sequence information for those with high raw reads and mapping to viral nucleotides 289–485.

sv-CoV2 small RNAs fragments	Genome position	Sequence	Length (nt)	Raw reads	
				Sample 1	Sample 2
sv-CoV2-346	346–382	CGUACGUGGCUUUGGAGACUCCGUGGAGGAGGUCUU	36	43,071	3,036
sv-CoV2-299	299–328	ACACACGUCCAACUCAGUUUGCCUGUUUU	29	1,931	636
sv-CoV2-404	404–443	AAAGAUGGCACUUGUGGCUUAGUAGAAGUUGAAAAAGGC	39	1,311	586
sv-CoV2-314	314–382	AGUUUGCCUGUUUUACAGGUUCGCGACGUGCUCGUACGUGGCUUUGGA GACUCCGUGG AGGAGGUCUU	68	126	13

interesting observations of newly discovered sv-CoV2 is that sv-CoV2-314 may have a similar tertiary structure as tRNAs and function as the potential precursor of 36 nt svCoV2-346 (**Figure 8**). Whether a tRNA-like shape (three-leafed clover) of svRNAs makes them as prone as tRNAs to the cleavage during SARS-CoV-2 infection will be investigated in the future. Recently, the cleavage of tRNAs has been reported to be regulated by nt modifications and tRNA anticodon loop is enriched with modification (Blanco et al., 2014; Ranjan and Rodnina, 2016). Therefore, it is possible that the anticodon and/or D loop experience nt modification changes in SARS-CoV-2 infection, resulting in the cleavage. It has been also previously reported that the cleavage of tRNAs is mediated by specific ribonuclease(s) (Lee et al., 2009; Wang et al., 2013; Zhou et al., 2017; Choi et al., 2020).

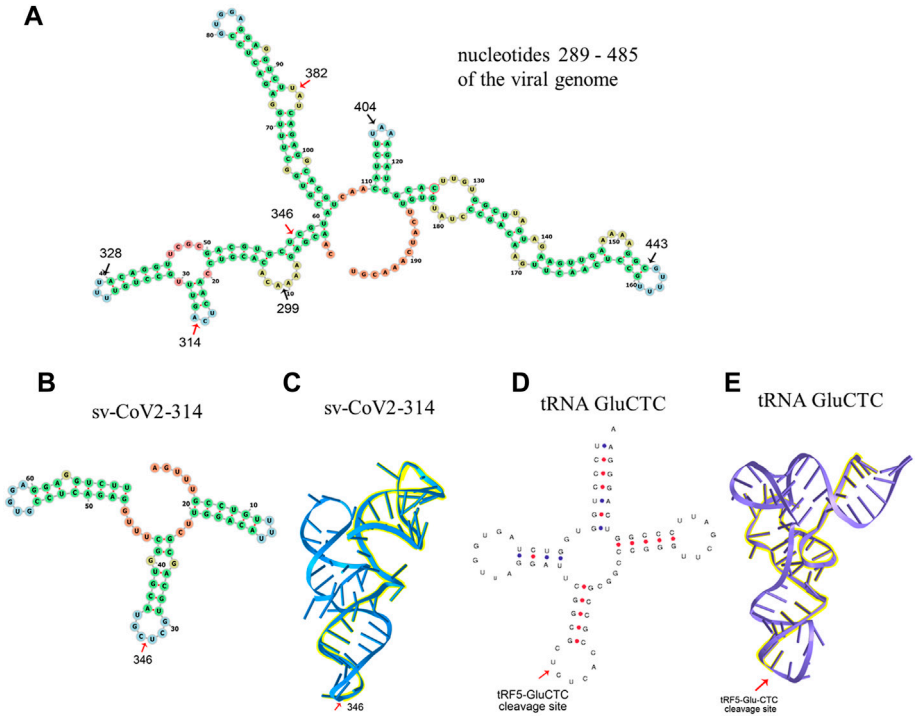

FIGURE 8 | Structure prediction of viral small RNA. **(A)** The secondary structure of viral nucleotides 289–485. The secondary **(B)** and tertiary **(C)** structure of sv-CoV2-314. The secondary **(D)** and tertiary **(E)** structure of a tRNA example GluCTC. Arrows indicated cleavage sites.

Therefore, it is also possible SARS-CoV-2 favors the activation of certain enzymes to enrich the corresponding sncRNA population. How viruses use the host proteins to control the biogenesis of sncRNAs is still unclear and awaits investigation.

In summary, we investigated COVID-19-impacted sncRNAs comprehensively using the NPS samples by T4 PNK-RNA-seq and modified qRT-PCR method. We are aware that our study has some limitations. For example, T4 PNK-RNA-seq may not catch all types of sncRNAs. In addition, our NPS samples were all from outpatient clinics, which set the limitation to study the correlation of tRF changes with the disease severity. We are closely working with our Molecular Diagnosis Laboratory to obtain the samples from outpatient, inpatient, and ICU services so that whether tRFs serve as disease biomarkers can be determined. Our recent publication on the correlation of tRF changes with Alzheimer's disease severity supports tRFs to be promising disease biomarkers (Wu et al., 2021). Other than biomarkers, the studies of tRFs in viral infections may also provide insight into therapeutic/prophylactic strategy development. In RSV infection, we found some induced tRFs promote viral replication (Wang et al., 2013; Zhou et al., 2017; Choi et al., 2020). Therefore, any mechanisms associated with their biogenesis and function would not only reveal potential targets to control viral replication but also benefit the ncRNA research community.

DATA AVAILABILITY STATEMENT

The datasets presented in this study can be found in online repositories. The names of the repository/repositories and accession number(s) can be found below: Gene Expression Omnibus accession number: GSE193555.

ETHICS STATEMENT

The studies involving human participants were reviewed and approved by University of Texas Medical. IRB committee. The patients/participants provided their written informed consent to participate in this study.

AUTHOR CONTRIBUTIONS

WW and XB wrote the manuscript; WW, E-JC, BW, KZ, contributed to the experiment performance and data analyses. LT, PH, RG, II, LH, and IL contribute to the deep seq data analyses and related methodology establishment. GH and JD developed IBM protocols for sample collection and NSP sample handling. JD, TW, and XB contributed to overall project management and experimental design.

FUNDING

This work was supported by grants from the NIH R01 AI116812, R21AG069226, and Research Pilot Grant from the Institute for Human Infections and Immunity (IHII) at UTMB to XB and NIH grants R01AI127744 (TW), R21 AI140569 (TW), and R21 EY029112 (TW).

ACKNOWLEDGMENTS

We thank Darby L. Buck for the manuscript editing.

SUPPLEMENTARY MATERIAL

The Supplementary Material for this article can be found online at: https://www.frontiersin.org/articles/10.3389/fmolb.2022.821137/full#supplementary-material

Supplementary Figure 1 | The pipeline of T4 PNK-RNA-seq and data analyses. **(A)** The flowchart of T4 PNK-RNA-seq. **(B)** The flowchart of the sequencing data analyses.

Supplementary Figure 2 | Biogenesis of tRF5s and tRF5DC. tRF5s are generated by the cleavage on the anticodon loop (black arrows); tRF5DCs are derived from the cleavage on the D arm (red or blue arrow) and anticodon loop (black arrows).

REFERENCES

Beermann, J., Piccoli, M.-T., Viereck, J., and Thum, T. (2016). Non-coding RNAs in Development and Disease: Background, Mechanisms, and Therapeutic Approaches. *Physiol. Rev.* 96, 1297–1325. doi:10.1152/physrev.00041.2015

Bhowmick, R., and Gappa-Fahlenkamp, H. (2016). Cells and Culture Systems Used to Model the Small Airway Epithelium. *Lung* 194, 419–428. doi:10.1007/s00408-016-9875-2

Blanco, S., Dietmann, S., Flores, J. V., Hussain, S., Kutter, C., Humphreys, P., et al. (2014). Aberrant Methylation of T RNA S Links Cellular Stress to Neuro-developmental Disorders. *EMBO J.* 33, 2020–2039. doi:10.15252/embj.201489282

Blanco-Melo, D., Nilsson-Payant, B. E., Liu, W.-C., Uhl, S., Hoagland, D., Møller, R., et al. (2020). Imbalanced Host Response to SARS-CoV-2 Drives Development of COVID-19. *Cell* 181, 1036–1045. doi:10.1016/j.cell.2020.04.026

Buchrieser, J., Dufloo, J., Hubert, M., Monel, B., Planas, D., Rajah, M. M., et al. (2021). Syncytia Formation by SARS-CoV-2-Infected Cells. *EMBO J.* 40, e107405. doi:10.15252/embj.2020107405

Chandorkar, P., Posch, W., Zaderer, V., Blatzer, M., Steger, M., Ammann, C. G., et al. (2017). Fast-track Development of an *In Vitro* 3D Lung/immune Cell Model to Study Aspergillus Infections. *Sci. Rep.* 7, 11644. doi:10.1038/s41598-017-11271-4

Cheng, Z., Cheng, L., Lin, J., Lunbiao, C., Chunyu, L., Guoxin, S., et al. (20212021). Verification of SARS-CoV-2-Encoded Small RNAs and Contribution to Infection-Associated Lung Inflammation. *bioRxiv* 2005, 444324. doi:10.1101/2021.05.16.444324

Choi, E. J., Wu, W., Zhang, K., Lee, I., Kim, I. H., Lee, Y. S., et al. (2020). ELAC2, an Enzyme for tRNA Maturation, Plays a Role in the Cleavage of a Mature tRNA to Produce a tRNA-Derived RNA Fragment during Respiratory Syncytial Virus Infection. *Front. Mol. Biosci.* 7, 609732. doi:10.3389/fmolb.2020.609732

Choudhuri, S. (2010). Small Noncoding RNAs: Biogenesis, Function, and Emerging Significance in Toxicology. *J. Biochem. Mol. Toxicol.* 24, 195–216. doi:10.1002/jbt.20325

Dozmorov, M. G., Giles, C. B., Koelsch, K. A., and Wren, J. D. (2013). Systematic Classification of Non-coding RNAs by Epigenomic Similarity. *BMC Bioinformatics* 14 Suppl 14 (Suppl. 14), S2. doi:10.1186/1471-2105-14-S14-S2

Fabian, M. R., and Sonenberg, N. (2012). The Mechanics of miRNA-Mediated Gene Silencing: a Look under the Hood of miRISC. *Nat. Struct. Mol. Biol.* 19, 586–593. doi:10.1038/nsmb.2296

Fu, H., Feng, J., Liu, Q., Sun, F., Tie, Y., Zhu, J., et al. (2009). Stress Induces tRNA Cleavage by Angiogenin in Mammalian Cells. *FEBS Lett.* 583, 437–442. doi:10.1016/j.febslet.2008.12.043

Fu, Z., Wang, J., Wang, Z., Sun, Y., Wu, J., Zhang, Y., et al. (2021). A Virus-Derived microRNA-like Small RNA Serves as a Serum Biomarker to Prioritize the COVID-19 Patients at High Risk of Developing Severe Disease. *Cell Discov* 7, 48. doi:10.1038/s41421-021-00289-8

Giraldez, M. D., Spengler, R. M., Etheridge, A., Goicochea, A. J., Tuck, M., Choi, S. W., et al. (2019). Phospho-RNA-seq: a Modified Small RNA-Seq Method that Reveals Circulating mRNA and lncRNA Fragments as Potential Biomarkers in Human Plasma. *EMBO J.* 38.e101695. doi:10.15252/embj.2019101695

Grundhoff, A., and Sullivan, C. S. (2011). Virus-encoded microRNAs. *Virology* 411, 325–343. doi:10.1016/j.virol.2011.01.002

Hafner, M., Landgraf, P., Ludwig, J., Rice, A., Ojo, T., Lin, C., et al. (2008). Identification of microRNAs and Other Small Regulatory RNAs Using cDNA Library Sequencing. *Methods* 44, 3–12. doi:10.1016/j.ymeth.2007.09.009

Hasan, M. M., Akter, R., Ullah, M. S., Abedin, M. J., Ullah, G. M., and Hossain, M. Z. (2014). A Computational Approach for Predicting Role of Human MicroRNAs in MERS-CoV Genome. *Adv. Bioinformatics* 2014, 967946. doi:10.1155/2014/967946

Hiemstra, P. S., Grootaers, G., van der Does, A. M., Krul, C. A. M., and Kooter, I. M. (2018). Human Lung Epithelial Cell Cultures for Analysis of Inhaled Toxicants: Lessons Learned and Future Directions. *Toxicol. Vitro* 47, 137–146. doi:10.1016/j.tiv.2017.11.005

Hofacker, I. L. (2003). Vienna RNA Secondary Structure Server. *Nucleic Acids Res.* 31, 3429–3431. doi:10.1093/nar/gkg599

Honda, S., Loher, P., Shigematsu, M., Palazzo, J. P., Suzuki, R., Imoto, I., et al. (2015). Sex Hormone-dependent tRNA Halves Enhance Cell Proliferation in Breast and Prostate Cancers. *Proc. Natl. Acad. Sci. USA* 112, E3816–E3825. doi:10.1073/pnas.1510077112

Hou, J., and Yao, C. (2021). Potential Prognostic Biomarkers of Lung Adenocarcinoma Based on Bioinformatic Analysis. *Biomed. Res. Int.* 2021, 8859996. doi:10.1155/2021/8859996

Hussain, M., Torres, S., Schnettler, E., Funk, A., Grundhoff, A., Pijlman, G. P., et al. (2012). West Nile Virus Encodes a microRNA-like Small RNA in the 3' Untranslated Region Which Up-Regulates GATA4 mRNA and Facilitates Virus Replication in Mosquito Cells. *Nucleic Acids Res.* 40, 2210–2223. doi:10.1093/nar/gkr848

Ivanov, P., O'Day, E., Emara, M. M., Wagner, G., Lieberman, J., and Anderson, P. (2014). G-quadruplex Structures Contribute to the Neuroprotective Effects of Angiogenin-Induced tRNA Fragments. *Proc. Natl. Acad. Sci. USA* 111, 18201–18206. doi:10.1073/pnas.1407361111

Karolchik, D., Hinrichs, A. S., Furey, T. S., Roskin, K. M., Sugnet, C. W., Haussler, D., et al. (2004). The UCSC Table Browser Data Retrieval Tool. *Nucleic Acids Res.* 32, D493–D496. doi:10.1093/nar/gkh103

Khan, M. A.-A. -K., Sany, M. R. U., Islam, M. S., and Islam, A. B. M. M. K. (2020). Epigenetic Regulator miRNA Pattern Differences Among SARS-CoV, SARS-CoV-2, and SARS-CoV-2 World-wide Isolates Delineated the Mystery behind the Epic Pathogenicity and Distinct Clinical Characteristics of Pandemic COVID-19. *Front. Genet.* 11, 765. doi:10.3389/fgene.2020.00765

Lee, Y. S., Shibata, Y., Malhotra, A., and Dutta, A. (2009). A Novel Class of Small RNAs: tRNA-Derived RNA Fragments (tRFs). *Genes Dev.* 23, 2639–2649. doi:10.1101/gad.1837609

Li, X., Fu, Z., Liang, H., Wang, Y., Qi, X., Ding, M., et al. (2018). H5N1 Influenza Virus-specific miRNA-like Small RNA Increases Cytokine Production and Mouse Mortality via Targeting poly(rC)-Binding Protein 2. *Cell Res* 28, 157–171. doi:10.1038/cr.2018.3

Liu, S., Chen, Y., Ren, Y., Zhou, J., Ren, J., Lee, I., et al. (2018). A tRNA-Derived RNA Fragment Plays an Important Role in the Mechanism of Arsenite -induced Cellular Responses. *Sci. Rep.* 8, 16838. doi:10.1038/s41598-018-34899-2

Mallick, B., Ghosh, Z., and Chakrabarti, J. (2009). MicroRNome Analysis Unravels the Molecular Basis of SARS Infection in Bronchoalveolar Stem Cells. *PLoS One* 4, e7837. doi:10.1371/journal.pone.0007837

Max, K. E. A., Bertram, K., Akat, K. M., Bogardus, K. A., Li, J., Morozov, P., et al. (2018). Human Plasma and Serum Extracellular Small RNA Reference Profiles and Their Clinical Utility. *Proc. Natl. Acad. Sci. USA* 115, E5334–E5343. doi:10.1073/pnas.1714397115

Morales, L., Oliveros, J. C., Fernandez-Delgado, R., tenOever, B. R., Enjuanes, L., and Sola, I. (2017). SARS-CoV-Encoded Small RNAs Contribute to Infection-Associated Lung Pathology. *Cell Host & Microbe* 21, 344–355. doi:10.1016/j.chom.2017.01.015

Mossel, E. C., Huang, C., Narayanan, K., Makino, S., Tesh, R. B., and Peters, C. J. (2005). Exogenous ACE2 Expression Allows Refractory Cell Lines to Support Severe Acute Respiratory Syndrome Coronavirus Replication. *J. Virol.* 79, 3846–3850. doi:10.1128/jvi.79.6.3846-3850.2005

Perez, J. T., Varble, A., Sachidanandam, R., Zlatev, I., Manoharan, M., Garcia-Sastre, A., et al. (2010). Influenza A Virus-Generated Small RNAs Regulate the Switch from Transcription to Replication. *Proc. Natl. Acad. Sci.* 107, 11525–11530. doi:10.1073/pnas.1001984107

Plieskatt, J. L., Rinaldi, G., Feng, Y., Levine, P. H., Easley, S., Martinez, E., et al. (2014). Methods and Matrices: Approaches to Identifying miRNAs for Nasopharyngeal Carcinoma. *J. Transl Med.* 12, 3. doi:10.1186/1479-5876-12-3

Popenda, M., Szachniuk, M., Antczak, M., Purzycka, K. J., Lukasiak, P., Bartol, N., et al. (2012). Automated 3D Structure Composition for Large RNAs. *Nucleic Acids Res.* 40, e112. doi:10.1093/nar/gks339

Qin, C., Xu, P. P., Zhang, X., Zhang, C., Liu, C. B., Yang, D. G., et al. (2020). Pathological Significance of tRNA-Derived Small RNAs in Neurological Disorders. *Neural Regen. Res.* 15, 212–221. doi:10.4103/1673-5374.265560

Rajput, R., Sharma, J., Nair, M. T., Khanna, M., Arora, P., and Sood, V. (2020). Regulation of Host Innate Immunity by Non-coding RNAs during Dengue Virus Infection. *Front. Cel. Infect. Microbiol.* 10, 588168. doi:10.3389/fcimb.2020.588168

Ranjan, N., and Rodnina, M. V. (2016). tRNA Wobble Modifications and Protein Homeostasis. *Translation* 4, e1143076. doi:10.1080/21690731.2016.1143076

Romano, G., Veneziano, D., Acunzo, M., and Croce, C. M. (2017). Small Non-coding RNA and Cancer. *Carcinogenesis* 38, 485–491. doi:10.1093/carcin/bgx026

Schwarz, D. S., Tomari, Y., and Zamore, P. D. (2004). The RNA-Induced Silencing Complex Is a Mg2+-dependent Endonuclease. *Curr. Biol.* 14, 787–791. doi:10.1016/j.cub.2004.03.008

Schweitzer, K. S., Crue, T., Nall, J. M., Foster, D., Sajuthi, S., Correll, K. A., et al. (2021). Influenza Virus Infection Increases ACE2 Expression and Shedding in Human Small Airway Epithelial Cells. *Eur. Respir. J.* 58, 2003988. doi:10.1183/13993003.03988-2020

Selitsky, S. R., Baran-Gale, J., Honda, M., Yamane, D., Masaki, T., Fannin, E. E., et al. (2015). Small tRNA-Derived RNAs Are Increased and More Abundant Than microRNAs in Chronic Hepatitis B and C. *Sci. Rep.* 5, 7675. doi:10.1038/srep07675

Shen, Y., Yu, X., Zhu, L., Li, T., Yan, Z., and Guo, J. (2018). Transfer RNA-Derived Fragments and tRNA Halves: Biogenesis, Biological Functions and Their Roles in Diseases. *J. Mol. Med.* 96, 1167–1176. doi:10.1007/s00109-018-1693-y

Sun, C., Fu, Z., Wang, S., Li, J., Li, Y., Zhang, Y., et al. (2018). Roles of tRNA-Derived Fragments in Human Cancers. *Cancer Lett.* 414, 16–25. doi:10.1016/j.canlet.2017.10.031

Tycowski, K. T., Guo, Y. E., Lee, N., Moss, W. N., Vallery, T. K., Xie, M., et al. (2015). Viral Noncoding RNAs: More Surprises. *Genes Dev.* 29, 567–584. doi:10.1101/gad.259077.115

Vaz, C., Ahmad, H. M., Sharma, P., Gupta, R., Kumar, L., Kulshreshtha, R., et al. (2010). Analysis of microRNA Transcriptome by Deep Sequencing of Small RNA Libraries of Peripheral Blood. *BMC Genomics* 11, 288. doi:10.1186/1471-2164-11-288

Wang, Q., Lee, I., Ren, J., Ajay, S. S., Lee, Y. S., and Bao, X. (2013). Identification and Functional Characterization of tRNA-Derived RNA Fragments (tRFs) in Respiratory Syncytial Virus Infection. *Mol. Ther.* 21, 368–379. doi:10.1038/mt.2012.237

Weng, K.-F., Hung, C.-T., Hsieh, P.-T., Li, M.-L., Chen, G.-W., Kung, Y.-A., et al. (2014). A Cytoplasmic RNA Virus Generates Functional Viral Small RNAs and Regulates Viral IRES Activity in Mammalian Cells. *Nucleic Acids Res.* 42, 12789–12805. doi:10.1093/nar/gku952

Weston, S., Coleman, C. M., Haupt, R., Logue, J., Matthews, K., Li, Y., et al. (2020). Broad Anti-coronavirus Activity of Food and Drug Administration-Approved Drugs against SARS-CoV-2 *In Vitro* and SARS-CoV *In Vivo*. *J. Virol.* 94, e01218. doi:10.1128/JVI.01218-20

World Health, O. (2021). *World Health Organization*. Geneva.

Wu, W., Choi, E. J., Lee, I., Lee, Y. S., and Bao, X. (2020) Non-Coding RNAs and Their Role in Respiratory Syncytial Virus (RSV) and Human Metapneumovirus (hMPV) Infections. 12(3):345.doi:10.3390/v12030345

Wu, W., Lee, I., Spratt, H., Fang, X., and Bao, X. (2021). tRNA-Derived Fragments in Alzheimer's Disease: Implications for New Disease Biomarkers and Neuropathological Mechanisms. *Jad* 79, 793–806. doi:10.3233/jad-200917

Zhang, H., Rostami, M. R., Leopold, P. L., Mezey, J. G., O'Beirne, S. L., Strulovici-Barel, Y., et al. (2020). Expression of the SARS-CoV-2 ACE2 Receptor in the Human Airway Epithelium. *Am. J. Respir. Crit. Care Med.* 202, 219–229. doi:10.1164/rccm.202003-0541oc

Zhou, J., Liu, S., Chen, Y., Fu, Y., Silver, A. J., Hill, M. S., et al. (2017). Identification of Two Novel Functional tRNA-Derived Fragments Induced in Response to Respiratory Syncytial Virus Infection. *J. Gen. Virol.* 98, 1600–1610. doi:10.1099/jgv.0.000852

Zhu, L., Liu, X., Pu, W., and Peng, Y. (2018). tRNA-derived Small Non-coding RNAs in Human Disease. *Cancer Lett.* 419, 1–7. doi:10.1016/j.canlet.2018.01.015

Zhu, N., Zhang, D., Wang, W., Li, X., Yang, B., Song, J., et al. (2020). A Novel Coronavirus from Patients with Pneumonia in China, 2019. *N. Engl. J. Med.* 382, 727–733. doi:10.1056/nejmoa2001017

Conflict of Interest: The authors declare that the research was conducted in the absence of any commercial or financial relationships that could be construed as a potential conflict of interest.

Publisher's Note: All claims expressed in this article are solely those of the authors and do not necessarily represent those of their affiliated organizations, or those of the publisher, the editors and the reviewers. Any product that may be evaluated in this article, or claim that may be made by its manufacturer, is not guaranteed or endorsed by the publisher.

frontiers | Frontiers in Molecular Biosciences

MINI REVIEW
published: 13 April 2022
doi: 10.3389/fmolb.2022.888424

Function and Therapeutic Implications of tRNA Derived Small RNAs

Briana Wilson[1] *and Anindya Dutta*[2]*

[1]Department of Biochemistry and Molecular Genetics, University of Virginia School of Medicine, Charlottesville, VA, United States, [2]Department of Genetics, University of Alabama, Birmingham, AL, United States

tRNA derived small RNAs are mainly composed of tRNA fragments (tRFs) and tRNA halves (tiRs). Several functions have been attributed to tRFs and tiRs since their initial characterizations, spanning all aspects of regulation of the Central Dogma: from nascent RNA silencing, to post-transcriptional gene silencing, and finally, to translational regulation. The length distribution, sequence diversity, and multifaceted functions of tRFs and tiRs positions them as attractive new models for small RNA therapeutics. In this review, we will discuss the principles of tRF biogenesis and function in order to highlight their therapeutic potential.

Keywords: tRNA fragments, RNA therapeutics, translation inhibition, post-transcriptional regulation of gene expression, RNA silencing

OPEN ACCESS

Edited by:
Yong Sun Lee,
National Cancer Center, South Korea

Reviewed by:
Patrick Provost,
Laval University, Canada

***Correspondence:**
Anindya Dutta
duttaa@uab.edu

Specialty section:
This article was submitted to Molecular Diagnostics and Therapeutics, a section of the journal Frontiers in Molecular Biosciences

Received: *02 March 2022*
Accepted: *28 March 2022*
Published: *13 April 2022*

Citation:
Wilson B and Dutta A (2022) Function and Therapeutic Implications of tRNA Derived Small RNAs. Front. Mol. Biosci. 9:888424. doi: 10.3389/fmolb.2022.888424

INTRODUCTION

The widespread introduction of small RNA sequencing technologies has uncovered a wide variety of non-microRNA (miRNA) small RNAs (nmsRNA) (Lee et al., 2009; Falaleeva and Stamm, 2013; Jackowiak et al., 2017; Cherlin et al., 2020). tRNA fragments (tRFs) and tRNA halves (tiRs) are one of the most highly abundant class of small RNAs, and depending on the cell type or condition, may reach higher levels than miRNAs (Sharma et al., 2016). Initially thought to be degradation products of tRNAs, the smaller tRFs were systematically characterized and found to have discrete length peaks (Kumar et al., 2014). Later, the longer tiRs were discovered and were found to be the result of tRNA cleavage by angiogenin (ANG) during stress (Yamasaki et al., 2009).

Initial characterizations focused primarily on tRFs having a miRNA-like mechanism, due to the similar size distribution between miRNAs and tRFs (Lee et al., 2009; Haussecker et al., 2010). To date, however, several other functions have been identified, covering all aspects of the Central Dogma including nascent RNA silencing, post-transcriptional gene silencing, and translational regulation (Yamasaki et al., 2009; Haussecker et al., 2010; Guzzi et al., 2018; Kuscu et al., 2018; Fricker et al., 2019; Di Fazio et al., 2022). While tRFs and tiRs have experienced a boom in basic biological and functional (**Table 1**) insights, miRNAs and siRNAs have experienced a renaissance in their therapeutic applications. Although many reviews focus on the role of tRFs and tiRs in disease and as potential biomarkers (Jia et al., 2020; Zeng et al., 2020; Fagan et al., 2021; Zong et al., 2021), here, we will discuss recent tRF and tiR functional insights, with emphasis on their potential therapeutic applications.

BIOGENESIS OF tRNA Fragments and tRNA Halves

tRNA derived small RNAs are divided into two major classes based on length: shorter tRFs and longer tRNA halves (**Figure 1**). The two major classes can be further subdivided based on the

TABLE 1 | The multifaceted functions of tRFs and tiRs.

Function	tRF type	tRF Examples	References
Post-transcriptional gene silencing (*via* association with RISC)	tRF-5s	several tRF-5s (bind AGO1,3,4)	Kumar et al. (2014)
	tRF-3s	several tRF-5s (bind AGO1,3,4)	Kumar et al. (2014)
	tRF-3	tRF-3001a,tRF-3003a, tRF-3009a	Kuscu et al. (2018)
	tRF-3	cand14	Haussecker et al. (2010)
	tRF-3	CU1276	Maute et al. (2013)
	tRF-3	Bj-tRF001,Bj-tRF002	Ren et al. (2019)
	tRF-5	Bj-tRF003	Ren et al. (2019)
	tRF-5	tRF5-GluCTC	Deng et al. (2015)
Role in cell proliferation	tRF-1	tRF-1001	Lee et al. (2009)
Endogenous retroviral reverse transcriptional silencing	tRF-3	tRF ETn (18 nt) (MERV)	Schorn et al. (2017)
Exogenous retroviral reverse transcriptional silencing	tRF-3	PBSncRNA (HIV)	Yeung et al. (2009)
Exogenous retroviral reverse transcriptional enhancement	tRF-3	tRF-3019 (HTLV-1)	Ruggero et al. (2014)
Endogenous retroviral post-transcriptional silencing	tRF-3	tRF ETn (22 nt) (MERV)	Schorn et al. (2017)
Endogenous retroviral chromatin mediated silencing	tRF-5	tRF-GlyGCC (MERVL)	Sharma et al. (2018), Boskovic et al. (2020)
Nascent RNA silencing	tRF-3 (precursor)	tsRNA SPINT1	Di Fazio et al. (2022)
	tRF-5	tsRNA LINC00665	Di Fazio et al. (2022)
	tRF-5	tsRNA EGFR/MET	Di Fazio et al. (2022)
	i-tRF	tsRNA BCL2	Di Fazio et al. (2022)
Translational gene silencing	tRF-5	Val-tRF	Gebetsberger et al. (2012)
	tRF-5	tRF(Gln)	Sobala and Hutvagner (2013)
	tRF-5	tRF(Val)	Sobala and Hutvagner (2013)
	tRF-5	tRF(Lys)	Sobala and Hutvagner (2013)
	tiRs	stress-induced tiRs	Yamasaki et al. (2009)
	tiR-5	tRNA-Ala	Ivanov et al. (2011)
	tiR-5	tRNA-GlyGCC	Ivanov et al. (2011)
	tiR-5	tRNA-GlyCCC	Ivanov et al. (2011)
	tiR-5	tRNA-Cys	Ivanov et al. (2011)
	tiR-3	tRNA-Pro	Ivanov et al. (2011)
Translational enhancement	tiR-3	tRNA-ThrAGU (*T. brucei*)	Fricker et al. (2019)
	tRF-3	tRNA-LeuCAG	Kim et al. (2017)
RNA protein binding	i-tRFs	tRNA-Glu,-Asp,-Tyr,-Gly (binds YBX1)	Goodarzi et al. (2015)
	tRF-3	tRNA-Glu (binds NCL)	Falconi et al. (2019)
	tiRs	20 ANG-dependent tiRs (binds Cytochrome C)	Saikia et al. (2014)
	tRF-1	tRF_U3_1 (binds SSB/La)	Cho et al. (2019)

location from which they arise on the parental tRNA. tRNA halves are 31–40 nucleotides long and generally arise from a mature parental tRNA (Kumar et al., 2016; Su et al., 2020). tRNA halves are classified based on whether it comes from the 5′ or 3′ end (tiR-5s come from the 5′ end, tiR-3s from the 3′ end). tRFs are generally between 14 and 30 nucleotides. tRF-5s come from the 5′ end of the mature parental tRNA. tRF-3s arise from the mature parental 3′ end; tRF-1s come from the trailer of the parental precursor tRNA. tRF-5s and tRF-3s can be further subclassified based on length distribution, with peaks of tRF-5s at 14 to 16 nucleotides (tRF-5a), 22 to 24 nucleotides (tRF-5b), and 28 to 30 nucleotides (tRF-5c). tRF-3s have peak lengths at around 18 nucleotides (tRF-3a) and 22 nucleotides (tRF-3b) (Kumar et al., 2016; Su et al., 2020).

The discrete length distributions of tRFs suggest specific cleavage by cellular ribonucleases. However, with the exception of tRF-1s, a general biogenesis mechanism for highly expressed tRFs remains to be elucidated. tRF-1s were one of the first tRFs to be characterized (Lee et al., 2009). tRF-1s arise from RNase Z (also known as ELAC1/2) cleavage of the precursor tRNA trailer sequence (**Figure 1**). tRF-5s and tRF-3s on the other hand, have a generally unelucidated biogenesis mechanism (**Figure 1**). Several groups have suggested the role of DICER1 in tRF biogenesis (Maute et al., 2013; Liu S. et al., 2018; Reinsborough et al., 2019; Di Fazio et al., 2022), however DICER1 knockout cell lines still have unaltered amounts of several highly abundant tRF-5s, tRF-3s, and tRF-1s (Kumar et al., 2016; Kuscu et al., 2018). Although DICER1 may not play a general role in tRF biogenesis, some tRFs may be produced by DICER1 cleavage. For example, Hasler et al. (2016) found that in the absence of the tRNA maturation protein SSB/La, some tRNAs may fold into an alternative structure, producing a hairpin (Hasler et al., 2016). This hairpin structure is then an optimal substrate for DICER1 cleavage. Additionally, Di Fazio et al. (2022) show that a subset of tRFs decrease under DICER1 knockdown conditions, and that tRNAs incubated with DICER1 can produce tRFs (Di Fazio et al., 2022). The discrepancy between Di Fazio et al. (2022) and Kumar et al. (2016) or Kuscu et al. (2018) may be due to the tRFs analyzed. Perhaps the different approaches for DICER1 depletion also affect the levels of tRFs. One technical limitation of both studies is that no spike-ins were used. Since miRNAs make up the majority of reads in small RNA sequencing data, and total mapped reads are used to normalize small RNA sequencing data, a substantial amount of

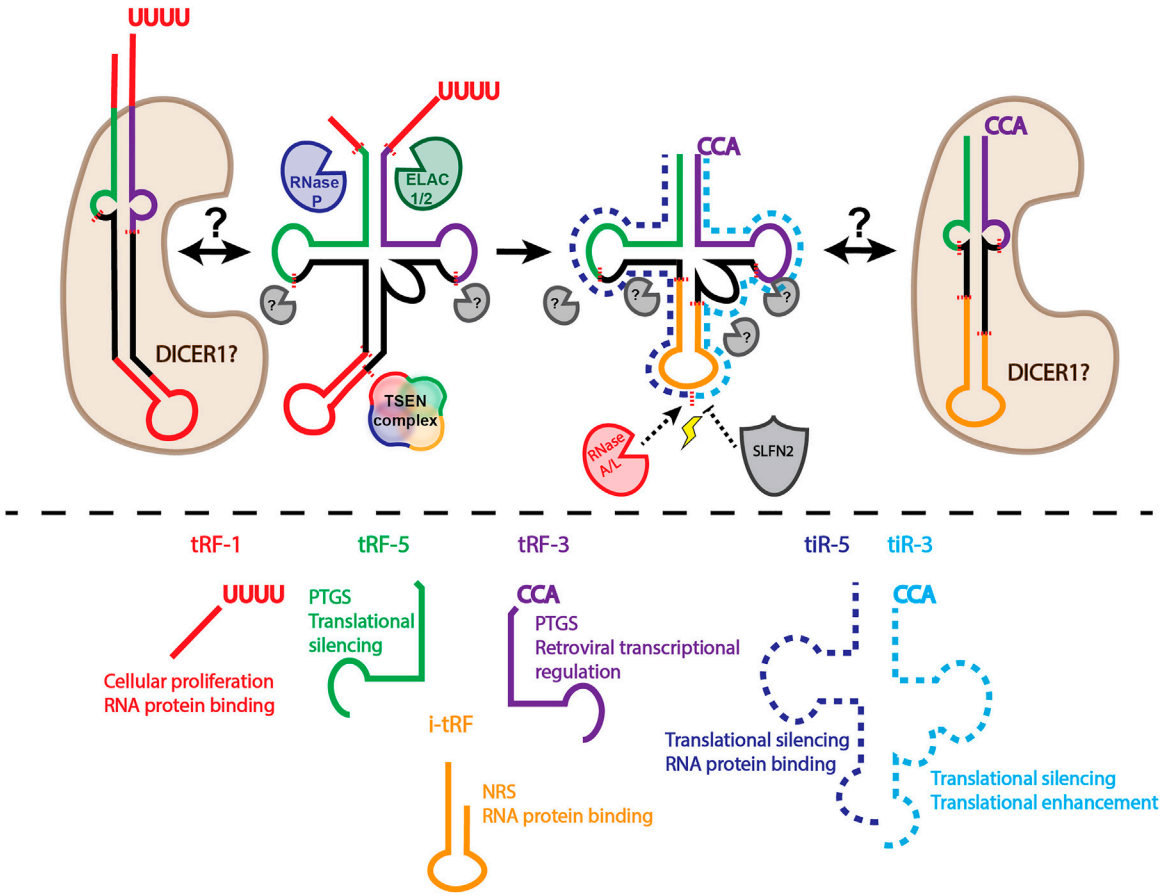

FIGURE 1 | Biogenesis and classification of tRFs and tRNA halves. Above dashed line: tRNAs undergo extensive processing and modification to generate a mature tRNA capable of being amino acylated. Precursor tRNAs have 5′ leader sequences removed by RNase P. 3′ trailer sequences removed by ELAC1/2 (also known as RNase Z) produces tRF-1s. Introns must be removed by the TSEN complex. Addition of a non-templated CCA, along with installment of necessary RNA modifications completes tRNA maturation. Cleavage of the mature tRNA produces tRFs classified based on length and origin on the parental tRNA. It is unclear if DICER1 is responsible for tRF biogenesis when tRNAs are folded in an alternative hairpin structure, rather than the canonical cloverleaf structure. It is important to note that DICER1 knockout does not eliminate production of many tRFs, leaving the identity of the enzyme that is necessary for tRF biogenesis unknown. In stressful conditions (lightning bolt), RNase A family members, such as ANG, cleave mature tRNAs in the anticodon loop, producing tRNA halves (tiRs). SLFN2 can block ANG mediated tRNA cleavage under stress conditions. Below dashed line: classification of tRFs and tiRs and the top two functions associated with each class based on the amount of experimental evidence. The functions also represent the potential therapeutic application for each tRF/tiR class. PTGS, post-transcriptional gene silencing; NRS, nascent RNA silencing.

bias can be introduced. Finally, a DICER1 dependent and DICER1 independent biogenesis mechanism are not incompatible. Perhaps, as Hasler et al. (2016) have shown for a particular subset of tRFs, some tRNAs can fold into a hairpin structure, making them a higher affinity DICER1 substrate, while other tRNAs are more likely to form a canonical cloverleaf structure (**Figure 1**). The propensity of a particular tRNA to fold into a hairpin vs. cloverleaf and how this influences tRF biogenesis is understudied. However, it would not be surprising if there were cell type variations due to differential tRNA expression, modification, or protein binding. As such, these experiments would require a modification-aware tRNA folding approach.

tiR biogenesis may also have more than one mechanism. Initially, tiRs were found to be upregulated under various stress conditions, giving them the name stress-induced tRNA halves. The RNase IV enzyme, angiogenin (ANG), was identified to be the enzyme responsible for tiR production under stress conditions and the 5′-terminal oligoguanylate (TOG) motif was found to be present in these tiRs (Ivanov et al., 2011; Saikia et al., 2014; Honda et al., 2015; Liu S. et al., 2018; Hogg et al., 2020). However, ANG KO does not reduce the levels of basally expressed (non-stress induced) tiRs (Su et al., 2019). Evidence of tiR production by other RNases is accumulating. RNase L was found to produce tiRs in a TOG independent manner (Donovan et al., 2017). Other RNase A family members have also been suggested to play a role in tiR production (Akiyama et al., 2019). These findings highlight the granularity of tRF and tiR production: ultimately, the

identification of a grand, unifying biogenesis mechanism for all tRFs and tiRs may not be attainable.

FUNCTION OF tRFs and tiRs

tRFs Enter RISC and Engage in Post-transcriptional Gene Silencing

In order to highlight the potential of tRFs to enhance therapeutic small RNA development, it is important to understand their endogenous cellular roles. The first report of a biological function for tRFs was reported for tRF-1001 (Lee et al., 2009). This tRF was highly abundant in cancer cell lines and was found to be required for cell proliferation. Of note, no detectable miRNA-like function was found for tRF-1001 in this study. The mechanism by which tRF-1001 regulates cellular proliferation still remains to be determined, but a miRNA-like mechanism is unlikely.

The lack of miRNA-like functions for tRF-1s was also established in another study (Haussecker et al., 2010). Transfection of a reporter and an oligonucleotide antisense to cand45 (tRFdb ID tRF-1001) did not derepress the luciferase reporter. Surprisingly, the reporter was further repressed by anti-tRF-1001 introduction. These results may be explained by a mechanism in which addition of an antisense oligo stabilizes tRF-1001, rather than interfering with its function. Interestingly, a more global meta-analysis of tRFs associated with AGO proteins revealed a striking absence of tRF-1s with AGO1-4 (Kumar et al., 2014). Both results make it clear that tRF-1s generally lack base-pair mediated repression of target mRNAs under basal conditions.

In the one case that tRF-1s are associated with miRNA-like repression, the tRF-1 is generated by DICER1 cleavage. DICER1 cleavage of tRNAs can occur when the precursor tRNA maturation protein, SSB/La, is depleted (Hasler et al., 2016). Under these conditions, RNase Z cannot cleave the precursor trailer sequence, allowing the tRNA to possibly form a hairpin, a substrate amenable to DICER1 cleavage. Overexpression of the tRF-1, either *via* mimic transfection, shRNA, or parental tRNA mediated overexpression led to repression of a luciferase reporter. Although these data clearly support a role for tRF-1 mediated repression, it is unclear if the effects are mediated by the SSB/La-DICER1 regulatory axis, as the parental tRNA overexpression followed by luciferase reporter was not conducted in SSB/La or DICER1 deficient cells.

Unlike tRF-1s, tRF-3s have been shown to readily enter RISC and repress gene expression in a base-pairing specific manner. As alluded to previously, overexpression of parental tRNAs leads to a direct upregulation of tRF expression. Parental tRNA overexpression leads to tRF-3001a, -3003a, and -3009a generation and entry into AGO for efficient repression of luciferase reporters (Kuscu et al., 2018). Haussecker et al. (2010) also showed that type I tRFs (tRF-3s) can behave like miRNAs because transfection of an antisense oligo derepressed a luciferase reporter. In the context of cancer, CU1276 (tRF-3027b) was found to be absent from germinal center derived lymphomas, present in normal germinal centers, and can downregulate RPA1 in a sequence specific manner (Maute et al., 2013). For tRF-3 the evidence is strong that the repression does not require DICER1, because tRNA overexpression mediated repression of tRF-3 reporters continues in DICER1 knock-out cells (Kuscu et al., 2018). Importantly, the repression of tRF-3 targets when tRNAs are overexpressed requires AGO and requires seed-match with the 3' UTR of the target (Kuscu et al., 2018).

The difference between the ability of tRF-1s and tRF-3s to repress target gene expression is unclear. The answer may lie in the inherent differences between the two classes: 1) different biogenesis enzymes (Vogel et al., 2005); 2) tRF-1s are likely to be single stranded (Lee et al., 2009), while the biogenesis of tRF-3s may involve a double stranded intermediate; or 3) undescribed sequence or modification difference; 4) differential association with RISC accessory proteins (Haussecker et al., 2010).

Another report found that two tRF-3s and one tRF-5 produced by rhizobial bacteria are enriched in soybean root nodules (Ren et al., 2019). These tRFs appeared to regulate soybean host genes in a miRNA-like manner because rhizobial tRF targets were predicted using plant miRNA target rules, overexpression of mimic rhizobial tRFs repressed predicted targets, and depletion of rhizobial tRFs resulted in an increase in predicted targets. A tRF-5 was also identified to regulate gene expression post-transcriptionally *via* base-pairing in the context of respiratory syncytial virus (RSV) infection (Deng et al., 2015). In this case, a tRF-5 derived from GluCTC downregulated expression of APOER2, which enhanced RSV replication. These findings highlight the ability of tRFs to behave like bona fide miRNAs, function in viral pathogenesis, and function across the kingdoms of life.

Perhaps one of the most important roles for tRFs may be in the function of stem cells and germ cells, hinting at a fundamental and primordial function for this class of small RNAs derived from tRNAs. tRFs have been found to be highly expressed in mouse stem cells where they suppress retrotransposition of endogenous retroviruses (Schorn et al., 2017). The 18 nucleotide tRF-3as accomplish this by blocking reverse transcription. 22 nucleotide tRF-3bs suppress retrotransposition *via* post-transcriptional silencing of retrotransposon gene expression. tRF's ability to interact with a retroelement may not come as a surprise, since retroviruses usurp host cell tRNAs for priming in reverse transcription (Mak and Kleiman, 1997). In another example of tRF's roles in early embryogenesis and germ cells, tRFs were found to be highly abundant in mature mouse sperm (Sharma et al., 2016; Sharma et al., 2018). tRF-5 from tRNA-GlyGCC (tRF-GG) was determined to be a repressor of MERVL *via* regulation of histone protein level and Cajal-body dependent noncoding RNAs (Boskovic et al., 2020). Finally, it has been shown that tRFs derived from tRNA primers can inhibit HIV reverse transcription (Yeung et al., 2009), or enhance HTLV-1 reverse transcription (Ruggero et al., 2014).

Therapeutic Potential of tRFs in Post-transcriptional Gene Silencing

Interestingly, most studies that determine tRF mediated repression, either endogenously or *via* tRNA or tRF mimic overexpression, observe at most a 40–60% reduction in target luciferase reporter expression (Haussecker et al., 2010; Maute et al., 2013; Kuscu et al., 2018). This is perhaps due to the fact that

most tRFs appear to enter AGO1, 3 and 4, rather than AGO2 which has slicer activity. Overexpression of either AGO2 (Haussecker et al., 2010; Maute et al., 2013) or knockout of DICER1 (Kuscu et al., 2018) in these systems leads to enhanced repression. These data suggest that availability of AGO2 binding is essential for miRNA-like efficiency in repression. This makes potential tRF-like therapeutics less useful if maximal repression of the target gene is required, which may lead to questioning of the utility of tRF mediated post-transcriptional gene silencing as a therapeutic approach. However, the moderate attenuation of gene expression mediated by tRFs may prove useful in disease contexts in which gene expression needs to be knocked down, but some degree of expression is still required for normal function. For example, Beckwith-Wiedemann syndrome is an imprinting disorder in which IGF2, among other genes, expression is too high (Wang et al., 2019; Borjas Mendoza and Mendez, 2021). IGF2 is a necessary gene for intrauterine growth and development, so too much repression of this gene would be detrimental. In fact, loss of IGF2 expression leads to Russell-Silver syndrome, a congenital growth syndrome which leads to failure to thrive (Saal et al., 2002). Thus, the correct balance of IGF2 expression needs to be achieved, and a tRF-like mechanism may be more amenable to this sort of repression, rather than siRNA or miRNA-like approaches.

tRFs can Regulate Nascent RNA Expression

One of the newest functions of tRFs is in nascent RNA silencing (Di Fazio et al., 2022). DICER1 dependent tRFs were found to target introns of genes in the nucleus in an AGO2 dependent manner. Nuclear functions of RISC have been reported (Gagnon et al., 2014), however, this is the first time tRFs have been attributed with this function. One potential reason tRFs may be uniquely suited to regulate nuclear gene expression either co- or post-transcriptionally may be their single stranded nature. David Corey and colleagues reported that single stranded small RNAs can readily bind nuclear AGO2, whereas double stranded siRNAs can only bind cytoplasmic AGO2, likely due to the nucleus missing accessory double stranded RNA loading factors.

There may be several reasons that tRFs are able to engage in nascent RNA silencing besides their single strandedness. One underexplored feature may be the modifications present on tRFs. It is possible that certain modifications allow tRFs to enter the nucleus and regulate gene expression. Although exciting, a more thorough understanding of nascent RNA silencing machinery and biochemistry will be necessary if it is to become a potential therapeutic modality.

tRFs and tiRs can Alter Translation

tRF-3s, and under certain conditions, tRF-1s, have been shown to regulate gene expression post-transcriptionally *via* base-pairing (Haussecker et al., 2010; Maute et al., 2013; Deng et al., 2015; Kuscu et al., 2018; Ren et al., 2019). Sobala and Hutvagner suggested that tRF-5s do not function in this way, and in fact are capable of reducing mRNA translation in the absence of base-pairing (Sobala and Hutvagner, 2013). In particular, a "GG" dinucleotide appears to be necessary, but not sufficient, to mediate repression of a luciferase reporter (Sobala and Hutvagner, 2013). These tRFs repress translation by associating with polysomes. This work is in line with previous work showing that tRNA fragments and halves derived from the 5′ end of tRNAs generally inhibit translation across the domains of life (Yamasaki et al., 2009; Zhang et al., 2009; Ivanov et al., 2011; Gebetsberger et al., 2012). tiR-5s can be produced under stress conditions. For example, stress induced by arsenite treatment, heat shock, and UV radiation induced cleavage of tRNAs *via* ANG, which led to translation inhibition in a phospho-eIF2α independent manner (Yamasaki et al., 2009). In a follow-up study, tiRs were found to work with YB-1 to displace eIF4G/A and eIF4F from uncapped mRNAs and m7G caps, respectively (Ivanov et al., 2011). Four to five guanines, or 5′ terminal oligo guanine (5′-TOG) motifs, were also found to be important for translation inhibition in this study, as tiR-5s from tRNA-Ala and tRNA-Cys with 5′-TOG motifs inhibit translation much more efficiently than tiRs without the motif. In sum, tiR-5s and tRF-5s seem to reduce global translation, and multiple guanines seem to be important for this mechanism.

As opposed to tiR-5s, much less seems to be known about tiR-3 function. A tiR-3 derived from tRNA-ThrAGU was found to be upregulated in starvation conditions in *Trypanosoma brucei*, one of the parasitic protozoans that causes the neglected disease sleeping sickness (Fricker et al., 2019). In contrast to tRF-5s and tiR-5s, the tiR-3 stimulated translation during starvation recovery (Fricker et al., 2019). Perhaps targeting this tiR-3 and preventing translation stimulation in post-starvation protozoa could be an alternative therapeutic approach for sleeping sickness caused by this subspecies.

Therapeutic Potential of tRF and tiR Translation Inhibition

The ability of tRFs and tiRs to regulate global translation sets up a potential paradigm for designing a new class of small RNA therapeutics. tRF-5s and tiR-5s may be designed to inhibit translation in disease states where an aberrant upregulation in translation is essential for pathogenesis. For example, mRNA translation is an essential process in rapidly proliferating cancer cells (Malina et al., 2012). The mTOR inhibitor everolimus is used alone or as part of chemotherapeutics regimens in breast cancer, renal clear cell carcinoma, subependymal giant cell astrocytoma, and advanced neuroendocrine tumors (DRUGBANK, 2022). In the case of renal clear cell carcinoma, patients often develop resistance to mTOR inhibitors everolimus and temsirolimus (Voss et al., 2011). In the future, it will be interesting to evaluate the effectiveness of tRF-5/tiR-5 mediated global translation inhibition as a cancer therapy.

The benefit of tRF and tiR mediated translation inhibition as a therapeutic approach is that it does not require the target cell to contain or efficiently use the RNA interference machinery. This is especially important in the context of bacteria, which does not have a system analogous to RNA interference. Antimicrobial resistance is one of the top 10 global health threats to humanity according to the World Health Organization (WHO, 2022), therefore novel approaches are needed to address this issue. tRNA fragments were first described in *E. coli* (Levitz et al.,

1990), but only recently has research into the global expression and biological roles of tRFs in microbes been conducted (Li and Stanton, 2021). Of note, several currently used antibiotics are small molecule inhibitors of translation (Chellat et al., 2016), positioning tRF and tiR mediated inhibition of translation as a viable approach. The development of antisense oligonucleotides as antibiotics is of great interest due to the ease of design, alterations in response to resistance, and clear targeting (Kole et al., 2012; Xue et al., 2018). Delivery of oligonucleotides is a grand challenge in eukaryotic oligonucleotide therapeutics (Hammond et al., 2021), and this challenge is no different in prokaryotes. However, conjugating oligonucleotides to peptides, vitamin B12, or encapsulation in nanoparticles has greatly improved the delivery of oligonucleotides into bacteria (Xue et al., 2018). It is also becoming clear that microbes (including Gram positive bacteria) are able to package RNAs and other cargo into extracellular vesicles (Domingues and Nielsen, 2017; Liu Y. et al., 2018; Toyofuku et al., 2019). These vesicles enable cross-talk between other bacteria as well as the host. As mammalian extracellular vesicles and other nanoparticles are being developed as vectors for carrying small RNA therapies (Bost et al., 2021), it is conceivable that bacterial vesicles may also function as drug delivery vehicles. This seems to be the case and has been an active area of study (Li and Liu, 2020). Most antibiotic oligonucleotide therapy development focuses on antisense technology, however, tRFs and tiRs that inhibit translation could also be conjugated or encapsulated into delivery vehicles and could provide another tool in the antibiotic oligonucleotide therapy toolbox.

Of note, one limitation of tRF/tiR antibiotics might be the role that tiRs appear to play in the regulation of the RNA repair operon (Hughes et al., 2020). The function of this operon is important for survival following DNA damage, and tiR-5s bind the CARF domain of RtcR, leading to oligomerization and activation of the RNA repair operon. Potentially giving a growth advantage to bacteria with DNA damage may be circumvented by utilizing tiR based therapies without a 3′ cyclic phosphate (3′ cP), as a 3′ cP was necessary for optimal CARF domain binding. The role of alternative 3′ ends in tRF/tiR mediated translation inhibition requires further study.

Other Functions of tRFs

tRFs can Enhance Translation of Specific Transcripts

A surprising connection between tRFs and ribosomes was recently discovered. A 22 nucleotide tRF-3 derived from LeuCAG tRNA was found to bind and enhance the translation of RPS15 and RPS28 ribosomal mRNA (Kim et al., 2017). The tRF-3 binds RPS28 mRNA in the coding region across vertebrates and within the 3′ UTR in primates. The enhancement of translation is post-initiation and is conserved between mouse and human (Kim et al., 2019). Loss of this tRF results in apoptosis of cells in an orthotopic hepatocellular carcinoma model, indicating its importance in proliferation and tumorigenesis. These findings indicate that tRFs can be oncogenic.

tRFs can Bind Proteins and Affect Their Function

There are also reports of tRFs binding proteins and altering their function. For example, YBX1 binds to oncogenic transcripts and stabilizes them (Goodarzi et al., 2015). Internal tRFs (i-tRFs) derived from the anticodon region of parental tRNAs from Glu, Asp, Tyr, and Gly have a consensus sequence that binds and sequesters YBX1 from oncogenic transcripts, destabilizing them. These i-tRFs, therefore, function as tumor suppressors. A tumor suppressor tRF-3 derived from Glu tRNA was found to be expressed in normal mammary tissue but not breast cancer (Falconi et al., 2019). This tRF-3 could bind nucleolin (NCL), which sequestered NCL away from p53 mRNA and enhanced p53 mRNA translation (Falconi et al., 2019). In another study, 20 ANG dependent tiRs were found to interact with cytochrome c and reduce apoptosis in hyperosmotic conditions (Saikia et al., 2014). Finally, tRFs have also been implicated in viral pathogenesis. During tRNA maturation SSB/La binds to the trailer sequence and aids in tRNA maturation. Cho et al. (2019) found that SSB/La could interact with tRF_U3_1, derived from tRNA-Ser(TGA) also known as tRF-1001, and become sequestered in the cytoplasm. Since SSB/La binds to hepatitis C viral (HCV) internal ribosomal entry sites (IRES) (Pudi et al., 2003), sequestration of SSB/La by tRF_U3_1 reduced translation *via* the HCV IRES (Cho et al., 2019).

As we discover more biological roles of tRFs and tiRs and delineate their functions from miRNAs, we may begin to develop unique tRF-mimic and tRF antagonist based therapeutics. Such therapies are being developed for miRNAs, although there are no miRNA therapeutics in phase III clinical trials (Zhang et al., 2021). One major roadblock for miRNA based therapeutics that is absent in siRNA based therapeutics is the large number of putative miRNA targets, such that sponging or overexpression of miRNA may cause off-target effects (Zhang et al., 2021). This may also be a major roadblock in tRF based therapeutics, although rigorous prediction and validation of tRF targets is still in its infancy.

Delivery of Oligonucleotide Therapeutics is a Major Challenge

Delivery of oligonucleotides to their site of action is a major challenge (Dowdy, 2017; Roberts et al., 2020; Hammond et al., 2021). tRF based therapeutics would have many of the same delivery issues. Oligonucleotide delivery can be broadly classified into two steps: 1) tissue delivery, and 2) cytoplasmic delivery or endosomal escape. Tissue specific delivery of oligonucleotides is more amenable to organs that are involved in blood filtration, such as the liver and kidney. Tissue delivery is also currently more amenable to organ systems that can be directly accessed *via* injection, such as the eye or brain and spinal cord by intrathecal injection. Furthermore, Alnylam has had success with liver specific delivery of siRNA-based therapies that are conjugated to N-acetylgalactosamine (GalNAc) (Springer and Dowdy, 2018). Lipid nanoparticles (LNPs) also enable more targeted delivery into tissues. LNPs have been successfully used for delivery of COVID-19 mRNA vaccines and the recently approved PCSK9 siRNA for the treatment of hypercholesterolemia (Fitzgerald et al., 2017; Buschmann et al., 2021).

Delivery of small RNAs to tissues may also be enhanced by encapsulation in extracellular vesicles (O'Brien et al., 2020). In support of the use of extracellular vesicles as tRF and tiR delivery agents, tRFs and tiRs are enriched in T cell extracellular vesicles (Chiou et al., 2018). tRFs were packaged into extracellular vesicles and released from activated T cells. Reduced expression of tRFs that are normally packaged and released leads to enhanced T cell activation. Although the effect of endogenous extracellular vesicle tRFs and tiRs on recipient cells is underexplored, it is clear that overexpressed tiRs can be delivered to recipient cells and alter gene expression (Gámbaro et al., 2020). Mouse epididymosomes can also deliver tRF-5s to maturing sperm, which ultimately represses MERVL (Sharma et al., 2016).

Another challenge for tissue delivery is oligonucleotide stability in circulation (Paunovska et al., 2022). Much of this issue has been solved, either by encapsulation of the oligonucleotide in an LNP, or by installment of RNA modifications (Yu et al., 2019). Interestingly, tRNAs, and likely tRFs, are one of the most highly modified RNAs in the cell, which may confer some enhanced stability in the circulation (Pan, 2018).

The second challenge of delivery, endosomal escape, is still a major unresolved bottleneck in the oligonucleotide therapeutics field (Dowdy, 2017). Small molecules such as nigericin and chloroquine have been found to enhance endosomal escape (Heath et al., 2019; Orellana et al., 2019), however, these compounds are too toxic for clinical use (Brown et al., 2020). It does appear that LNP platforms are better suited for endosomal escape than GalNAc conjugated siRNA mediated delivery, but this comes at the expense of duration of action (Brown et al., 2020). Any tRF or tiR therapeutic would also need to overcome these barriers.

A Word of Caution for tRNA Based Therapeutics

Although tRNA based therapies are outside the scope of this review, it is a burgeoning field of development because nonsense suppressor tRNAs can prevent the formation of truncated, dysfunctional proteins (Porter et al., 2021). It is clear, however, that overexpressed tRNAs produce tRNA fragments. These tRNA fragments may cause off-target effects and lead to unpredictable side effects. In order to circumvent these effects, the biogenesis of tRFs and tiRs must continue to be thoroughly investigated. For example, it is clear that certain modifications can affect the production of tRFs ((He et al., 2021; Nagayoshi et al., 2021) and reviewed in (Lyons et al., 2018)). Parental tRNA cleavage induced by reactive oxygen species can also be prevented in T cells by binding Schlafen 2 (SLFN2) (Yue et al., 2021) (**Figure 1**). Findings like these will enable rational design of stable tRNA therapeutics.

CONCLUSIONS AND FUTURE DIRECTIONS

It is clear that tRFs/tiRs have important roles in biology in all domains of life. Mechanistically, tRFs/tiRs function differently, even between and within class distinctions. General trends in tRF/tiR's role in regulating nascent gene silencing, post-transcriptional gene silencing, and mRNA translation make this class of small RNAs one of the most versatile classes discovered to date. Small RNA therapeutics based on basic knowledge about miRNA function are experiencing a renaissance, with several RNAi based therapeutics on the market. Perhaps tRFs and tiR based therapeutics will follow suit. In order for tRFs/tiRs to reach the clinic, several challenges must be addressed. For example, it is clear that tRF-5s and tiR-5s can behave as protein synthesis inhibitors. What is less clear is whether there is an RNA modification or RNA sequence code that is important for tRF-5 and tiR-5 mediated protein synthesis inhibition. For example, PUS7 mediated pseudouridylation is important for protein synthesis inhibition in stem cells (Guzzi et al., 2018; Guzzi et al., 2022). Since tRNAs have on average thirteen modifications per molecule (Pan, 2018), it would not be surprising if other tRF/tiR modifications regulate protein synthesis, perhaps in a combinatorial or tissue specific manner. tRF/tiR modifications may provide other useful roles and insights into tRF and tiR based therapeutics. For example, tRF and tiR modifications from species adapted to extreme conditions, such as some bacteria and archea (Babski et al., 2014; Li and Stanton, 2021), may be useful for further stabilization of synthetic tRFs and tiRs or confer novel functions.

Another challenge is understanding the role that tRFs play in nascent RNA silencing and post-transcriptional gene silencing. Do all tRFs follow the same rules (i.e. seed based pairing, supplemental base pairing, etc) as miRNAs when it comes to post-transcriptional gene silencing? What role do tRF modifications play in nascent RNA silencing and post-transcriptional gene silencing? Since most tRF target prediction tools are built on miRNA-based assumptions and rules or more general complementary pairing (Li et al., 2021; Xiao et al., 2021; Zhou et al., 2021), are we capturing the most robust tRF targets? Finally, it is unclear what features of tRFs/tiRs make them more likely to behave primarily as miRNAs, interact with RNA binding proteins, or interact with other RNAs. In order for tRFs/tiRs to be useful in the clinical setting, these questions will need to be addressed.

AUTHOR CONTRIBUTIONS

BW and AD conceived and contributed to the writing of the manuscript. All authors read and approved the submitted version of the manuscript.

FUNDING

This work was supported by NIH grant R01 AR067712 (to AD) and the NIH NCI Grant F30 CA254134 (to BW).

REFERENCES

Akiyama, Y., Lyons, S., Fay, M. M., Abe, T., Anderson, P., and Ivanov, P. (2019). Multiple Ribonuclease A Family Members Cleave Transfer RNAs in Response to Stress. *bioRxiv*, 811174. doi:10.1101/811174

Babski, J., Maier, L.-K., Heyer, R., Jaschinski, K., Prasse, D., Jäger, D., et al. (2014). Small Regulatory RNAs in Archaea. *RNA Biol.* 11, 484–493. doi:10.4161/rna.28452

Borjas Mendoza, P. A., and Mendez, M. D. (2021). "Beckwith Wiedemann Syndrome," in *StatPearls* (Treasure Island, FL: StatPearls Publishing). Available at: https://www.ncbi.nlm.nih.gov/pubmed/32644419.

Boskovic, A., Bing, X. Y., Kaymak, E., and Rando, O. J. (2020). Control of Noncoding RNA Production and Histone Levels by a 5′ tRNA Fragment. *Genes Dev.* 34, 118–131. doi:10.1101/gad.332783.119

Bost, J. P., Barriga, H., Holme, M. N., Gallud, A., Maugeri, M., Gupta, D., et al. (2021). Delivery of Oligonucleotide Therapeutics: Chemical Modifications, Lipid Nanoparticles, and Extracellular Vesicles. *ACS Nano* 15, 13993–14021. doi:10.1021/acsnano.1c05099

Brown, C. R., Gupta, S., Qin, J., Racie, T., He, G., Lentini, S., et al. (2020). Investigating the Pharmacodynamic Durability of GalNAc-siRNA Conjugates. *Nucleic Acids Res.* 48, 11827–11844. doi:10.1093/nar/gkaa670

Buschmann, M. D., Carrasco, M. J., Alishetty, S., Paige, M., Alameh, M. G., and Weissman, D. (2021). Nanomaterial Delivery Systems for mRNA Vaccines. *Vaccines* 9, 65. doi:10.3390/vaccines9010065

Chellat, M. F., Raguž, L., and Riedl, R. (2016). Targeting Antibiotic Resistance. *Angew. Chem. Int. Ed.* 55, 6600–6626. doi:10.1002/anie.201506818

Cherlin, T., Magee, R., Jing, Y., Pliatsika, V., Loher, P., and Rigoutsos, I. (2020). Ribosomal RNA Fragmentation into Short RNAs (rRFs) Is Modulated in a Sex- and Population of Origin-specific Manner. *BMC Biol.* 18, 38. doi:10.1186/s12915-020-0763-0

Chiou, N.-T., Kageyama, R., and Ansel, K. M. (2018). Selective Export into Extracellular Vesicles and Function of tRNA Fragments during T Cell Activation. *Cel Rep.* 25, 3356–3370. doi:10.1016/j.celrep.2018.11.073

Cho, H., Lee, W., Kim, G.-W., Lee, S.-H., Moon, J.-S., Kim, M., et al. (2019). Regulation of La/SSB-dependent Viral Gene Expression by Pre-tRNA 3′ Trailer-Derived tRNA Fragments. *Nucleic Acids Res.* 47, 9888–9901. doi:10.1093/nar/gkz732

Deng, J., Ptashkin, R. N., Chen, Y., Cheng, Z., Liu, G., Phan, T., et al. (2015). Respiratory Syncytial Virus Utilizes a tRNA Fragment to Suppress Antiviral Responses through a Novel Targeting Mechanism. *Mol. Ther.* 23, 1622–1629. doi:10.1038/mt.2015.124

Di Fazio, A., Schlackow, M., Pong, S. K., Alagia, A., and Gullerova, M. (2022). Dicer Dependent tRNA Derived Small RNAs Promote Nascent RNA Silencing. *Nucleic Acids Res.* 50, 1734–1752. doi:10.1093/nar/gkac022

Domingues, S., and Nielsen, K. M. (2017). Membrane Vesicles and Horizontal Gene Transfer in Prokaryotes. *Curr. Opin. Microbiol.* 38, 16–21. doi:10.1016/j.mib.2017.03.012

Donovan, J., Rath, S., Kolet-Mandrikov, D., and Korennykh, A. (2017). Rapid RNase L-Driven Arrest of Protein Synthesis in the dsRNA Response without Degradation of Translation Machinery. *RNA* 23, 1660–1671. doi:10.1261/rna.062000.117

Dowdy, S. F. (2017). Overcoming Cellular Barriers for RNA Therapeutics. *Nat. Biotechnol.* 35, 222–229. doi:10.1038/nbt.3802

DRUGBANK (2022). Everolimus. Available at: https://go.drugbank.com/drugs/DB01590 (Accessed February 21, 2022).

Fagan, S. G., Helm, M., and Prehn, J. H. M. (2021). tRNA-derived Fragments: A New Class of Non-coding RNA with Key Roles in Nervous System Function and Dysfunction. *Prog. Neurobiol.* 205, 102118. doi:10.1016/j.pneurobio.2021.102118

Falaleeva, M., and Stamm, S. (2013). Processing of snoRNAs as a New Source of Regulatory Non-coding RNAs. *Bioessays* 35, 46–54. doi:10.1002/bies.201200117

Falconi, M., Giangrossi, M., Zabaleta, M. E., Wang, J., Gambini, V., Tilio, M., et al. (2019). A Novel 3′-tRNAGlu-Derived Fragment Acts as a Tumor Suppressor in Breast Cancer by Targeting Nucleolin. *FASEB J.* 33, 13228–13240. doi:10.1096/fj.201900382RR

Fitzgerald, K., White, S., Borodovsky, A., Bettencourt, B. R., Strahs, A., Clausen, V., et al. (2017). A Highly Durable RNAi Therapeutic Inhibitor of PCSK9. *N. Engl. J. Med.* 376, 41–51. doi:10.1056/NEJMoa1609243

Fricker, R., Brogli, R., Luidalepp, H., Wyss, L., Fasnacht, M., Joss, O., et al. (2019). A tRNA Half Modulates Translation as Stress Response in Trypanosoma Brucei. *Nat. Commun.* 10, 118. doi:10.1038/s41467-018-07949-6

Gámbaro, F., Li Calzi, M., Fagúndez, P., Costa, B., Greif, G., Mallick, E., et al. (2020). Stable tRNA Halves Can Be Sorted into Extracellular Vesicles and Delivered to Recipient Cells in a Concentration-dependent Manner. *RNA Biol.* 17, 1168–1182. doi:10.1080/15476286.2019.1708548

Gagnon, K. T., Li, L., Chu, Y., Janowski, B. A., and Corey, D. R. (2014). RNAi Factors Are Present and Active in Human Cell Nuclei. *Cel Rep.* 6, 211–221. doi:10.1016/j.celrep.2013.12.013

Gebetsberger, J., Zywicki, M., Künzi, A., and Polacek, N. (2012). tRNA-Derived Fragments Target the Ribosome and Function as Regulatory Non-coding RNA inHaloferax Volcanii. *Archaea* 2012, 1–11. doi:10.1155/2012/260909

Goodarzi, H., Liu, X., Nguyen, H. C. B., Zhang, S., Fish, L., and Tavazoie, S. F. (2015). Endogenous tRNA-Derived Fragments Suppress Breast Cancer Progression *via* YBX1 Displacement. *Cell* 161, 790–802. doi:10.1016/j.cell.2015.02.053

Guzzi, N., Cieśla, M., Ngoc, P. C. T., Lang, S., Arora, S., Dimitriou, M., et al. (2018). Pseudouridylation of tRNA-Derived Fragments Steers Translational Control in Stem Cells. *Cell* 173, 1204–1216. doi:10.1016/j.cell.2018.03.008

Guzzi, N., Muthukumar, S., Cieśla, M., Todisco, G., Ngoc, P. C. T., Madej, M., et al. (2022). Pseudouridine-modified tRNA Fragments Repress Aberrant Protein Synthesis and Predict Leukaemic Progression in Myelodysplastic Syndrome. *Nat. Cel Biol.* 24, 299–306. doi:10.1038/s41556-022-00852-9

Hammond, S. M., Aartsma-Rus, A., Alves, S., Borgos, S. E., Buijsen, R. A. M., Collin, R. W. J., et al. (2021). Delivery of Oligonucleotide-based Therapeutics: Challenges and Opportunities. *EMBO Mol. Med.* 13, e13243. doi:10.15252/emmm.202013243

Hasler, D., Lehmann, G., Murakawa, Y., Klironomos, F., Jakob, L., Grässer, F. A., et al. (2016). The Lupus Autoantigen La Prevents Mis-Channeling of tRNA Fragments into the Human MicroRNA Pathway. *Mol. Cel* 63, 110–124. doi:10.1016/j.molcel.2016.05.026

Haussecker, D., Huang, Y., Lau, A., Parameswaran, P., Fire, A. Z., and Kay, M. A. (2010). Human tRNA-Derived Small RNAs in the Global Regulation of RNA Silencing. *RNA* 16, 673–695. doi:10.1261/rna.2000810

He, C., Bozler, J., Janssen, K. A., Wilusz, J. E., Garcia, B. A., Schorn, A. J., et al. (2021). TET2 Chemically Modifies tRNAs and Regulates tRNA Fragment Levels. *Nat. Struct. Mol. Biol.* 28, 62–70. doi:10.1038/s41594-020-00526-w

Heath, N., Osteikoetxea, X., de Oliveria, T. M., Lázaro-Ibáñez, E., Shatnyeva, O., Schindler, C., et al. (2019). Endosomal Escape Enhancing Compounds Facilitate Functional Delivery of Extracellular Vesicle Cargo. *Nanomedicine* 14, 2799–2814. doi:10.2217/nnm-2019-0061

Hogg, M. C., Rayner, M., Susdalzew, S., Monsefi, N., Crivello, M., Woods, I., et al. (2020). 5′ValCAC tRNA Fragment Generated as Part of a Protective Angiogenin Response Provides Prognostic Value in Amyotrophic Lateral Sclerosis. *Brain Commun.* 2, fcaa138. doi:10.1093/braincomms/fcaa138

Honda, S., Loher, P., Shigematsu, M., Palazzo, J. P., Suzuki, R., Imoto, I., et al. (2015). Sex Hormone-dependent tRNA Halves Enhance Cell Proliferation in Breast and Prostate Cancers. *Proc. Natl. Acad. Sci. U.S.A.* 112, E3816–E3825. doi:10.1073/pnas.1510077112

Hughes, K. J., Chen, X., Burroughs, A. M., Aravind, L., and Wolin, S. L. (2020). An RNA Repair Operon Regulated by Damaged tRNAs. *Cel Rep.* 33, 108527. doi:10.1016/j.celrep.2020.108527

Ivanov, P., Villen, J., Gygi, S. P., Anderson, P., and Anderson, P. (2011). Angiogenin-induced tRNA Fragments Inhibit Translation Initiation. *Mol. Cel* 43, 613–623. doi:10.1016/j.molcel.2011.06.022

Jackowiak, P., Hojka-Osinska, A., Philips, A., Zmienko, A., Budzko, L., Maillard, P., et al. (2017). Small RNA Fragments Derived from Multiple RNA Classes - the Missing Element of Multi-Omics Characteristics of the Hepatitis C Virus Cell Culture Model. *BMC Genomics* 18, 502. doi:10.1186/s12864-017-3891-3

Jia, Y., Tan, W., and Zhou, Y. (2020). Transfer RNA-Derived Small RNAs: Potential Applications as Novel Biomarkers for Disease Diagnosis and Prognosis. *Ann. Transl. Med.* 8, 1092. doi:10.21037/atm-20-2797

Kim, H. K., Fuchs, G., Wang, S., Wei, W., Zhang, Y., Park, H., et al. (2017). A Transfer-RNA-Derived Small RNA Regulates Ribosome Biogenesis. *Nature* 552, 57–62. doi:10.1038/nature25005

Kim, H. K., Xu, J., Chu, K., Park, H., Jang, H., Li, P., et al. (2019). A tRNA-Derived Small RNA Regulates Ribosomal Protein S28 Protein Levels after Translation

Initiation in Humans and Mice. *Cel Rep.* 29, 3816–3824. doi:10.1016/j.celrep.2019.11.062

Kole, R., Krainer, A. R., and Altman, S. (2012). RNA Therapeutics: beyond RNA Interference and Antisense Oligonucleotides. *Nat. Rev. Drug Discov.* 11, 125–140. doi:10.1038/nrd3625

Kumar, P., Anaya, J., Mudunuri, S. B., and Dutta, A. (2014). Meta-analysis of tRNA Derived RNA Fragments Reveals that They Are Evolutionarily Conserved and Associate with AGO Proteins to Recognize Specific RNA Targets. *BMC Biol.* 12, 78. doi:10.1186/s12915-014-0078-0

Kumar, P., Kuscu, C., and Dutta, A. (2016). Biogenesis and Function of Transfer RNA-Related Fragments (tRFs). *Trends Biochem. Sci.* 41, 679–689. doi:10.1016/j.tibs.2016.05.004

Kuscu, C., Kumar, P., Kiran, M., Su, Z., Malik, A., and Dutta, A. (2018). tRNA Fragments (tRFs) Guide Ago to Regulate Gene Expression post-transcriptionally in a Dicer-independent Manner. *RNA* 24, 1093–1105. doi:10.1261/rna.066126.118

Lee, Y. S., Shibata, Y., Malhotra, A., and Dutta, A. (2009). A Novel Class of Small RNAs: tRNA-Derived RNA Fragments (tRFs). *Genes Dev.* 23, 2639–2649. doi:10.1101/gad.1837609

Levitz, R., Chapman, D., Amitsur, M., Green, R., Snyder, L., and Kaufmann, G. (1990). The Optional *E. coli* Prr Locus Encodes a Latent Form of Phage T4-Induced Anticodon Nuclease. *EMBO J.* 9, 1383–1389. doi:10.1002/j.1460-2075.1990.tb08253.x

Li, R., and Liu, Q. (2020). Engineered Bacterial Outer Membrane Vesicles as Multifunctional Delivery Platforms. *Front. Mater.* 7, 202. doi:10.3389/fmats.2020.00202

Li, Z., and Stanton, B. A. (2021). Transfer RNA-Derived Fragments, the Underappreciated Regulatory Small RNAs in Microbial Pathogenesis. *Front. Microbiol.* 12, 687632. doi:10.3389/fmicb.2021.687632

Li, N., Shan, N., Lu, L., and Wang, Z. (2021). tRFtarget: a Database for Transfer RNA-Derived Fragment Targets. *Nucleic Acids Res.* 49, D254–D260. doi:10.1093/nar/gkaa831

Liu, S., Chen, Y., Ren, Y., Zhou, J., Ren, J., Lee, I., et al. (2018a). A tRNA-Derived RNA Fragment Plays an Important Role in the Mechanism of Arsenite -induced Cellular Responses. *Sci. Rep.* 8, 16838. doi:10.1038/s41598-018-34899-2

Liu, Y., Defourny, K. A. Y., Smid, E. J., and Abee, T. (2018b). Gram-Positive Bacterial Extracellular Vesicles and Their Impact on Health and Disease. *Front. Microbiol.* 9, 1502. doi:10.3389/fmicb.2018.01502

Lyons, S. M., Fay, M. M., and Ivanov, P. (2018). The Role of RNA Modifications in the Regulation of tRNA Cleavage. *FEBS Lett.* 592, 2828–2844. doi:10.1002/1873-3468.13205

Mak, J., and Kleiman, L. (1997). Primer tRNAs for Reverse Transcription. *J. Virol.* 71, 8087–8095. doi:10.1128/JVI.71.11.8087-8095.1997

Malina, A., Mills, J. R., and Pelletier, J. (2012). Emerging Therapeutics Targeting mRNA Translation. *Cold Spring Harbor. Perspect. Biol.* 4, a012377. doi:10.1101/cshperspect.a012377

Maute, R. L., Schneider, C., Sumazin, P., Holmes, A., Califano, A., Basso, K., et al. (2013). tRNA-derived microRNA Modulates Proliferation and the DNA Damage Response and Is Down-Regulated in B Cell Lymphoma. *Proc. Natl. Acad. Sci. U.S.A.* 110, 1404–1409. doi:10.1073/pnas.1206761110

Nagayoshi, Y., Chujo, T., Hirata, S., Nakatsuka, H., Chen, C.-W., Takakura, M., et al. (2021). Loss of Ftsj1 Perturbs Codon-specific Translation Efficiency in the Brain and Is Associated with X-Linked Intellectual Disability. *Sci. Adv.* 7, eabf3072. doi:10.1126/sciadv.abf3072

O'Brien, K., Breyne, K., Ughetto, S., Laurent, L. C., and Breakefield, X. O. (2020). RNA Delivery by Extracellular Vesicles in Mammalian Cells and its Applications. *Nat. Rev. Mol. Cel Biol.* 21, 585–606. doi:10.1038/s41580-020-0251-y

Orellana, E. A., Abdelaal, A. M., Rangasamy, L., Tenneti, S., Myoung, S., Low, P. S., et al. (2019). Enhancing MicroRNA Activity through Increased Endosomal Release Mediated by Nigericin. *Mol. Ther. Nucleic Acids* 16, 505–518. doi:10.1016/j.omtn.2019.04.003

Pan, T. (2018). Modifications and Functional Genomics of Human Transfer RNA. *Cell Res.* 28, 395–404. doi:10.1038/s41422-018-0013-y

Paunovska, K., Loughrey, D., and Dahlman, J. E. (2022). Drug Delivery Systems for RNA Therapeutics. *Nat. Rev. Genet.* doi:10.1038/s41576-021-00439-4

Porter, J. J., Heil, C. S., and Lueck, J. D. (2021). Therapeutic Promise of Engineered Nonsense Suppressor tRNAs. *WIREs RNA* 12, e1641. doi:10.1002/wrna.1641

Pudi, R., Abhiman, S., Srinivasan, N., and Das, S. (2003). Hepatitis C Virus Internal Ribosome Entry Site-Mediated Translation Is Stimulated by Specific Interaction of Independent Regions of Human La Autoantigen. *J. Biol. Chem.* 278, 12231–12240. doi:10.1074/jbc.M210287200

Reinsborough, C. W., Ipas, H., Abell, N. S., Nottingham, R. M., Yao, J., Devanathan, S. K., et al. (2019). BCDIN3D Regulates tRNAHis 3' Fragment Processing. *Plos Genet.* 15, e1008273. doi:10.1371/journal.pgen.1008273

Ren, B., Wang, X., Duan, J., and Ma, J. (2019). Rhizobial tRNA-Derived Small RNAs Are Signal Molecules Regulating Plant Nodulation. *Science* 365, 919–922. doi:10.1126/science.aav8907

Roberts, T. C., Langer, R., and Wood, M. J. A. (2020). Advances in Oligonucleotide Drug Delivery. *Nat. Rev. Drug Discov.* 19, 673–694. doi:10.1038/s41573-020-0075-7

Ruggero, K., Guffanti, A., Corradin, A., Sharma, V. K., De Bellis, G., Corti, G., et al. (2014). Small Noncoding RNAs in Cells Transformed by Human T-Cell Leukemia Virus Type 1: a Role for a tRNA Fragment as a Primer for Reverse Transcriptase. *J. Virol.* 88, 3612–3622. doi:10.1128/JVI.02823-13

Saal, H. M., Harbison, M. D., and Netchine, I. (2002). "Silver-Russell Syndrome," in *GeneReviews®*. Editors M. P. Adam, H. H. Ardinger, R. A. Pagon, S. E. Wallace, L. J. H. Bean, K. W. Gripp, et al. (Seattle, WA: University of Washington, Seattle). Available at: https://www.ncbi.nlm.nih.gov/pubmed/20301499.

Saikia, M., Jobava, R., Parisien, M., Putnam, A., Krokowski, D., Gao, X.-H., et al. (2014). Angiogenin-Cleaved tRNA Halves Interact with Cytochrome C, Protecting Cells from Apoptosis during Osmotic Stress. *Mol. Cel. Biol.* 34, 2450–2463. doi:10.1128/MCB.00136-14

Schorn, A. J., Gutbrod, M. J., LeBlanc, C., and Martienssen, R. (2017). LTR-Retrotransposon Control by tRNA-Derived Small RNAs. *Cell* 170, 61–71. doi:10.1016/j.cell.2017.06.013

Sharma, U., Conine, C. C., Shea, J. M., Boskovic, A., Derr, A. G., Bing, X. Y., et al. (2016). Biogenesis and Function of tRNA Fragments during Sperm Maturation and Fertilization in Mammals. *Science* 351, 391–396. doi:10.1126/science.aad6780

Sharma, U., Sun, F., Conine, C. C., Reichholf, B., Kukreja, S., Herzog, V. A., et al. (2018). Small RNAs Are Trafficked from the Epididymis to Developing Mammalian Sperm. *Develop. Cel* 46, 481–494. doi:10.1016/j.devcel.2018.06.023

Sobala, A., and Hutvagner, G. (2013). Small RNAs Derived from the 5′ End of tRNA Can Inhibit Protein Translation in Human Cells. *RNA Biol.* 10, 553–563. doi:10.4161/rna.24285

Springer, A. D., and Dowdy, S. F. (2018). GalNAc-siRNA Conjugates: Leading the Way for Delivery of RNAi Therapeutics. *Nucleic Acid Ther.* 28, 109–118. doi:10.1089/nat.2018.0736

Su, Z., Kuscu, C., Malik, A., Shibata, E., and Dutta, A. (2019). Angiogenin Generates Specific Stress-Induced tRNA Halves and Is Not Involved in tRF-3-Mediated Gene Silencing. *J. Biol. Chem.* 294, 16930–16941. doi:10.1074/jbc.RA119.009272

Su, Z., Wilson, B., Kumar, P., and Dutta, A. (2020). Noncanonical Roles of tRNAs: tRNA Fragments and beyond. *Annu. Rev. Genet.* 54, 47–69. doi:10.1146/annurev-genet-022620-101840

Toyofuku, M., Nomura, N., and Eberl, L. (2019). Types and Origins of Bacterial Membrane Vesicles. *Nat. Rev. Microbiol.* 17, 13–24. doi:10.1038/s41579-018-0112-2

Vogel, A., Schilling, O., Späth, B., and Marchfelder, A. (2005). The tRNase Z Family of Proteins: Physiological Functions, Substrate Specificity and Structural Properties. *Biol. Chem.* 386, 1253–1264. doi:10.1515/BC.2005.142

Voss, M. H., Molina, A. M., and Motzer, R. J. (2011). mTOR Inhibitors in Advanced Renal Cell Carcinoma. *Hematol. Oncol. Clin. North Am.* 25, 835–852. doi:10.1016/j.hoc.2011.04.008

Wang, K. H., Kupa, J., Duffy, K. A., and Kalish, J. M. (2019). Diagnosis and Management of Beckwith-Wiedemann Syndrome. *Front. Pediatr.* 7, 562. doi:10.3389/fped.2019.00562

WHO (2022). Antimicrobial Resistance. Available at: https://www.who.int/news-room/fact-sheets/detail/antimicrobial-resistance (Accessed February 21, 2022).

Xiao, Q., Gao, P., Huang, X., Chen, X., Chen, Q., Lv, X., et al. (2021). tRFTars: Predicting the Targets of tRNA-Derived Fragments. *J. Transl. Med.* 19, 88. doi:10.1186/s12967-021-02731-7

Xue, X.-Y., Mao, X.-G., Zhou, Y., Chen, Z., Hu, Y., Hou, Z., et al. (2018). Advances in the Delivery of Antisense Oligonucleotides for Combating Bacterial Infectious Diseases. *Nanomedicine: Nanotechnol. Biol. Med.* 14, 745–758. doi:10.1016/j.nano.2017.12.026

Yamasaki, S., Ivanov, P., Hu, G.-F., and Anderson, P. (2009). Angiogenin Cleaves tRNA and Promotes Stress-Induced Translational Repression. *J. Cel Biol.* 185, 35–42. doi:10.1083/jcb.200811106

Yeung, M. L., Bennasser, Y., Watashi, K., Le, S.-Y., Houzet, L., and Jeang, K.-T. (2009). Pyrosequencing of Small Non-coding RNAs in HIV-1 Infected Cells: Evidence for the Processing of a Viral-Cellular Double-Stranded RNA Hybrid. *Nucleic Acids Res.* 37, 6575–6586. doi:10.1093/nar/gkp707

Yu, A.-M., Jian, C., Yu, A. H., and Tu, M.-J. (2019). RNA Therapy: Are We Using the Right Molecules? *Pharmacol. Ther.* 196, 91–104. doi:10.1016/j.pharmthera.2018.11.011

Yue, T., Zhan, X., Zhang, D., Jain, R., Wang, K.-W., Choi, J. H., et al. (2021). SLFN2 protection of tRNAs from Stress-Induced Cleavage Is Essential for T Cell-Mediated Immunity. *Science* 372, eaba4220. doi:10.1126/science.aba4220

Zeng, T., Hua, Y., Sun, C., Zhang, Y., Yang, F., Yang, M., et al. (2020). Relationship between tRNA -derived Fragments and Human Cancers. *Int. J. Cancer* 147, 3007–3018. doi:10.1002/ijc.33107

Zhang, S., Sun, L., and Kragler, F. (2009). The Phloem-Delivered RNA Pool Contains Small Noncoding RNAs and Interferes with Translation. *Plant Physiol.* 150, 378–387. doi:10.1104/pp.108.134767

Zhang, S., Cheng, Z., Wang, Y., and Han, T. (2021). The Risks of miRNA Therapeutics: In a Drug Target Perspective. *Drug Des. Devel. Ther.* 15, 721–733. doi:10.2147/DDDT.S288859

Zhou, Y., Peng, H., Cui, Q., and Zhou, Y. (2021). tRFTar: Prediction of tRF-Target Gene Interactions *via* Systemic Re-analysis of Argonaute CLIP-Seq Datasets. *Methods* 187, 57–67. doi:10.1016/j.ymeth.2020.10.006

Zong, T., Yang, Y., Zhao, H., Li, L., Liu, M., Fu, X., et al. (2021). tsRNAs: Novel Small Molecules from Cell Function and Regulatory Mechanism to Therapeutic Targets. *Cell Prolif* 54, e12977. doi:10.1111/cpr.12977

Conflict of Interest: The authors declare that the research was conducted in the absence of any commercial or financial relationships that could be construed as a potential conflict of interest.

Publisher's Note: All claims expressed in this article are solely those of the authors and do not necessarily represent those of their affiliated organizations, or those of the publisher, the editors and the reviewers. Any product that may be evaluated in this article, or claim that may be made by its manufacturer, is not guaranteed or endorsed by the publisher.

frontiers | Frontiers in Molecular Biosciences

ORIGINAL RESEARCH
published: 27 April 2022
doi: 10.3389/fmolb.2022.835590

Comparative Analysis of Long Non-Coding RNA Expression and Immune Response in Mild and Severe COVID-19

*Yongting Zhang, Fan Shi, Yuchong Wang, Yuting Meng, Qiong Zhang, Kaihang Wang, Ping Zeng and Hongyan Diao**

State Key Laboratory for Diagnosis and Treatment of Infectious Diseases, National Clinical Research Center for Infectious Disease, Collaborative Innovation Center for Diagnosis and Treatment of Infectious Diseases, The First Affiliated Hospital, College of Medicine, Zhejiang University, Hangzhou, China

OPEN ACCESS

Edited by:
Yong Sun Lee,
National Cancer Center, South Korea

Reviewed by:
Rafael B. Polidoro,
Indiana University Bloomington, United States
Thomaz Lüscher Dias,
Federal University of Minas Gerais, Brazil, in collaboration with reviewer RP Khalid Muhammad,
United Arab Emirates University, United Arab Emirates

***Correspondence:**
Hongyan Diao
diaohy@zju.edu.cn

Specialty section:
This article was submitted to Molecular Diagnostics and Therapeutics, a section of the journal Frontiers in Molecular Biosciences

Received: *14 December 2021*
Accepted: *21 March 2022*
Published: *27 April 2022*

Citation:
Zhang Y, Shi F, Wang Y, Meng Y, Zhang Q, Wang K, Zeng P and Diao H (2022) Comparative Analysis of Long Non-Coding RNA Expression and Immune Response in Mild and Severe COVID-19. Front. Mol. Biosci. 9:835590. doi: 10.3389/fmolb.2022.835590

Background: Coronavirus disease 2019 (COVID-19) is a worldwide emergency, caused by severe acute respiratory syndrome coronavirus 2 (SARS-CoV-2). Long non-coding RNAs (lncRNAs) do not encode proteins but could participate in immune response.

Methods: In our study, 39 COVID-19 patients were enrolled. The microarray of peripheral blood mononuclear cells from healthy and COVID-19 patients was applied to identify the expression profiles of lncRNAs and mRNAs. Identified differentially expressed (DE) lncRNAs were validated by qRT-PCR. Then, the lncRNA–mRNA network was constructed and visualized using Cytoscape (3.6.1) based on the Pearson correlation coefficient. The enrichment of DE mRNAs was analyzed using Metascape. The difference in frequencies of immune cells and cytokines was detected using CIBERSORT and ImmPort based on DE mRNAs.

Results: All patients with COVID-19 displayed lymphopenia, especially in T cells, and hyper-inflammatory responses, including IL-6 and TNF-α. Four immune-related lncRNAs in COVID-19 were found and further validated, including AC136475.9, CATG00000032642.1, G004246, and XLOC_013290. Functional analysis enriched in downregulation of the T-cell receptor and the antigen processing and presentation as well as increased apoptotic proteins, which could lead to T-cell cytopenia. In addition, they participated in monocyte remodeling, which contributed to releasing cytokines and chemokines and then recruiting more monocytes and aggravating the clinical severity of COVID-19 patients.

Conclusion: Taken together, four lncRNAs were in part of immune response in COVID-19, which was involved in the T-cell cytopenia by downregulating the antigen processing and presentation, the T-cell receptor, and an increased proportion of monocytes, with a distinct change in cytokines and chemokines.

Keywords: COVID-19, lncRNA, PBMC, T-cell, monocyte

INTRODUCTION

The coronavirus disease 2019 (COVID-19) outbreak has caused a worldwide emergency owing to its rapid spread and high mortality rate. Mostly, COVID-19 patients may have asymptomatic or mild symptoms, while severe patients can develop pneumonia to acute respiratory or multiorgan failure and death (Yang Y et al.,2020).

Multiple studies, focused on COVID-19, have highlighted the changes in peripheral immune response, including marked pro-inflammatory cytokine release and pronounced lymphopenia, especially reduction in T cells (Song et al., 2020). Therefore, there is an urgent need for further studies on the host immune response to screen prognostic and diagnostic indicators and to provide appropriate therapeutic interventions for severe COVID-19.

Long non-coding RNAs (LncRNAs) are a class of molecules with more than 200 nucleotides in length, which are incapable of coding proteins but participate in the regulation of gene expression through epigenetic, transcriptional, and post-transcriptional changes (Shen et al., 2020).

Recent studies primarily demonstrated that lncRNAs took part in various biological and physiological processes, including the cell cycle and proliferation, apoptosis, and differentiation (Wang et al., 2014). Lnc-DC was exclusively upregulated in DCs during DC differentiation, with regulation of CD40, CD80, CD86, and HLA-DR. The knockdown of lnc-DC failed to present antigens, activate T-cells, and induce cytokine production (Chen et al., 2017).

Therefore, it is essential to explore the potential of lncRNA in peripheral immune response to provide immunotherapy targets in COVID-19. In this study, we applied microarrays to investigate the potential lncRNA of peripheral blood mononuclear cells (PBMCs) from COVID-19 patients.

MATERIALS AND METHODS

Patients

Thirty-nine COVID-19 patients and five healthy donors were enrolled, admitted in The First Affiliated Hospital, Zhejiang University School of Medicine, between 28th January and 20th February, 2020. COVID-19 was confirmed using the SARS-CoV-2-specific RT-PCR test. The patients (**Supplementary Table 1**) were diagnosed with the severe, who required critical care and met one or more of following criteria: dyspnea and respiratory rate ≥30 time/min, blood oxygen saturation ≤93%, PaO_2/FiO_2 ratio <300 mmHg, and lung infiltrates on CT scan >50% within 24–48 h, or those who exhibited respiratory failure, septic shock, and/or multiple organ dysfunction/failure. Meanwhile, all patients' demographics, clinical characteristics, and laboratory results are shown in **Tables 1**, **2**.

Isolated RNA From Peripheral Blood Mononuclear Cells

Sequencing samples are organized in three sets of five, including five healthy donors, five mild COVID-19, and five severe COVID-19, with matched ages and genders and exclusion of patients with any comorbidity. PBMCs were isolated from peripheral venous blood by Ficoll density gradient centrifugation. Isolated cells were treated using RNAiso Plus (TAKARA) reagents under the instruction of the manufacturer for RNA isolation.

Microarray Analysis

For preparations of rRNA depleted sequencing, mRNA was purified using the mRNA-ONLY™ Eukaryotic mRNA Isolation Kit (Epicenter). Then, fluorescent cRNA, which was amplified and transcribed from mRNA, was generated using the Arraystar Flash RNA Labeling Kit (Arraystar). A measure of 3 μg of purified cRNA per sample using the RNeasy Mini Kit (Qiagen) was used for hybridizations through Arraystar Human LncRNA Microarray V5.0 and then was washed, fixed, and scanned through the Agilent DNA Microarray Scanner (part number G2505C).

Data Analysis

The gathered array images were analyzed using Agilent Feature Extraction software (version 11.0.1.1). The GeneSpring GX v12.1 software package (Agilent Technologies) normalized and processed the raw data. The flags from at least five out of 15 samples were positive in present or marginal ("All Targets Value"), and then the selected mRNAs were used for further analysis. The Benjamini corrected the *p*-values to control the false discovery rate (FDR). Differentially expressed genes (DEGs) conformed to the following criteria: adjusted *p*-value ≤ 0.05 and fold-change ≥2 between pairwise combinations of two groups. Also, DE lncRNAs (Raw ≥100) were further analyzed. The weighted gene co-expression network was constructed using the WGCNA package (R, Bioconductor), while the normalized expression index of genes (both mRNA and lncRNA) with top 30% standard deviation was chosen as an input. A gene tree was plotted to present the results of hierarchical clustering, and the dynamic tree-cutting algorithm was applied to segment the gene modules. Finally, the gene lists constituting each module were extracted for further analysis (Zhang and Horvath, 2005).

DE mRNAs, related to lncRNAs, were concluded based on the Pearson correlation coefficient (absolute value ≥ 0.9, *p*-value ≤ 0.01). Metascape Resource was applied for the GO and KEGG pathway annotations (https://metascape.org/gp/index.html). GO or KEGG pathways/terms with *p*-value < 0.01, a minimum count of 3, and an enrichment factor >1.5 were defined as a threshold, in which the term was statistically enriched. Heatmaps, ggplot2, correlation heatmaps, and bar plots were obtained by lc-bio.cn. online analysis. GO terms, Sankey diagrams, and principal component analysis (PCA) were obtained by http://www.bioinformatics.com.cn. CIBERSORT assessed the immune subtype, according to the expression file (https://cibersortx.stanford.edu/). ImmPort focused on immunologically relevant gene sets for analyzing cytokines and chemokines associated with lncRNAs (http://www.immport.org/).

Construction of the Long Non-Coding RNA–mRNA Co-Expression Network

The lncRNA–mRNA network was constructed and visualized using Cytoscape (3.6.1) based on the Pearson correlation

TABLE 1 | Demographics and clinical characteristics of all patients.

Variable/Group	Normal	Mild (26)	Severe (13)	*p*-value
Age (years)	-	44.5	72	<0.05
Male (%)	-	13 (50%)	9 (70%)	NS
Onset of symptoms to hospital admission, days	-	6.5 (3–20)	9 (4–14)	<0.05
Exposure to Wuhan	-	11 (42%)	4 (31%)	NS
Any comorbidity				
Hypertension	-	7 (27%)	10 (77%)	<0.05
Diabetes	-	3 (8%)	2 (15%)	NS
Malignancy	-	0	0	
Chronic liver disease	-	0	0	
Fever				
Highest temperature (°C)				
<37.3	-	4 (15%)	3 (23%)	
37.3–38.0	-	13 (50%)	6 (46%)	
38.1–39.0	-	8 (30%)	2 (15%)	
>39.0	-	1 (5%)	2 (15%)	
Cough	-	14 (54%)	9 (69%)	NS
Expectoration	-	13 (50%)	6 (46%)	NS
Myalgia or fatigue	-	8 (31%)	1 (8%)	NS
Nausea and vomiting	-	1 (4%)	1 (8%)	NS
Sore throat	-	3 (12%)	0	NS
Shortness of breath	-	5 (20%)	2 (15%)	NS
Chest pain	-	2 (8%)	0	NS
Diarrhea	-	2 (8%)	4 (31%)	NS

Data are median or n (%), compared by the Mann–Whitney U-test or χ^2 test between mild and severe COVID-19.

TABLE 2 | Laboratory results of hospitalized patients with infected SARS-Cov-2.

Laboratory results	Normal range	Normal	Mild (26)	Severe (13)	*p*-value
Laboratory results	4.0–10.0*109	-	5.1	13	<0.05
Leukocyte (10E9/L)	2.0–7.0*109	-	3.3	11.9	<0.01
Neutrophil (10E9/L)	0.8–4.0*109	-	0.8	0.5	<0.01
Lymphocyte (10E9/L)	3.68–5.13	-	4.3	3.95	NS
Red blood cells (10E12/L)	113–151	-	130.5	121	NS
Hemoglobin (g/L)	101–320	-	197	174	<0.05
Platelet (10E9/L)	0–700	-	400	705	<0.01
D-dimer (ug/L)	0.00–20.06	-	13.23	6.58	NS
IFN-γ (pg/ml)	0.00–2.31	-	3.82	7.94	<0.05
IL-10 (pg/ml)	0.00–4.13	-	1.14	2.09	NS
IL-2 (pg/ml)	0.00–6.61	-	13.58	47.18	<0.05
IL-6 (pg/ml)	0.00–33.27	-	9.345	22.51	NS
TNF-α (pg/ml)	70.0–140.0	-	137	126	NS
Complement3 (mg/dL)	10.0–40.0	-	43	34	<0.05
Complement4 (mg/dL)	0.00–8.00	-	9.42	67.95	NS
Hypersensitive C-reactive protein (mg/L)	0.00–0.05	-	0.04	0.09	<0.01
Procalcitonin (ng/ml)	0–40	-	36	46	NS
Brain natriuretic peptide (pg/ml)	7–40	-	13	17	NS
ALT (U/L)	13–35	-	20	19	NS
AST (U/L)	100.0–420.0	-	218	218	NS
Immune globulin (Ig)A (mg/dL)	860.0–1740.0	-	1330	1606	NS
Immune globulin (Ig)G (mg/dL)	30.0–220.0	-	115	60	NS
Immune globulin (Ig)M (mg/dL)	4.0–10.0*109	-	5.1	13	<0.05

Data are median, compared by the Mann–Whitney U-test between mild and severe COVID-19.

coefficient (absolute value ≥ 0.9, *p*-value ≤ 0.01). The protein–protein interaction (PPI) was established through the STRING database. The correlation between selected lncRNA and mRNA was analyzed using the co-expression network and Sankey diagrams (http://www.bioinformatics.com.cn).

Treatment of HuT 78 Cells With Spike-ECD and Hemagglutinin Proteins

The human monocytic cell line THP-1 and the human T-cell line HuT 78 were purchased from the Cell Bank of Type Culture Collection of the Chinese Academy of Sciences. THP-1 was cultured in the RPMI 1640 medium, supplemented with 10% fetal bovine serum (Gibco), 1% penicillin/streptomycin, and 100 ng/ml phorbol 12-myristate 13-acetate (PMA; MCE, United States). After 24 h, THP-1 cells were stimulated by 50 ng/ml spike protein of severe acute respiratory syndrome coronavirus 2 (SARS-CoV-2) (GenScript) or the hemagglutinin (HA) protein of influenza A H1N1 (A/California/04/2009) (Sino Biological) for 24 h. The cells were then co-cultured with HuT 78 for another 6 and 12 h, followed by RNA isolation and the subsequent qRT-PCR assay.

Quantitative RT-PCR

A measure of 1 μg of total RNA was reverse-transcribed to cDNA using HiScript II Q Select RT SuperMix (Vazyme). Quantitative real-time PCR was performed using SYBR qPCR Master Mix (Vazyme), and the amplifications were performed using QuantStudio 5 (Applied Biosystems). For quantification of gene expression, the 2-ΔΔCt method was used. The housekeeping gene glyceraldehyde-3-phosphate dehydrogenase (GAPDH) was used in all reactions as an endogenous control. The 5′–3′ sequences of primer pairs were as follows: GAPDH: GTCTCCTCT:GACTTC AAC AGCG (F) and ACCACCCTGTTGCTG TAG CCA A (R); AC005083.1: ACACCTCTGCCTCTATGGGA (F) and AGCCAG CCCTTTTGTCTGAT (R); AC136475.9: GGAGTTCCTTCCTTT CGCCT (F) and ATTACGTCCTGTGCACGCTC (R); XLOC_013290: GGGTATCAGGTGTCTGGGTG (F) and CCA GAAATCCTGCCACTCCG (R); G004246: TGCCAGTAGACC ATGACTCG (F) and TTTGGCACTCTTGGGCACTT (R); CATG00000032642.1: AGCACTTTGCAGAGGGACAC (F) and ACAGCAACAAGGGTTGAGGG (R); HLA-DRA: AGGTTG AGGGACGGAGATTT (F) and TGGCTGCATCTCGAGACT TT (R); HLA-DMA: GGGAGATGCTCCTGCCATTT (F) and AGCGATAGGAAACCCTCTGG (R); HLA-DMB: GAGCTG GCCACTCTAGTTACA (F) and GGAGAGGCATGGTAGCAT CA (R); HLA-DQB2: CCGTGGAGTGGCGACCT (F) and GAC ACAGGCAGCTAGGAATTCTG (R); HLA-DOA: CAACGG CCAAACTGTCACTG (F) and GTCATAGACGTCCTCGGC TG (R); LAT: GCAGACCCTTGGGGCCTA (F) and GCACAC ACAGTGCCATCAAC (R); VAV1: ACGTCGAGGTCAAGC ACATT (F) and GGCCTGCTGATGGTTCTCTT (R); LCK: GGAGGACCATGTGAATGGGG (F) and CATTTCGGATGA GCAGCGTG (R).

Statistical Analysis

GraphPad Prism 8.0 (GraphPad Software, San Diego, CA) was adopted for the t-test or Wilcoxon matched-pair test. Continuous variables were expressed as median (IQR) and compared using the Mann–Whitney U-test. Categorical measurement variables were displayed as count (%) and compared using the χ^2 test or Fisher's exact test. The Pearson correlation test was conducted to assess correlation between two quantitative variables. p-value < 0.05 was considered statistically significant.

RESULTS

Sample Collection and Identification of Biomarker Long Non-Coding RNAs by Microarrays

All patients' demographics, clinical characteristics, and laboratory results are shown in **Tables 1**, **2**. The severe group exhibited lymphopenia, especially in T-cell cytopenia, and hyper-cytokines, notably increased TNF-α and IL-6 (**Supplementary Figures S1A,B**).

To discover the underlying mechanism of specific immune response in COVID-19 patients, PBMCs were isolated from laboratory-confirmed mild (n = 5) and severe COVID-19 patients (n = 5) as well as healthy controls (n = 5). There was no significant difference in age between each other (**Supplementary Figure S1C**).

Then microarray was applied and analyzed as the flow chart (**Figure 1A**). The corresponding expression profiles, in which each row represents a separate gene and each column represented a separate individual, were presented with clustered heatmaps, according to the severity of COVID-19 (**Figure 1B**). The volcano plots of DE lncRNAs (Raw ≥100) and DE mRNAs were shown by adjusted p-values (p-value < 0.05) and FC ratios (|log2FC|≥ 1) **Supplementary Figure S2**).

To screen out lncRNA signatures, UpSet analysis was performed in each comparison group (**Figure 1C**). Two types of lncRNAs were defined as candidate lncRNA biomarkers: 1) lncRNAs consistently downregulated (13) and 2) lncRNAs consistently upregulated (18). The lncRNAs were filtered by p-value ≦ 0.01 and the length of lncRNAs among 400–3000 nts and the difference between pairwise combinations of two groups, and only 5 lncRNAs conform to the criteria, including AC005083.1, AC136475.9, CATG00000032642.1, G004246, and XLOC_013290 (p < 0.001) (**Figure 1D**). These lncRNAs significantly increased in COVID-19, especially in severe COVID-19.

Validation of Selected Long Non-Coding RNAs by Quantitative RT-PCR

For further validation of selected lncRNAs, we performed qRT-PCR. After stimulation with the S-protein and HA for 0, 6, and 12 h, we observed that four of five lncRNA, including AC136475.9, CATG00000032642.1, G004246, and XLOC_013290, significantly increased, excluding AC005083.1. (**Figures 2A,B**), consistent with the aforementioned microarray results. Also, the results suggested that the immune response to H1N1 and SARS-COV-2 was obviously different.

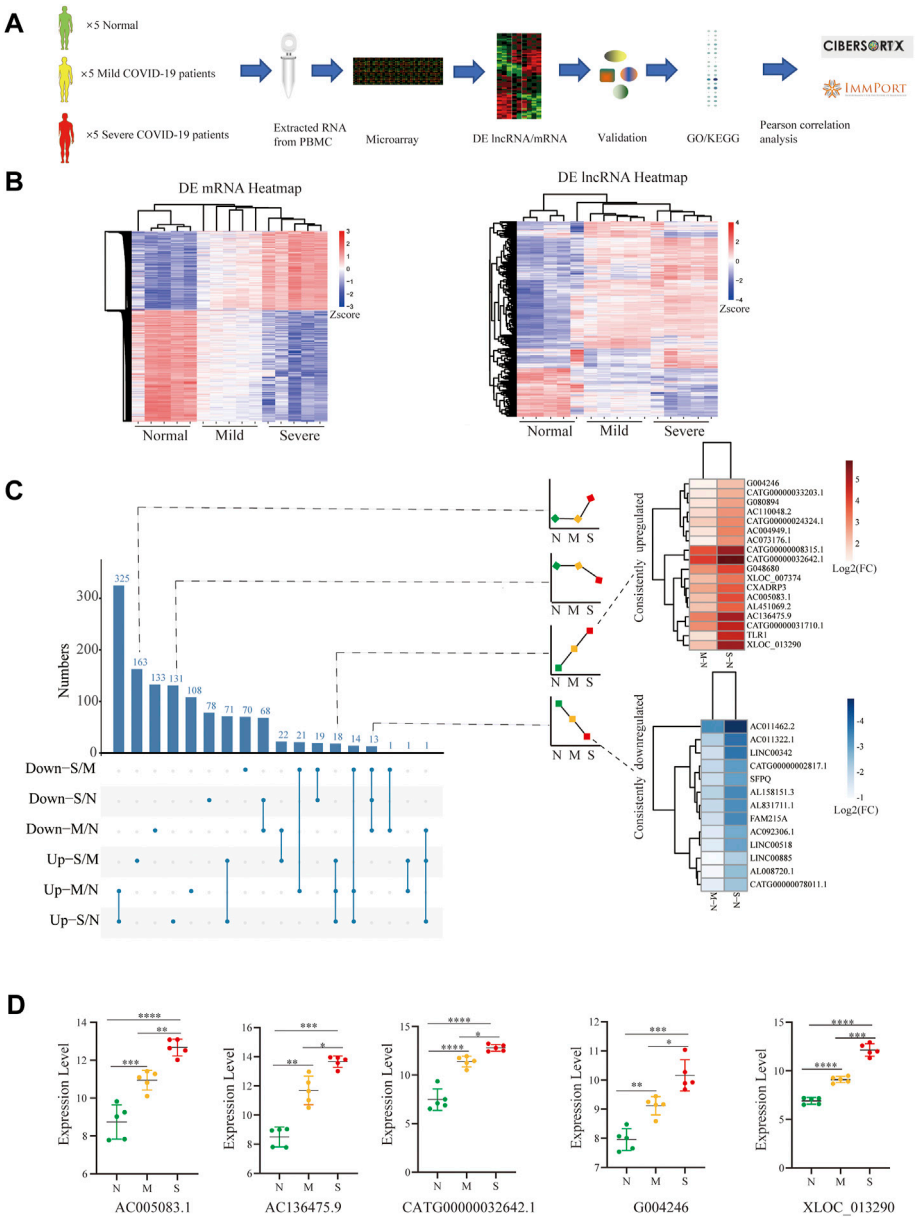

FIGURE 1 | Identification of biomarker lncRNAs. **(A)** Research experimental design. **(B)** Heatmap comparison of DE lncRNAs and mRNAs within PBMCs from normal control (n = 5), mild (n = 5), and severe (n = 5) patients; each row and column respectively represent a separate gene and individual. **(C)** UpSet plot shows the number of DE lncRNAs with different tendencies; the heatmap shows the consistently increased or decreased lncRNAs by log2FC between mild vs. normal and severe vs. normal. **(D)** Filtered by p-value ≦ 0.01 and the length of lncRNAs among 400–3000 nts and the difference between pairwise combinations of two groups, with expression of lncRNAs in each group. N (Normal: n = 5), M (Mild: n = 5), and S (Severe: n = 5). Comparisons were done using the ANOVA test. Mild and severe patients were colored by yellow and red, respectively. Statistical comparisons are indicated by the arrows; $*p < 0.05$, $**p < 0.01$, $***p < 0.001$, $****p < 0.0001$; Mild and severe patients were colored by yellow and red, respectively.

Functional Enrichment With the Four Long Non-Coding RNAs in COVID-19

We performed WGCNA analysis, in which selected lncRNAs played the role in viral release from the host cell. (**Figure 3**). To better understand the function of lncRNAs in COVID-19, we computed the Pearson correlation coefficient (PCC) between mRNAs and four lncRNAs. We identified 2,890 mRNAs correlated with lncRNA biomarkers ($r > 0.9$ and $p \leq 0.01$) (**Supplementary Table 2**). Then, we performed GO and KEGG enrichment analysis (**Supplementary Table 3**).

The KEGG pathway was performed in **Figure 3**. "T-cell receptor signaling pathway," "antigen processing and presentation," and "apoptosis" were enriched in COVID-19, especially in severe patients. Surprisingly, *Staphylococcus aureus* infection was also

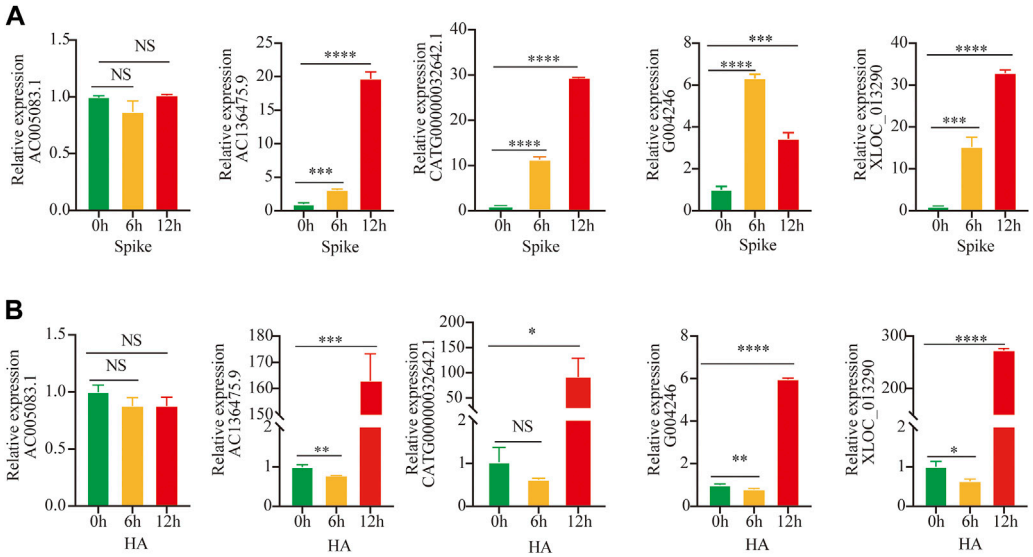

FIGURE 2 | Validation by Quantitative RT-PCR. **(A,B)** Expressions of lncRNAs were detected after stimulation by S-protein and HA for 0, 6, and 12 h in HuT 78 cell co-cultured with the activated THP-1; statistical comparisons are indicated by the arrows; $*p < 0.05$, $**p < 0.01$, $***p < 0.001$, $****p < 0.0001$; comparisons were done using the ANOVA test.

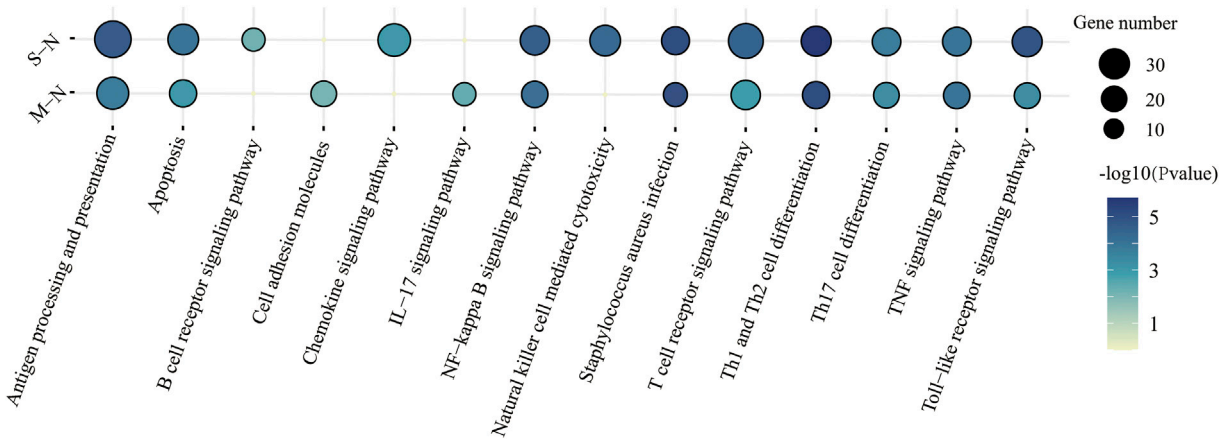

FIGURE 3 | KEGG functional characteristics for the predicted target genes of four lncRNAs in immune response between mild and severe COVID-19.

found in COVID-19 patients. It suggested that patients were more susceptible to bacteremia, such as Gram-positive bacteria (Cusumano et al., 2020).

Analysis of the Long Non-Coding RNA–mRNA Network in COVID-19

Based on the aforementioned KEGG pathway, with the Pearson correlation ($|R| > 0.94$ and $p \leq 0.01$), we constructed the lncRNA–mRNA co-expression network (**Figure 4A**). A total of 142 lncRNA–mRNA pairs were filtrated, and the top 24 genes were shown using the Sankey diagram (**Figure 4B**).

XLOC_013290 and CATG00000032642.1 were negatively correlated with HLA-DQB2 and HLA-DRB1, respectively (**Figure 4C**). Also, HLA-DRA, HL-DMA, and HL-DMB decreased in COVID-19, especially in severe cases, consistent with Mudd PA's result, who reported that abundances of HLA-DR of monocytes significantly reduced in COVID-19 (Mudd et al., 2020). After stimulation with the S-protein for 0, 6, and 12 h *in vitro*, the mRNA HLA-DOA-related antigen presentation appeared to have a decline in trend after an initial increase (**Supplementary Figure S4A**).

LAT, VAV1, ZAP70, and CARD11, as the key components of T-cell receptor, exhibited a significant decrease with severity in

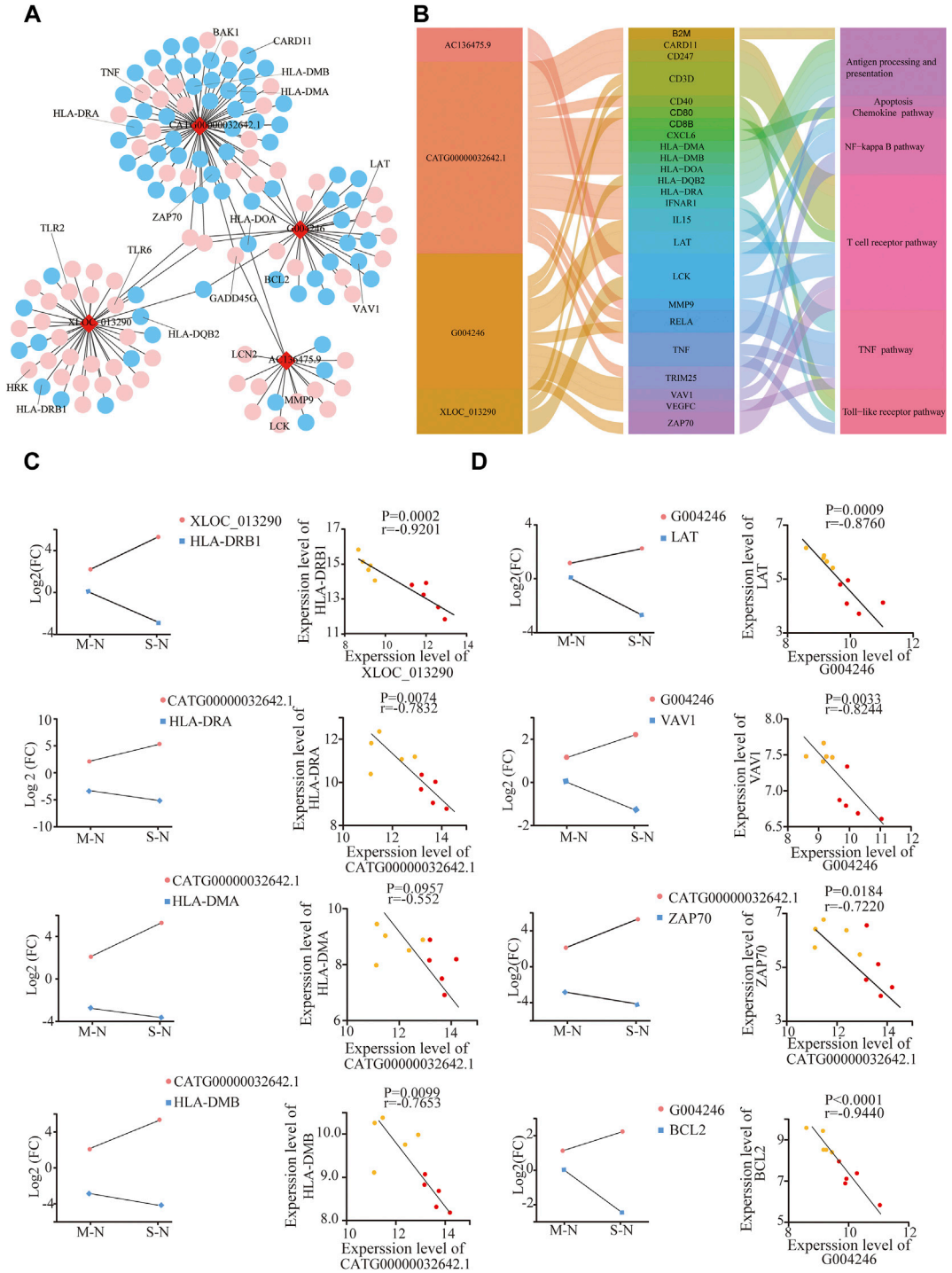

FIGURE 4 | Analysis of the lncRNA–mRNA network in COVID-19. **(A)** Integrated lncRNA–mRNA network; **(B)** 4 lncRNA and selected 24 mRNA are shown using the Sankey diagram; **(C,D)** correlation between lncRNA and targeted mRNAs in mild and severe groups compared to healthy controls, respectively. The Y-axes correspond to the log2FC of lncRNAs and mRNAs. The number of samples: M (n = 5) and S (n = 5); mild and severe patients were colored by yellow and red dots, respectively.

COVID-19, negative with G004246 and CATG00000032642.1. (**Figure 4D**). Meanwhile, the gene expression of VAV1 and LCK also declined, after stimulation with the S-protein for 12 h *in vitro* (**Supplementary Figure S4B**). Moreover, BCL2, an important antiapoptotic protein, shows a decreasing trend in COVID-19. Also, GADD45G, HRK, and BAK, as proapoptotic

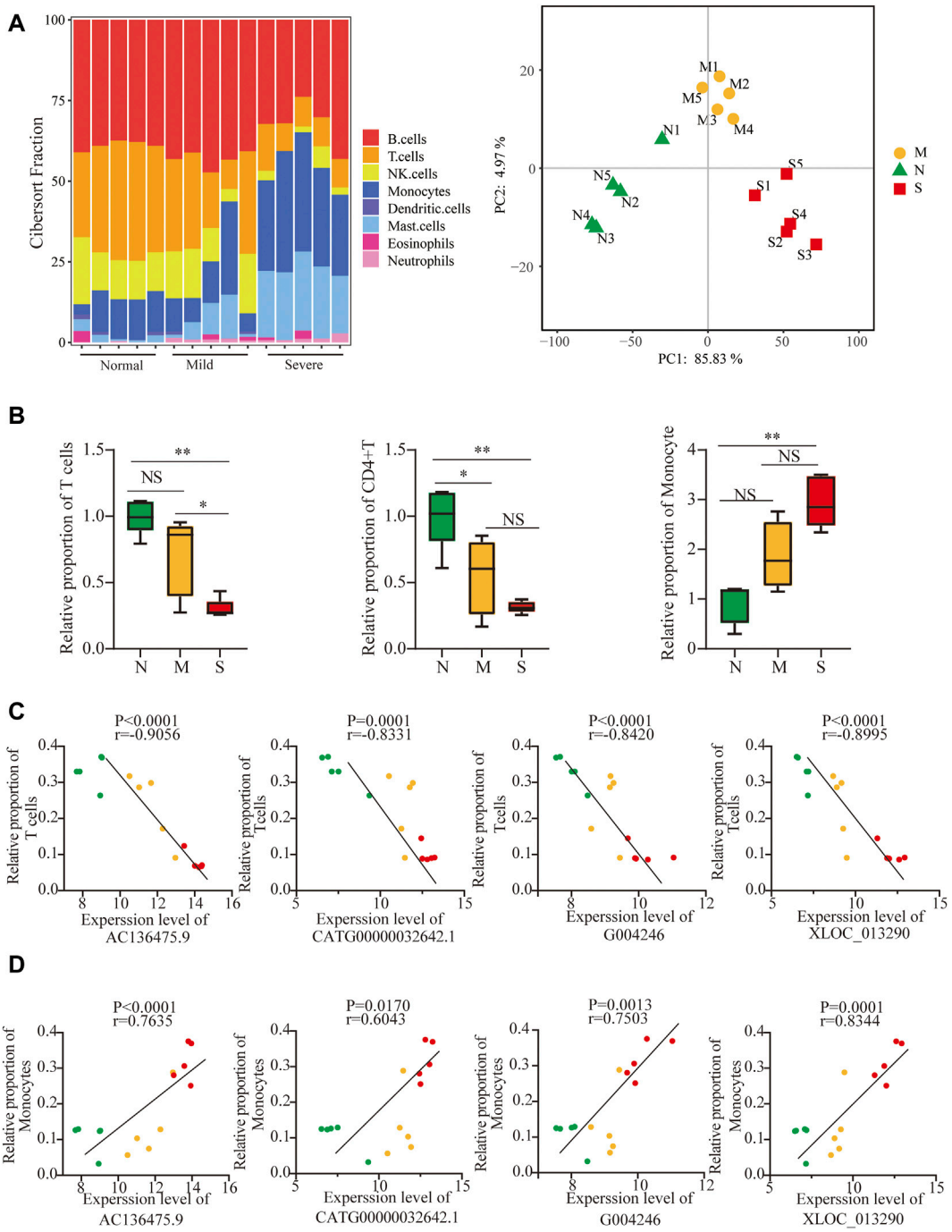

FIGURE 5 | Validation of lncRNAs as biomarkers by differences in immune cell compositions. **(A)** Profiles of immune subtypes are shown using bar plots; PCA between normal and COVID-19. **(B)** Difference in immune subtypes among three groups is shown using the Mann–Whitney test, including T cells, CD4+ T cells, and monocytes. **(C, D)** Correlation between 4 lncRNAs and T cells and monocytes in normal, mild, and severe groups. The normal, mild, and severe patients were colored by green, yellow, and red dots, respectively. ns: non-significant; *$p < 0.05$; **$p < 0.01$.

proteins, showed a significant increase with severity in COVID-19 (**Figure 4D**, **Supplementary Figure S4C**). These results indicated that SARS-CoV2 could induce T-cell apoptosis. Also, higher levels of both TLR2 and TLR6 genes were observed with the severity of COVID-19 (**Supplementary Figure S4D**) (Taniguchi-Ponciano et al., 2021). These results implied that lncRNAs could participate in T-cell reduction, with the dysfunction of TCR and HLA as well as increased apoptotic proteins.

Validation of Long Non-Coding RNAs as Biomarkers by Differences in Immune Cell Compositions, Especially in T-Cell Cytopenia

Next, to further identify whether lncRNAs play a role in T-cell cytopenia under COVID-19 conditions, the potential mRNAs of lncRNAs were applied with CIBERSORT and eight major cell subpopulations were successfully identified in peripheral blood using the bar plot. (**Figure 5A**). Principal component analysis (PCA) showed that there were significant differences in immune cell composition, also in the severity of COVID-19 (**Figure 5A**).

The fraction of total T cells was lower in COVID-19 (**Figure 5B**), especially in CD4T, and not in CD8T (**Supplementary Figure S5A**), and only marginal differences in B cells were observed (**Supplementary Figure S5A**). The adaptive immune cell subsets were depleted in COVID-19, including follicular helper T cells (TFh), regulatory T cells (Tregs) cells, and gamma delta T (γδT) cells (**Supplementary Figure S5B**). Surprisingly, the proportion of monocytes significantly increased in COVID-19 (**Figure 5B**). In contrast, the frequencies of activated natural killer (NK) cells and dendritic cells (DCs) decreased in both mild and severe COVID-19 (**Supplementary Figure S5C**). The frequency of neutrophils increased slightly in COVID-19, although the neutrophils were normally excluded from PBMCs (**Supplementary Figure S5C**). Furthermore, 4 lncRNAs were negatively correlated with T-cell cytopenia but positively correlated with an increased frequency of monocytes (**Figures 5C,D**). It implied that 4 lncRNAs might participate in not only T-cell cytopenia but also increased monocytes.

Monocytes have been implicated in the physiopathology of COVID-19, and differences in transcriptional signatures about monocytes are shown in **Supplementary Figure S6A** based on Aaron J. Wilk's single-cell RNA sequencing (scRNA-seq) (Wilk et al., 2020). Both Mudd et al. (2020) and Zhou et al. (2021) reported SARS-CoV2 could inhibit antigen-presenting ability in monocytes, which led to T-cell cytopenia.

Furthermore, both Wen et al. (2020) and Zhou F et al. (2020) observed that monocytes significantly increased and proved that pro-inflammatory cytokines and chemokines genes were also upregulated. A distinct change in cytokines and chemokines was shown in mild and severe COVID-19, derived from ImmPort (Bhattacharya et al., 2018), which were associated with lncRNAs ($|R| > 0.90$ and $p \leq 0.01$). (**Supplementary Figure S6B,C**).

It indicated that SARS-Cov2 led to the upregulation of lncRNA, T-cell cytopenia, and transcriptional differences of monocytes, with a distinct change in cytokines and chemokines, especially in severe COVID-19.

DISCUSSION

Previous studies reported lncRNAs played a potential role in immune response. In order to find the lncRNA associated with COVID-19, we performed a whole genome microarray of PBMCs from COVID-19 and healthy donors.

In this study, we have demonstrated that 1) lncRNAs AC136475.9, CATG00000032642.1, G004246, and XLOC_013290 are active participants in COVID-19; 2) their function enriched in dysregulation of TCR and HLA as well as increased apoptotic proteins, which could be in part of T-cell cytopenia; and 3) they also participated in monocyte reprogramming, with a distinct change in cytokines and chemokines.

Both the routine laboratory results and bioinformatics analysis demonstrated that lymphopenia in the periphery was the prominent feature in COVID-19, which was similar to recently published data (Giamarellos-Bourboulis et al., 2020; Huang et al., 2020; Tan et al., 2020; Chen et al., 2020) (**Supplementary Figure S1**). Also, lymphocyte counts in severe cases performed lower than those in mild cases, which implied that the degree of lymphocytopenia was relevant to the severity of COVID-19 (Qin et al., 2020; Wang et al., 2020). Moreover, our results showed that the absolute number or frequency of several immune subsets in severe COVID-19 significantly decreased compared to that in mild COVID-19, including CD4 T cells, CD8 T cells, and natural killer cells (Kuri-Cervantes et al., 2020) (**Supplementary Figure S1**, **Figure 5**).

Several explanations accounted for lymphopenia, caused by SARS-CoV-2. First, the peripheral lymphopenia is possibly attributed to the redistribution or recruitment of lymphocytes from the periphery to the respiratory tract or lymphoid organs, accompanied by the accumulation of lymphocytes (Liao et al., 2020; Wichmann et al., 2020). Second, enrichment analysis included the "apoptosis signaling pathway," and viral infection of lymphocytes might lead to cell death by apoptosis, necrosis, or pyroptosis (Yue et al., 2018; Tan et al., 2007). Last, increased levels of cytokines may be associated with lymphopenia. TNF-a led to lymphocyte apoptosis, particularly for CD8 T-cell apoptosis (Mehta et al., 2018). IL-10 was known as an immunosuppressive effect, which also induced CD4 T and CD8 T inactivation (Brooks et al., 2006). Type-I IFN had an impact on lymphocyte proliferation, apoptosis, and expression of cytokines and cytokine receptors and disrupted modulation of S1P-S1P1 for lymphocyte recirculation (Kamphuis et al., 2006). Moreover, COVID-19 patients who were admitted had a substantial accumulation of inflammatory cytokines, including TNF-a, IL-6, IL-2, and IL-10 (**Supplementary Figure S1B**), especially in severe COVID-19.

Meanwhile, increased plasma inflammatory biomarkers were accompanied by worsened symptoms, including C-reactive protein, ferritin, and D-dimers, and neutrophil-to-lymphocyte ratio (Wu et al., 2020; Ruan et al., 2020; Zhou et al.,2020). Although the fraction of T cells decreased in severe COVID-19, the frequency of monocytes and the levels of inflammatory cytokines and chemokines evidently increased (Chen et al., 2020; Gong et al., 2020; Huang et al., 2020; Qin et al., 2020; Yang L et al., 2020). The aforementioned results indicated there is a potential interaction between T-cell reduction and an increased proportion in monocytes.

Aaron J. Wilk found that the phenotype of the monocyte was remodeled, in which the $CD16^+$ monocyte was depleted, but they did not find the series of pro-inflammatory cytokine genes coding in the monocyte (Wilk et al., 2020). A single-cell analysis of PBMCs from COVID-19 found that $CD14^+$ monocytes were significantly increased, while an observed decrease was shown in $CD16^+$ monocytes (Wen et al., 2020; Huang et al., 2021). Zhou Y et al. (2020) not only observed that $CD14^+CD16^+$ monocytes significantly increased but also proved that monocytes secreted a large amount of IL-6 and GM-CSF. Moreover, substantial pro-inflammatory cytokines and chemokines genes, associated with $CD14^+$ monocytes, were upregulated, such as IL1β, JUN, and CCL4 (Wen et al., 2020). In addition, they suggested that pro-inflammatory monocytes contribute to the potential cytokine storm and also implied that various cytokines and chemokines migrate to lung and lymph organs and then activate a series of inflammatory immune cells and aggravate lung injury.

Despite the extensive clinical research studies on lncRNAs, several questions still need to be further addressed. Several risk factors, which affected the expression of peripheral lncRNAs, must be observed to make more accurate predictions of potential lncRNAs. First, Pujadas et al. (2020) reported that there is an independent relationship between high viral load and mortality. Among the enrolled patients in isolation wards or intensive care units, the absolute viral load was not measured. The laboratory result of SARS-COV-2 was positive or not. It is difficult to determine the accuracy of lncRNAs in the development and progression of COVID-19. Second, recent research indicated that some of the risk factors could alter the potential lncRNA expression in peripheral immune response, including age (Lee et al., 2012), sex (Scully et al., 2020), and some other comorbidities. In our studies, the majority of the samples were male. As a specific biomarker in COVID-19, whether lncRNAs were applied to female or not, it is needed to be further verified. Furthermore, as the positive control, patients, who did not suffer from COVID-19 but from pneumonia or acute respiratory distress syndrome, were not enrolled, and the specificity of non-coding RNA biomarkers still need validation.

CONCLUSION

In this study, we reported the potential lncRNAs and their correlation with T-cell cytopenia and an increased frequency of monocytes in COVID-19. Our analysis provided bases for therapeutic targets in COVID-19 as well as the SARS-CoV-2-specific vaccines.

DATA AVAILABILITY STATEMENT

The datasets presented in this study can be found in online repositories. The names of the repository/repositories and accession number(s) can be found in the article/ **Supplementary Material**.

ETHICS STATEMENT

The studies involving human participants were reviewed and approved by the Clinical Research Ethics Committee of The First Affiliated Hospital, School of Medicine, Zhejiang University (Approval notice 2020-38). The patients/participants provided their written informed consent to participate in this study. Written informed consent was obtained from the individual(s) for the publication of any potentially identifiable images or data included in this article.

AUTHOR CONTRIBUTIONS

YZ and HD conceived and designed the study. YZ, FS and YW performed the experiments and statistical and bioinformatic analysis. YM, QZ, KW and PZ collected and characterized samples. YZ and HD wrote and edited the manuscript. All authors read and approved the final manuscript.

FUNDING

This work was supported by the Key Research and Development Plan of Zhejiang Province (2019C04005) and the National Key Research and Development Program of China (2018YFC2000500).

SUPPLEMENTARY MATERIAL

The Supplementary Material for this article can be found online at: https://www.frontiersin.org/articles/10.3389/fmolb.2022.835590/full#supplementary-material

Supplementary Figure S1 | Difference of peripheral lymphocyte subsets and cytokines in COVID-19 patients. **(A)** Cell counts or frequency of lymphocytes, neutrophils, monocytes, CD3+ T cells, CD4+ T cells, CD8+ T cells, NK cells, and B cells in mild and severe groups were analyzed. **(B)** Levels of IL-6, TNF-a, IFN-γ, IL-2, and IL-10 from mild and severe patients. **(C)** Characteristics of all subjects for the microarray. The shaded region shows the normal range of the indicated cell subset. M: mild; S: severe; Mild and severe patients were colored by yellow and red, respectively. The data were compared by the Mann–Whitney U-test. ns: non-significant; $*p < 0.05$, $**p < 0.01$, $***p < 0.001$, $****p < 0.0001$.

Supplementary Figure S2 | Volcano plot of DE lncRNAs and mRNAs among three groups.

Supplementary Figure S3 | WGCNA was performed for analysis of co-relation between lncRNA and mRNA. The brown and green modules respectively are AC136475.9, G004246, XLOC_013290, and CATG00000032642.1.

Supplementary Figure S4 | Expression and correlation of lncRNAs and mRNA; **(A, B)** Expression of mRNA, related antigen presentation, and TCR were detected by RT-PCR after stimulation by S-protein and HA for 0, 6, and 12 hours in HuT 78 cells co-cultured with the activated THP-1; **(C)** correlation between lncRNAs and apoptosis; **(D)** correlation between lncRNAs and TLRs. Statistical comparisons are indicated by the arrows; ns: non-significant; $*p < 0.05$, $**p < 0.01$; Comparisons were done by the ANOVA test.

Supplementary Figure S5 | Difference in immune cells among three groups; the normal, mild, and severe patients were colored by green, yellow, and red, respectively. Data were compared by the Mann–Whitney test; ns: non-significant; $*p < 0.05$; $**p < 0.01$.

Supplementary Figure S6 | Cytokine and chemokine profiles in COVID-19 patients. **(A)** Heatmap of DE genes related to monocytes; **(B)** number of genes in 17 immune-related pathways; **(C)** heatmap comparison of chemokines and cytokines; **(D)** correlation heatmap between 4 lncRNAs with cytokines and chemokines. *p*-values generated by one-way ANOVA with multiple comparisons by Tukey's test. ns: non-significant; *p < 0.05; **p < 0.01, ***p < 0.001, ****p < 0.0001.

REFERENCES

Bhattacharya, S., Dunn, P., Thomas, C. G., Smith, B., Schaefer, H., Chen, J., et al. (2018). ImmPort, toward Repurposing of Open Access Immunological Assay Data for Translational and Clinical Research. *Sci. Data* 5, 180015. doi:10.1038/sdata.2018.15

Brooks, D. G., Trifilo, M. J., Edelmann, K. H., Teyton, L., McGavern, D. B., and Oldstone, M. B. A. (2006). Interleukin-10 Determines Viral Clearance or Persistence *In Vivo*. *Nat. Med.* 12 (11), 1301–1309. doi:10.1038/nm1492

Chen, G., Wu, D., Guo, W., Cao, Y., Huang, D., Wang, H., et al. (2020). Clinical and Immunological Features of Severe and Moderate Coronavirus Disease 2019. *J. Clin. Invest.* 130 (5), 2620–2629. doi:10.1172/JCI137244

Chen, Y. G., Satpathy, A. T., and Chang, H. Y. (2017). Gene Regulation in the Immune System by Long Noncoding RNAs. *Nat. Immunol.* 18 (9), 962–972. doi:10.1038/ni.3771

Cusumano, J. A., Dupper, A. C., Malik, Y., Gavioli, E. M., Banga, J., Berbel Caban, A., et al. (2020). Staphylococcus aureus Bacteremia in Patients Infected with COVID-19: A Case Series. *Open Forum Infect. Dis.* 7 (11), ofaa518. doi:10.1093/ofid/ofaa518

Giamarellos-Bourboulis, E. J., Netea, M. G., Rovina, N., Akinosoglou, K., Antoniadou, A., Antonakos, N., et al. (2020). Complex Immune Dysregulation in COVID-19 Patients with Severe Respiratory Failure. *Cell Host & Microbe* 27 (6), 992–1000. e3. doi:10.1016/j.chom.2020.04.009

Gong, J., Dong, H., Xia, Q.-S., Huang, Z.-y., Wang, D.-k., Zhao, Y., et al. (2020). Correlation Analysis between Disease Severity and Inflammation-Related Parameters in Patients with COVID-19: a Retrospective Study. *BMC Infect. Dis.* 20 (1), 963. doi:10.1186/s12879-020-05681-5

Huang, C., Wang, Y., Li, X., Ren, L., Zhao, J., Hu, Y., et al. (2020). Clinical Features of Patients Infected with 2019 Novel Coronavirus in Wuhan, China. *The Lancet* 395 (10223), 497–506. doi:10.1016/S0140-6736(20)30183-5

Huang, L., Shi, Y., Gong, B., Jiang, L., Zhang, Z., Liu, X., et al. (2021). Dynamic Blood Single-Cell Immune Responses in Patients with COVID-19. *Sig Transduct Target. Ther.* 6 (1), 110. doi:10.1038/s41392-021-00526-2

Kamphuis, E., Junt, T., Waibler, Z., Forster, R., and Kalinke, U. (2006). Type I Interferons Directly Regulate Lymphocyte Recirculation and Cause Transient Blood Lymphopenia. *Blood* 108 (10), 3253–3261. doi:10.1182/blood-2006-06-027599

Kuri-Cervantes, L., Pampena, M. B., Meng, W., Rosenfeld, A. M., Ittner, C. A. G., Weisman, A. R., et al. (2020). Comprehensive Mapping of Immune Perturbations Associated with Severe COVID-19. *Sci. Immunol.* 5 (49), eabd7114. doi:10.1126/sciimmunol.abd7114

Lee, N., Shin, M. S., and Kang, I. (2012). T-cell Biology in Aging, with a Focus on Lung Disease. *Journals Gerontol. Ser. A: Biol. Sci. Med. Sci.* 67A (3), 254–263. doi:10.1093/gerona/glr237

Liao, M., Liu, Y., Yuan, J., Wen, Y., Xu, G., Zhao, J., et al. (2020). Single-cell Landscape of Bronchoalveolar Immune Cells in Patients with COVID-19. *Nat. Med.* 26 (6), 842–844. doi:10.1038/s41591-020-0901-9

Mehta, A. K., Gracias, D. T., and Croft, M. (2018). TNF Activity and T Cells. *Cytokine* 101, 14–18. doi:10.1016/j.cyto.2016.08.003

Mudd, P. A., Crawford, J. C., Turner, J. S., Souquette, A., Reynolds, D., Bender, D., et al. (2020). Distinct Inflammatory Profiles Distinguish COVID-19 from Influenza with Limited Contributions from Cytokine Storm. *Sci. Adv.* 6 (50), eabe3024. doi:10.1126/sciadv.abe3024

Pujadas, E., Chaudhry, F., McBride, R., Richter, F., Zhao, S., Wajnberg, A., et al. (2020). SARS-CoV-2 Viral Load Predicts COVID-19 Mortality. *Lancet Respir. Med.* 8 (9), e70. doi:10.1016/S2213-2600(20)30354-4

Qin, C., Zhou, L., Hu, Z., Zhang, S., Yang, S., Tao, Y., et al. (2020). Dysregulation of Immune Response in Patients with Coronavirus 2019 (COVID-19) in Wuhan, China. *Clin. Infect. Dis.* 71 (15), 762–768. doi:10.1093/cid/ciaa248

Ruan, Q., Yang, K., Wang, W., Jiang, L., and Song, J. (2020). Clinical Predictors of Mortality Due to COVID-19 Based on an Analysis of Data of 150 Patients from Wuhan, China. *Intensive Care Med.* 46 (5), 846–848. doi:10.1007/s00134-020-05991-x

Scully, E. P., Haverfield, J., Ursin, R. L., Tannenbaum, C., and Klein, S. L. (2020). Considering How Biological Sex Impacts Immune Responses and COVID-19 Outcomes. *Nat. Rev. Immunol.* 20 (7), 442–447. doi:10.1038/s41577-020-0348-8

Shen, Y., Peng, X., and Shen, C. (2020). Identification and Validation of Immune-Related lncRNA Prognostic Signature for Breast Cancer. *Genomics* 112 (3), 2640–2646. doi:10.1016/j.ygeno.2020.02.015

Song, J.-W., Zhang, C., Fan, X., Meng, F.-P., Xu, Z., Xia, P., et al. (2020). Immunological and Inflammatory Profiles in Mild and Severe Cases of COVID-19. *Nat. Commun.* 11 (1), 3410. doi:10.1038/s41467-020-17240-2

Tan, L., Wang, Q., Zhang, D., Ding, J., Huang, Q., Tang, Y.-Q., et al. (2020). Lymphopenia Predicts Disease Severity of COVID-19: a Descriptive and Predictive Study. *Sig Transduct Target. Ther.* 5 (1), 33. doi:10.1038/s41392-020-0148-4

Tan, Y.-X., Tan, T. H. P., Lee, M. J.-R., Tham, P.-Y., Gunalan, V., Druce, J., et al. (2007). Induction of Apoptosis by the Severe Acute Respiratory Syndrome Coronavirus 7a Protein Is Dependent on its Interaction with the Bcl-X L Protein. *J. Virol.* 81 (12), 6346–6355. doi:10.1128/JVI.00090-07

Taniguchi-Ponciano, K., Vadillo, E., Mayani, H., Gonzalez-Bonilla, C. R., Torres, J., Majluf, A., et al. (2021). Increased Expression of Hypoxia-Induced Factor 1α mRNA and its Related Genes in Myeloid Blood Cells from Critically Ill COVID-19 Patients. *Ann. Med.* 53 (1), 197–207. doi:10.1080/07853890.2020.1858234

Wang, F., Nie, J., Wang, H., Zhao, Q., Xiong, Y., Deng, L., et al. (2020). Characteristics of Peripheral Lymphocyte Subset Alteration in COVID-19 Pneumonia. *J. Infect. Dis.* 221 (11), 1762–1769. doi:10.1093/infdis/jiaa150

Wang, P., Xue, Y., Han, Y., Lin, L., Wu, C., Xu, S., et al. (2014). The STAT3-Binding Long Noncoding RNA Lnc-DC Controls Human Dendritic Cell Differentiation. *Science* 344 (6181), 310–313. doi:10.1126/science.1251456

Wen, W., Su, W., Tang, H., Le, W., Zhang, X., Zheng, Y., et al. (2020). Immune Cell Profiling of COVID-19 Patients in the Recovery Stage by Single-Cell Sequencing. *Cell Discov* 6, 31. doi:10.1038/s41421-020-0168-9

Wichmann, D., Sperhake, J.-P., Lütgehetmann, M., Steurer, S., Edler, C., Heinemann, A., et al. (2020). Autopsy Findings and Venous Thromboembolism in Patients with COVID-19. *Ann. Intern. Med.* 173 (4), 268–277. doi:10.7326/M20-2003

Wilk, A. J., Shankar, R. D., Shen-Orr, S. S., Thomson, E., Wiser, J., Butte, A. J., et al. (2020). A Single-Cell Atlas of the Peripheral Immune Response in Patients with Severe COVID-19. *Nat. Med.* 26 (7), 1070–1076. doi:10.1038/s41591-020-0944-y

Wu, C., Chen, X., Cai, Y., Xia, J. a., Zhou, X., Xu, S., et al. (2020). Risk Factors Associated with Acute Respiratory Distress Syndrome and Death in Patients with Coronavirus Disease 2019 Pneumonia in Wuhan, China. *JAMA Intern. Med.* 180 (7), 934–943. doi:10.1001/jamainternmed.2020.0994

Yang, L., Liu, S., Liu, J., Zhang, Z., Wan, X., Huang, B., et al. (2020). COVID-19: Immunopathogenesis and Immunotherapeutics. *Sig Transduct Target. Ther.* 5(1), 128. doi:10.1038/s41392-020-00243-2

Yang, Y., Shen, C., Li, J., Yuan, J., Wei, J., Huang, F., et al. (2020). Plasma IP-10 and MCP-3 Levels Are Highly Associated with Disease Severity and Predict the Progression of COVID-19. *J. Allergy Clin. Immunol.* 146 (1), 119–127. e4. doi:10.1016/j.jaci.2020.04.027

Yue, Y., Nabar, N. R., Shi, C.-S., Kamenyeva, O., Xiao, X., Hwang, I.-Y., et al. (2018). SARS-coronavirus Open Reading Frame-3a Drives Multimodal Necrotic Cell Death. *Cell Death Dis* 9 (9), 904. doi:10.1038/s41419-018-0917-y

Zhang, B., and Horvath, S. (2005). A General Framework for Weighted Gene Co-expression Network Analysis. *Stat. Appl. Genet. Mol. Biol.* 4. Article17. doi:10.2202/1544-6115.1128

Zhou, F., Yu, T., Du, R., Fan, G., Liu, Y., Liu, Z., et al. (2020). Clinical Course and Risk Factors for Mortality of Adult Inpatients with COVID-19 in Wuhan,

China: a Retrospective Cohort Study. *The Lancet* 395(10229), 1054–1062. doi:10.1016/S0140-6736(20)30566-3

Zhou, Y., Fu, B., Zheng, X., Wang, D., Zhao, C., Qi, Y., et al. (2020). Pathogenic T-Cells and Inflammatory Monocytes Incite Inflammatory Storms in Severe Covid-19 Patients. *Natl. Sci. Rev.* 7 (6), 998–1002. doi:10.1093/nsr/nwaa041

Zhou, Z., Huang, C., Zhou, Z., Huang, Z., Su, L., Kang, S., et al. (2021). Structural Insight Reveals SARS-CoV-2 ORF7a as an Immunomodulating Factor for Human CD14+ Monocytes. *iScience* 24 (3), 102187. doi:10.1016/j.isci.2021.102187

Conflict of Interest: The authors declare that the research was conducted in the absence of any commercial or financial relationships that could be construed as a potential conflict of interest.

Publisher's Note: All claims expressed in this article are solely those of the authors and do not necessarily represent those of their affiliated organizations or those of the publisher, the editors, and the reviewers. Any product that may be evaluated in this article or claim that may be made by its manufacturer is not guaranteed or endorsed by the publisher.

frontiers | Frontiers in Molecular Biosciences

ORIGINAL RESEARCH
published: 28 June 2022
doi: 10.3389/fmolb.2022.909312

Nematode microRNAs can Individually Regulate Interferon Regulatory Factor 4 and mTOR in Differentiating T Helper 2 Lymphocytes and Modulate Cytokine Production in Macrophages

Julien Soichot[1], *Nathalie Guttmann*[1], *Hubert Rehrauer*[2], *Nicole Joller*[3] and *Lucienne Tritten*[1*†]

[1]Institute of Parasitology, Vetsuisse Faculty, University of Zurich, Zurich, Switzerland, [2]Functional Genomics Center Zurich, ETH Zurich/University of Zurich, Zurich, Switzerland, [3]Department of Quantitative Biomedicine, University of Zurich, Zurich, Switzerland

OPEN ACCESS

Edited by:
Yong Sun Lee,
National Cancer Center, South Korea

Reviewed by:
Ann-Kristin Östlund Farrants,
Stockholm University, Sweden
Mrigank Srivastava,
Central Drug Research Institute (CSIR), India

***Correspondence:**
Lucienne Tritten
Lucienne.tritten@uzh.ch

†Present address:
Lucienne Tritten,
Swiss Tropical and Public Health Institute, University of Basel, Switzerland

Specialty section:
This article was submitted to Molecular Diagnostics and Therapeutics, a section of the journal Frontiers in Molecular Biosciences

Received: 31 March 2022
Accepted: 27 May 2022
Published: 28 June 2022

Citation:
Soichot J, Guttmann N, Rehrauer H, Joller N and Tritten L (2022) Nematode microRNAs can Individually Regulate Interferon Regulatory Factor 4 and mTOR in Differentiating T Helper 2 Lymphocytes and Modulate Cytokine Production in Macrophages. Front. Mol. Biosci. 9:909312. doi: 10.3389/fmolb.2022.909312

Parasitic nematodes are masterful immunomodulators. This class of pathogens has evolved a spectrum of sophisticated strategies to regulate and evade host immune responses, mediated through the release of various molecules. In this context, the release of microRNAs (miRNAs), short post-transcriptional regulators of gene expression, has been of particular interest in the host-parasite interplay. Evidence that parasite-derived miRNAs modulate host innate and adaptive immune responses has become increasingly compelling. However, since miRNAs are usually contained in extracellular vesicles containing other mediators, it is difficult to assign an observed effect on host cells to miRNAs specifically. Here, the effects of some abundantly secreted miRNAs by nematodes used as models of gastrointestinal infections (*Heligmosomoides polygyrus bakeri*, *Trichuris muris* and *Ascaris suum*) were evaluated, addressing the potential of parasite miRNAs to impair *in vitro* differentiation of two important types of immune cells in the context of helminth infections, Th2 lymphocytes and macrophages. Mimicking a continuous exposure to low concentrations of nematode miRNAs, the interferon gamma signaling, the IL-2/STAT5 signaling, and the mTOR signaling pathways were identified as downregulated by Hpo-miR-71-5p. Interferon regulatory factor 4 (*Irf4*) was validated as a target of Hpo-miR-71-5p, while *Mtor* is targeted by Asu-miR-791-3p, abundant in the *T. muris* secretions. By trend, Hpo-miR-71-5p impacts mildly but consistently on the amounts of inflammatory cytokines in unpolarized macrophages but leads to slightly increased IL-10 level in alternatively activated cells. In addition, our data suggests that transfected miRNAs remain for days in recipient cells, and that Hpo-miR-71-5p can incorporate into mouse Argonaute protein complexes. Nematode miRNAs can impair both innate and adaptive arms of host immunity. Hpo-miR-71-5p in particular, absent in mammals, interacts with host genes and pathways with crucial involvement in anthelmintic immune responses. This report brings new insights into the dynamics of miRNA-driven immunomodulation and highlights putative targeted pathways. Although the absolute repression is subtle, it is expected that

the dozens of different miRNAs released by nematodes may have a synergistic effect on surrounding host cells.

Keywords: parasitic nematode, microRNA, immunomodulation, T cells, macrophages, IRF4, mTOR, cytokines

INTRODUCTION

Parasitic helminths are macroscopic pathogens of plants and animals, including humans. In 2013, over 2 billion human cases were attributed to the main helminth species (Herricks et al., 2017). In 2020, 24% of the world's population was infected with soil-transmitted helminths (*Ascaris lumbricoides*, *Trichuris trichiura*, and the hookworms *Necator americanus* and *Ancylostoma duodenale*), affecting primarily the poorest and most deprived populations of tropical and subtropical areas of the world (World Health Organization, 2020). However, helminth infections cause not only diseases of the poor but also have a colossal economic impact in Western countries, especially in the livestock industry. Gastrointestinal (GI) nematodes alone cause production losses in up to 50% of ruminant farms analyzed in several European studies (Charlier et al., 2014). Improvements in diagnostics and control interventions will be crucial, as the development of drug resistance has been fast and severe, for the most part in livestock parasites (Kaplan and Vidyashankar, 2012; Selzer and Epe, 2020).

Upon host colonization, helminth infections and resulting diseases tend to become stable and chronic. This is at least in part due to the exceptional abilities of this class of pathogens to manipulate their hosts and modify surrounding tissues to their own advantage (Maizels and McSorley, 2016).

The so-called "modified type 2 immunity" elicited by helminths in their mammalian hosts is characterized by a $CD4^+$ T helper 2 (Th2)-driven response, accompanied by regulatory T cell (Treg) subsets that dampen inflammation (Allen and Maizels, 2011; Girgis et al., 2013). Th2 responses confer partial resistance to parasitic worms and help control infection and inflammation while promoting wound healing. While hosts mount immune responses to constrain the detrimental impact of such infections, helminths have evolved a spectrum of sophisticated strategies to regulate and evade host immune responses. As a result, the immune pathways that would be engaged to lead to worm expulsion are neutralized, and immunity is globally dampened, also affecting responses to unrelated bystander antigens (Maizels and McSorley, 2016). These effects are mediated through the release of parasite-derived molecules of various types.

Excretory/secretory (E/S) molecules of the phylum *Nematoda* have been studied extensively for their immunomodulatory properties. E/S soluble proteins in particular affect host immune responses through various mechanisms from mimicking host molecules, to inhibiting immune processes, degrading key host molecules, or facilitating entry into and movement within hosts (Bellafiore et al., 2008; Hewitson et al., 2009; Shepherd et al., 2015; Tritten et al., 2021). Other types of molecules contribute to the continuous dialogue between helminth and host, including glycans, lipids (Whitehead et al., 2020) and nucleic acids (Buck et al., 2014; Sotillo et al., 2020). Following pioneering studies demonstrating host gene modulatory effects of nematode microRNAs (miRNAs) (Buck et al., 2014), non-coding RNAs have been of particular interest in the host-parasite interplay. miRNAs are short post-transcriptional regulators of gene expression that are integral to virtually all biological processes in eukaryotes. Silencing of the partially complementary mRNA targets occurs through a combination of translational repression and/or mRNA destabilization, ultimately leading to mRNA degradation (Jonas and Izaurralde, 2015). For their regulatory functions, miRNAs associate with protein complexes including Argonaute proteins (AGO), part of the RNA induced silencing complex. The way a targeted mRNA becomes silenced depends on the degree of complementarity between miRNA and the mRNA site. Full complementarity enables catalytically active AGO to cleave the mRNA directly, while incompletely complementary miRNAs require recruitment of additional protein partners to mediate silencing through a combination of repression, deadenylation, decapping, and degradation of the transcript (Jonas and Izaurralde, 2015). miRNA-driven repression is characterized by both redundancy and pleiotropy in targeted genes and pathways. Evidence that parasite-derived miRNAs modulate host innate and adaptive immune responses has become increasingly compelling (Coakley et al., 2015, 2016). Available data suggest a widespread incorporation of helminth miRNAs into a broad range of host cells. Various crucial host immune functions are repressed by nematode miRNAs *in vitro* following internalization of parasite-derived extracellular vesicles (EVs), as well as *in vivo* (Buck et al., 2014; Zamanian et al., 2015; Coakley et al., 2017; Eichenberger et al., 2018a; Liu et al., 2019; Meningher et al., 2020; Tran et al., 2021). miRNAs released from *Litomosoides sigmodontis* were preferentially detected in host macrophages *in vivo* (Quintana et al., 2019), similar to miRNAs from *Schistosoma japonicum* EVs (Liu et al., 2019). miRNAs found in *S. japonicum* EVs regulated host macrophage functions and are able to incorporate into mouse AGO2 *in vitro* (Liu et al., 2019). *Schistosoma mansoni* EV-contained miRNAs are taken up by host T helper cells and impair Th2 differentiation by targeting MAP3K7 and inhibiting NF-κB activity. The same paper reported the presence of *S. mansoni* miRNAs in Peyer's patches and mesenteric lymph nodes of infected hosts (Meningher et al., 2020). Similarly, *Haemonchus contortus*-derived circulating miRNAs were detected in infected sheep lymph nodes (Gu et al., 2017). The trematode *Fasciola hepatica* hijacks host miRNA machinery in macrophages, where they negatively regulate production of inflammatory cytokines and modulate early immune response to the parasite (Tran et al., 2021). Several gaps remain in our understanding of host gene repression by helminth miRNAs (Claycomb et al.,

2017). Currently, it seems that in order to regulate host genes, helminth miRNAs must be loaded onto host AGO2 proteins, taking advantage of the effector machinery in place (Donnelly and Tran, 2021), an interaction likely dictated by miRNA sequence and structure, and perhaps also by cell-specific needs (Ricafrente et al., 2020; Brosnan et al., 2021; Donnelly and Tran, 2021; Luo et al., 2021).

In addition to cells of the innate immune system such as macrophages, important recipient cells of nematode miRNAs (Quintana et al., 2019), a few reports indicate that T lymphocyte development and differentiation may be commonly targeted by helminth-derived miRNAs (Duguet et al., 2020; Meningher et al., 2020). Here, we studied the effects of some abundantly secreted miRNAs by nematodes used as models of gastrointestinal infections (*Heligmosomoides polygyrus bakeri*, *Trichuris muris* and *Ascaris suum*). Computational target predictions in the mouse genome identified the master transcription factor of Th2 differentiation *Gata3* among other important genes. We addressed the potential of parasite miRNAs to impair Th2 and macrophage differentiation *in vitro*, which evolved as a response to helminth infections and confer some degree of anthelmintic resistance (Allen and Maizels, 2011). We showed that crucial pathways for the differentiation into Th2 cells are downregulated by transfection of synthetic nematode miRNAs and validated interactions with some of their predicted targets. By trend, macrophages exposed to nematode miRNAs produced reduced amounts of inflammatory cytokines. We conclude that nematode miRNAs can impair both the innate and adaptive arms of host immunity by interacting with essential genes.

MATERIALS AND METHODS

Bioinformatics Analysis

Secreted miRNA lists from *H. polygyrus bakeri*, *T. muris*, and *A. suum* were retrieved from the literature (Buck et al., 2014; Tritten et al., 2017; Eichenberger et al., 2018b; Hansen et al., 2019). Target prediction in the mouse genome for the top 20 most abundant miRNAs was performed as described previously (Duguet et al., 2020) using the TargetScan software package v. 7 (http://www.targetscan.org), implemented as a standalone workflow under iPortal (Kunszt et al., 2015) and openBIS (Bauch et al., 2011), using default parameters (Agarwal et al., 2015). The model takes 14 different features of the miRNA, miRNA site, or mRNA into account to predict which sites within mRNAs are most effectively targeted by miRNAs and further relies on a multi-species alignment of 3′UTR across 84 vertebrate species derived from the UCSC genome browser. Results were deposited in Mendeley Data: https://data.mendeley.com//datasets/358nm9mhpr/1). Predicted targets were screened using R Studio (4.0.3 (R Core Team, 2017)) against lists of typical gene markers and molecules involved in development of Th2 cells (Stubbington et al., 2015; Zhu, 2015), as well as all mouse genes listed in the 15 KEGG pathways under 5.1. "Immune system" (Kanehisa et al., 2017) accessed in May-June 2018. KEGG pathways comprised: Hematopoietic cell lineage, Toll-like receptor signaling pathway, NOD-like receptor signaling pathway, C-type lectin receptor signaling pathway, Natural killer cell mediated cytotoxicity, Antigen processing and presentation, T cell receptor signaling, Th1 and Th2 cell differentiation, Th17 cell differentiation, IL-17 signaling pathway, Fc epsilon RI signaling pathway, Fc gamma R-mediated phagocytosis, Leukocyte transendothelial migration, Intestinal immune network for IgA production, and Chemokine signaling pathway.

T Cell Differentiation

Wild-type female C57BL/6J mice were ordered from Envigo (Netherlands) and euthanized with CO_2 between 5 and 12 weeks of age to isolate naïve $CD4^+$ T cells. The spleen and the inguinal, axillary, brachial, and cervical lymph nodes were dissected and processed as described (Flaherty and Reynolds, 2015), with some modifications. Under sterile conditions, tissues were crushed against a 100 μm cell strainer (Corning) and filtered through a second 100 μm cell strainer. Cells were pelleted at 475 x *g* for 5 min at 4°C. Cells from lymph nodes were resuspended in sterile PBS and kept on ice. Splenic cells were resuspended in 1 ml ACK lysis buffer (Gibco) for 1 min to remove erythrocytes and washed twice with PBS.

Naïve $CD4^+$ T cells were purified by depletion of memory $CD4^+$ T cells and non-$CD4^+$ T cells using a mouse Naïve $CD4^+$ T cell Isolation Kit (Miltenyi Biotec) on LS columns (Miltenyi Biotec), following the manufacturer's instructions. Isolated naïve $CD4^+$ T cells were counted and cultured in anti-CD3ε (clone 145-2C11, eBioscience) and α-CD28 (clone 37.51, eBioscience) coated plates in 500 μl RPMI complete (RPMI-1640 containing 10% v/v FBS (Corning), 100 U/ml penicillin, 100 μg/ml streptomycin, 2 mM L-glutamine and 50 μM β-mercaptoethanol), supplemented with 10 ng/ml recombinant mouse IL-4 (Biolegend), 30 U/ml recombinant human IL-2 (Biolegend), and 5 μg/ml anti-IFN-γ (clone XMG1.2, eBioscience), and 2 μg/ml anti-CD28 (Flaherty and Reynolds, 2015)). Cells were cultured at 37°C, 5% CO_2. After 48 h, 500 μl fresh RPMI complete were added to each well. Cells were counted at 72 h and seeded at 1×10^6 cells/ml in RPMI complete containing only 20 U/ml recombinant human IL-2 (Biolegend) and 5 μg/ml anti-mouse IFN-γ (clone XMG1.2, eBioscience). After 92 h in culture, cells were re-stimulated at 1×10^6 cells/ml with 1 μg/ml anti-CD3ε (clone 145-2C11, eBioscience) for 4 h prior to RNA extraction, or with 1 μg/ml ionomycin (Merck) and 10 ng/ml PMA (Sigma-Aldrich) for 4 h with the addition of 3 μg/ml brefeldin A (ThermoFisher Scientific) for the last 3 h for FACS analysis, as described (Flaherty and Reynolds, 2015). Total RNA was extracted using an RNeasy Plus mini kit (Qiagen). RNA concentration was quantified using a Qubit 4 Fluorometer. Prior to FACS analysis, cells were treated with 10 μg/ml brefeldin A and with a dilution of 1:1,000 Live/Dead Fixable Near-IR Dead Cell Stain Kit (Invitrogen) according to the manufacturer's instructions. Cells were fixed and permeabilized with a BD Cytofix/Cytoperm kit (BD Biosciences) and intracellular staining was carried out with APC anti-mouse IFN-γ antibody (Biolegend) diluted 1:20 and PE-efluor610 anti-mouse IL-13 antibody (Invitrogen) diluted 1:100. Data were acquired on a Cytoflex S flow cytometer (Beckman Coulter) and further analyzed in FlowJo Software v10.8.

Compensation matrix was created using VersaComp Antibody Capture Bead Kit (Beckman Coulter).

Differentiating T Cell miRNA Transfection

Cells were transfected with synthetic miRNAs once or several times at various time points, between 0 and 90 h after culture start. We used mirVana miRNA mimics (Ambion, LifeTechnologies) of Hpo-miR-71-5p (mature sequence: UGA AAGACAUGGGUAGUGAGAC), Hpo-miR-100-5p (mature sequence: AACCCGUAGAUCCGAACUUGUGU), and Hpo-miR-10021-5p (mature sequence: UGAGAUCAUCACCAU AAGCACA), as they are among the most abundant freely circulating miRNAs found in *H. polygyrus bakeri* culture supernatants (Buck et al., 2014; Tritten et al., 2017). We used additionally Hpo-miR-1-3p (mature sequence: UGGAAUGUA AAGAAGUAUGUA) the mirVana miRNA mimic universal negative control #1 (Ambion, LifeTechnologies), a random sequence miRNA mimic molecule validated to not produce identifiable effects on known miRNA function in human cells. miRNA mimics were transfected into 2×10^5—1×10^6 cells using lipofectamine RNAiMax (Invitrogen) and OPTI-MEM I 1x (Gibco) following the manufacturer's protocol at final concentrations of 10 nM or 50 nM. A combination of miR-71, miR-10021, and miR-100 was also tested at the same total concentration (e.g., 3.33 nM of each individual miRNA). Information on miRNAs used in this work is provided in more detail in Supplementary Table S4.

Transfection Efficiency and Imaging

The proportion of transfected Th2 cells was determined by FACS analysis following transfection with 50 nM BLOCK-iT fluorescent oligo (Invitrogen) and lipofectamine RNAiMax (Invitrogen) as described above. The proportion of FITC-labeled cells was determined 1–48 h post-transfection in cells at various stages throughout the differentiation protocol (from naïve $CD4^+$ T cells to 96 h in culture) exposed to i) BLOCK-iT fluorescent oligo + lipofectamine, ii) BLOCK-iT fluorescent oligo without lipofectamine and iii) lipofectamine only. Cells transfected with 40 nM BLOCK-iT fluorescent oligo were imaged 1 and 3 h post-transfection and co-stained with LysoTracker Red DND-99 (Invitrogen) for live cell imaging in a Leica DMI6000 B inverted fluorescence microscope (Leica Microsystems, Germany) equipped with a Leica DFC365 FX camera (Leica) and recorded using the LAS X software (Leica). Images were compiled in ImageJ (v.1.53k).

Transcriptome Analysis

Total RNA from 3 independent experiments of differentiating Th2 cells treated every 24 h with 10 nM miRNA was quality controlled using the fragment analyzer (Agilent Technologies, Santa Clara, CA, United States) at the Functional Genomics Center Zurich. Subsequent library preparation and sequencing was performed using Illumina Truseq mRNA library protocol. RNA sequencing was performed using an Illumina Novaseq 6000 sequencer with single read 100bp. Sequencing reads were aligned using STAR (Spliced Transcripts Alignment to a Reference) (Dobin et al., 2013) with the Ensembl mouse genome build GRCm38.p6 (provided by GENCODE M23 release) as reference. Gene expression values were obtained with the function featureCounts from the R package Rsubread (Liao et al., 2013). Differential expressed (DE) genes analysis was computed with the Bioconductor package EdgeR. Determination of cell types and their proportion in our samples was assessed by Digital Sorting Algorithm (Zhong et al., 2013). Following the analysis of the estimated cell type fractions, DE genes were computed comparing different miRNA treatments versus the universal negative control, or versus lipofectamine (the transfection reagent) only, using the donor mouse as experimental factor. Variability caused by differences in cell type composition was estimated and modeled using the RUVSeq package (Risso et al., 2014). Raw data was deposited on GEO https://www.ncbi.nlm.nih.gov/geo/query/acc.cgi?acc=GSE180829 (reviewer token: qrchacisjnojnmv) DE genes (cutoff: $p < 0.01$) were subjected to pathway analysis in Enrichr (Kuleshov et al., 2016; Xie et al., 2021), using the MSigDB Hallmark 2020 as library (Liberzon et al., 2015).

Macrophage Assays–miRNA Transfections and Polarization

Raw 264.7 blood macrophages (cell line 91062702, ECACC) were seeded at a density of 5×10^5 cells in 500 µl DMEM 1x (Gibco) containing 10% v/v FBS (Corning), 100 U/ml penicillin, and 100 µg/ml streptomycin, and transfected with 100 nM mirVana mimics (list) and lipofectamine RNAiMax (Invitrogen). After 24 h, cells were collected, washed with PBS and resuspended in 500 µl fresh media without further addition (M0: neutral activation status), or polarized with 20 ng/ml IFN-γ (Biolegend) and 100 ng/ml lipopolysaccharide (eBioscience; M1: classical activation), or 10 ng/ml recombinant mouse IL-4 (Biolegend; M2: alternative activation). Cells were incubated for 6 h at 37°C, 5% CO_2, and collected for RNA isolation. Supernatants were centrifuged for 10 min at 1,500 x *g*, 4°C to remove debris and frozen at -80°C. The experiment was conducted 3 times independently.

Luminex Assay–Cytokines in Supernatants

Supernatants from Raw 264.7 macrophages were analyzed on a Luminex FlexMAP 3D using a Milliplex MAP Mouse Cytokine/Chemokine Magnetic kit (MCYTMAG-70K-PX32; Merck Millipore) for the simultaneous measurement of 32 cytokines and chemokines, following the manufacturer's recommendations. Median fluorescent intensity data were analyzed in GraphPad Prism (v. 9.2.0) using a five-parameter logistic curve-fitting method for calculating cytokine/chemokine concentration as recommended by the manufacturer. Data were produced for 3 independent experimental replicates. Concentrations and the Dunnett's test were computed in RStudio.

Reporter Assays

Predicted target sites were inserted on the pmirGLO dual luciferase miRNA target expression vector (Promega) and

cloned into HeLa cells. Briefly, 20,000 cells were seeded into Costar flat-bottom white 96-well plates in 200 µl media (DMEM 1x high-glucose (Gibco) containing 10% v/v FBS (Corning), 100 U/ml penicillin and 100 µg/ml streptomycin) and allowed to attach for 24 h at 37°C, 5% CO_2. HeLa cells were co-transfected with 200 ng/well vector (with or without target site insert) and different miRNA concentrations (50, 25, or 0 nM) using lipofectamine reagent 3000 (Invitrogen), following manufacturer's instructions. Cells were lysed and luminescence was quantified sequentially (Firefly followed by Renilla) using the Dual-Glo luciferase assay system (Promega). Assays were conducted 3 times independently, with 5-6 well per condition. A two-step normalization analysis was undertaken to quantify luciferase relative activity (Campos-Melo et al., 2014). Dunnett's tests were performed for each miRNA concentrations separately, with the luminescence ratios obtained on the vector containing the insert versus those obtained from the empty vector, as described (Campos-Melo et al., 2014).

Mouse AGO2 Pull Down Assays and RT-qPCR

To verify that synthetic miRNAs were incorporated into host cell silencing machinery, differentiating mouse Th2 cells were transfected at 92 h with 75 nM mirVana mimic Hpo-miR-71-5p, which is a nematode-specific miRNA, absent in mammalian cells. Mouse AGO2 pull-down assays followed by miRNA isolation were conducted 4 h later using a microRNA Isolation kit Mouse Ago2 (Fujifilm). For each condition (Hpo-miR-71-5p transfected and untransfected samples), 4×10^6 cells were used in 3 biological replicates representing different donor mice. The same procedure was applied to fresh mesenteric lymph nodes from 2 *H. polygyrus bakeri* infected mice. A custom-designed stem-loop RT-qPCR assay (modified from (Tritten et al., 2014); stem-loop primer for RT: 5′-CCA GTG CAG GGT CCG AGG TA-3′, forward primer: 5′-TCG GGT AGT GAA AGA CAT GGG TAG T-3′, universal reverse primer: 5′-CCA GTG CAG GGT CCG AGG TA-3′, probe: 5′- FAM - CGC ACT GGA TAC GAC GTC TC-MGBQ5 - 3′) was employed to detect the presence of transfected Hpo-miR-71-5p in miRNAs isolated from mouse Ago2 pull-downs. We used the RT Maxima H Minus reverse transcriptase (Thermo Scientific) and the TaqMan Fast Advanced master mix (Applied Biosystems); amplification was performed on a QuantStudio 7 Flex real-time PCR system (Applied Biosystems/Life Technologies).

Ethics Approval

Ethical clearance for work involving mice was obtained from the Cantonal Veterinary Office of Zurich (permit number ZH186/18). All experiments were conducted in accordance with the Swiss cantonal and national regulations on animal experimentation. The *H. polygyrus bakeri* life cycle is maintained by Prof. J. Keiser at the Swiss TPH (University of Basel), under license 2070 granted by the Cantonal Veterinary Office of Basel-Stadt.

RESULTS

Hypothesizing that nematode miRNAs present at higher concentrations may have a greater impact on host gene expression, we focused our analysis arbitrarily on the 20 miRNAs most abundantly secreted by three parasitic species, *H. polygyrus bakeri*, *T. muris* and *A. suum* (Supplementary Table S1). Genes resulting from target predictions of these miRNAs were matched to genes functionally relevant for T cells and macrophages. The number of predicted interactions between miRNAs and each gene—regardless of the nature of the predicted miRNA binding site and without taking overlapping binding sites into consideration—highlights putative differences in miRNA-mediated host gene regulation by the three nematodes (Supplementary Table S2). For instance, *Gata3* is predicted to be targeted 5x by *H. polygyrus bakeri*, 1x by *T. muris*, and 8x by *A. suum* miRNAs. Guided by the transcriptional network and positive feedback regulation during Th2 cell differentiation (summarized in (Yang et al., 2013; Zhu, 2015), **Figure 1**), we functionally validated several predicted targets of interest in differentiating Th2 cells. Several key elements of the transcriptional network for Th2 differentiation represent computationally predicted targets (**Figure 1**). Among them were genes encoding the Th2 master regulator GATA3 and the IL-4Rα, another molecule central to Th2 immunity elicited against helminths (Allen and Maizels, 2011). Also, the mechanistic target of rapamycin (mTOR) was among the predicted gene targets of *T. muris* secreted miRNAs. The most frequently targeted genes by *H. polygyrus bakeri* and *A. suum* abundantly secreted miRNAs: *D1ertd622e* (or macrophage immunometabolism regulator (MACIR)), predicted to be targeted 169x and 162x, respectively, followed by cAMP response element modulator (*Crem* 113x and 119x, respectively), and *Mapk10*, (84x and 85x, respectively). miRNAs secreted by *T. muris* were predicted to target *D1ertd622e* 191x, *Crem* 113x, and catenin delta 1 (*Ctnnd1*), 79x (Supplementary Table S2).

Individual Abundant Nematode miRNAs Enter Host Cells but do Not Abrogate Th2 Differentiation or Proliferation

To reproduce the regular or constant exposure to worm secretions, as expected during an ongoing infection, the impact of daily transfections with synthetic nematode miRNA on cell proliferation was monitored at 92 h in several experiments (two to eight replicated per condition). Cell counts were not significantly different across miRNA treatments or controls (p = 0.58, **Figure 2A**).

The proportion of Th2 cells, measured by flow cytometry at 96 h and defined by expression of IL-13, varied markedly across experiments (**Figure 2B**). This was also observed with cells from different individual mice of the same batch (age and sex matched, but not necessarily litter mates). On average per transfection condition, only 7.66% (±3.45%; based on 2 experiments) of cells exposed to the 3-miRNA combination (combo; miR-71 + miR-100 + miR-10021) expressed IL-13; 12.23% (±5.45% miR-71) and

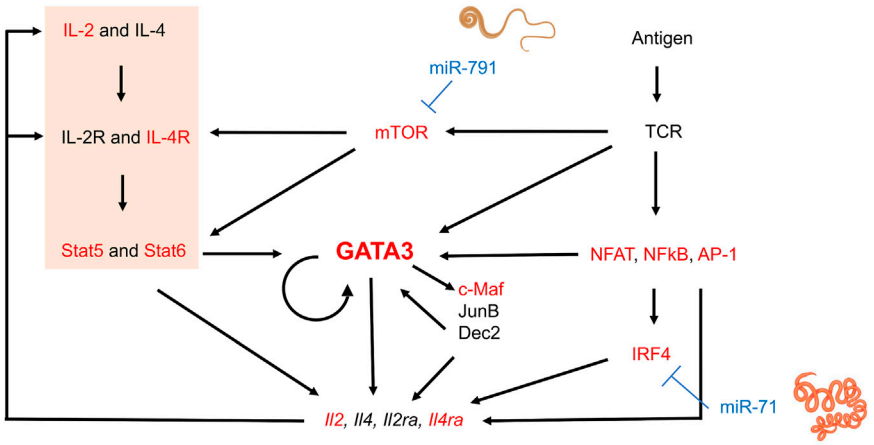

FIGURE 1 | Schematic transcriptional network and positive regulation during Th2 lymphocyte differentiation and interference by nematode miRNAs. Elements in red represent genes of which at least some isoforms represent predicted targets of the 20 most abundantly secreted *H. polygyrus bakeri, T. muris* and *A. suum* miRNAs. Briefly, T cell receptor (TCR) stimulation activates downstream molecules such as nuclear factor of activated T-cells (NFAT), nuclear factor-κB (NFκB), and AP-1, in turn leading to upregulation of interferon regulatory factor 4 (IRF4) (Zhu, 2015). IL-4-mediated Stat6 activation and other signaling pathways also induce GATA3 expression. GATA3 may directly or indirectly regulate Th2 cytokine expression by inducing other transcription factors such as c-Maf, JunB, or Dec2, some of which may further sustain GATA3 expression. The IL-2—Stat5 axis is also crucial for Th2 cytokine production and was significantly downregulated by our transfected miRNAs (orange block). Activated T cells produce IL-2 and IL-4, among others, upregulating IL-2 and IL-4 receptors, creating a positive feedback loop. mTOR in the complex mTORC2 is required for Th2 differentiation *via* two mechanisms: i) repression of expression of negative regulators of IL4-R and STAT6, and ii) promotion of NF-κB-mediated transcription (Chi, 2012). Some elements of this image were created with Biorender.com

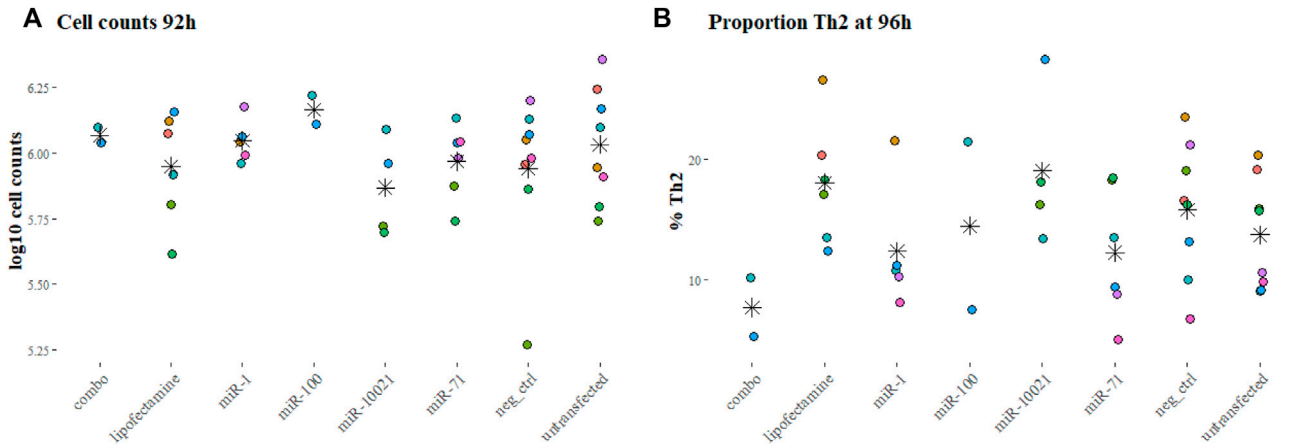

FIGURE 2 | Cell counts and proportions of fully differentiated Th2 cells. Cell counts after 92 h into culture **(A)** and proportion of Th2 cells at the end of the experiments (96 h, **(B)**, as reflection of IL-13 positive labeling, measured by FACS. Colors indicate independent experiments; stars indicate the mean for each miRNA treatment. Cell counts are expressed in $\log_{10}$ of average cell counts.

19.0% (±6.49%; miR-10021) of cells were considered fully differentiated Th2. Untransfected cells reached on average 13.69% (±4.62%) of Th2; cells exposed to the universal negative control (UNC) showed on average 15.79% (±5.64%) differentiated Th2 cells (**Figure 2B**). Th2 proportions across treatments and controls were not significantly different (p = 0.20). The remaining cells were most likely not fully differentiated or uncommitted as *in vitro* differentiation procedures usually yield a maximum of 25% of Th2 cells (Flaherty and Reynolds, 2015). Cells expressing IFN-γ were in the range of 1% of the population or below, confirming a clean Th2 culture.

Transfection efficiency in macrophages and differentiating Th2 lymphocytes was assessed with a fluorescently labeled oligonucleotide (**Figure 3**). Unpolarized and alternatively activated macrophages (M2) showed a high rate of oligo uptake (>80%), only when the transfection reagent was used. In contrast, M1 macrophages showed a lower transfection efficiency, with a third of cells displaying fluorescence. Regardless of time in culture and differentiation status, at least

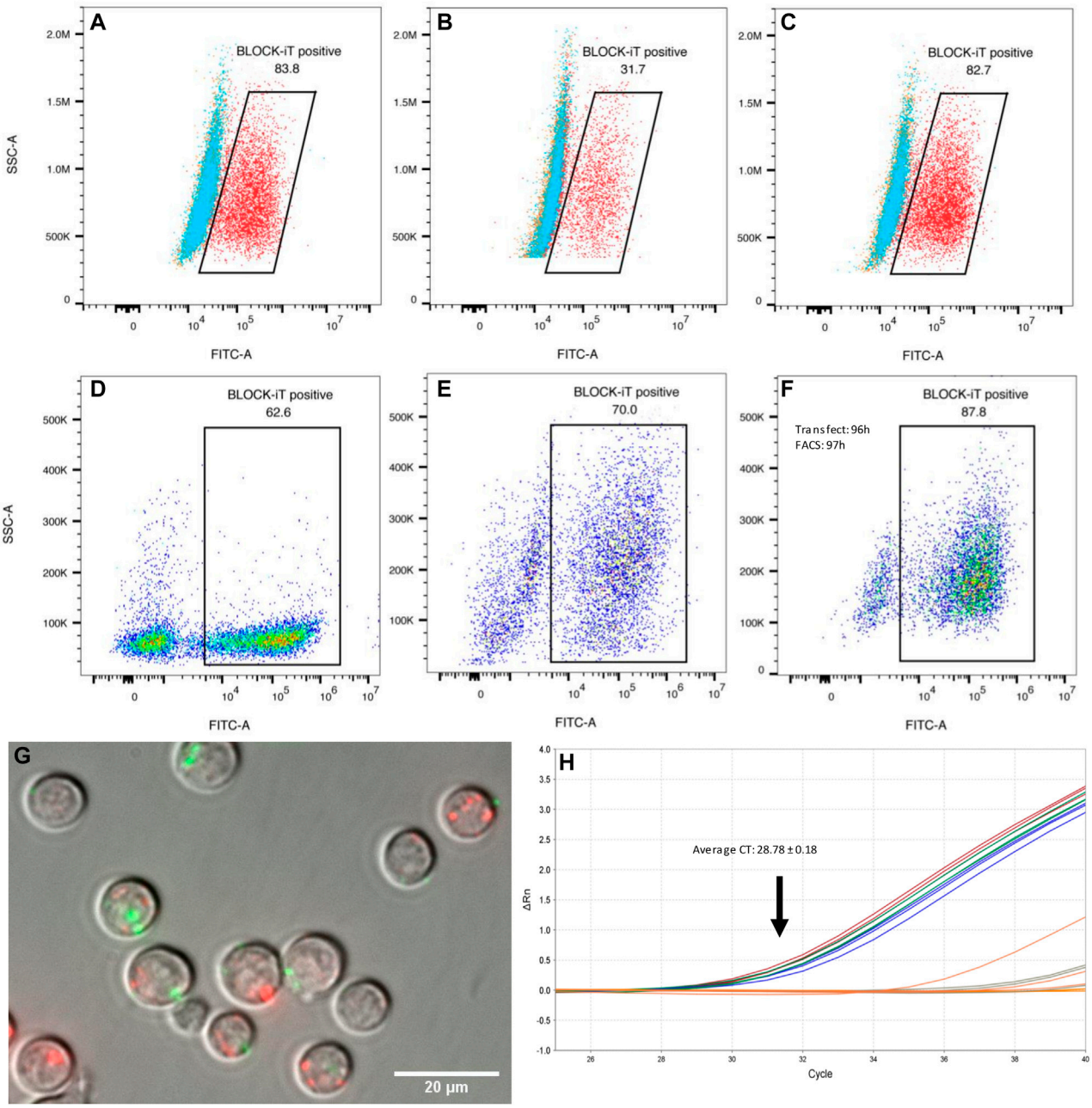

FIGURE 3 | Transfection efficiency. **(A–C)** Raw 264.7 macrophages (mϕ) transfected with a fluorescent oligonucleotide (representative examples). **(A)** 83.8% of unpolarized macrophages showed FITC fluorescence 1 h post transfection with BLOCK-iT fluorescent oligonucleotide (FITC labeled) and lipofectamine (red). Cells exposed to the oligo only are shown in blue, or to the transfection reagent only, in orange. **(B)** Classically activated macrophages (M1) showed only 31.7% transfection efficiency with the fluorescent oligo and lipofectamine (red). **(C)** Alternatively activated macrophages (M2) showed a high transfection efficiency, similar to M0 cells, with 82.7% cells showing FITC labeling. Transfection efficiency in differentiating Th2 cells **(D–F)**. $CD4^+$ naïve T cells were transfected with BLOCK-iT fluorescent oligo upon start of the differentiation protocol (day 0). Transfection efficiency was measured after 1 h **(D)** and again after 48 h **(E)**. Cells transfected at the end of the differentiation protocol (96 h) showed 87.8% of FITC-labelled cells when the oligo was introduced into cells with lipofectamine **(F)**. **(G)** Live cell imaging of transfected differentiating Th2 cells. $CD4^+$ T cells were transfected at 96 h of Th2 differentiation with a FITC-labelled oligo (green) and imaged 1 h post-transfection (magnification: 60 x). Lysosomes were stained with Lyso-Tracker red DND-99 (red). There is a priori no co-localization between introduced oligonucleotides and lysosomes. **(H)** Real-time PCR amplification of Hpo-miR-71-5p from miRNA following mouse AGO pull-downs, 4 h after transfection of Th2 cells with miRNA mimics. miRNA transfected samples are represented by blue, red, and green replicate curves.

TABLE 1 | Most strongly up- and downregulated pathways. DE genes ($p < 0.01$) were submitted to Enrichr for pathway enrichment against the MSigDB Hallmark 2020 library. Combo: combination of miR-100, miR-10021, and miR-71 in equal parts, where the total amount of miRNA introduced is the same as for individual miRNAs (i.e., 10 nM). UNC: universal negative control. Data for miR-100, miR1 and combo are from two independent experiments only.

Downregulated Pathways by miRNA transfection Compared with the UNC miRNA			
	Pathway Name	**Adj. *p*-value**	**Contributing genes**
miR-100* vs UNC	-	-	-
miR-71 vs UNC	Interferon Gamma Response	<0.01	*IFITM3, EIF4E3, IRF4, PSMA2*
	IL-2/STAT5 Signaling	0.04	*IFITM3, IRF4, CD48*
	mTORC1 Signaling	0.04	*EBP, TFRC, CCNG1*
miR-10021 vs UNC	-	-	-
Combo* vs UNC	Interferon Alpha Response	0.07	*LGALS3BP, IFIH1, LY6E*
miR-1* vs UNC	Protein Secretion	0.06	*AP2S1, VPS45, SEC24D*
	Oxidative Phosphorylation	0.06	*UQCRQ, MRPS11, MRPS12, ATP6V1D*
	mTORC1 Signaling	0.06	*SLC9A3R1, SQSTM1, ATP6V1D, NFKBIB*
	Myc Targets V1	0.06	*PSMA2, RUVBL2, NHP2, SNRPA*
Transfection reagent vs UNC	IL-2/STAT5 Signaling	<0.01	*PENK, LRRC8C, PIM1, LIF, CD48*
	mTORC1 Signaling	0.01	*TFRC, DHCR24, TMEM97, ATP6V1D*
	Inflammatory Response	0.01	*OSM, LIF, LTA, CD48*
	Fatty Acid Metabolism	0.04	*GPD2, FASN, DHCR24*
Upregulated pathways by miRNA transfection compared with the UNC miRNA			
-	**Pathway name**	**Adj. p-value**	**Contributing genes**
Transfection reagent vs UNC	TNF-alpha signaling *via* NF-kB	<0.01	*NR4A1, BTG2, EGR2, IRF1, PDE4B, MXD1*
	Apoptosis	0.01	*TGFBR3, BTG2, CASP7, BCL2L11, IRF1*
	Interferon Gamma Response	0.01	*CASP7, IRF1, PDE4B, JAK2, SAMHD1*
	Complement	0.01	*CASP7, SRC, BRPF3, IRF1, JAK2*
	UV Response Up	0.03	*NR4A1, BTG2, BCL2L11, IRF1*
	IL-2/STAT5 Signaling	0.04	*CTLA4, CAPN3, MXD1, IGF1R*
	Inflammatory Response	0.04	*BTG2, IRF1, PDE4B, MXD1*
	heme Metabolism	0.04	*BTG2, CIR1, TENT5C, KDM7A*

60% of live $CD4^+$ T cells showed detectable signal by FACS analysis, as early as 1 h post-exposure to lipofectamine-oligonucleotide complexes. The signal was still detectable in 64.8 and 70% of cells 48 h post-transfection (2 samples, one of them shown in **Figures 3D,E**). A maximum of 10% of cells exposed to the oligonucleotide only (without transfection reagent) showed staining. Live cell imaging 1 h post-transfection allowed the detection of FITC-labeled oligonucleotide in small clusters, which did not co-localize with lysosomes and other acidic organelles (**Figure 3G**). However, this does not exclude the possibility that diffusion of oligonucleotides into the cytosol may have occurred. Lipofectamine transfection reagents are typically expected to deliver their contents *via* fusion with the cell membrane, rather than by active endocytosis, thereby releasing their cargo into the cytosol.

Nematode miR-71 Incorporates Into AGO2 Protein Complexes in Transfected Differentiating Th2 Cells to Regulate Mouse Gene Expression

Our understanding of host gene repression by helminth miRNAs remains incomplete. A currently popular concept is that helminth miRNAs must be loaded onto host silencing protein complexes (AGO2 in particular) to regulate host genes (Donnelly and Tran 2021). This interaction is likely to be at least partially dictated by miRNA sequence and structure (Luo et al., 2021). Because miR-71 is specifically expressed by nematodes and does not have a close homolog in mammalian systems, we asked whether it would also be able to interact with host AGO2. Differentiating Th2 cells (after 92 h in culture) were transfected with miR-71; cells were lysed for AGO2 precipitation after 4 h, followed by miRNA isolation. As expected, the mature Hpo-miR-71-5p was detected by RT-qPCR (Average CT = 28.78 ± 0.18) in transfected cells but not detected in untransfected cells (CT > 37; **Figure 3H**). However, using the same real-time PCR assay, miR-71 was not detected in the mesenteric lymph nodes from *H. polygyrus bakeri* infected mice, likely present below the detection capacity of the assay.

Nematode miRNAs Downregulate Critical Genes and Pathways of the Th2 Differentiation Process

Throughout the 4-day differentiation, $CD4^+$ cells were transfected daily with low doses (10 nM) of the three most abundant *H. polygyrus bakeri* secreted miRNAs, to reproduce

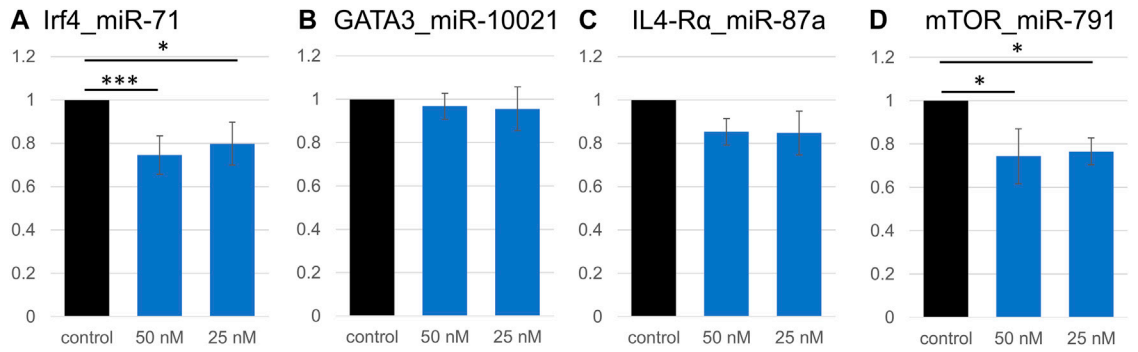

FIGURE 4 | Validation of direct interactions between miRNAs and predicted targets. Relative luciferase activity is significantly decreased due to the insertion of a miR-71 binding site on *Irf4* **(A)**. Signal repression was stronger at 50 nM miRNA ($p < 0.001$, *t*-test) than at 25 nM ($p = 0.02$). Similarly, 50 nM or 25 nM miR-791 led to a decrease in luminescence signal ($p = 0.02$ and $p = 0.03$, respectively; **(D)**, confirming an interaction between miR-791 and its predicted binding site in *Mtor*. No significant decrease in luminescence was detected in all other miRNA:binding site combinations (*Gata3*:miR-10021 **(B)**, and *Il4ra*:miR-87a **(C)**). $^{*}p < 0.05$, $^{***}p < 0.01$.

the expected constant pressure exerted by nematode miRNAs on surrounding host cells. A whole transcriptome analysis was carried out with total RNA collected after 4 days in culture. Sequenced transcripts from three independent differentiation-transfection experiments resulting from a whole transcriptome analysis displayed strong batch effects and inter-individual variability across donor mice. To correct for non-specific responses upon introduction of nucleic acids into cells, all pairwise comparisons were made against treatment with UNC, for which no target is known. Only between 11 and 110 genes were DE across comparisons between synthetic miRNA treatments and the UNC miRNA, cutoff: $p < 0.01$, across all fold-changes and FDRs (**Table 1**, Supplementary Table S3). No upregulated pathways appeared below the *p*-value threshold of 0.05, except in the comparison between the transfection reagent without miRNA and the UNC. The upregulation of these eight pathways can be interpreted as non-specifically downregulated by the UNC miRNA. Some of these overlap with pathways downregulated by other miRNAs, however, without overlap of the contributing genes.

A closer look at the most strongly up- and downregulated genes provides further insights into the effects of nematode miRNA mimics on expression of individual genes. SpiB, a transcription factor associated with the DN3 stage in T cells, was among genes with the highest fold change after transfection with miR-71, miR-100, and miR-10021 individually or in combination. Among the most strongly downregulated genes, a large fraction shows involvement in cell metabolism, with no unique functions in T lymphocytes. Determinants of lysosomal function (e.g., transcription factor EB (*Tfeb*) and N-sulfoglucosamine sulfohydrolase (*Sgsh*)) were downregulated. Of special interest was the downregulation of interferon-inducible transmembrane (IFITM) proteins (*Ifitm3*) and homeodomain-only protein homeobox (*Hopx*), both associated with $CD4^+$ T cells differentiation potential (Opejin et al., 2020; Yánez et al., 2019, 2020). CD48 is crucial for $CD4^+$ T cell activation, as observed in CD48-deficient mice (González-Cabrero et al., 1999); however, downregulation by miR-71 is likely non-specific since *Cd48* expression was decreased by the transfection reagent alone. The mTOR signaling controls multiple effector T cell fates, including Th2. mTORC1 regulates exit from quiescence of naïve T cells, which undergo metabolic reprogramming (Yang et al., 2013). For instance, mTORC1 activates transcription factors (e.g., HIF-1α and MYC), which in turn stimulate transcription of the transferrin receptor (TFRC; downregulated upon miR-71 treatment), required to import cofactor Fe^{3+} to support cell growth and proliferation (Truillet et al., 2017). Among molecules of the transcriptional network and positive regulation of Th2 lymphocyte differentiation (**Figure 1**), our transcriptome analysis did not confirm significant regulation of *Gata3, Il4ra, Nfat, NFkB,* or *c-Maf.* However, interferon regulatory factor 4 (*Irf4*) showed a modest but significant decrease (log2 FC = -0.19) in miR-71 exposed cells. IRF4 promotes differentiation of naïve $CD4^+$ T cells into Th2, Th9, Th17, or T follicular helper cells. It is required for functional effector regulatory T cells, as well as for the differentiation of many myeloid, lymphoid, and dendritic cells (Huber and Lohoff, 2014). Several mechanisms exist: IRF4 may promote IL-4 production by binding to the IL-4 promoter directly and in cooperation with members of the NFAT transcription factor family, by indirectly regulating IL-2-mediated Th2 expansion, or by upregulating GATA3 expression. In fact, overexpression of GATA3 may rescue IL-4 production in $Irf4^{-/-}$ Th2 cells, suggesting a pivotal role for IRF4-dependent GATA3 expression for T cell differentiation into Th2 (Lohoff et al., 2002; Huber and Lohoff, 2014). IRF4 expression is primarily induced by antigen receptor engagement, stimulation with LPS, or signaling induced by CD40 or IL-4 (Gupta et al., 1999). In T cells, its expression declines after reaching peaking levels within a few hours following TCR stimulation, when cells return to a resting state (Huber and Lohoff, 2014). IRF4 also likely acts in conjunction with BATF and JUN. Finally, IL-2—STAT5 signaling is among pathways tuned down by miR-71, *via* downregulation of several genes, which is another key

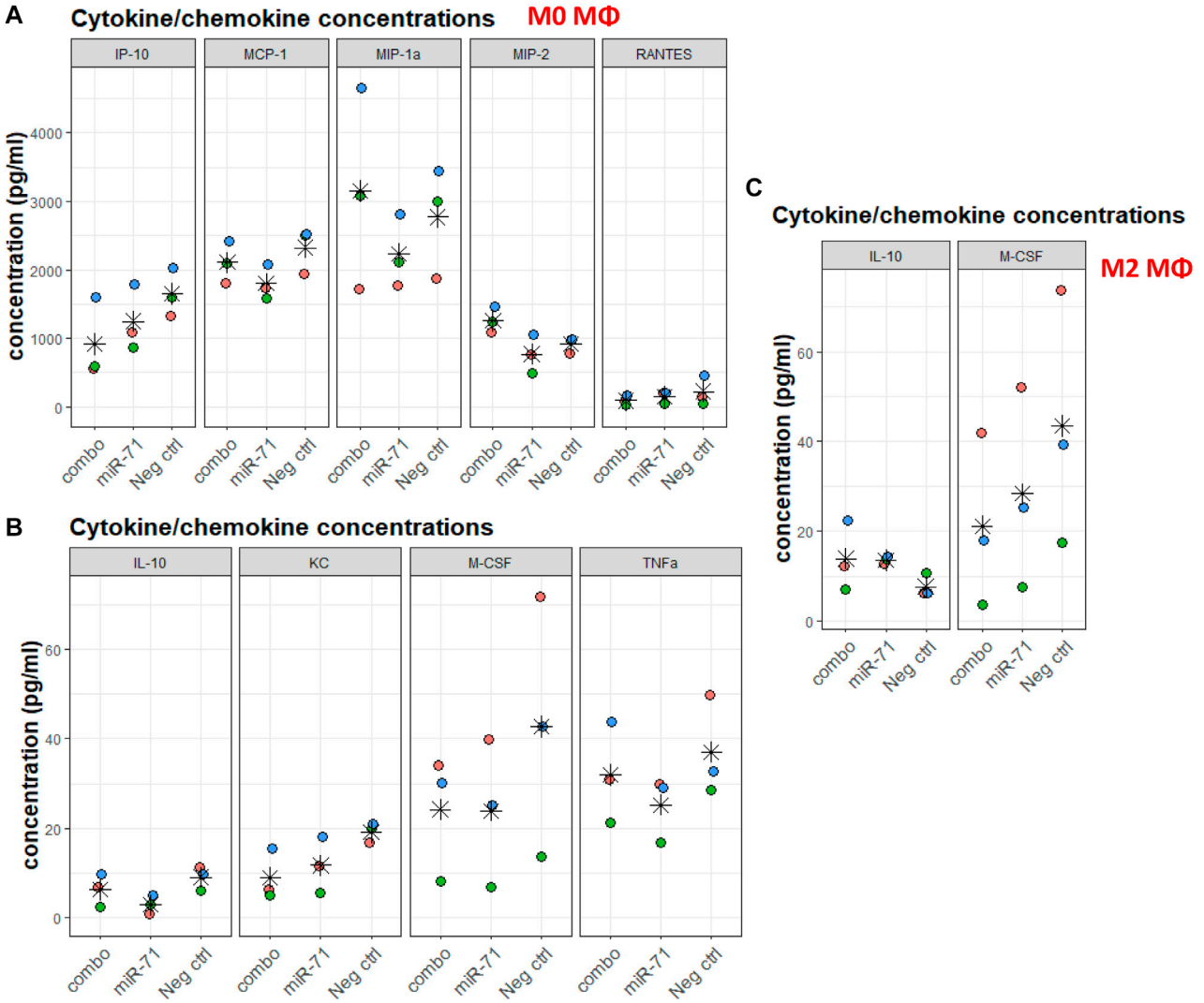

FIGURE 5 | Cytokine/chemokine concentrations in supernatants of macrophages exposed to nematode miRNAs. For each analyte, colors indicate replicates, stars indicate the mean across three data points. **(A,B)** Chemokine/cytokine concentration (in pg/ml) varying upon miRNA transfection of M0 macrophages. **(C)** Chemokine/cytokine concentration (in pg/ml) varying upon miRNA transfection and polarization toward the alternative activation profile M2. IP-10: IFN-γ-induced protein 10 (Cxcl10); MCP-1: monocyte chemoattractant protein 1 (CCl2); MIP-1a: macrophage inhibitory protein 1a; MIP-2: macrophage inhibitory protein 2; RANTES: regulated upon activation, normal T cell expressed and presumably secreted (CCl5); IL-10: interleukin 10; KC: keratinocytes-derived chemokine (CxCl1); M-CSF: macrophage colony-stimulating factor (Csf1); TNF-α: tumor necrosis factor 1α. All concentrations were within range of detection 3.2–10,000 pg/ml (and 12.8–40,000 pg/ml for IL-13). Statistical significance of variation across conditions was performed against Neg. ctrl (UNC) using the Dunnett's test.

element of the transcriptional network for Th2 cell differentiation.

Nematode miRNAs Interact Directly With Predicted Binding Sites on Host Genes

Because of expected compensatory regulatory mechanisms and potential indirect effects in cell systems, we investigated the accuracy of some computationally predicted targets. Four genes were selected from the Th2 transcriptional network, and from the downregulated pathways identified by RNA sequencing. Predicted binding sites for several miRNAs in *Gata3*, *Irf4*, *Mtor*, *Il4ra*, and Arginase 1 (*Arg1*) were cloned into the pmirGLO dual luciferase vector (Supplementary Table S4). These genes present multiple miRNA binding sites; miRNAs with the most promising computed context scores (TargetScan) were selected for validation. We validated that a direct interaction occurs between the cloned predicted miR-71 binding site on the *Irf4* mRNA, which supports results from the transcriptome analysis; exposure to 50 nM miR-71 (+ transfection reagent) led to a 25% reduction in luminescence, while 25 nM led to a 20% reduction (**Figure 4**). Similarly, the interaction between *Mtor* and miR-791 was confirmed, 50 and 25 nM miRNA leading to reduction of the relative Luciferase activity by 22 and 20%, respectively. In both

cases, there was a very mild concentration dependence, in which the higher miRNA concentrations had a slightly more pronounced effect. The minor difference between both concentrations likely suggests saturation of the system, where only one binding site was cloned into the luciferase plasmid. We could not confirm an interaction between *Gata3* and miR-10021 or miR-71 (relative luciferase activity unchanged, not shown). miR-87a was found to be weakly interact with *Il4ra*, which did not reach significance levels. miR-71 did not affect luminescence signals when its most likely binding site on *Il4ra* was inserted into the vector. There was no identifiable interaction between miR-100 and its predicted site on *Mtor* and on *Arg1*.

miR-71 Impacts Macrophage Cytokine Expression

Helminths and helminth EVs influence macrophages. The individual capacity of miRNAs (as opposed to whole EVs, containing many other molecules) to modulate the capacity of macrophages to differentiate was assessed. Without further stimuli, Raw 264.7 macrophages are unpolarized (M0). Cells were transfected with miR-71 alone or combined with miR-100 and miR-10021 (combo), or with the UNC; 24 h later, polarization was initiated either toward the classical activation profile (M1) or the alternative activation profile, associated with Th2 responses (M2). Supernatants were collected after 6 h for multiplex cytokine/chemokine analysis. Among the 32 measured analytes, most variation was observed in the unpolarized M0 population. Despite substantial variation across three biological replicates, the direction of regulation is reproducible across independent experiments and thus, lends some confidence in the data, although based on a tiny sample size, that did not reach significance. While more samples will be necessary to obtain fully conclusive results, in most cases, miR-71 showed an inhibitory effect by trend, compared to the UNC. IP-10 (CxCl10), MCP-1 (CCl2), MIP-1a, MIP-2, RANTES (CCl5) (**Figure 5A**), IL-10, KC (CxCl1), M-CSF (Csf1), and TNF-α, showed slight reductions in concentration (**Figure 5B**). The picture is not so clear regarding the effects produced by transfection with the three-miRNA combination, suggesting that the other two miRNAs (miR-100 and miR-10021) do not have the same effect as miR-71. It also shows concentration-dependence, as miR-71 is diluted 1:3 in the combo treatment, unless the other miRNAs have a stimulatory effect on cytokine production. Cytokine/chemokine concentrations produced by M1 macrophages were not affected by miR-71 or the miRNA combination compared to the UNC. In M2 supernatants, only IL-10 and M-CSF showed altered levels compared to the UNC, however, with large inter-replicate variation for M-CSF (**Figure 5C**). In M2 macrophages, IL-10 was mildly increased upon prior exposure to miR-71, which would support an active regulatory role of this helminth miRNA by acting on innate immune cells in type 2 immune responses. IP-10 is predicted to be targeted by miR-100 (see Supplementary Table S4 and target predictions: https://data.mendeley.com//datasets/358nm9mhpr/1). miR-71 is predicted to target transcripts of MIP-1a, KC, M-CSF *via* 7mer-1 or 7mer-8 binding sites. miR-1 is predicted to target MIP-1a and M-CSF *via* both kinds of 7mer sites as well. Similarly, miR-10021 is predicted to bind to MIP and M-CSF, while miR-100 is predicted to interact with IP-10. TNF-α, MCP-1, and RANTES were not among putative targets of the miRNAs we used in transfection experiments.

DISCUSSION

Parasitic helminths are large eukaryotic pathogens with complex life histories that tend to persist for relatively long periods of time in their hosts. Through the release of molecular messages in their surroundings, they master the art of host manipulation. A contribution of EVs in interspecific crosstalk has been increasingly documented. However, EVs represent inhomogeneous entities showing a great molecular diversity derived from parent cells. It is difficult to assign an observed effect on host cells to a specific molecule in this case. Differentiating helminth products that are important for infection from those that are not involved in the 'negotiations' between hosts and parasites will likely require a thorough breakdown of the molecular spectrum constituting E/S products (ESP), using models that can reduce the complexity of host-parasite communication.

Previously, *H. polygyrus bakeri* EVs were shown to have various effects on MODE-K cells (an intestinal cell line) (Buck et al., 2014). The most strongly downregulated gene was *Dusp1* (dual-specificity phosphatase 1), a regulator of MAPK signaling associated with dampening the type 1 pro-inflammatory responses. Another gene significantly downregulated by exosomes is *Il1rl1* (also known as IL33R in humans), the ligand-specific subunit of the receptor for IL-33, key in responses to helminths (Buck et al., 2014; Coakley et al., 2017).

Heligmosomoides polygyrus bakeri, *T. muris* and *A. suum* are commonly used as models of human intestinal infections. They infect laboratory mice for at least a part of their life cycle. Previous studies suggested macrophages and T cells as particularly exposed to nematode secreted miRNAs and predicted a functional impairment (Quintana et al., 2019; Duguet et al., 2020; Meningher et al., 2020). In this work, a small fraction of the miRNA complement of helminth ESP was examined for host gene regulatory properties in cells of the innate and adaptive arms of immunity. Helminths typically elicit a Th2 effector cell polarization, along with the induction of a prominent regulatory T cell (Treg) population. To assess whether nematode miRNAs are indeed capable of modulating T cell differentiation or proliferation, we relied on a simplistic conditioning *in vitro* model (without reaching the fully differentiated state), that allowed for manipulation but has a limited ability to reflect the complexity and intercellular interactions required to produce an immune response *in vivo*. Moreover, despite our effort to expose cells repeatedly, our assay setup likely did not accurately mirror the constant exposure of local immune cells to helminth products. miRNA overexpression studies have shown that cells start to recover normal gene expression levels as soon as 12 h post-transfection, indicating that effects are transient (Jin et al., 2015). The combination of low

miRNA concentrations and punctate transfections may have contributed to the observation of only a small number of DE genes in the transcriptome analysis. Nevertheless, the approach identified IRF4 (also known as NF-EM5, PIP, MUM1, or ICSAT), a crucial and direct interactor of GATA3, the master regulator of Th2 differentiation, as a target of one of the most abundantly secreted nematode miRNAs. Repression observed in reporter assays was in the range of prior observations with nematode miRNAs (Buck et al., 2014; Meningher et al., 2020). Of note, dendritic cells (DCs) expressing IRF4 (IRF4+ CD11c+ CD11b+ DCs) are potent drivers of type 2 immunity in *T. muris* infection, while other DC populations are associated with establishment of chronic infections (Mayer et al., 2017; Else et al., 2020). *T. muris*, however, does not express miR-71, and hence, does not rely on this particular modulatory mechanism (Sotillo et al., 2020; White et al., 2020). In macrophages too, the mTORC2-IRF4 signaling axis is essential for alternative activation (M2), a profile observed upon *H. polygyrus bakeri* infection. Hence, given the importance of IRF4 at several levels in the anti-helminth immune response(s), modulation of this gene is expected to have functional consequences. This will require verifications, especially in additional cell types such as DCs or macrophages, given their prominent role in responses to nematode infections.

To validate additional and potentially crucial nematode miRNA targets in Th2 cell differentiation, we selected a number of miRNA:mRNA sites for closer examination using reporter assays. We confirmed an interaction between miR-791 and its binding site on *Mtor*. Th2 cell differentiation requires mTORC2 activity (Delgoffe et al., 2011). In addition, the mTORC1-mediated pathway links signal-dependent metabolic reprogramming (through CD28 or TCR) to exit the quiescent state, and subsequently orchestrate cell proliferation and fate decisions. Together with Raptor, the mTORC1 complex connects glucose metabolism to cytokine responsiveness and Th2 cell differentiation and expansion (Yang et al., 2013). EVs released from the filarial nematode *Brugia malayi,* enriched for miR-100, miR-71, miR-34, and miR-7, downregulate the host mTOR pathway as well (Ricciardi et al., 2021). Their target predictions agreed with ours, in that miR-100 was predicted to target mTOR, among other mRNAs (e.g., eukaryotic translation initiation factor 4E binding protein 1 (EIF4E3BP1)) in the mTOR signaling pathway. EIF4E3BP1 was not identified among the targets of miRNAs from our nematode species, but *Eif4e3* was among downregulated genes following transfection with miR-71, according to transcriptomics data. Recent evidence shows that EIF4E3 acts in re-programming the translatome to promote 'stress resistance' and adaptation and is recruited the mTOR pathway is inhibited (Weiss et al., 2021). A further gene downregulated by miR-71 treatment was *Ifitm3*, which is constitutively expressed in $CD4^+$ T cells and is downregulated upon cell activation. In a mouse model and in contrast to *Ifitm2*, *Ifitm3* deletion did not reduce the Th2 response; hence, its role in a context of cell polarization remains incompletely understood (Yánez et al., 2019). *Ifitm3* was not among direct targets of the transfected miRNAs, hence, the effect is likely indirect.

Raw 264.7 macrophages transfected with miR-71 or the miRNA combo (miR-71, miR-100, miR-10021 combined) resulted in mild alterations of mRNAs encoding some cytokines/chemokines. Especially in non-polarized cells, cytokine levels were low at baseline and differences subtle. Although not statistically significant and based on limited sample sizes, miR-71 exposure led to systematically decreased analyte levels by trend, compared to UNC treatment, and the direction of regulation was reproducible across independent experiments. In both non-polarized (M0) and alternatively activated macrophages, miR-71 and the miRNA combination decreased macrophage colony-stimulating factor (M-CSF) levels. M-CSF is required for macrophage differentiation. Lowered M-CSF levels might lead to impairment of the innate immune response and weakened macrophage capacity to respond appropriately to worm infection. While Zamanian and colleagues reported substantial increases in monocyte chemoattractant protein (MCP-1), macrophage inhibitory protein 2 (MIP-2), RANTES, and TNF-α following uptake of *B. malayi* larvae EVs, in line with the classical activation profile, we observed the opposite upon introduction of miR-71 into cells. EVs, however, represent more complex entities than just a handful of miRNAs, and EV composition (including miRNAs) tend to vary in a species- and stage-specific manner (Zamanian et al., 2015; Sotillo et al., 2020). Decreases in IP-10 (IFN-γ-induced protein, or CxCl10), MIP-1, and KC (CxCl1, a neutrophil chemoattractant), and increased levels of IL-10 (an anti-inflammatory cytokine) in M2 macrophages suggest that miR-71 (and to some extent combo, where miR-71 is "diluted" with other miRNAs) has potential both anti-inflammatory and immunosuppressing properties and would overall favor polarization toward the alternative activation profile.

In general, miRNAs are considered key mediators in development, activation and regulation of immune cells (Arora et al., 2017). In light of their redundant and pleiotropic properties, it is likely that only a handful of different miRNAs are not sufficient to produce a phenotype. Indeed, we did not observe any significant difference in terms of cell counts or Th2 proportions. miRNA-driven silencing is often relatively subtle: they are "micromanagers" contributing to of regulatory circuits and control fine-tune of protein expression (Arora et al., 2017). In addition, cells are expected to have many compensatory mechanisms to function when one pathway gets slowed down. Hence, it is likely that the cumulative effects of multiple different miRNAs may have more pronounced, synergistic effects on host cells.

In *C. elegans*, miR-71 promotes longevity and stress resistance (Boulias and Horvitz, 2012). In addition, miR-71 is specifically required for the starvation-induced stress response and plays a critical role in long-term survival by repressing the expression of insulin receptor/PI3K pathway genes and genes acting downstream or in parallel to the pathway (Zhang et al., 2011): mutating miR-71 drastically reduces the survival rate of animals in first stage larvae (L1) diapause (Zhang et al., 2011), a stress-resistant, developmentally

quiescent, and long-lived larval stage. In *Echinococcus multilocularis*, miR-71 is required for metacestode normal development *in vitro* (Pérez et al., 2019). Taken together and integrating data presented here, it is likely that miR-71 fulfills multiple roles, both endogenously and exogenously.

Only few predicted targets have translated into validated targets using reporter assays. Generally, the most effective canonical site types are the 8mer sites, where a Watson–Crick match to mature miRNA positions two to eight with an A opposite position 1 is observed (Lewis et al., 2005; Agarwal et al., 2015), followed by 7mer sites. Finally, 6mer site types are associated with weaker preferential conservation and much lower efficacy (Friedman et al., 2009; Agarwal et al., 2015). In line with this, the predicted 6mer sites on IL4-Rα and GATA3 upon interaction with miR-71 resulted in no decrease in luminescence in reporter assays. Binding sites between miR-71 and IRF4 and mTOR and miR-791 were 8mer-1a, and 7mer-m8, respectively. Despite optimal site conservation, GATA3 and IL-4Rα are not confirmed as biochemical targets of miR-10021 (8mer-1a) and miR-87a (7mer-m8), respectively. Therefore, predicted targets, even with high context scores and optimal site conservation parameters, require experimental validation.

The fact that a nematode-specific miRNA, without a close mammalian homologue, may incorporate into host AGO protein complexes support the hypothesis that the silencing machinery does not need to be transferred along with small RNAs (Donnelly and Tran, 2021). miR-71 was not detected in mesenteric lymph nodes of *H. polygyrus bakeri* infected mice, likely present below the detection level of the assay. Meningher et al. reported measurable amounts of miR-10 and Bantam from the mesenteric lymph nodes and Peyer's patches of *S. mansoni* infected mice, but not in the inguinal lymph node nor in the spleen (Meningher et al., 2020); adult worms reside in the mesenteric and small intestine venules and hence, have a more direct contact with lymphoid tissue surrounding the parasite, than would do the gastrointestinal nematodes.

Whether nematode miRNA concentrations achieve biologically relevant *in vivo* (for local and systemic effects) is currently under investigation in our laboratory. However, the low miRNA doses (10 nM for 2×10^5 to 1×10^6 cells) we used in the present work support the hypothesis that they might indeed at least have mild but reliable local regulatory effects.

This work demonstrates that repeated exposure to low concentrations of lipid-encased synthetic nematode miRNAs can result in a mild modulation of host gene expression *in vitro*, which was partially confirmed by reporter assays. In particular, abundant GI nematode miRNA sequences may get loaded onto host AGO proteins and target important components of the Th2 differentiation process: IRF4 and mTOR. Immunomodulatory effects exerted by individual parasite miRNAs are very mild in comparison to whole worms or EVs but are in line with their proposed roles as fine-tuning entities of gene and protein expression. Further mechanistic insights are required in order to fully grasp the extent of miRNA-mediated host modulation.

DATA AVAILABILITY STATEMENT

The datasets presented in this study can be found in online repositories. The names of the repository/repositories and accession number(s) can be found below: https://data.mendeley.com//datasets/358nm9mhpr/1, 10.17632/358nm9mhpr.1, https://www.ncbi.nlm.nih.gov/geo/, GSE180829.

ETHICS STATEMENT

The animal study was reviewed and approved by the Cantonal Veterinary Office of Zurich (permit number ZH186/18) and by the Cantonal Veterinary Office of Basel-Stadt (permit number 2070).

AUTHOR CONTRIBUTIONS

LT conceptualized the study and obtained funding. LT and NJ designed the work. LT did the initial bioinfomatics work. JS, NG, and LT performed the experiments and analyzed the data. HR analyzed the transcriptomics data. JS and LT wrote the manuscript. All authors revised and approved the final manuscript.

FUNDING

This work was supported by the Swiss National Science Foundation (PZ00P3_168080) and by the Bank Vontobel Charitable Foundation, both granted to LT.

ACKNOWLEDGMENTS

We thank Prof. Jennifer Keiser for granting access to material from *H. polygyrus bakeri* infected mice. The laboratory work was partly performed using the logistics of the Center for Clinical Studies at the Vetsuisse Faculty of the University of Zurich. We acknowledge Next Generation Sequencing lab of the Functional Genomics Center Zurich for supporting the RNA-seq experiments. We thank the Institute of Medical Virology of the University of Zurich and Dr. Irene Abela and Selina Epp for the Luminex apparatus and their assistance. We are grateful to Fiorella Ruchti (Institute of Virology, University of Zurich) for her kind assistance with flow cytometry experiments.

SUPPLEMENTARY MATERIAL

The Supplementary Material for this article can be found online at: https://www.frontiersin.org/articles/10.3389/fmolb.2022.909312/full#supplementary-material

REFERENCES

Agarwal, V., Bell, G. W., Nam, J.-W., and Bartel, D. P. (2015). Predicting Effective microRNA Target Sites in Mammalian mRNAs. *eLife* 4. doi:10.7554/eLife.05005

Allen, J. E., and Maizels, R. M. (2011). Diversity and Dialogue in Immunity to Helminths. *Nat. Rev. Immunol.* 11, 375–388. doi:10.1038/nri2992

Arora, N., Tripathi, S., Singh, A. K., Mondal, P., Mishra, A., and Prasad, A. (2017). Micromanagement of Immune System: Role of miRNAs in Helminthic Infections. *Front. Microbiol.* 8, 586. doi:10.3389/fmicb.2017.00586

Bauch, A., Adamczyk, I., Buczek, P., Elmer, F.-J., Enimanev, K., Glyzewski, P., et al. (2011). openBIS: a Flexible Framework for Managing and Analyzing Complex Data in Biology Research. *BMC Bioinforma.* 12, 468. doi:10.1186/1471-2105-12-468

Bellafiore, S., Shen, Z., Rosso, M.-N., Abad, P., Shih, P., and Briggs, S. P. (2008). Direct Identification of the *Meloidogyne incognita* Secretome Reveals Proteins with Host Cell Reprogramming Potential. *PLoS Pathog.* 4, e1000192. doi:10.1371/journal.ppat.1000192

Boulias, K., and Horvitz, H. R. (2012). The *C. elegans* microRNA Mir-71 Acts in Neurons to Promote Germline-Mediated Longevity through Regulation of DAF-16/FOXO. *Cell. Metab.* 15, 439–450. doi:10.1016/j.cmet.2012.02.014

Brosnan, C. A., Palmer, A. J., and Zuryn, S. (2021). Cell-type-specific Profiling of Loaded miRNAs from *Caenorhabditis elegans* Reveals Spatial and Temporal Flexibility in Argonaute Loading. *Nat. Commun.* 12, 2194. doi:10.1038/s41467-021-22503-7

Buck, A. H., Coakley, G., Simbari, F., McSorley, H. J., Quintana, J. F., Le Bihan, T., et al. (2014). Exosomes Secreted by Nematode Parasites Transfer Small RNAs to Mammalian Cells and Modulate Innate Immunity. *Nat. Commun.* 5, 5488. doi:10.1038/ncomms6488

Campos-Melo, D., Droppelmann, C., Volkening, K., and Strong, M. (2014). Comprehensive Luciferase-Based Reporter Gene Assay Reveals Previously Masked Up-Regulatory Effects of miRNAs. *Ijms* 15, 15592–15602. doi:10.3390/ijms150915592

Charlier, J., van der Voort, M., Kenyon, F., Skuce, P., and Vercruysse, J. (2014). Chasing Helminths and Their Economic Impact on Farmed Ruminants. *Trends Parasitol.* 30, 361–367. doi:10.1016/j.pt.2014.04.009

Chi, H. (2012). Regulation and Function of mTOR Signalling in T Cell Fate Decisions. *Nat. Rev. Immunol.* 12, 325–338. doi:10.1038/nri3198

Claycomb, J., Abreu-Goodger, C., and Buck, A. H. (2017). RNA-mediated Communication between Helminths and Their Hosts: The Missing Links. *RNA Biol.* 14, 436–441. doi:10.1080/15476286.2016.1274852

Coakley, G., Buck, A. H., and Maizels, R. M. (2016). Host Parasite Communications-Messages from Helminths for the Immune System. *Mol. Biochem. Parasitol.* 208, 33–40. doi:10.1016/j.molbiopara.2016.06.003

Coakley, G., Maizels, R. M., and Buck, A. H. (2015). Exosomes and Other Extracellular Vesicles: The New Communicators in Parasite Infections. *Trends Parasitol.* 31, 477–489. doi:10.1016/j.pt.2015.06.009

Coakley, G., McCaskill, J. L., Borger, J. G., Simbari, F., Robertson, E., Millar, M., et al. (2017). Extracellular Vesicles from a Helminth Parasite Suppress Macrophage Activation and Constitute an Effective Vaccine for Protective Immunity. *Cell. Rep.* 19, 1545–1557. doi:10.1016/j.celrep.2017.05.001

Delgoffe, G. M., Pollizzi, K. N., Waickman, A. T., Heikamp, E., Meyers, D. J., Horton, M. R., et al. (2011). The Kinase mTOR Regulates the Differentiation of Helper T Cells through the Selective Activation of Signaling by mTORC1 and mTORC2. *Nat. Immunol.* 12, 295–303. doi:10.1038/ni.2005

Dobin, A., Davis, C. A., Schlesinger, F., Drenkow, J., Zaleski, C., Jha, S., et al. (2013). STAR: Ultrafast Universal RNA-Seq Aligner. *Bioinformatics* 29, 15–21. doi:10.1093/bioinformatics/bts635

Donnelly, S., and Tran, N. (2021). Commandeering the Mammalian Ago2 miRNA Network: a Newly Discovered Mechanism of Helminth Immunomodulation. *Trends Parasitol.* 37, 1031–1033. doi:10.1016/j.pt.2021.09.001

Duguet, T. B., Soichot, J., Kuzyakiv, R., Malmström, L., and Tritten, L. (2020). Extracellular Vesicle-Contained microRNA of *C. elegans* as a Tool to Decipher the Molecular Basis of Nematode Parasitism. *Front. Cell. Infect. Microbiol.* 10, 217. doi:10.3389/fcimb.2020.00217

Eichenberger, R. M., Ryan, S., Jones, L., Buitrago, G., Polster, R., Montes de Oca, M., et al. (2018a). Hookworm Secreted Extracellular Vesicles Interact with Host Cells and Prevent Inducible Colitis in Mice. *Front. Immunol.* 9, 850. doi:10.3389/fimmu.2018.00850

Eichenberger, R. M., Talukder, M. H., Field, M. A., Wangchuk, P., Giacomin, P., Loukas, A., et al. (2018b). Characterization of *Trichuris muris* Secreted Proteins and Extracellular Vesicles Provides New Insights into Host-Parasite Communication. *J. Extracell. Vesicles* 7, 1428004. doi:10.1080/20013078.2018.1428004

Else, K. J., Keiser, J., Holland, C. V., Grencis, R. K., Sattelle, D. B., Fujiwara, R. T., et al. (2020). Whipworm and Roundworm Infections. *Nat. Rev. Dis. Prim.* 6, 44. doi:10.1038/s41572-020-0171-3

Flaherty, S., and Reynolds, J. M. (2015). Mouse Naive CD4+ T Cell Isolation and *In Vitro* Differentiation into T Cell Subsets. *JoVE* 98, 52739. doi:10.3791/52739

Friedman, R. C., Farh, K. K.-H., Burge, C. B., and Bartel, D. P. (2009). Most Mammalian mRNAs Are Conserved Targets of microRNAs. *Genome Res.* 19, 92–105. doi:10.1101/gr.082701.108

Girgis, N. M., Gundra, U. M., and Loke, P. n. (2013). Immune Regulation during Helminth Infections. *PLoS Pathog.* 9, e1003250. doi:10.1371/journal.ppat.1003250

González-Cabrero, J., Wise, C. J., Latchman, Y., Freeman, G. J., Sharpe, A. H., and Reiser, H. (1999). CD48-deficient Mice Have a Pronounced Defect in CD4 + T Cell Activation. *Proc. Natl. Acad. Sci. U.S.A.* 96, 1019–1023. doi:10.1073/pnas.96.3.1019

Gu, H. Y., Marks, N. D., Winter, A. D., Weir, W., Tzelos, T., McNeilly, T. N., et al. (2017). Conservation of a microRNA Cluster in Parasitic Nematodes and Profiling of miRNAs in Excretory-Secretory Products and Microvesicles of *Haemonchus contortus*. *PLoS Negl. Trop. Dis.* 11, e0006056. doi:10.1371/journal.pntd.0006056

Gupta, S., Jiang, M., Anthony, A., and Pernis, A. B. (1999). Lineage-specific Modulation of Interleukin 4 Signaling by Interferon Regulatory Factor 4. *J. Exp. Med.* 190, 1837–1848. doi:10.1084/jem.190.12.1837

Hansen, E. P., Fromm, B., Andersen, S. D., Marcilla, A., Andersen, K. L., Borup, A., et al. (2019). Exploration of Extracellular Vesicles from *Ascaris suum* Provides Evidence of Parasite-Host Cross Talk. *J. Extracell. Vesicles* 8, 1578116. doi:10.1080/20013078.2019.1578116

Herricks, J. R., Hotez, P. J., Wanga, V., Coffeng, L. E., Haagsma, J. A., Basáñez, M.-G., et al. (2017). The Global Burden of Disease Study 2013: What Does it Mean for the NTDs? *PLoS Negl. Trop. Dis.* 11, e0005424. doi:10.1371/journal.pntd.0005424

Hewitson, J. P., Grainger, J. R., and Maizels, R. M. (2009). Helminth Immunoregulation: The Role of Parasite Secreted Proteins in Modulating Host Immunity. *Mol. Biochem. Parasitol.* 167, 1–11. doi:10.1016/j.molbiopara.2009.04.008

Huber, M., and Lohoff, M. (2014). IRF4 at the Crossroads of Effector T-Cell Fate Decision. *Eur. J. Immunol.* 44, 1886–1895. doi:10.1002/eji.201344279

Jin, H. Y., Gonzalez-Martin, A., Miletic, A. V., Lai, M., Knight, S., Sabouri-Ghomi, M., et al. (2015). Transfection of microRNA Mimics Should Be Used with Caution. *Front. Genet.* 6, 340. doi:10.3389/fgene.2015.00340

Jonas, S., and Izaurralde, E. (2015). Towards a Molecular Understanding of microRNA-Mediated Gene Silencing. *Nat. Rev. Genet.* 16, 421–433. doi:10.1038/nrg3965

Kanehisa, M., Furumichi, M., Tanabe, M., Sato, Y., and Morishima, K. (2017). KEGG: New Perspectives on Genomes, Pathways, Diseases and Drugs. *Nucleic Acids Res.* 45, D353–D361. doi:10.1093/nar/gkw1092

Kaplan, R. M., and Vidyashankar, A. N. (2012). An Inconvenient Truth: Global Worming and Anthelmintic Resistance. *Veterinary Parasitol.* 186, 70–78. doi:10.1016/j.vetpar.2011.11.048

Kuleshov, M. V., Jones, M. R., Rouillard, A. D., Fernandez, N. F., Duan, Q., Wang, Z., et al. (2016). Enrichr: a Comprehensive Gene Set Enrichment Analysis Web Server 2016 Update. *Nucleic Acids Res.* 44, W90–W97. doi:10.1093/nar/gkw377

Kunszt, P., Blum, L., Hullár, B., Schmid, E., Srebniak, A., Wolski, W., et al. (2015). iPortal: the Swiss Grid Proteomics Portal: Requirements and New Features Based on Experience and Usability Considerations. *Concurr. Comput. Pract. Exper.* 27, 433–445. doi:10.1002/cpe.3294

Lewis, B. P., Burge, C. B., and Bartel, D. P. (2005). Conserved Seed Pairing, Often Flanked by Adenosines, Indicates that Thousands of Human Genes Are microRNA Targets. *Cell.* 120, 15–20. doi:10.1016/j.cell.2004.12.035

Liao, Y., Smyth, G. K., and Shi, W. (2013). The Subread Aligner: Fast, Accurate and Scalable Read Mapping by Seed-And-Vote. *Nucleic Acids Res.* 41, e108. doi:10.1093/nar/gkt214

Liberzon, A., Birger, C., Thorvaldsdóttir, H., Ghandi, M., Mesirov, J. P., and Tamayo, P. (2015). The Molecular Signatures Database Hallmark Gene Set Collection. *Cell. Syst.* 1, 417–425. doi:10.1016/j.cels.2015.12.004

Liu, J., Zhu, L., Wang, J., Qiu, L., Chen, Y., Davis, R. E., et al. (2019). *Schistosoma japonicum* Extracellular Vesicle miRNA Cargo Regulates Host Macrophage Functions Facilitating Parasitism. *PLoS Pathog.* 15, e1007817. doi:10.1371/journal.ppat.1007817

Lohoff, M., Mittrücker, H.-W., Prechtl, S., Bischof, S., Sommer, F., Kock, S., et al. (2002). Dysregulated T Helper Cell Differentiation in the Absence of Interferon Regulatory Factor 4. *Proc. Natl. Acad. Sci. U.S.A.* 99, 11808–11812. doi:10.1073/pnas.182425099

Luo, Q.-J., Zhang, J., Li, P., Wang, Q., Zhang, Y., Roy-Chaudhuri, B., et al. (2021). RNA Structure Probing Reveals the Structural Basis of Dicer Binding and Cleavage. *Nat. Commun.* 12, 3397. doi:10.1038/s41467-021-23607-w

Maizels, R. M., and McSorley, H. J. (2016). Regulation of the Host Immune System by Helminth Parasites. *J. Allergy Clin. Immunol.* 138, 666–675. doi:10.1016/j.jaci.2016.07.007

Mayer, J. U., Demiri, M., Agace, W. W., MacDonald, A. S., Svensson-Frej, M., and Milling, S. W. (2017). Different Populations of CD11b+ Dendritic Cells Drive Th2 Responses in the Small Intestine and Colon. *Nat. Commun.* 8, 15820. doi:10.1038/ncomms15820

Meningher, T., Barsheshet, Y., Ofir-Birin, Y., Gold, D., Brant, B., Dekel, E., et al. (2020). Schistosomal Extracellular Vesicle-enclosed miRNAs Modulate Host T Helper Cell Differentiation. *EMBO Rep.* 21, e47882. doi:10.15252/embr.201947882

Opejin, A., Surnov, A., Misulovin, Z., Pherson, M., Gross, C., Iberg, C. A., et al. (2020). A Two-step Process of Effector Programming Governs CD4+ T Cell Fate Determination Induced by Antigenic Activation in the Steady State. *Cell. Rep.* 33, 108424. doi:10.1016/j.celrep.2020.108424

Pérez, M. G., Spiliotis, M., Rego, N., Macchiaroli, N., Kamenetzky, L., Holroyd, N., et al. (2019). Deciphering the Role of miR-71 in *Echinococcus multilocularis* Early Development *In Vitro*. *PLoS Negl. Trop. Dis.* 13, e0007932. doi:10.1371/journal.pntd.0007932

Quintana, J. F., Kumar, S., Ivens, A., Chow, F. W. N., Hoy, A. M., Fulton, A., et al. (2019). Comparative Analysis of Small RNAs Released by the Filarial Nematode *Litomosoides sigmodontis In Vitro* and *In Vivo*. *PLoS Negl. Trop. Dis.* 13, e0007811. doi:10.1371/journal.pntd.0007811

R Core Team (2017). R: A Language and Environment for Statistical Computing. Vienna, Austria: R Foundation for Statistical Computing.

Ricafrente, A., Nguyen, H., Tran, N., and Donnelly, S. (2020). An Evaluation of the *Fasciola hepatica* miRnome Predicts a Targeted Regulation of Mammalian Innate Immune Responses. *Front. Immunol.* 11, 608686. doi:10.3389/fimmu.2020.608686

Ricciardi, A., Bennuru, S., Tariq, S., Kaur, S., Wu, W., Elkahloun, A. G., et al. (2021). Extracellular Vesicles Released from the Filarial Parasite *Brugia malayi* Downregulate the Host mTOR Pathway. *PLoS Negl. Trop. Dis.* 15, e0008884. doi:10.1371/journal.pntd.0008884

Risso, D., Ngai, J., Speed, T. P., and Dudoit, S. (2014). Normalization of RNA-Seq Data Using Factor Analysis of Control Genes or Samples. *Nat. Biotechnol.* 32, 896–902. doi:10.1038/nbt.2931

Selzer, P. M., and Epe, C. (2021). Antiparasitics in Animal Health: Quo Vadis? *Trends Parasitol.* 37, 77–89. doi:10.1016/j.pt.2020.09.004

Shepherd, C., Navarro, S., Wangchuk, P., Wilson, D., Daly, N. L., and Loukas, A. (2015). Identifying the Immunomodulatory Components of Helminths. *Parasite Immunol.* 37, 293–303. doi:10.1111/pim.12192

Sotillo, J., Robinson, M. W., Kimber, M. J., Cucher, M., Ancarola, M. E., Nejsum, P., et al. (2020). The Protein and microRNA Cargo of Extracellular Vesicles from Parasitic Helminths - Current Status and Research Priorities. *Int. J. Parasitol.* 50, 635–645. doi:10.1016/j.ijpara.2020.04.010

Stubbington, M. J., Mahata, B., Svensson, V., Deonarine, A., Nissen, J. K., Betz, A. G., et al. (2015). An Atlas of Mouse CD4+ T Cell Transcriptomes. *Biol. Direct* 10, 14. doi:10.1186/s13062-015-0045-x

Tran, N., Ricafrente, A., To, J., Lund, M., Marques, T. M., Gama-Carvalho, M., et al. (2021). *Fasciola hepatica* Hijacks Host Macrophage miRNA Machinery to Modulate Early Innate Immune Responses. *Sci. Rep.* 10, 14. doi:10.1038/s41598-021-86125-1

Tritten, L., Ballesteros, C., Beech, R., Geary, T. G., and Moreno, Y. (2021). Mining Nematode Protein Secretomes to Explain Lifestyle and Host Specificity. *PLoS Negl. Trop. Dis.* 15, e0009828. doi:10.1371/journal.pntd.0009828

Tritten, L., Burkman, E., Moorhead, A., Satti, M., Geary, J., Mackenzie, C., et al. (2014). Detection of Circulating Parasite-Derived microRNAs in Filarial Infections. *PLoS Negl. Trop. Dis.* 8, e2971. doi:10.1371/journal.pntd.0002971

Tritten, L., Tam, M., Vargas, M., Jardim, A., Stevenson, M. M., Keiser, J., et al. (2017). Excretory/secretory Products from the Gastrointestinal Nematode *Trichuris muris*. *Exp. Parasitol.* 178, 30–36. doi:10.1016/j.exppara.2017.05.003

Truillet, C., Cunningham, J. T., Parker, M. F. L., Huynh, L. T., Conn, C. S., Ruggero, D., et al. (2017). Noninvasive Measurement of mTORC1 Signaling with 89Zr-Transferrin. *Clin. Cancer Res.* 23, 3045–3052. doi:10.1158/1078-0432.CCR-16-2448

Weiss, B., Allen, G. E., Kloehn, J., Abid, K., Jaquier-Gubler, P., and Curran, J. A. (2021). eIF4E3 Forms an Active eIF4F Complex during Stresses (eIF4FS) Targeting mTOR and Re-programs the Translatome. *Nucleic Acids Res.* 49, 5159–5176. doi:10.1093/nar/gkab267

White, R., Kumar, S., Chow, F. W.-N., Robertson, E., Hayes, K. S., Grencis, R. K., et al. (2020). Extracellular Vesicles from *Heligmosomoides bakeri* and *Trichuris muris* Contain Distinct microRNA Families and Small RNAs that Could Underpin Different Functions in the Host. *Int. J. Parasitol.* 50, 719–729. doi:10.1016/j.ijpara.2020.06.002

Whitehead, B., Boysen, A. T., Mardahl, M., and Nejsum, P. (2020). Unique Glycan and Lipid Composition of Helminth-Derived Extracellular Vesicles May Reveal Novel Roles in Host-Parasite Interactions. *Int. J. Parasitol.* 50, 647–654. doi:10.1016/j.ijpara.2020.03.012

World Health Organization (2020). Soil-transmitted Helminth Infections. Avaliable At: https://www.who.int/news-room/fact-sheets/detail/soil-transmitted-helminth-infections (Accessed 9 9, 21).

Xie, Z., Bailey, A., Kuleshov, M. V., Clarke, D. J. B., Evangelista, J. E., Jenkins, S. L., et al. (2021). Gene Set Knowledge Discovery with Enrichr. *Curr. Protoc.* 1, e90. doi:10.1002/cpz1.90

Yánez, D. C., Ross, S., and Crompton, T. (2020). The IFITM Protein Family in Adaptive Immunity. *Immunology* 159, 365–372. doi:10.1111/imm.13163

Yánez, D. C., Sahni, H., Ross, S., Solanki, A., Lau, C. I., Papaioannou, E., et al. (2019). IFITM Proteins Drive Type 2 T Helper Cell Differentiation and Exacerbate Allergic Airway Inflammation. *Eur. J. Immunol.* 49, 66–78. doi:10.1002/eji.201847692

Yang, K., Shrestha, S., Zeng, H., Karmaus, P. W. F., Neale, G., Vogel, P., et al. (2013). T Cell Exit from Quiescence and Differentiation into Th2 Cells Depend on Raptor-mTORC1-Mediated Metabolic Reprogramming. *Immunity* 39, 1043–1056. doi:10.1016/j.immuni.2013.09.015

Zamanian, M., Fraser, L. M., Agbedanu, P. N., Harischandra, H., Moorhead, A. R., Day, T. A., et al. (2015). Release of Small RNA-Containing Exosome-like Vesicles from the Human Filarial Parasite *Brugia malayi*. *PLoS Negl. Trop. Dis.* 9, e0004069. doi:10.1371/journal.pntd.0004069

Zhang, X., Zabinsky, R., Teng, Y., Cui, M., and Han, M. (2011). microRNAs Play Critical Roles in the Survival and Recovery of *Caenorhabditis elegans* from Starvation-Induced L1 Diapause. *Proc. Natl. Acad. Sci. U.S.A.* 108, 17997–18002. doi:10.1073/pnas.1105982108

Zhong, Y., Wan, Y.-W., Pang, K., Chow, L. M., and Liu, Z. (2013). Digital Sorting of Complex Tissues for Cell Type-specific Gene Expression Profiles. *BMC Bioinforma.* 14, 89. doi:10.1186/1471-2105-14-89

Zhu, J. (2015). T Helper 2 (Th2) Cell Differentiation, Type 2 Innate Lymphoid Cell (ILC2) Development and Regulation of Interleukin-4 (IL-4) and IL-13 Production. *Cytokine* 75, 14–24. doi:10.1016/j.cyto.2015.05.010

Conflict of Interest: The authors declare that the research was conducted in the absence of any commercial or financial relationships that could be construed as a potential conflict of interest.

Publisher's Note: All claims expressed in this article are solely those of the authors and do not necessarily represent those of their affiliated organizations, or those of the publisher, the editors and the reviewers. Any product that may be evaluated in this article, or claim that may be made by its manufacturer, is not guaranteed or endorsed by the publisher.

frontiers | Frontiers in Molecular Biosciences

REVIEW
published: 08 July 2022
doi: 10.3389/fmolb.2022.915993

Roles of Non-Coding RNAs in Primary Biliary Cholangitis

Yaqin Zhang[1†], *Ziying Jiao*[2†], *Mingwei Chen*[3], *Bing Shen*[2] *and Zongwen Shuai*[1*]

[1]*Department of Rheumatology, The First Affiliated Hospital of Anhui Medical University, Hefei, China,* [2]*Department of Physiology, School of Basic Medicine of Anhui Medical University, Hefei, China,* [3]*Department of Endocrinology, The First Affiliated Hospital of Anhui Medical University, Hefei, China*

Primary biliary cholangitis (PBC) is an autoimmune-mediated chronic cholestatic liver disease, fatigue, and skin itching are the most common clinical symptoms. Its main pathological feature is the progressive damage and destruction of bile duct epithelial cells. Non-coding RNA (NcRNA, mainly including microRNA, long non-coding RNA and circular RNA) plays a role in the pathological and biological processes of various diseases, especially autoimmune diseases. Many validated ncRNAs are expected to be biomarkers for the diagnosis or treatment of PBC. This review will elucidate the pathogenesis of PBC and help to identify potential ncRNA biomarkers for PBC.

Keywords: primary biliary cholangitis, non-coding RNA, autoimmunity, ursodeoxycholic acid, biomarker

OPEN ACCESS

Edited by:
Inhan Lee,
miRcore, United States

Reviewed by:
Ze-Hua Zhao,
Shandong University, China
Enqiang Chen,
Sichuan University, China

****Correspondence:***
Zongwen Shuai
shuaizongwen@ahmu.edu.cn

†These authors have contributed equally to this work

Specialty section:
This article was submitted to Molecular Diagnostics and Therapeutics, a section of the journal Frontiers in Molecular Biosciences

Received: *08 April 2022*
Accepted: *20 June 2022*
Published: *08 July 2022*

Citation:
Zhang Y, Jiao Z, Chen M, Shen B and Shuai Z (2022) Roles of Non-Coding RNAs in Primary Biliary Cholangitis. Front. Mol. Biosci. 9:915993. doi: 10.3389/fmolb.2022.915993

INTRODUCTION

Primary biliary cholangitis (PBC) is a chronic cholestatic liver disease mediated by autoimmunity. Fatigue and pruritus are the most common clinical symptoms, usually preceding the appearance of jaundice by years (Erice et al., 2018; Beuers et al., 2015). The main histological features are chronic progressive damage and destruction of bile duct epithelial cells (non-suppurative cholangitis), portal inflammation (mainly lymphocytes, plasma cells, and eosinophils) and increased fibrosis (Poupon, 2010; Tsuneyama et al., 2017; Pandit and Samant, 2022). PBC is globally distributed and can occur in all races and ethnicities. A recent meta-analysis (Lv et al., 2021) showed that both the incidence and prevalence of PBC are on the rise globally, with an annual incidence rate of 0.23/100,000–5.31/100,000, and a prevalence of 1.91/100,000–40.2/100,000. The highest in North America and Nordic countries (Kim et al., 2000; Koulentaki et al., 2014; Metcalf et al., 1997; Marschall et al., 2019), and the lowest in Canada (Witt-Sullivan et al., 1990) and Australia (Watson et al., 1995). Population-based epidemiological data on PBC are still lacking in China. A recent meta-analysis (Zeng et al., 2019) estimated that the prevalence of PBC in China was 20.5/100,000, ranking second in the Asia-Pacific region after Japan. **Figure 1**. The cause of PBC is unknown, and may be caused by a highly complex interaction between genetic and environmental factors. There is also extensive evidence that inflammation and immune disorders have an important impact on PBC. The disease mostly affects middle-aged women (i.e., 85%–90% patients onset at 40–60 years old), with female-to-male ratios is about 1:10, while higher mortality was described in men (Gonzalez and Washington, 2018). Moreover, there are also recent literature of increasing in male PBC (Lleo et al., 2016). This may be related to additional environmental exposures, higher prevalence of viral hepatitis, greater awareness of the disease by physicians and patients and unknown gender factors that may modulate immunity (Lleo et al., 2016). The specific reasons need to be further explored.

PBC was also previously known as primary biliary cirrhosis. The name change reflects the fact that cirrhosis only occurs in the late stage, so it is difficult to correctly identify patients with early disease. According to the AASLD (American Association for the Study of Liver Diseases), two of the

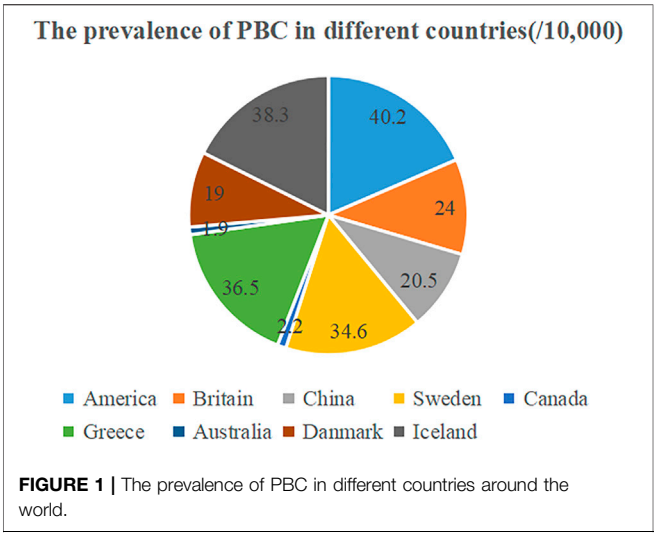

FIGURE 1 | The prevalence of PBC in different countries around the world.

following three criteria are met to confirm the diagnosis of PBC: 1) biochemical evidence of cholestasis based on alkaline phosphatase (ALP) elevation; 2) anti-mitochondrial antibody (AMA) positivity; 3) histological evidence of intrahepatic destructive cholangitis (Carey et al., 2015). Among them, serum AMA, especially the positive AMA-M2 subtype, has high sensitivity and specificity for the diagnosis of PBC, and are recognized as distinct diagnostic biomarkers. There is also a PBC patient subpopulation (~5%–10%) who have the same clinical and histological features as classic PBC, but AMAs are negative even with the most sensitive detection methods. For these patients, the diagnosis is mainly based on liver biopsy (Kouroumalis et al., 2018). However, problems can arise in the presence of ascites or infection and are not easily accepted by patients.

The first-line treatment of PBC is the daily administration of ursodeoxycholic acid (UDCA), which improves prognosis in ~2/3 of patients in early stage of the disease. This means up to 40% of patients have an incomplete response to UDCA, and the long-term survival rate is lower than that of the general population (Parés et al., 2006). UDCA was approved by the United States FDA (Food and Drug Administration) in 2016 as a second-line treatment for patients with primary biliary cholangitis who are unresponsive to UDCA; however, approximately 50% of patients might need additional treatments to reach therapeutic goals. Otherwise, these patients may progress to liver transplantation or even die (Gulamhusein and Hirschfield, 2020). Therefore, identification of novel and promising biomarkers is crucial for PBC early diagnosis and (or) treatment.

Non-coding RNA (NcRNA) refers to a functional RNA molecule that cannot be translated into protein. They can perform their respective biological functions at the RNA level (Wang et al., 2019). Due to increasing development of microarray sequencing techniques, accumulating data have suggested ncRNAs play important roles in regulating autoimmunity and inflammation (Kempinska-Podhorodecka et al., 2017; Young et al., 2017; Wang et al., 2018a). In addition, different cells and tissues have different ncRNA expression profiles (Chen et al., 2016; Katsumi et al., 2016; Zheng et al., 2017a; Erice et al., 2018; Xiang et al., 2019). Erice studies have shown that miR-506 is overexpressed in cholangiocytes of PBC, induces PBC-like characteristics in cholangiocytes and promotes immune activation (Erice et al., 2018). Dai et al. compared miRNAs in renal biopsy samples from patients with class II lupus nephritis (LN) and nephrectomy samples from patients with renal tumors. The results showed that there were 66 differentially regulated miRNAs (36 upregulated and the remaining 30 downregulated) in lupus nephritis patients (Dai et al., 2009). Wu et al. showed that linc0949 and linc0597 were significantly decreased in patients with SLE compared with patients with RA and healthy control subjects. Moreover, linc0949 was positively correlated with SLEDAI-2K scores and negatively correlated with complement component C3 levels (Wu et al., 2015). However, the roles of these specifically expressed ncRNAs in the pathogenesis of PBC have not been fully elucidated.

In the present review, some functional ncRNAs are listed in **Table 1**, mainly including microRNAs (miRNAs), long non-coding RNAs (lncRNAs), and circular RNAs (circRNAs) (Katsushima et al., 2014; Nakagawa et al., 2017; Wang et al., 2017; Wasik et al., 2017; Afonso et al., 2018; Wasik et al., 2020). We aimed to elucidate the dysregulated ncRNAs in PBC that contribute to the understanding of the pathogenesis of PBC by reviewing all currently published studies. Most importantly, helping to identify those aberrantly expressed ncRNAs in PBC will facilitate the exploration of promising biomarkers for early diagnosis and treatment of PBC.

MICRORNAS AND PRIMARY BILIARY CHOLANGITIS

Broad Roles of MicroRNAs in Various Diseases

MiRNAs are evolutionarily conserved, non-coding small RNAs of 18–25 nucleotides in length. MiRNAs incompletely bind to complementary sequences in the 3′ untranslated region (3′UTR) of messenger RNA (mRNA) and regulate the expression of target genes at the post-transcriptional level by promoting the degradation of mRNA or repressing its translation (Tavasolian et al., 2018). MiRNAs can regulate about 90% of protein-coding genes and play important roles in various biological processes such as metabolism, cell differentiation, proliferation, apoptosis, and the maintenance of immune homeostasis (Alvarez-Garcia and Miska, 2005; Baltimore et al., 2008; Check Hayden, 2008). Disturbances in miRNAs expression profiles are associated with a variety of human diseases, including autoimmune diseases, such as systemic lupus erythematosus (SLE), PBC, and rheumatoid arthritis (RA) (Young et al., 2017; Wang et al., 2018a; Erice et al., 2018). Some of them have been proposed as non-invasive biomarkers of disease.

As shown in **Table 1**, various miRNAs were dysregulated in PBC. These miRNAs can regulate target genes of cytokines, oxidative stress, immunity and inflammation-related

TABLE 1 | Aberrant expressed ncRNAs in PBC.

NcRNA	Target	Site	Expression	Signaling	Role	References
MiRNA						
miR-506	AE2/InsP3R3	Intrahepatic bile ducts	Up	---	Binds the 3′UTR region of AE2 mRNA, prevents protein translation; Decreased AE2 activity; Impair bile secretion	Erice et al. (2018)
miR-155	SOCS-1	Liver tissues	Up	VDR-miRNA 155-SOCS1 pathway	Sustained inflammatory responses are elicited through the VDR-miRNA155-SOCS1 pathway	Kempinska-Podhorodecka et al. (2017)
miR-139-5p	c-FOS/TNF-α	Serum Liver tissues (lymphocytes or hepatocytes)	Down Up-lymphocytes Down-hepatocytes	NF-κB signaling	Regulated TNF-α and c-FOS.	Katsumi et al. (2016)
miR-21/miR-150	cMyb/ RASGRP1/ DNMT1	Serum, liver tissue, and PBMC in AMA (-) patient	Up	---	A feature of anti-mitochondrial antibody-negative PBC.	Wasik et al. (2020)
miR-425	N-Ras	Peripheral blood $CD4^+$ T cell	Down	TCR signaling	Downregulation of inflammatory cytokines (IL-2 and IFN-γ)	Nakagawa et al. (2017)
miR-223-3p/miR-21-5p	TGFBR1	Peripheral blood B cells	Down	TGF-β1 signaling	Associated with progression of PBC.	Wang et al. (2017)
miR-34a/miR-132	NRF2	Liver tissues	Down	Oxidative stress	Oxidative stress; Autophagy	Wasik et al. (2017)
miR-21	CDK2AP1	Liver tissues	Up	Regulated necrosis	MiR-21 ablation ameliorates liver damage and necroptosis	Afonso MB, et al., (2018)
miR-92a	IL-17A	Plasma and PBMC	Down	Th17 signaling	Direct regulation of IL-17A	Liang et al. (2016)
miR-181a	BCL-2	Peripheral blood $CD4^+$ T cell	Down	TCR signaling	Regulated Th17 cells distribution *via* upregulated BCL-2	Song et al. (2018)
miR-122a/miR-26a miR-328/miR-299-5p	---/EZH2 ---	Liver tissues	Down Up	Apoptosis/ inflammation/oxidative stress/metabolism	Affected cell proliferation, apoptosis, inflammation, oxidative stress, and metabolism	Padgett et al. (2009)
miR-26a	IL-17A	Th17 cell	Up	---	Regulates IL-17, induces apoptosis and proliferation	Tang (2009)
miR-34a	TGIF2	Peripheral blood	Up	TGF-β1/Smad	Induction of EMT and fibrosis in intrahepatic bile duct epithelium	Pan et al. (2021)
Circulating miRNAs						
miR-299-5p	---	Peripheral blood	Up	---	MiR-299-5p was associated with ALP, γ-GT, TBIL and immunoglobulin M levels	Katsushima, et al. (2014)
let-7b	---	PBMC	Down	---	miR-let-7b expression was correlated with Mayo risk scores, IL-18 and ALP.	Qian et al. (2013)
miR-451a/miR-642-3p	---	Plasma exosomes	Up	---	Regulated the expression of the co-stimulatory molecules CD86 and CD80 in peripheral antigen-presenting cells	Tomiyama et al. (2017)
miR-197-3p/miR-505-3p	---	Serum	Down	---	As a clinical biomarker for PBC.	Ninomiya et al. (2013)
miR-122-5p/miR-141-3p miR-26b-5p	---	Serum	Up Down	---	As potential biomarkers of PBC.	Tan et al., (2014)

(Continued on following page)

TABLE 1 | (*Continued*) Aberrant expressed ncRNAs in PBC.

NcRNA	Target	Site	Expression	Signaling	Role	References
miR-4311/miR-4714-3p	---	Serum	Down	---	Potential biomarkers for use in the development of treatment of patients with refractory PBC.	Sakamoto et al. (2016)
miR-122/miR-378			Up			
miR-155-5p	AKT3	PBMC	Down	MAPK/TCR/BCR signaling	A new disease marker of PBC.	Yang. et al. (2013)
miR-150-5p	---		Up			
LncRNA						
lncRNA NONHSAT250451.1	EGR1	PBMC	Up	Inflammation/immune activation/TCR signaling/NF-κB signaling/chemokine signaling	It is involved in inflammation, immune cell activation, TCR signaling pathway, etc., which may be related to the occurrence of PBC.	Xiang et al. (2019)
lncRNA AK053349	---	Peripheral blood $CD8^+$ T cell and PBMC	Up	Autoimmunity and T lymphocyte activation	Targeted regulation of EGR1 may be involved in the occurrence of PBC.	Pang et al. (2009)
lncRNA XIST	Inflammatory cytokines	NK and $CD4^+$ T lymphocytes	Up	Th1/Th17	Stimulated the secretion of IFN-γ, IL-17, TGF-β and ROR-γ T cells, and increase the proportion of Th1 and Th7 cells, led to the occurrence of PBC.	She (2020)
lncRNA H19	---	Liver tissue	Up	HSC activation and proliferation	Promoted HSC activation and proliferation, aggravate PBC.	(Li et al. (2018a); Liu et al. (2019); Li et al. (2020a))
CircRNA						
circ_402458/ circ_087631/ circ_406329	hsa-miR-522-3p/hsa-miR-943	Plasma	Up	Inflammation-related signaling	Candidate biomarkers for PBC.	Zheng et al. (2017a)
circ_407176/ circ_082319			Down			

--- represents unknown.

PBMC, peripheral blood lymphocyte mononuclear cells; EMT, epithelial-mesenchymal transition; ALP, alkaline phosphatase; γ-GT, γ-glutamyl transpeptidase; TBIL, total bilirubin; TCR, T cell receptor; BCR, B cell receptor; NF-κB, nuclear factor-κB; MAPK, mitogen-activated protein kinase; HSC, hepatic stellate cell.

molecules, thereby participating in the pathogenesis or/and progression of PBC (Padgett et al., 2009; Qian et al., 2013; Liang et al., 2016; Erice et al., 2018; Song et al., 2018). Several published literatures have extensively explored the molecular mechanisms of differentially expressed miRNAs in PBC, particularly regarding their altering effects on inflammation and autoimmunity (Liang et al., 2016; Nakagawa et al., 2017; Erice et al., 2018).

The Role of MiR-506 in the Pathogenesis of Primary Biliary Cholangitis

Anion exchanger 2 (AE2) is essential in the maintenance of the protective bicarbonate- rich umbrella on the surface of BECs *via* regulation of biliary HCO_3^- secretion, which shields BECs from noxious luminal bile acids (Rodrigues et al., 2018). Banales et al. (2012) demonstrated that miR-506 is upregulated in cholangiocytes from PBC patients, binds the 3′UTR region of AE2 mRNA and prevents protein translation, resulting in diminished AE2 activity and impaired biliary secretory functions. Given the putative pathogenic role of decreased AE2 in PBC, miR-506 may constitute a potential therapeutic target for this disease. Furthermore, miR-506 also regulates other genes involved in maintaining the integrity of bicarbonate umbrellas, the type III inositol 1,4,5-triphosphate receptor, an important regulator of calcium release from cholangiocytes (Ananthanarayanan et al., 2015; Erice et al., 2018). Under physiological conditions, acetylcholine increases the level of inositol triphosphate (InsP3) in cholangiocytes, resulting in an increase in the level of cytoplasmic Ca^{2+}. Apical Cl^- secretion is further stimulated by the Ca^{2+} activated Cl^- channel transmembrane protein 16F (TMEM16A), ultimately leading to bicarbonate secretion through AE2 (Minagawa et al., 2007). The downregulation of InsP3R3 expression in cholangiocytes from PBC patients leads to decreased intracellular Ca^{2+} signaling and bicarbonate secretion, thereby triggering cholestasis (Shibao et al., 2003). InsP3R3 mRNA contains two highly conserved miR-506 binding sites, both of which are functional. In miR-506-overexpressed cholangiocytes, InsP3R3 mRNA and protein levels were reduced, resulting in a marked reduction in Ca^{2+} release from the endoplasmic reticulum and failure of bile secretion

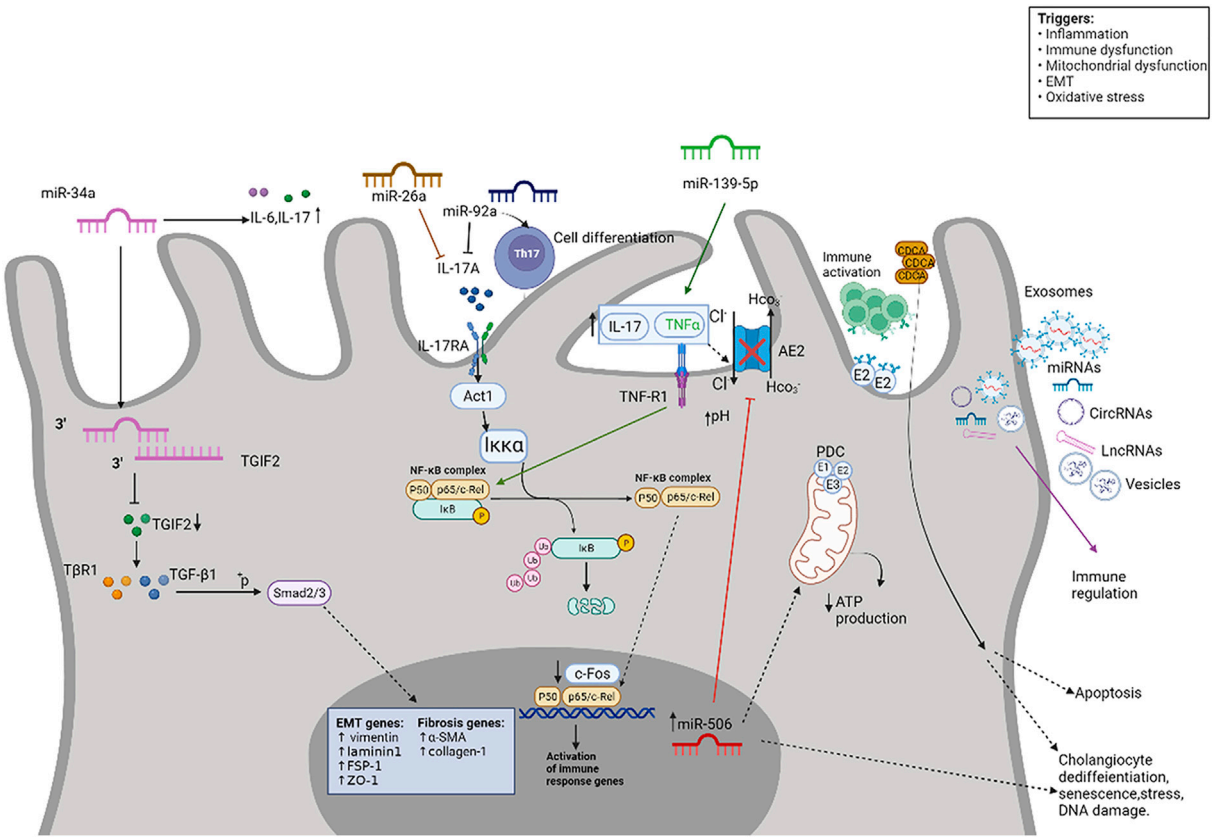

FIGURE 2 | Signaling pathway of miRNAs in PBC. MiRNA are involved in regulating inflammation and autoimmunity. Some miRNAs are encapsulated in nanovesicles and exert critical effects on inflammatory and immune cells. miRNAs participate in PBC inflammation and autoimmune disorders primarily through NF-κB, TGF-β1, Th17, and so on.

(Ananthanarayanan et al., 2015). *In vitro* data demonstrate that upregulation of proinflammatory, profibrotic, and senescent markers in miR-506-overexpressing cholangiocytes results in increased cellular stress and increased sensitivity to toxic hydrophobic bile acids (Erice et al., 2018). These results suggest a mechanistic link between epigenetic regulation, cellular damage, and immune dysregulation in PBC. Banales' team further expiored the role of inflammatory factors, such as interleukins (IL)-1β, IL-6, IL-8, IL-12, IL-17, IL-18, tumor necrosis factor alpha (TNF-α) and interferon gamma (IFN-γ), transforming growth factor beta 1 (TGF-β1), estrogens (17β-estradiol, 17β-E2), bile acids [cholic acid (CA), UDCA and tauroursodeoxycholic (TUCA)] and other factors in regulating miR-506 expression in cholangiocytes and the role of miR-506 in cholangiocyte pathophysiology and immunomodulation in PBC. The result show different inflammatory factors enhance the expression of miR-506 in biliary epithelial cells. MiR-506 induces PBC-like features in cholangiocytes and promotes immune activation (Erice et al., 2018). **Figure 2**. Intriguingly, miR-506 is an X- linked miRNA localized to Xq27.3, which helps explain the possibility that females predominate in PBC disease, although whether this hypothesis applies to human remains to be demonstrated (Arora et al., 2013).

Expression Profiles of MicroRNAs in Peripheral Blood and Liver Tissue of Primary Biliary Cholangitis Patients

Liang et al. (2016) used microarrays to identify 16 differentially expressed miRNAs (9 miRNAs upregulated and 7 miRNAs downregulated) in plasma from 3 PBC patients and 3 healthy controls. The most prominent finding was the downregulation of miR-92a, and the expression of miR-92a was negatively correlated with the Th17 cell population. Furthermore, the expression of miR-92a was colocalized with IL-17A in peripheral blood mononuclear cells (PBMCs) of patients, implying a direct regulation of IL-17A by miR-92a. Notably, studies have shown that Th17 cells and the IL-17 secreted by the cells may induce epithelial-mesenchymal transition (EMT) in intrahepatic bile ducts through IL-17A-IL-17RA-Act1 activation of the NF-κB pathway, and participate in the progression of PBC disease (Huang et al., 2016). **Figure 2**. Domestic studies have found that there are differences in the expression of miR-26a in initial $CD4^+$ T cells, memory $CD4^+$ T cells and effector $CD4^+$

T cells of PBC patients, and no expression in Jurkat cells (human T cell line). The authors then cultured Th17 cells (derived from human $CD4^+$ T cells) and transfected pre-miR-26a and anti-miR-26a, respectively. The results showed that compared with the normal control, the cells transfected with pre-miR-26a significantly decreased IL-17, significantly decreased the activities of NF-κB and AP-1, and induced increased apoptosis after activation; transfected with anti-miR-26a cells, IL-17 mRNA, NF-κB and AP-1 activities were significantly increased, cell proliferation activity increased, and apoptosis induced by activation decreased. The luciferase reporter further demonstrated that miRNA-26a could indeed regulate IL-17. Therefore, this study shows that miRNA-26a regulates the function of Thl7 cells by affecting apoptosis and cell proliferation activities induced by IL-17 activation (Tang, 2009). **Figure 2**. The above studies demonstrate that miRNAs may play a significant role in the fibrosis of bile duct epithelial cells in PBC patients through IL-17.

Pan et al. (2021) found that miR-34a was significantly overexpressed in the serum of PBC patients (30 PBC vs.30 controls). miR-34a upregulation inhibits proliferation of intrahepatic bile duct epithelium and increases mesenchymal markers zonula occluden-1 (ZO-1), laminin 1, vimentin and fibroblast-specific protein 1 (FSP-1) and expression of fibrotic markers α-SMA, and collagen I. The authors further demonstrated that miR-34a targets TGIF2 to induce EMT and fibrosis in intrahepatic bile duct epithelium through the TGF-β1/smad pathway (Pan et al., 2021). **Figure 2**. MiR-139-5p was significantly downregulated in clinically advanced PBC compared to control. *In situ* hybridization and RT-qPCR showed that the expression of miR-139-5p in lymphocytes of PBC patients was higher than that of lymphocytes of other liver diseases (chronic viral hepatitis and autoimmune hepatitis), while miR-139-5p in hepatocytes of PBC was lower than that in other liver disease, suggesting that lymphocytes are the main source of miR-139-5p. *In vitro* studies showed that with the upregulation of miR-139-5p, the level of TNF-α in the cell supernatant was significantly increased, the transcription of the c-FOS gene was inhibited, and the NF-κB signaling pathway was finally activated. Activation of NF-κB further induces the production of TNF-α, and increased levels of TNF-α may accelerate bile duct injury through positive feedback. The authors revealed a novel inflammation-regulatory mechanism between TNF-α and c-FOS transcription through miR-139-5p in the NF-κB pathway (Katsumi et al., 2016). **Figure 2**. Therefore, miR-139-5p could become not only a biomarker of disease progression, but also a novel therapeutic target for patients with progressive PBC. In addition, the expression of miR-155 was enhanced in PBMCs and liver tissues of PBC patients, accompanied by vitamin D receptor (VDR) mRNA and protein, cytokine signaling inhibitor 1 (SOCS1) protein expression decreased, indicating that the decreased VDR expression may lead to the dysregulation of the negative feedback loop through the VDR-miRNA155-SOCS1 pathway, thereby triggering a sustained inflammatory response (Kempinska-Podhorodecka et al., 2017). Padgett et al. (2009) analyzed liver tissue from 6 patients with end-stage PBC and 5 control subjects using a miRNA microarray platform. The results showed that 35 differentially expressed miRNAs (11 upregulated and 24 downregulated) were identified in the liver tissue of PBC patients compared with the liver tissue of normal controls. The targets they predicted were associated with the regulation of cell proliferation, apoptosis, inflammation, oxidative stress, and metabolism. According to the above studies, we can conclude that miRNAs may be derived from various immune cells and play a significant effect in the occurrence and development of PBC by inflammatory factors and immune-inflammatory pathways (such as TGF-β1/smad, TCR, NF-κB, and so on). Subsequent studies on miRNAs and PBC can start from immune cells and immune-inflammation-related pathways. Subsequent studies on miRNAs and PBC can start from immune cells (not only B cells, T cells, but also Th17 cells, Treg cells, macrophages, etc.), inflammatory factors and immune-inflammation-related pathways.

MicroRNAs and Therapeutic Targets for Primary Biliary Cholangitis

Nakagawa et al. (2017) examined total RNAs of $CD4^+$ T cells from 6 PBC patients and 6 healthy controls using miRNA microarrays. The authors found that the expression levels of 16 miRNAs were significantly different in PBC patients compared with healthy controls ($p < 0.05$, fold change >1.2). Among them, five of these miRNAs were significantly downregulated in PBC patients by qRT-PCR. The integral analysis of miRNA and mRNA identified four significantly downregulated miRNAs (miR-181a, miR-181b, miR-374b, and miR-425) related to the T-cell receptor (TCR) signaling pathway in $CD4^+$ T cells of PBC. N-Ras, a regulator of the TCR signaling pathway, was found to be targeted by all four identified miRNAs. In addition, *in vitro* assays confirmed that decreased miR-425 strongly induced inflammatory cytokines (IL-2 and IFN-γ) *via* N-Ras upregulation in the TCR signaling pathway. Therefore, the restoration of decreased miR-425 or the suppression of N-Ras may be promising for an immunotherapeutic strategy against PBC.

The authors believe that miR-122 is the most noteworthy therapeutic target for PBC. MiR-122 is a conserved liver-specific miRNA, accounting for 70% of total liver miRNAs (Chang et al., 2008). Multiple studies have shown that miR-122 plays a key role in lipid metabolism (Esau et al., 2006), cell differentiation (Kim et al., 2011), liver polyploidy (Hsu et al., 2016), hepatitis C virus replication (Luna et al., 2015), acetaminophen toxicity (Chowdhary et al., 2017; Yang et al., 2021), liver fibrosis in innate immunity of hepatocytes (Xu et al., 2019). Decreased miR-122 expression was found in HCV-negative liver cancer and was associated with metastasis in hepatocellular carcinoma (HCC) patients (Coulouarn et al., 2009; Tsai et al., 2009).

Tan et al. (2014) analyzed miRNA expression by Illumina sequencing of serum samples from 3 PBC patients and 3 controls and assessed the expression of selected miRNAs in a screened

group ($n = 40$) by qRT-PCR. A logistic regression model was then constructed using the training cohort ($n = 192$) and validated with another cohort ($n = 142$). The results showed that serum miR-122-5p levels were elevated in PBC patients. Compared with ALP and ANA, the miRNA panel (hsa-miR-122-5p, hsa-miR-141-3p, and hsa-miR-26b-5p) was a more sensitive and specific biomarker for PBC (Tan et al., 2014). Circulating miR-122 levels have been reported to correlate with liver histological stage, inflammation grade, and ALT activity (Lewis and Jopling, 2010; Zhang et al., 2010; Hu et al., 2012; Wang et al., 2012; Iino et al., 2013). MiR-122 expression was significantly decreased in a carbon tetrachloride (CCl4)-induced mouse model of liver fibrosis and HCC (Li et al., 2013; Hayes and Chayama, 2016). Similarly, Padgett et al. (2009) used the miRNA array platform to analyze the liver tissue of 6 patients with end-stage PBC and 5 control subjects, and the results showed that miR-122 was also downregulated in the liver tissue of PBC patients. This is an interesting result. It means that the liver may overexpress miR-122 compensatory in the early stage of PBC. However, most of miR-122 reaches the peripheral circulation, which increases miR-122 in peripheral circulation in PBC patients; or in PBC patients, other tissues, organs or cells abnormally express miR-122 in addition to the liver. The above-mentioned known immune cells and inflammatory factors play an important role in the occurrence and development of PBC. Therefore, the authors speculate that in the peripheral blood of PBC patients, various immune cells are activated (such as T cells, B cells, Th cells, Treg cells, macrophages, etc.) abnormally expressing miR-122 increases the level of miR-122 in serum/plasma. MiR-122 is a negative regulator of liver fibrosis. Li et al. (2013) found that miR-122 inhibited the proliferation and activation of Lx2 in hepatic stellate cells (HSC) by targeting P4HA1, regulating collagen production, and inhibiting liver fibrosis.

Tsai et al. (2012) generated a mutant mouse strain with a germline deletion of *Mir122a* using homologous recombination (*Mir122a*$^{-/-}$). Histological examination of the livers of Mir122a−/− mice revealed extensive lipid accumulation and reduced glycogen storage, as well as inflammation and fibrosis, compared with WT controls. A strong positive reaction to the anti-F4/80 antibody, which is specific for mouse macrophages and monocytes, was detected in the Mir122a−/− livers. Teng et al. (2020) also found that knockout of miR-122 in mouse liver developed spontaneous liver fibrosis. Therefore, the authors speculate that miR-122 may be a novel gene therapy strategy for patients with advanced PBC, especially targeting the liver. Whether the anti-fibrotic mechanism of miR-122 is related to its regulation of hepatic fatty acid and cholesterol synthesis still needs to be further explored (Esau et al., 2006; Naderi et al., 2017). In addition, due to the ability of miR-122 to enhance HCV replication, vigilance and monitoring of HCV infection should be exercised when using miR-122 (Luna et al., 2015). In the early stage of PBC, the main lesions are chronic inflammation and fibrosis of the intrahepatic bile ducts. Whether miR-122 can regulate the proliferation and apoptosis of intrahepatic bile duct cells has not been reported in the literature. This is also the direction our research group is working on.

Immunomodulatory Role of Exosomal MicroRNAs in Primary Biliary Cholangitis

Extracellular vesicles (EVs) are nano- or micro-lipid bilayer spheres produced by different cells. They are released into the extracellular space where they participate in intercellular communications. They are also found in bile and contain miRNAs (Li et al., 2014). Several nanovesicle-delivered miRNAs have been identified that are specifically expressed in PBC and play a modifying role in inflammation and autoimmunity (Olaizola et al., 2018). Exosomes are small vesicles formed by budding from endosomal membrane and released to extracellular by fusion with plasma membrane, which are important mediators of intercellular communication (Hirsova et al., 2016a; Martínez and Andriantsitohaina, 2017). Recent studies have reported that exosomes-mediated transfer of ncRNAs, proteins and lipids are associated with a variety of human diseases, including liver disease (Bala et al., 2012; Hirsova et al., 2016a; Debabrata and Mukhopadhyay, 2017; Pan et al., 2017; Szabo and Momen-Heravi, 2017). Hepatic epithelial cells, including cholangiocytes and hepatocytes, are exosomes-releasing cells (Masyuk et al., 2010; Masyuk et al., 2013; Hirsova et al., 2016b; Worst et al., 2017). Tomiyama et al. (2017) found plasma-derived exosomal miR-451a and miR-642a-3p were increased in PBC patients compared with healthy controls, and could regulate the expression of the co-stimulatory molecules such as CD86 and CD80 in peripheral antigen-presenting cells. **Figure 2**. In conclusion, accumulating evidence points to the critical role of miRNAs in regulating inflammation and autoimmunity, and many mature miRNAs are expected to be candidate biomarkers and therapeutic targets for PBC (Ninomiya et al., 2013; Qian et al., 2013; Yang, 2013; Katsushima et al., 2014; Tan et al., 2014; Sakamoto et al., 2016).

LONG NON-CODING RNA AND PRIMARY BILIARY CHOLANGITIS

Expression Profiles of Long Non-Coding RNAs in Autoimmune Diseases

LncRNAs are highly conserved RNA sequences >200 nucleotides in length that can epigenetically regulate gene expression and broadly affect cellular biological processes (Mercer et al., 2009; Ponting et al., 2009). Published literature on lncRNA have been focused on cancer (Chan and Tay, 2018; Mitobe et al., 2018; Tian et al., 2018), and studies on lncRNA in innate immunity are relatively scarce, accounting for only about 4% of all lncRNA papers (Robinson et al., 2020). With increasing interest of lncRNA in autoimmune diseases, it has been found that different autoimmune diseases (including PBC) have specific lncRNA expression profiles in different cells and tissues (Zhang et al., 2013; Sigdel et al., 2015; Hur et al., 2019; Liang et al., 2019). Previous studies have shown that the lncRNA AK053349 is highly expressed in $CD8^+$ T cells and is associated with autoimmunity and T lymphocyte activation (Pang et al., 2009). Zhang et al. (2013) wrote in his doctoral dissertation that the lncRNA AK053349 was increased in PBMC

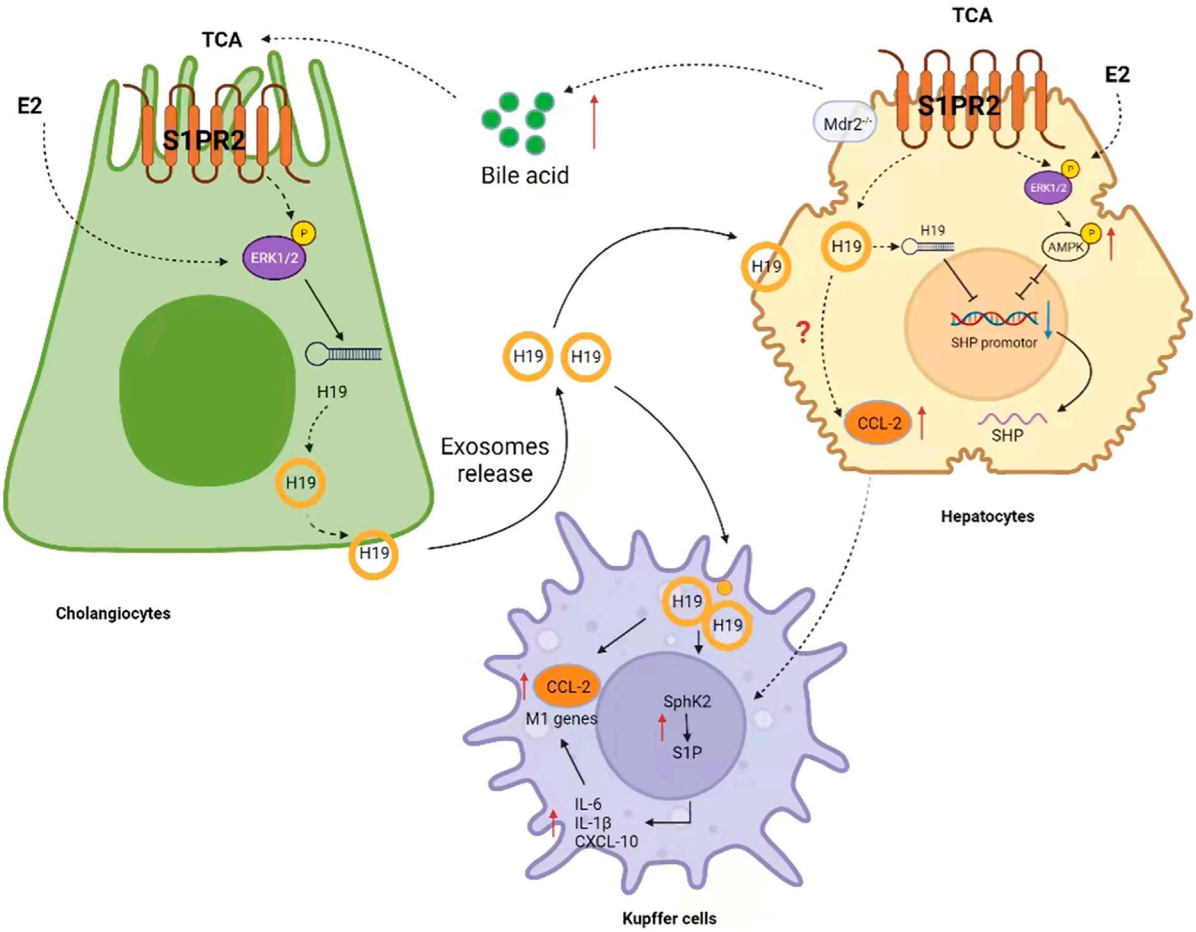

FIGURE 3 | Molecular mechanism of lncRNAH19 promoting cholestasis and activating macrophages.

of PBC patients and positively correlated with the Mayo risk score, emphasizing its potential relevance to the pathogenesis of PBC and worthy of further study (Zhang et al., 2013). Another recent domestic study (She, 2020) found that the expression level of lncRNA XIST in NK cells and $CD4^+$ T lymphocytes of PBC patients was significantly higher than that of healthy controls, and could be clearly located in the nucleus. The high expression of lncRNA XIST in Naïve $CD4^+$ T cells of PBC patients can promote the proliferation of Naïve $CD4^+$ T cells, stimulate the secretion of IFN-γ, IL-17, TGF-β and ROR-γ T cells, and increase the proportion of Th1 and Th7 cells, which led to the occurrence of PBC. This further supports the critical role of immune cells and inflammatory factors, especially IL-17 in PBC disease.

Exosomal Long Non-Coding RNA H19 Promotes Bile Duct Proliferation and Liver Fibrosis

Huiping Zhou et al. (Li et al., 2017) used $Mdr2^{-/-}$ mice as an animal model of cholestatic biliary disease. Their study showed that H19 expression was significantly increased in the liver and bile duct cells of female $Mdr^{2-/-}$ mice compared with male $Mdr2^{-/-}$ mice, and that abnormal H19 expression was associated with the severity of biliary fibrosis in female $Mdr2^{-/-}$ mice. Knockdown of H19 alleviate cholestatic liver injury in female $Mdr2^{-/-}$ mice. Furthermore, both Taurocholic acid (TCA) and Estradiol 2 (E2) upregulated the expression of H19, but there was no superposition or synergy. The role of H19 in cholestatic injury in female $Mdr2^{-/-}$ mice may be related to extracellular regulated protein kinase 1/2 (ERK1/2) signaling pathway. In a follow up study, Huiping Zhou's team further demonstrated that exosomal H19 is derived from bile duct cells and transferred to hepatocytes, inhibit the expression of small heterodimeric partner (SHP) in hepatocytes and promote cholestatic injury (Li et al., 2018a). **Figure 3**. To further determine the effect of H19 expression in the progression of liver fibrosis, the authors examined the expression levels of hepatic H19, Ck19, and fibrosis marker genes (Acta2, Loxl2, and Collagen 1) in both male and female 2-week bile duct ligation (BDL) mice and in 100 day old female $Mdr2^{-/-}$ mice and perform a linear analysis. The results showed that the expression level of hepatic H19 was significantly positively correlated with Ck19 and fibrosis marker genes. Similarly, in primary sclerosing cholangitis (PSC) and PBC patients, the hepatic mRNA levels of H19, CK19,

and fibrosis marker genes were all increased. In BDL mice with H19 knockout (H19KO-BDL), collagen deposition and α-SMA-positive fibroblast distribution near the bile ducts of mice were significantly reduced. H19 deficiency also significantly alleviated serum AST, ALT, ALP, and total bile acid (TBA) levels induced by BDL. H19 deficiency in DKO (Mdr2 and H19 double knockout) mice significantly reduced bile duct proliferation, immune cell infiltration and fibrosis in the periportal area. Next, the authors isolated exosomes from H19-enriched and H19-free (control) cholangiocytel culture medium and injected mice *via* tail vein. The results showed that bile duct proliferation, hepatic inflammation, collagen deposition, and fibroblast activation were more severe in mice treated with H19-enriched exosomes when compared to those treated with control exosomes. This effect is related to the promotion of hepatic stellate cell (HSC) activation and proliferation by exosomal H19 (Liu et al., 2019). Furthermore, cholangiocyte-derived exosomal H19 promotes macrophage activation, differentiation, chemotaxis and liver inflammation through the CCL-2/CCR-2 signaling pathway. **Figure 3**. H19-deficiency ameliorates the liver cholestasis and macrophage activation in both BDL and $Mdr2^{-/-}$ Mice (Li et al., 2020a). Thus, exosomal H19 represents a noninvasive biomarker and potential therapeutic target for cholestatic disease. Notably, $Mdr2^{-/-}$ mice are actually a suitable model for PSC and not an animal model for PBC disease. What role lncRNA H19 plays in PBC disease and whether the molecular mechanism is the same remains to be discussed.

CIRCULAR RNAS AND PRIMARY BILIARY CHOLANGITIS

CircRNA is an endogenous non-coding RNA, the most representative characteristic of which is the covalently closed RNA circle (Salzman, 2016; Ouyang et al., 2017). Circularization results in resistance and high stability of RNA to exonuclease-mediated degradation. In addition, circRNAs are abundant and evolutionarily conserved in the cytoplasm. These properties make circRNAs potentially more suitable as clinical biomarkers than other types of RNAs (Jeck and Sharpless, 2014; Lasda and Parker, 2014; Li et al., 2015). Most importantly, the expression profiles of circRNAs are specific in different cell types and can generally be found in peripheral blood, exosomes, and tissues. Due to their various forms of epigenetic modifications, circRNAs play important roles in various diseases, such as cancer, neurologic disorders and cardiovascular diseases (Zhao et al., 2017; Yang et al., 2018a; Ojha et al., 2018; Sheng et al., 2018). Ma et al. (2019) showed that circARSP91 promotes cancer immune surveillance by regulating NK cells in liver cancer, suggesting a key role of circRNAs in tumor immunity. Furthermore, circRNA Malat-1 is thought to act as a key regulator of alloimmune rejection by promoting dendritic cell-induced T cell exhaustion and regulatory T cell generation, suggesting a critical role for circRNAs in adaptive immunity (Zhang et al., 2018). In conclusion, circRNAs play key roles not only in innate immunity but also in adaptive immunity.

In recent years, accumulated studies have shown that circRNAs are closely related to the occurrence and development of autoimmune diseases (Yang et al., 2018b), including SLE (Li et al., 2018b; Wang et al., 2018b), RA (Zheng et al., 2017b), PBC (Zheng et al., 2017a), etc. Zheng et al. (2017a) used microarray to identify 22 aberrantly expressed circRNAs (18 upregulated, 4 downregulated) in the plasma of PBC patients. Notably, PBC patients who did not receive UDCA had higher levels of hsa-circ-402458 than those who received UDCA. Hsa-circ-402458 may target hsa-miR-943 and hsa-miR-522-3p. For miR-522-3p, it may be an effective target for regulating chronic inflammatory diseases. Therefore, the authors speculate that hsa-circ-402458 may act as a miRNA sponge to regulate inflammation-related pathways, thereby promoting the development of PBC. Unfortunately, there are few studies on the relationship between circRNAs and PBC, and the molecular mechanism behind the regulation of circRNAs in PBC disease is still unclear. Whether circRNAs, like miRNAs and/or lncRNAs, play a role in PBC through signaling pathways such as TGF-β, NF-κB, TLR, TCR and oxidative stress, remains to be further explored.

CONCLUSION AND FUTURE DIRECTIONS

Studies on ncRNAs in human biology have gained much interest in the scientific world in recent years (Kapoor et al., 2021; Makkos et al., 2021; Wang et al., 2021). The role of ncRNAs in immune regulation, inflammation and autoimmunity can be of significant translational implication in medicine. Although specific expression profiles of miRNAs, lnRNAs, and cirRNAs have been well-documented in the literature (Padgett et al., 2009; Sigdel et al., 2015; Zheng et al., 2017a), the underlying mechanisms of ncRNAs in the development of PBC is unclear and may involve autoimmune regulatory pathways such as TGF-B1, NF-kB, Th17, and TCR. Furthermore, the effects of ncRNAs in oxidative stress, apoptosis, immune cells homing, and others in PBC are also confounding factors. Further studies including a combination of wet-bench studies and the use of bioinformatics tools (Li et al., 2020b; Zhu and Leung, 2021) to discover the target gene networks of non-coding RNAs are necessary to decipher the mechanistic role of ncRNAs in the pathogenesis of PBC and their potential application as diagnostic markers and/or therapeutic checkpoints.

AUTHOR CONTRIBUTIONS

YZ wrote the manuscript, and ZJ assisted in the drawing. MC, BS, and ZS revised the manuscript.

FUNDING

This work was supported by the Natural Foundation of Anhui Province (NO.1808085MH279).

REFERENCES

Afonso, M. B., Rodrigues, P. M., Simão, A. L., Gaspar, M. M., Carvalho, T., Borralho, P., et al. (2018). miRNA-21 Ablation Protects against Liver Injury and Necroptosis in Cholestasis. *Cell Death Differ.* 25 (5), 857–872. doi:10.1038/s41418-017-0019-x

Alvarez-Garcia, I., and Miska, E. A. (2005). MicroRNA Functions in Animal Development and Human Disease. *Development* 132 (21), 4653–4662. doi:10.1242/dev.02073

Ananthanarayanan, M., Banales, J. M., Guerra, M. T., Spirli, C., Munoz-Garrido, P., Mitchell-Richards, K., et al. (2015). Post-Translational Regulation of the Type III Inositol 1,4,5-trisphosphate Receptor by miRNA-506. *J. Biol. Chem.* 290 (1), 184–196. doi:10.1074/jbc.M114.587030

Arora, H., Qureshi, R., and Park, W.-Y. (2013). miR-506 Regulates Epithelial Mesenchymal Transition in Breast Cancer Cell Lines. *PLoS One* 8 (5), e64273. doi:10.1371/journal.pone.0064273

Bala, S., Petrasek, J., Mundkur, S., Catalano, D., Levin, I., Ward, J., et al. (2012). Circulating microRNAs in Exosomes Indicate Hepatocyte Injury and Inflammation in Alcoholic, Drug-Induced, and Inflammatory Liver Diseases. *Hepatology* 56 (5), 1946–1957. doi:10.1002/hep.25873

Baltimore, D., Boldin, M. P., Rao, R. M. R. M., O'ConnellRao, D. S., and Taganov, K. D. (2008). MicroRNAs: New Regulators of Immune Cell Development and Function. *Nat. Immunol.* 9 (8), 839–845. doi:10.1038/ni.f.209

Banales, J. M., Sáez, E., Úriz, M., Sarvide, S., Urribarri, A. D., Splinter, P., et al. (2012). Upregulation of microRNA 506 Leads to Decreased Cl−/HCO3− Anion Exchanger 2 Expression in Biliary Epithelium of Patients with Primary Biliary Cirrhosis. *Hepatology* 56 (2), 687–697. doi:10.1002/hep.25691

Beuers, U., Gershwin, M. E., Gish, R. G., Invernizzi, P., Jones, D. E. J., Lindor, K., et al. (2015). Changing Nomenclature for PBC: From 'cirrhosis' to 'cholangitis'. *J. Hepatology* 63 (5), 1285–1287. doi:10.1016/j.jhep.2015.06.031

Carey, E. J., Ali, A. H., and Lindor, K. D. (2015). Primary Biliary Cirrhosis. *Lancet* 386 (10003), 1565–1575. doi:10.1016/s0140-6736(15)00154-3

Chan, J., and Tay, Y. (2018). Noncoding RNA:RNA Regulatory Networks in Cancer. *Ijms* 19 (5), 1310. doi:10.3390/ijms19051310

Chang, J., Guo, J.-T., Jiang, D., Guo, H., Taylor, J. M., and Block, T. M. (2008). Liver-specific microRNA miR-122 Enhances the Replication of Hepatitis C Virus in Nonhepatic Cells. *J. Virol.* 82 (16), 8215–8223. doi:10.1128/jvi.02575-07

Check Hayden, E. (2008). Thousands of Proteins Affected by miRNAs. *Nature* 454 (7204), 562. doi:10.1038/454562b

Chen, J.-Q., Papp, G., Szodoray, P., and Zeher, M. (2016). The Role of microRNAs in the Pathogenesis of Autoimmune Diseases. *Autoimmun. Rev.* 15 (12), 1171–1180. doi:10.1016/j.autrev.2016.09.003

Chowdhary, V., Teng, K.-y., Thakral, S., Zhang, B., Lin, C.-h., Wani, N., et al. (2017). miRNA-122 Protects Mice and Human Hepatocytes from Acetaminophen Toxicity by Regulating Cytochrome P450 Family 1 Subfamily A Member 2 and Family 2 Subfamily E Member 1 Expression. *Am. J. Pathology* 187 (12), 2758–2774. doi:10.1016/j.ajpath.2017.08.026

Coulouarn, C., Factor, V. M., Andersen, J. B., Durkin, M. E., and Thorgeirsson, S. S. (2009). Loss of miR-122 Expression in Liver Cancer Correlates with Suppression of the Hepatic Phenotype and Gain of Metastatic Properties. *Oncogene* 28 (40), 3526–3536. doi:10.1038/onc.2009.211

Dai, Y., Sui, W., Lan, H., Yan, Q., Huang, H., and Huang, Y. (2009). Comprehensive Analysis of microRNA Expression Patterns in Renal Biopsies of Lupus Nephritis Patients. *Rheumatol. Int.* 29 (7), 749–754. doi:10.1007/s00296-008-0758-6

Debabrata, J. M., and Mukhopadhyay, D. (2017). Exosomes and Their Role in the Micro-/macro-environment: a Comprehensive Review. *J. Biomed. Res.* 31 (5), 386–394. doi:10.7555/jbr.30.20150162

Erice, O., Munoz-Garrido, P., Vaquero, J., Perugorria, M. J., Fernandez-Barrena, M. G., Saez, E., et al. (2018). MicroRNA-506 Promotes Primary Biliary Cholangitis-like Features in Cholangiocytes and Immune Activation. *Hepatology* 67 (4), 1420–1440. doi:10.1002/hep.29533

Esau, C., Davis, S., Murray, S. F., Yu, X. X., Pandey, S. K., Pear, M., et al. (2006). miR-122 Regulation of Lipid Metabolism Revealed by *In Vivo* Antisense Targeting. *Cell Metab.* 3 (2), 87–98. doi:10.1016/j.cmet.2006.01.005

Gonzalez, R. S., and Washington, K. (2018). Primary Biliary Cholangitis and Autoimmune Hepatitis. *Surg. Pathol. Clin.* 11 (2), 329–349. doi:10.1016/j.path.2018.02.010

Gulamhusein, A. F., and Hirschfield, G. M. (2020). Primary Biliary Cholangitis: Pathogenesis and Therapeutic Opportunities. *Nat. Rev. Gastroenterol. Hepatol.* 17 (2), 93–110. doi:10.1038/s41575-019-0226-7

Hayes, C., and Chayama, K. (2016). MicroRNAs as Biomarkers for Liver Disease and Hepatocellular Carcinoma. *Ijms* 17 (3), 280. doi:10.3390/ijms17030280

Hirsova, P., Ibrahim, S. H., Krishnan, A., Verma, V. K., Bronk, S. F., Werneburg, N. W., et al. (2016). Lipid-Induced Signaling Causes Release of Inflammatory Extracellular Vesicles from Hepatocytes. *Gastroenterology* 150 (4), 956–967. doi:10.1053/j.gastro.2015.12.037

Hirsova, P., Ibrahim, S. H., Verma, V. K., Morton, L. A., Shah, V. H., LaRusso, N. F., et al. (2016). Extracellular Vesicles in Liver Pathobiology: Small Particles with Big Impact. *Hepatology* 64 (6), 2219–2233. doi:10.1002/hep.28814

Hsu, S. H., Delgado, E. R., Otero, P. A., Teng, K. Y., Kutay, H., Meehan, K. M., et al. (2016). MicroRNA-122 Regulates Polyploidization in the Murine Liver. *Hepatology* 64 (2), 599–615. doi:10.1002/hep.28573

Hu, J., Xu, Y., Hao, J., Wang, S., Li, C., and Meng, S. (2012). MiR-122 in Hepatic Function and Liver Diseases. *Protein Cell* 3 (5), 364–371. doi:10.1007/s13238-012-2036-3

Huang, Q., Chu, S., Yin, X., Yu, X., Kang, C., Li, X., et al. (2016). Interleukin-17A-Induced Epithelial-Mesenchymal Transition of Human Intrahepatic Biliary Epithelial Cells: Implications for Primary Biliary Cirrhosis. *Tohoku J. Exp. Med.* 240 (4), 269–275. doi:10.1620/tjem.240.269

Hur, K., Kim, S.-H., and Kim, J.-M. (2019). Potential Implications of Long Noncoding RNAs in Autoimmune Diseases. *Immune Netw.* 19 (1), e4. doi:10.4110/in.2019.19.e4

Iino, I., Kikuchi, H., Miyazaki, S., Hiramatsu, Y., Ohta, M., Kamiya, K., et al. (2013). Effect of miR-122 and its Target Gene Cationic Amino Acid Transporter 1 on Colorectal Liver Metastasis. *Cancer Sci.* 104 (5), 624–630. doi:10.1111/cas.12122

Jeck, W. R., and Sharpless, N. E. (2014). Detecting and Characterizing Circular RNAs. *Nat. Biotechnol.* 32 (5), 453–461. doi:10.1038/nbt.2890

Kapoor, P., Chowdhry, A., Bagga, D. K., Bhargava, D., and Aishwarya, S. (2021). MicroRNAs in Oral Fluids (Saliva and Gingival Crevicular Fluid) as Biomarkers in Orthodontics: Systematic Review and Integrated Bioinformatic Analysis. *Prog. Orthod.* 22 (1), 31. doi:10.1186/s40510-021-00377-1

Katsumi, T., Ninomiya, M., Nishina, T., Mizuno, K., Tomita, K., Haga, H., et al. (2016). MiR-139-5p Is Associated with Inflammatory Regulation through C-FOS Suppression, and Contributes to the Progression of Primary Biliary Cholangitis. *Lab. Invest.* 96 (11), 1165–1177. doi:10.1038/labinvest.2016.95

Katsushima, F., Takahashi, A., Sakamoto, N., Kanno, Y., Abe, K., and Ohira, H. (2014). Expression of Micro-RNAs in Peripheral Blood Mononuclear Cells from Primary Biliary Cirrhosis Patients. *Hepatol. Res.* 44 (10), E189–E197. doi:10.1111/hepr.12198

Kempinska-Podhorodecka, A., Milkiewicz, M., Wasik, U., Ligocka, J., Zawadzki, M., Krawczyk, M., et al. (2017). Decreased Expression of Vitamin D Receptor Affects an Immune Response in Primary Biliary Cholangitis via the VDR-miRNA155-SOCS1 Pathway. *Ijms* 18 (2), 289. doi:10.3390/ijms18020289

Kim, N., Kim, H., Jung, I., Kim, Y., Kim, D., and Han, Y.-M. (2011). Expression Profiles of miRNAs in Human Embryonic Stem Cells during Hepatocyte Differentiation. *Hepatol. Res.* 41 (2), 170–183. doi:10.1111/j.1872-034X.2010.00752.x

Kim, W. R., Lindor, K. D., Locke, G. R., 3rd, Therneau, T. M., Homburger, H. A., Batts, K. P., et al. (2000). Epidemiology and Natural History of Primary Biliary Cirrhosis in a U.S. Community. *Gastroenterology* 119 (6), 1631–1636. doi:10.1053/gast.2000.20197

Koulentaki, M., Mantaka, A., Sifaki-Pistolla, D., Thalassinos, E., Tzanakis, N., and Kouroumalis, E. (2014). Geoepidemiology and Space-Time Analysis of Primary Biliary Cirrhosis in Crete, Greece. *Liver Int.* 34 (7), e200–e207. doi:10.1111/liv.12479

Kouroumalis, E., Samonakis, D., and Voumvouraki, A. (2018). Biomarkers for Primary Biliary Cholangitis: Current Perspectives. *Hmer* 10, 43–53. doi:10.2147/hmer.s135337

Lasda, E., and Parker, R. (2014). Circular RNAs: Diversity of Form and Function. *Rna* 20 (12), 1829–1842. doi:10.1261/rna.047126.114

Lewis, A. P., and Jopling, C. L. (2010). Regulation and Biological Function of the Liver-specific miR-122. *Biochem. Soc. Trans.* 38 (6), 1553–1557. doi:10.1042/bst0381553

Li, B., Dong, J., Yu, J., Fan, Y., Shang, L., Zhou, X., et al. (2020). Pinpointing miRNA and Genes Enrichment over Trait-Relevant Tissue Network in Genome-wide Association Studies. *BMC Med. Genomics* 13 (Suppl. 11), 191. doi:10.1186/s12920-020-00830-w

Li, J., Ghazwani, M., Zhang, Y., Lu, J., Li, J., Fan, J., et al. (2013). miR-122 Regulates Collagen Production via Targeting Hepatic Stellate Cells and Suppressing P4HA1 Expression. *J. Hepatology* 58 (3), 522–528. doi:10.1016/j.jhep.2012.11.011

Li, L.-J., Zhu, Z.-W., Zhao, W., Tao, S.-S., Li, B.-Z., Xu, S.-Z., et al. (2018). Circular RNA Expression Profile and Potential Function of Hsa_circ_0045272 in Systemic Lupus Erythematosus. *Immunology* 155 (1), 137–149. doi:10.1111/imm.12940

Li, L., Masica, D., Ishida, M., Tomuleasa, C., Umegaki, S., Kalloo, A. N., et al. (2014). Human Bile Contains microRNA-Laden Extracellular Vesicles that Can Be Used for Cholangiocarcinoma Diagnosis. *Hepatology* 60 (3), 896–907. doi:10.1002/hep.27050

Li, P., Chen, S., Chen, H., Mo, X., Li, T., Shao, Y., et al. (2015). Using Circular RNA as a Novel Type of Biomarker in the Screening of Gastric Cancer. *Clin. Chim. Acta* 444, 132–136. doi:10.1016/j.cca.2015.02.018

Li, X., Liu, R., Huang, Z., Gurley, E. C., Wang, X., Wang, J., et al. (2018). Cholangiocyte-derived Exosomal Long Noncoding RNA H19 Promotes Cholestatic Liver Injury in Mouse and Humans. *Hepatology* 68 (2), 599–615. doi:10.1002/hep.29838

Li, X., Liu, R., Wang, Y., Zhu, W., Zhao, D., Wang, X., et al. (2020). Cholangiocyte-Derived Exosomal lncRNA H19 Promotes Macrophage Activation and Hepatic Inflammation under Cholestatic Conditions. *Cells* 9 (1), 190. doi:10.3390/cells9010190

Li, X., Liu, R., Yang, J., Sun, L., Zhang, L., Jiang, Z., et al. (2017). The Role of Long Noncoding RNA H19 in Gender Disparity of Cholestatic Liver Injury in Multidrug Resistance 2 Gene Knockout Mice. *Hepatology* 66 (3), 869–884. doi:10.1002/hep.29145

Liang, D.-Y., Hou, Y.-Q., Luo, L.-J., and Ao, L. (2016). Altered Expression of miR-92a Correlates with Th17 Cell Frequency in Patients with Primary Biliary Cirrhosis. *Int. J. Mol. Med.* 38 (1), 131–138. doi:10.3892/ijmm.2016.2610

Liang, J., Chen, W., and Lin, J. (2019). LncRNA: An All-Rounder in Rheumatoid Arthritis. *J. Transl. Int. Med.* 7 (1), 3–9. doi:10.2478/jtim-2019-0002

Liu, R., Li, X., Zhu, W., Wang, Y., Zhao, D., Wang, X., et al. (2019). Cholangiocyte-Derived Exosomal Long Noncoding RNA H19 Promotes Hepatic Stellate Cell Activation and Cholestatic Liver Fibrosis. *Hepatology* 70 (4), 1317–1335. doi:10.1002/hep.30662

Lleo, A., Jepsen, P., Morenghi, E., Carbone, M., Moroni, L., Battezzati, P. M., et al. (2016). Evolving Trends in Female to Male Incidence and Male Mortality of Primary Biliary Cholangitis. *Sci. Rep.* 6, 25906. doi:10.1038/srep25906

Luna, J. M., Scheel, T. K. H., Danino, T., Shaw, K. S., Mele, A., Fak, J. J., et al. (2015). Hepatitis C Virus RNA Functionally Sequesters miR-122. *Cell* 160 (6), 1099–1110. doi:10.1016/j.cell.2015.02.025

Lv, T., Chen, S., Li, M., Zhang, D., Kong, Y., and Jia, J. (2021). Regional Variation and Temporal Trend of Primary Biliary Cholangitis Epidemiology: A Systematic Review and Meta-analysis. *J. Gastroenterology Hepatology* 36 (6), 1423–1434. doi:10.1111/jgh.15329

Ma, Y., Zhang, C., Zhang, B., Yu, H., and Yu, Q. (2019). circRNA of AR-suppressed PABPC1 91 B-p E-nhances the C-ytotoxicity of N-atural K-iller C-ells against H-epatocellular C-arcinoma via U-pregulating UL16 B-inding P-rotein 1. *Oncol. Lett.* 17 (1), 388–397. doi:10.3892/ol.2018.9606

Makkos, A., Ágg, B., Petrovich, B., Varga, Z. V., Görbe, A., and Ferdinandy, P. (2021). Systematic Review and Network Analysis of microRNAs Involved in Cardioprotection against Myocardial Ischemia/reperfusion Injury and Infarction: Involvement of Redox Signalling. *Free Radic. Biol. Med.* 172, 237–251. doi:10.1016/j.freeradbiomed.2021.04.034

Marschall, H.-U., Henriksson, I., Lindberg, S., Söderdahl, F., Thuresson, M., Wahlin, S., et al. (2019). Incidence, Prevalence, and Outcome of Primary Biliary Cholangitis in a Nationwide Swedish Population-Based Cohort. *Sci. Rep.* 9 (1), 11525. doi:10.1038/s41598-019-47890-2

Martínez, M. C., and Andriantsitohaina, R. (2017). Extracellular Vesicles in Metabolic Syndrome. *Circ. Res.* 120 (10), 1674–1686. doi:10.1161/circresaha.117.309419

Masyuk, A. I., Huang, B. Q., Ward, C. J., Gradilone, S. A., Banales, J. M., Masyuk, T. V., et al. (2010). Biliary Exosomes Influence Cholangiocyte Regulatory Mechanisms and Proliferation through Interaction with Primary Cilia. *Am. J. Physiology-Gastrointestinal Liver Physiology* 299 (4), G990–G999. doi:10.1152/ajpgi.00093.2010

Masyuk, A. I., Masyuk, T. V., and Larusso, N. F. (2013). Exosomes in the Pathogenesis, Diagnostics and Therapeutics of Liver Diseases. *J. Hepatology* 59 (3), 621–625. doi:10.1016/j.jhep.2013.03.028

Mercer, T. R., Dinger, M. E., and Mattick, J. S. (2009). Long Non-coding RNAs: Insights into Functions. *Nat. Rev. Genet.* 10 (3), 155–159. doi:10.1038/nrg2521

Metcalf, J., Bhopal, R., Gray, J., Howel, D., and James, O. (1997). Incidence and Prevalence of Primary Biliary Cirrhosis in the City of Newcastle upon Tyne, England. *Int. J. Epidemiol.* 26 (4), 830–836. doi:10.1093/ije/26.4.830

Minagawa, N., Nagata, J., Shibao, K., Masyuk, A. I., Gomes, D. A., Rodrigues, M. A., et al. (2007). Cyclic AMP Regulates Bicarbonate Secretion in Cholangiocytes through Release of ATP into Bile. *Gastroenterology* 133 (5), 1592–1602. doi:10.1053/j.gastro.2007.08.020

Mitobe, Y., Takayama, K.-i., Horie-Inoue, K., and Inoue, S. (2018). Prostate Cancer-Associated lncRNAs. *Cancer Lett.* 418, 159–166. doi:10.1016/j.canlet.2018.01.012

Naderi, M., Pazouki, A., Arefian, E., Hashemi, S. M., Jamshidi-Adegani, F., Gholamalamdari, O., et al. (2017). Two Triacylglycerol Pathway Genes, CTDNEP1 and LPIN1, Are Down-Regulated by Hsa-miR-122-5p in Hepatocytes. *Arch. Iran. Med.* 20 (3), 165–171.

Nakagawa, R., Muroyama, R., Saeki, C., Goto, K., Kaise, Y., Koike, K., et al. (2017). miR-425 Regulates Inflammatory Cytokine Production in CD4+ T Cells via N-Ras Upregulation in Primary Biliary Cholangitis. *J. Hepatology* 66 (6), 1223–1230. doi:10.1016/j.jhep.2017.02.002

Ninomiya, M., Kondo, Y., Funayama, R., Nagashima, T., Kogure, T., Kakazu, E., et al. (2013). Distinct microRNAs Expression Profile in Primary Biliary Cirrhosis and Evaluation of miR 505-3p and miR197-3p as Novel Biomarkers. *PLoS One* 8 (6), e66086. doi:10.1371/journal.pone.0066086

Ojha, R., Nandani, R., Chatterjee, N., and Prajapati, V. K. (2018). Emerging Role of Circular RNAs as Potential Biomarkers for the Diagnosis of Human Diseases. *Adv. Exp. Med. Biol.* 1087, 141–157. doi:10.1007/978-981-13-1426-1_12

Olaizola, P., Lee-Law, P. Y., Arbelaiz, A., Lapitz, A., Perugorria, M. J., Bujanda, L., et al. (2018). MicroRNAs and Extracellular Vesicles in Cholangiopathies. *Biochimica Biophysica Acta (BBA) - Mol. Basis Dis.* 1864 (4 Pt B), 1293–1307. doi:10.1016/j.bbadis.2017.06.026

Ouyang, Q., Wu, J., Jiang, Z., Zhao, J., Wang, R., Lou, A., et al. (2017). Microarray Expression Profile of Circular RNAs in Peripheral Blood Mononuclear Cells from Rheumatoid Arthritis Patients. *Cell Physiol. Biochem.* 42 (2), 651–659. doi:10.1159/000477883

Padgett, K. A., Lan, R. Y., Leung, P. C., Lleo, A., Dawson, K., Pfeiff, J., et al. (2009). Primary Biliary Cirrhosis Is Associated with Altered Hepatic microRNA Expression. *J. Autoimmun.* 32 (3-4), 246–253. doi:10.1016/j.jaut.2009.02.022

Pan, L., Liang, W., Fu, M., Huang, Z.-h., Li, X., Zhang, W., et al. (2017). Exosomes-mediated Transfer of Long Noncoding RNA ZFAS1 Promotes Gastric Cancer Progression. *J. Cancer Res. Clin. Oncol.* 143 (6), 991–1004. doi:10.1007/s00432-017-2361-2

Pan, Y., Wang, J., He, L., and Zhang, F. (2021). MicroRNA-34a Promotes EMT and Liver Fibrosis in Primary Biliary Cholangitis by Regulating TGF-β1/smad Pathway. *J. Immunol. Res.* 2021, 6890423. doi:10.1155/2021/6890423

Pandit, S., and Samant, H. (2022). "Primary Biliary Cholangitis," in *StatPearls* (Treasure Island FL: StatPearls Publishing LLC.). Copyright © 2022.

Pang, K. C., Dinger, M. E., Mercer, T. R., Malquori, L., Grimmond, S. M., Chen, W., et al. (2009). Genome-Wide Identification of Long Noncoding RNAs in CD8+T Cells. *J. Immunol.* 182 (12), 7738–7748. doi:10.4049/jimmunol.0900603

Parés, A., Caballería, L., and Rodés, J. (2006). Excellent Long-Term Survival in Patients with Primary Biliary Cirrhosis and Biochemical Response to Ursodeoxycholic Acid. *Gastroenterology* 130 (3), 715–720. doi:10.1053/j.gastro.2005.12.029

Ponting, C. P., Oliver, P. L., and Reik, W. (2009). Evolution and Functions of Long Noncoding RNAs. *Cell* 136 (4), 629–641. doi:10.1016/j.cell.2009.02.006

Poupon, R. (2010). Primary Biliary Cirrhosis: a 2010 Update. *J. Hepatology* 52 (5), 745–758. doi:10.1016/j.jhep.2009.11.027

Qian, C., Chen, S. X., Ren, C. L., Zhong, R. Q., Deng, A. M., and Qin, Q. (2013). [Abnormal Expression of miR-Let-7b in Primary Biliary Cirrhosis and its Clinical Significance]. *Zhonghua Gan Zang Bing Za Zhi* 21 (7), 533–536. doi:10.3760/cma.j.issn.1007-3418.2013.07.014

Robinson, E. K., Covarrubias, S., and Carpenter, S. (2020). The How and Why of lncRNA Function: An Innate Immune Perspective. *Biochimica Biophysica Acta (BBA) - Gene Regul. Mech.* 1863 (4), 194419. doi:10.1016/j.bbagrm.2019.194419

Rodrigues, P. M., Perugorria, M. J., Santos-Laso, A., Bujanda, L., Beuers, U., and Banales, J. M. (2018). Primary Biliary Cholangitis: A Tale of Epigenetically-Induced Secretory Failure? *J. Hepatology* 69 (6), 1371–1383. doi:10.1016/j.jhep.2018.08.020

Sakamoto, T., Morishita, A., Nomura, T., Tani, J., Miyoshi, H., Yoneyama, H., et al. (2016). Identification of microRNA Profiles Associated with Refractory Primary Biliary Cirrhosis. *Mol. Med. Rep.* 14 (4), 3350–3356. doi:10.3892/mmr.2016.5606

Salzman, J. (2016). Circular RNA Expression: Its Potential Regulation and Function. *Trends Genet.* 32 (5), 309–316. doi:10.1016/j.tig.2016.03.002

She, C. (2020). *Study on the Role of LncRNA XIST in Immune Cells of Primary Biliary Cholangitis*. Shandong, China: Qingdao University. doi:10.27262/d.cnki.gqdau.2020.000390

Sheng, J. Q., Liu, L., Wang, M. R., and Li, P. Y. (2018). Circular RNAs in Digestive System Cancer: Potential Biomarkers and Therapeutic Targets. *Am. J. Cancer Res.* 8 (7), 1142–1156.

Shibao, K., Hirata, K., Robert, M. E., and Nathanson, M. H. (2003). Loss of Inositol 1,4,5-trisphosphate Receptors from Bile Duct Epithelia Is a Common Event in Cholestasis. *Gastroenterology* 125 (4), 1175–1187. doi:10.1016/s0016-5085(03)01201-0

Sigdel, K. R., Cheng, A., Wang, Y., Duan, L., and Zhang, Y. (2015). The Emerging Functions of Long Noncoding RNA in Immune Cells: Autoimmune Diseases. *J. Immunol. Res.* 2015, 848790. doi:10.1155/2015/848790

Song, Y., Yang, H., Jiang, K., Wang, B.-M., and Lin, R. (2018). miR-181a Regulates Th17 Cells Distribution via Up-Regulated BCL-2 in Primary Biliary Cholangitis. *Int. Immunopharmacol.* 64, 386–393. doi:10.1016/j.intimp.2018.09.027

Szabo, G., and Momen-Heravi, F. (2017). Extracellular Vesicles in Liver Disease and Potential as Biomarkers and Therapeutic Targets. *Nat. Rev. Gastroenterol. Hepatol.* 14 (8), 455–466. doi:10.1038/nrgastro.2017.71

Tan, Y., Pan, T., Ye, Y., Ge, G., Chen, L., Wen, D., et al. (2014). Serum microRNAs as Potential Biomarkers of Primary Biliary Cirrhosis. *PLoS One* 9 (10), e111424. doi:10.1371/journal.pone.0111424

Tang, Y. (2009). *The Regulation of Micro RNA on Thl7 Cells in Patients with Primary Biliary Cirrhosis*. China: Second Military Medical University.

Tavasolian, F., Abdollahi, E., Rezaei, R., Momtazi-borojeni, A. A., Henrotin, Y., and Sahebkar, A. (2018). Altered Expression of MicroRNAs in Rheumatoid Arthritis. *J. Cell. Biochem.* 119 (1), 478–487. doi:10.1002/jcb.26205

Teng, K.-Y., Barajas, J. M., Hu, P., Jacob, S. T., and Ghoshal, K. (2020). Role of B Cell Lymphoma 2 in the Regulation of Liver Fibrosis in miR-122 Knockout Mice. *Biology* 9 (7), 157. doi:10.3390/biology9070157

Tian, T., Wang, M., Lin, S., Guo, Y., Dai, Z., Liu, K., et al. (2018). The Impact of lncRNA Dysregulation on Clinicopathology and Survival of Breast Cancer: A Systematic Review and Meta-Analysis. *Mol. Ther. - Nucleic Acids* 12, 359–369. doi:10.1016/j.omtn.2018.05.018

Tomiyama, T., Yang, G.-X., Zhao, M., Zhang, W., Tanaka, H., Wang, J., et al. (2017). The Modulation of Co-stimulatory Molecules by Circulating Exosomes in Primary Biliary Cirrhosis. *Cell Mol. Immunol.* 14 (3), 276–284. doi:10.1038/cmi.2015.86

Tsai, W.-C., Hsu, P. W.-C., Lai, T.-C., Chau, G.-Y., Lin, C.-W., Chen, C.-M., et al. (2009). MicroRNA-122, a Tumor Suppressor microRNA that Regulates Intrahepatic Metastasis of Hepatocellular Carcinoma. *Hepatology* 49 (5), 1571–1582. doi:10.1002/hep.22806

Tsai, W.-C., Hsu, S.-D., Hsu, C.-S., Lai, T.-C., Chen, S.-J., Shen, R., et al. (2012). MicroRNA-122 Plays a Critical Role in Liver Homeostasis and Hepatocarcinogenesis. *J. Clin. Invest.* 122 (8), 2884–2897. doi:10.1172/jci63455

Tsuneyama, K., Baba, H., Morimoto, Y., Tsunematsu, T., and Ogawa, H. (2017). Primary Biliary Cholangitis: Its Pathological Characteristics and Immunopathological Mechanisms. *J. Med. Invest.* 64 (1.2), 7–13. doi:10.2152/jmi.64.7

Wang, J., Yan, S., Yang, J., Lu, H., Xu, D., and Wang, Z. (2019). Non-coding RNAs in Rheumatoid Arthritis: From Bench to Bedside. *Front. Immunol.* 10, 3129. doi:10.3389/fimmu.2019.03129

Wang, X., Wen, X., Zhou, J., Qi, Y., Wu, R., Wang, Y., et al. (2017). MicroRNA-223 and microRNA-21 in Peripheral Blood B Cells Associated with Progression of Primary Biliary Cholangitis Patients. *PLoS One* 12 (9), e0184292. doi:10.1371/journal.pone.0184292

Wang, X. W., Heegaard, N. H. H., and Ørum, H. (2012). MicroRNAs in Liver Disease. *Gastroenterology* 142 (7), 1431–1443. doi:10.1053/j.gastro.2012.04.007

Wang, X., Zhang, C., Wu, Z., Chen, Y., and Shi, W. (2018). CircIBTK Inhibits DNA Demethylation and Activation of AKT Signaling Pathway via miR-29b in Peripheral Blood Mononuclear Cells in Systemic Lupus Erythematosus. *Arthritis Res. Ther.* 20 (1), 118. doi:10.1186/s13075-018-1618-8

Wang, Y., Fu, L., Lu, T., Zhang, G., Zhang, J., Zhao, Y., et al. (2021). Clinicopathological and Prognostic Significance of Long Non-coding RNA MIAT in Human Cancers: A Review and Meta-Analysis. *Front. Genet.* 12, 729768. doi:10.3389/fgene.2021.729768

Wang, Y., Zheng, F., Gao, G., Yan, S., Zhang, L., Wang, L., et al. (2018). MiR-548a-3p Regulates Inflammatory Response via TLR4/NF-κB Signaling Pathway in Rheumatoid Arthritis. *J. Cell Biochem.* 120, 1133–1140. doi:10.1002/jcb.26659

Wasik, U., Kempinska-Podhorodecka, A., Bogdanos, D. P., Milkiewicz, P., and Milkiewicz, M. (2020). Enhanced Expression of miR-21 and miR-150 Is a Feature of Anti-mitochondrial Antibody-Negative Primary Biliary Cholangitis. *Mol. Med.* 26 (1), 8. doi:10.1186/s10020-019-0130-1

Wasik, U., Milkiewicz, M., Kempinska-Podhorodecka, A., and Milkiewicz, P. (2017). Protection against Oxidative Stress Mediated by the Nrf2/Keap1 axis Is Impaired in Primary Biliary Cholangitis. *Sci. Rep.* 7, 44769. doi:10.1038/srep44769

Watson, R. G., Angus, P. W., Dewar, M., Goss, B., Sewell, R. B., and Smallwood, R. A. (1995). Low Prevalence of Primary Biliary Cirrhosis in Victoria, Australia. Melbourne Liver Group. *Gut* 36 (6), 927–930. doi:10.1136/gut.36.6.927

Witt-Sullivan, H., Heathcote, J., Cauch, K., Blendis, L., Ghent, C., Katz, A., et al. (1990). The Demography of Primary Biliary Cirrhosis in Ontario, Canada. *Hepatology* 12 (1), 98–105. doi:10.1002/hep.1840120116

Worst, T. S., von Hardenberg, J., Gross, J. C., Erben, P., Schnölzer, M., Hausser, I., et al. (2017). Database-augmented Mass Spectrometry Analysis of Exosomes Identifies Claudin 3 as a Putative Prostate Cancer Biomarker. *Mol. Cell. Proteomics* 16 (6), 998–1008. doi:10.1074/mcp.M117.068577

Wu, Y., Zhang, F., Ma, J., Zhang, X., Wu, L., Qu, B., et al. (2015). Association of Large Intergenic Noncoding RNA Expression with Disease Activity and Organ Damage in Systemic Lupus Erythematosus. *Arthritis Res. Ther.* 17 (1), 131. doi:10.1186/s13075-015-0632-3

Xiang, G., Fan, J., Ye, Z., Fu, X., Li, H., Zhang, H., et al. (2019). Differential Expression Analysis of Long-Chain Non-coding RNA in Peripheral Blood of Patients with Primary Biliary Cirrhosis. *Chongqing Med.* 48, 1149–1154.

Xu, H., Xu, S.-J., Xie, S.-J., Zhang, Y., Yang, J.-H., Zhang, W.-Q., et al. (2019). MicroRNA-122 Supports Robust Innate Immunity in Hepatocytes by Targeting the RTKs/STAT3 Signaling Pathway. *Elife* 8, e41159. doi:10.7554/eLife.41159

Yang, J., Chen, M., Cao, R. Y., Li, Q., and Zhu, F. (2018). The Role of Circular RNAs in Cerebral Ischemic Diseases: Ischemic Stroke and Cerebral Ischemia/Reperfusion Injury. *Adv. Exp. Med. Biol.* 1087, 309–325. doi:10.1007/978-981-13-1426-1_25

Yang, L., Fu, J., and Zhou, Y. (2018). Circular RNAs and Their Emerging Roles in Immune Regulation. *Front. Immunol.* 9, 2977. doi:10.3389/fimmu.2018.02977

Yang, Y. (2013). *Preliminary Study of microRNA as a New Disease Marker and its Function in Primary Biliary Cirrhosis*. China, Beijing: Peking Union Medical College.

Yang, Z., Wu, W., Ou, P., Wu, M., Zeng, F., Zhou, B., et al. (2021). MiR-122-5p Knockdown Protects against APAP-Mediated Liver Injury through Up-Regulating NDRG3. *Mol. Cell Biochem.* 476 (2), 1257–1267. doi:10.1007/s11010-020-03988-0

Young, N. A., Valiente, G. R., Hampton, J. M., Wu, L.-C., Burd, C. J., Willis, W. L., et al. (2017). Estrogen-regulated STAT1 Activation Promotes TLR8 Expression to Facilitate Signaling via microRNA-21 in Systemic Lupus Erythematosus. *Clin. Immunol.* 176, 12–22. doi:10.1016/j.clim.2016.12.005

Zeng, N., Duan, W., Chen, S., Wu, S., Ma, H., Ou, X., et al. (2019). Epidemiology and Clinical Course of Primary Biliary Cholangitis in the Asia-Pacific Region: a Systematic Review and Meta-Analysis. *Hepatol. Int.* 13 (6), 788–799. doi:10.1007/s12072-019-09984-x

Zhang, L., Huang, Y., Wang, H., Kong, W., Ye, X., Chen, Y., et al. (2013). Increased Expression of lncRNA AK053349 in Peripheral Blood Mononuclear Cells from Patients with Primary Biliary Cirrhosis and its Clinical Significance. *Int. J. Lab. Med.* 34 (20), 2656–2657+2659.

Zhang, Y., Jia, Y., Zheng, R., Guo, Y., Wang, Y., Guo, H., et al. (2010). Plasma microRNA-122 as a Biomarker for Viral-, Alcohol-, and Chemical-Related Hepatic Diseases. *Clin. Chem.* 56 (12), 1830–1838. doi:10.1373/clinchem.2010.147850

Zhang, Y., Zhang, G., Liu, Y., Chen, R., Zhao, D., McAlister, V., et al. (2018). GDF15 Regulates Malat-1 Circular RNA and Inactivates NFκB Signaling Leading to Immune Tolerogenic DCs for Preventing Alloimmune Rejection in Heart Transplantation. *Front. Immunol.* 9, 2407. doi:10.3389/fimmu.2018.02407

Zhao, Z., Li, X., Gao, C., Jian, D., Hao, P., Rao, L., et al. (2017). Peripheral Blood Circular RNA Hsa_circ_0124644 Can Be Used as a Diagnostic Biomarker of Coronary Artery Disease. *Sci. Rep.* 7, 39918. doi:10.1038/srep39918

Zheng, F., Yu, X., Huang, J., and Dai, Y. (2017). Circular RNA Expression Profiles of Peripheral Blood Mononuclear Cells in Rheumatoid Arthritis Patients, Based on Microarray Chip Technology. *Mol. Med. Rep.* 16 (6), 8029–8036. doi:10.3892/mmr.2017.7638

Zheng, J., Li, Z., Wang, T., Zhao, Y., and Wang, Y. (2017). Microarray Expression Profile of Circular RNAs in Plasma from Primary Biliary Cholangitis Patients. *Cell Physiol. Biochem.* 44 (4), 1271–1281. doi:10.1159/000485487

Zhu, H., and Leung, S.-w. (2021). MicroRNA Biomarkers of Type 2 Diabetes: A Protocol for Corroborating Evidence by Computational Genomics and Meta-Analyses. *PLoS One* 16 (4), e0247556. doi:10.1371/journal.pone.0247556

Conflict of Interest: The authors declare that the research was conducted in the absence of any commercial or financial relationships that could be construed as a potential conflict of interest.

Publisher's Note: All claims expressed in this article are solely those of the authors and do not necessarily represent those of their affiliated organizations, or those of the publisher, the editors and the reviewers. Any product that may be evaluated in this article, or claim that may be made by its manufacturer, is not guaranteed or endorsed by the publisher.

frontiers | Frontiers in Molecular Biosciences

TYPE Original Research
PUBLISHED 18 July 2022
DOI 10.3389/fmolb.2022.887686

OPEN ACCESS

EDITED BY
Yong Sun Lee,
National Cancer Center, South Korea

REVIEWED BY
Sihem Cheloufi,
University of California, United States
Aristeidis G. Telonis,
University of Miami, United States

*CORRESPONDENCE
Rune Ougland,
runoug@vestreviken.no
Anindya Dutta,
duttaa@uab.edu

†These authors have contributed equally to this work and share first authorship

SPECIALTY SECTION
This article was submitted to Molecular Diagnostics and Therapeutics, a section of the journal Frontiers in Molecular Biosciences

RECEIVED 01 March 2022
ACCEPTED 27 June 2022
PUBLISHED 18 July 2022

CITATION
Su Z, Monshaugen I, Klungland A, Ougland R and Dutta A (2022), Characterization of novel small non-coding RNAs and their modifications in bladder cancer using an updated small RNA-seq workflow.
Front. Mol. Biosci. 9:887686.
doi: 10.3389/fmolb.2022.887686

Characterization of novel small non-coding RNAs and their modifications in bladder cancer using an updated small RNA-seq workflow

Zhangli Su[1,2†], Ida Monshaugen[3,4,6†], Arne Klungland[3,5], Rune Ougland[3,6*] and Anindya Dutta[1,2*]

[1]Department of Genetics, University of Alabama at Birmingham, Birmingham, AL, United States, [2]Department of Biochemistry and Molecular Genetics, School of Medicine, University of Virginia, Charlottesville, VA, United States, [3]Department of Microbiology, Oslo University Hospital Rikshospitalet, Oslo, Norway, [4]Department of Molecular Medicine, Institute of Basic Medical Sciences, University of Oslo, Oslo, Norway, [5]Department of Biosciences, Faculty of Mathematics and Natural Sciences, University of Oslo, Oslo, Norway, [6]Department of Surgery, Baerum Hospital Vestre Viken Hospital Trust, Gjettum, Norway

Background: Bladder cancer (BLCA) is one of the most common cancer types worldwide. The disease is responsible for about 200,000 deaths annually, thus improved diagnostics and therapy is needed. A large body of evidence reveal that small RNAs of less than 40 nucleotides may act as tumor suppressors, oncogenes, and disease biomarkers, with a major focus on microRNAs. However, the role of other families of small RNAs is not yet deciphered. Recent results suggest that small RNAs and their modification status, play a role in BLCA development and are promising biomarkers due to their high abundance in the exomes and body fluids (including urine). Moreover, free modified nucleosides have been detected at elevated levels from the urine of BLCA patients. A genome-wide view of small RNAs, and their modifications, will help pinpoint the molecules that could be used as biomarker or has important biology in BLCA development.

Methods: BLCA tumor tissue specimens were obtained from 12 patients undergoing transurethral resection of non-muscle invasive papillary urothelial carcinomas. Genome-wide profiling of small RNAs less than 40 bases long was performed by a modified protocol with TGIRT (thermostable group II reverse transcriptase) to identify novel small RNAs and their modification status.

Results: Comprehensive analysis identified not only microRNAs. Intriguingly, 57 ± 15% (mean ± S.D.) of sequencing reads mapped to non-microRNA-small RNAs including tRNA-derived fragments (tRFs), ribosomal RNA-derived fragments (rRFs) and YRNA-derived fragments (YRFs). Misincorporation (mismatch) sites identified potential base modification positions on the small RNAs, especially on tRFs, corresponding to m^1A (N^1-methyladenosine), m^1G (N^1-methylguanosine) and $m^2{}_2G$ (N^2, N^2-dimethylguanosine). We also detected

mismatch sites on rRFs corresponding to known modifications on 28 and 18S rRNA.

Conclusion: We found abundant non-microRNA-small RNAs in BLCA tumor samples. Small RNAs, especially tRFs and rRFs, contain modifications that can be captured as mismatch by TGIRT sequencing. Both the modifications and the non-microRNA-small RNAs should be explored as a biomarker for BLCA detection or follow-up.

KEYWORDS

bladder cancer, non-coding RNA, small RNA, RNA modification, tRNA-derived fragment, rRNA-derived fragment, YRNA-derived fragment

Introduction

Bladder cancer (BLCA) is the sixth most common cancer worldwide with high morbidity and mortality rates. With 550,000 annual new incidents and 200,000 deaths, BLCA poses a significant disease burden globally (Bray et al., 2018). About 75% of incidents present as non-muscle invasive (NMIBC), consisting of a heterogeneous population of tumors (Kirkali et al., 2005; Burger et al., 2013). Currently there is no routine screening for NMIBC or BLCA in general. Patients with NMIBC usually display urinary tract symptoms i.e., hematuria, pain or frequent urination, and is then subject to cystoscopy as the first step in the diagnostic process. If the initial workup reveals a tumor, the affected individual often undergoes surgery. In addition, patients may receive radiation therapy, chemotherapy, immunotherapy and targeted therapy. Despite a 70–80% recurrence rate, NMIBC has a favorable prognosis and a 5-year survival rate greater than 85% (van Rhijn et al., 2009). However, up to 30% of NMIBC cases progress into more advanced stages with less favorable prognosis, and 5-year survival rate drops to about 5% for metastatic disease (Schrier et al., 2004; Sanli et al., 2017; Boegemann and Krabbe, 2020). This lifelong menace necessitates an exhaustive post-operative control scheme burdening both patients and healthcare systems. In fact, BLCA is in the top tier of the most expensive cancer type to treat, both when considering cost per patient and lifetime cost, in addition to the invaluable expense of life quality reduction (James and Gore, 2013). Thus, urgent improvement of diagnostics and follow-up is required. Despite tremendous effort, the development of sensitive biomarkers and non-invasive methods for cost-effective diagnostics and surveillance of patients remains a challenge. However, the family of small non-coding RNAs and their modifications, appear as a promising addition to the future clinical toolbox.

Non-coding RNAs (ncRNAs), including both long non-coding RNAs (lncRNAs) and small RNAs (sRNAs), have gained much attention lately for their key role as mediators of gene expression in cancer (Slack and Chinnaiyan, 2019). They are considered well-suited as therapeutic targets or agents due to their small size and chemical properties, which allow them to cross tissue barriers and reach tumor cell interior better than macromolecular antibody drugs (Li et al., 2020). In particular, the primary focus of sRNA research in BLCA has been directed towards microRNAs (miRNAs). Extensive RNA sequencing by The Cancer Genome Atlas reported epigenetic regulation of ncRNA, especially miRNAs, in BLCA (Yoshino et al., 2013; Cancer Genome Atlas Research, 2014). In recent years, dysregulated expression of hundreds of miRNAs have been reported in BLCA by large-scale analysis from close to 20 research groups (Lee et al., 2016). Functional studies suggest that miRNAs are involved in different aspects of BLCA development and progression (Li et al., 2011; Morais et al., 2014; Wang et al., 2015). Moreover, miRNAs dysregulated in tumor tissue can also be detected in biological fluids such as serum and urine, suggesting their potential usage as non-invasive diagnostic or prognostic tools (Yun et al., 2012; Armstrong et al., 2015; Fang et al., 2016; Borkowska et al., 2019; Yin et al., 2019).

Besides microRNAs, other emerging small RNAs are detected at high abundance thanks to the technological advances in next-generational sequencing. For example, tRNA-derived fragments (tRFs) have gained attention as their diverse biological functions are being discovered (Magee and Rigoutsos, 2020). These sRNAs have high promise due to their biological functions in different diseases and their high abundance in bodily fluids as recently reviewed (Su et al., 2020b). So far only a few reports focused on tRFs or other non-microRNA-small RNAs in BLCA. tRF expression showed context-dependent association with mRNA expression across 32 cancer types in TCGA, highlighting differences in tRF-mRNA connection by sex in bladder cancer (Telonis et al., 2019). Furthermore, analysis of TCGA data found association between elevated level of a specific tRF (5′-tRF-LysCTT) and early progression and poor outcome in BLCA (Papadimitriou et al., 2020), calling for further investigation of tRF functions in BLCA. In addition to tRFs, other small RNAs such as ribosomal

RNA-derived fragments (rRFs) and Y RNA-derived fragments (YRFs) have also been reported in humans but not investigated as much. Important to note, TCGA small RNA-seq data was collected focusing on microRNAs (~22 nucleotides long) and has a strict size cut-off of 30 nucleotides, losing potential information on RNAs longer than this size range.

Moreover, sRNAs harbor a range of chemical modifications providing a second layer of biological information (Zhang et al., 2016; Li et al., 2021). This modification information is often missing and even leads to under-representation of modification-containing sRNAs during conventional small RNA-seq library preparation (Shi et al., 2021). Enzyme-assisted library preparation improves the cloning of modification-containing sRNAs, and suggests that their abundance was formerly far under-appreciated. Altogether, there is a great need to understand the relative abundance of non-microRNA-small RNAs and modification status on different small RNAs, both of which have not been comprehensively profiled in BLCA samples.

We aimed to establish a workflow that can profile both microRNA (miRs) and non-miR small RNAs in a genome-wide fashion that can be applied to patient samples. Small RNA-seq has been a powerful method for high-throughput profiling and sequence-level information that is important for base-level analysis. However, regular small RNA-seq protocol is known to suffer from the stalling of the reverse transcriptase at sites containing modifications that disrupt Watson-Crick base-pairing, including but not limited to m^1A (N^1-methyladenosine), m^1G (N^1-methylguanosine), and m_2^2G (N^2, N^2-dimethylguanosine) (Behrens et al., 2021; Shi et al., 2021). Recently we showed TGIRT (thermostable group II intron reverse transcriptase) can be used in small RNA-seq to overcome under-cloning of m^1A-containing RNAs during regular small RNA-seq protocol, and further be used to identify the modification base position via mismatch (Su et al., 2022). The under-representation of m^1A-containing small RNAs and loss of quantitative mismatch ratio by a commonly used M-MuLV reverse transcriptase (ProtoScriptII) indicates the regular small RNA-seq pipeline is biased against m^1A-modified small RNAs. Intrigued by this result, we wondered whether TGIRT can also overcome and capture the other RNA modifications that disrupt Watson-Crick base-pairing. In addition to A-type mismatch, we noticed TGIRT also produced more G-type mismatch than ProtoScriptII from the same HEK293T RNAs (Supplementary Figure S1A), suggesting TGIRT can potentially capture modifications on guanosine as well. Here we report a comprehensive profiling of small RNAs and their modification status in BLCA patient samples by this modified small RNA-seq pipeline. From 12 tumor samples, we identified non-microRNA-small RNA reads that are comparable in abundance to microRNAs. These non-microRNA-small RNAs include tRNA-fragments, rRNA-fragments, Y-RNA-fragments, snoRNA-fragments and more. Their length distribution and cleavage patterns were distinctly different. RNA modification as indicated by TGIRT mismatch pattern was mostly found on tRFs over other small RNA types. Mismatch sites on specific tRFs correspond to known m^1A, m^1G and m_2^2G annotations on mature tRNAs, suggest a large proportion of tRFs harbor these modifications. Furthermore, mismatch sites were also identified on rRFs at known modification positions on 28 and 18S rRNAs. This analysis confirms the high potential of using TGIRT to enable modification-friendly profiling of small RNAs in clinical samples.

TABLE1 NMIBC patient information.

Patient #	Sex	Age range	Primary or recidive
Patient #1	Female	40-49	Primary
Patient #2	Male	70-79	Primary
Patient #3	Male	70-79	Primary
Patient #4	Male	60-69	Primary
Patient #5	Male	70-79	Primary
Patient #6	Male	>80	Primary
Patient #7	Male	60-69	Primary
Patient #8	Male	50-59	Primary
Patient #9	Male	40-49	Primary
Patient #10	Male	50-59	Primary
Patient #11	Male	>80	Primary
Patient #12	Female	70-79	Primary

Materials and methods

Human subject and sample collection

Patients diagnosed and treated for papillary urothelial NMIBC at the Vestre Viken Hospital Trust hospitals were enrolled in the study. Cold cup biopsies were harvested prior to surgical resection of the tumor, and the specimens were kept on −20°C in RNAlater preservation solution (Ambion #AM7020) until preparation and further analyses.

Anonymized collective patient information of the 12 samples used is listed in Table 1.

RNA extraction

Purification of total RNA was done using the RNAzol RT reagent (MRC Inc. #RN190). Subsequently RNA quality was determined using RNA ScreenTape on TapeStation (Agilent Tech. #5067-5576) or Agilent RNA 6000 Pico Kit on Bioanalyzer (Agilent Tech. #5067-1513).

Small RNA library preparation by TGIRT and sequencing

Small RNA-seq library preparation was performed as previously reported (Su et al., 2019; Su et al., 2020a) using NEBNext Small RNA Library Prep Set for Illumina (NEB #7330) with changes to use TGIRT for cDNA synthesis. TGIRT condition is based on m^1A mapping on polyA-enriched RNAs by TGIRT-seq (Li et al., 2017) with the modifications described below. Total RNAs of 0.3–1 μg were ligated with the corresponding 3′ and 5’ adaptor within the NEBNext kit. Ligated RNAs were converted to cDNA by 1 μL TGIRT-III enzyme (InGex #TGIRT50) per reaction at 60°C for 15 min. TGIRT reaction was carried out in buffer (50 mM Tris, pH 8.3, 75 mM KCl, 3 mM $MgCl_2$, 1 mM dNTP, 10 mM DTT) with addition of 1 μL RNase Inhibitor. The reaction is stopped by addition of 250 mM (final concentration) NaOH at 95°C for 3 min and 65°C for 15 min. Same amount of HCl was added to neutralize the reaction after the reaction cools down. The cDNA is further purified by QIAquick Nucleotide Removal Kit (Qiagen #28304) or ZYMO oligo clean and concentrator kit (ZYMO #D4060) or Dynabeads MyOne Silane (Thermo Fisher #37002D). cDNA is amplified by 15–16 cycles of PCR with indexed NEBNext primers (NEB #E6609). The individual amplified libraries were purified with ZYMO DNA Clean and Concentrator Kit (ZYMO #D4033) and run on 8% TBE polyacrylamide Novex gel (Thermo Fisher #EC6215). The position corresponding to RNA insert of 15–40 nucleotides long was cut out from the gel and purified *via* crush-and-soak method. Care was taken to cut the region longer than primer dimer and shorter than full-length tRNA. Gel-recovered eluate was purified and concentrated by ethanol precipitation according to NEB kit instruction. Final libraries were quantified by Qubit fluorometer and pooled for sequencing on Illumina sequencer.

HEK293T small RNA-seq data by ProtoScriptII and TGIRT can be accessed from GEO: GSE171040 (GSM5217188 and GSM5217193 for ProtoScriptII; GSM5217184 and GSM5217186 for TGIRT).

General mapping strategy for small RNA TGIRT-seq data analysis

Small RNA-seq data was analyzed similarly as before (Su et al., 2019; Su et al., 2020a). Briefly, cutadapt v1.15 (Martin, 2011) was used to trim 3′ adaptor sequence and discard trimmed read length shorter than 15 nt. To avoid mis-annotation of 5′ NEBNext adaptor sequence to hsa-miR-3168, reads containing 5′ adaptor sequence were discarded with cutadapt. In general, each library has 2–10 million mapped reads. Unitas v1.7.3 (Gebert et al., 2017) with SeqMap v1.0.13 (Jiang and Wong, 2008) was used to map small RNAs. Priority of mapping was given to first map the reads to miRBase Release 22 (Kozomara et al., 2019) human sequence. The remaining reads were mapped to other small RNA sequences including genomic tRNA database (Chan and Lowe, 2016) and Ensembl Release 97. Additional rRNA and YRNA reference sequences were used for rRF and YRF mapping: 18S (NR_145820.1), 5S (NR_023363.1), 28S (NR_003287.4) and 5.8S (NR_145821.1); RNY1 (NR_004391.1), RNY3 (NR_004392.1), RNY4 (NR_004393.1) and RNY5 (NR_001571.2). miRNA mapping was done allowing 2 non-templated 3’ nucleotides addition and 1 internal mismatch. Other nmsRNA mapping was done allowing 1 mismatch and 0 insertion/deletion, unless otherwise specified (for example Supplementary Figure S1). When a given read is mapped to multiple reference RNAs (multi-mapping), fractionated count was calculated assuming even distribution among all possible references. For all the analysis, reads per million (RPM) was calculated to adjust for total mapped reads in each library.

Mismatch calculation for small RNA TGIRT-seq data analysis

After initial mapping as above, tRF/rRF/YRF reads were re-mapped to only the corresponding reference RNAs with unitas v1.7.3 (Gebert et al., 2017) allowing 1 mismatch and 0 insertion/deletion. The mapping start/end position and mismatch position were recorded for each read. The reads were aggregated onto the whole length of reference RNAs into a coverage plot to facilitate visualization, with *X* axis representing each nucleotide position of the reference RNA and *Y* axis representing the abundance of all reads that covered that specific position. Mismatch index (on a scale of 0–100%) was calculated for each position by taking the reads with mismatch at that position and divided by total reads that covered that specific position. Mismatch index was visualized by color on the coverage plot (red means higher mismatch). For tRFs (Figure 4), coverage was aggregated by tRNA amino acid groups.

Coverage plot on secondary structure of YRNA-derived fragments

YRNA secondary structures were retrieved from RNAcentral v19 based on Rfam (RF00019). The dot-bracket notation was used to generate secondary structure plot by StructureEditor v6.1. To color each base based on the relative abundance, coverage of each base is normalized to the highest coverage for that YRNA.

Results

An updated small RNA-seq workflow for modification-friendly global analysis

We collected 12 NMIBC tumor samples (patient information summarized in Table 1) to test the updated

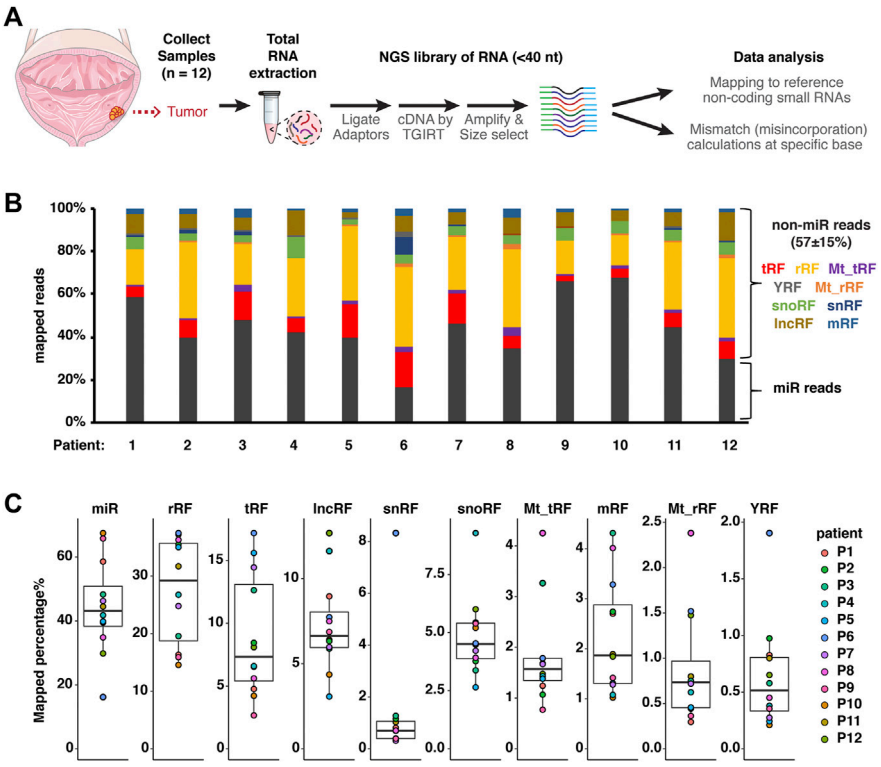

FIGURE 1
An updated small RNA-seq workflow for modification-friendly global analysis. **(A)** Scheme of collecting tumor samples from 12 NMIBC patients. Small RNA-sequencing libraries by TGIRT were prepared from total RNAs to profile relative abundance and potential RNA modifications (based on mismatch/misincorporation) for small RNAs less than 40 bases long. **(B)** Overall distribution of total mapped reads between microRNAs (dark grey) and non-microRNA small RNAs (nmsRNAs), including rRFs (yellow), tRFs (red) and more. **(C)** Distribution of mapped percentage for each sub-group of small RNAs shown as box-whisker plot. Box plot center represents median value, bounds represent upper and lower quartile, whiskers represent 1.5* interquartile range from the bounds.

small RNA-seq workflow (Figure 1A). High-quality total RNAs were used as input and first ligated with 3′ adaptor and 5’ adaptor. Ligated RNA was converted into cDNA by reverse transcriptase TGIRT, which has been shown to produce more mismatch (misincorporation) than hard-stop products at m^1A modification sites than other reverse transcriptases (Li et al., 2017; Su et al., 2022). When sequencing HEK293T RNAs, we noticed TGIRT protocol is better at capturing non-microRNA-small RNAs than the regular ProtoScriptII protocol (Supplementary Figure S1A). The higher G-type mismatch from the same HEK293T RNAs by TGIRT (Supplementary Figure S1B), suggests TGIRT might detect certain modifications on guanosine as well. To be noted, base modifications that disrupt base pairing such as m^1A, m^1G, m_2^2G are more prone to produce RT-induced mismatch, while other RNA modifications including m^6A and pseudouridine are less affected. Only the fully ligated and converted cDNAs can be further amplified by the next PCR amplification. Lastly, the PCR products are size selected experimentally to enrich for small RNAs of size less than 40 nucleotides long. To avoid ambiguous mapping of very short sequences, we only mapped reads that are at least 15 nucleotides long. Each clean read was first mapped to human microRNA sequences, and the remaining reads were then mapped to other reference sequences to identify non-microRNA-small RNAs (nmsRNA) (Supplementary Figure S1C). The largest increase in mapping of nmsRNAs (of 25–150%) was seen specifically with tRFs compared to other nmsRNAs (Supplementary Figure S1D). In contrast allowing indels of 1 nt did not increase mapping numbers (Supplementary Figure S1E). Overall we found a very high percentage of nmsRNA reads in these libraries, constituting 42–72% of all mapped reads (Figure 1B). The most abundant nmsRNAs include tRNA-derived fragments (tRFs), ribosomal RNA-derived fragments (rRFs), mitochondrial tRFs, mitochondrial rRFs, Y-RNA-derived fragments (YRFs), small nucleolar RNA-derived fragments (snoRFs), small nuclear RNA-derived fragments (snRFs), lncRNA-derived fragments (lncRFs) and protein-coding mRNA-derived fragments (mRFs). Among these, the four most abundant groups are rRFs, tRFs, snoRFs and lncRFs (Figure 1B). It was striking

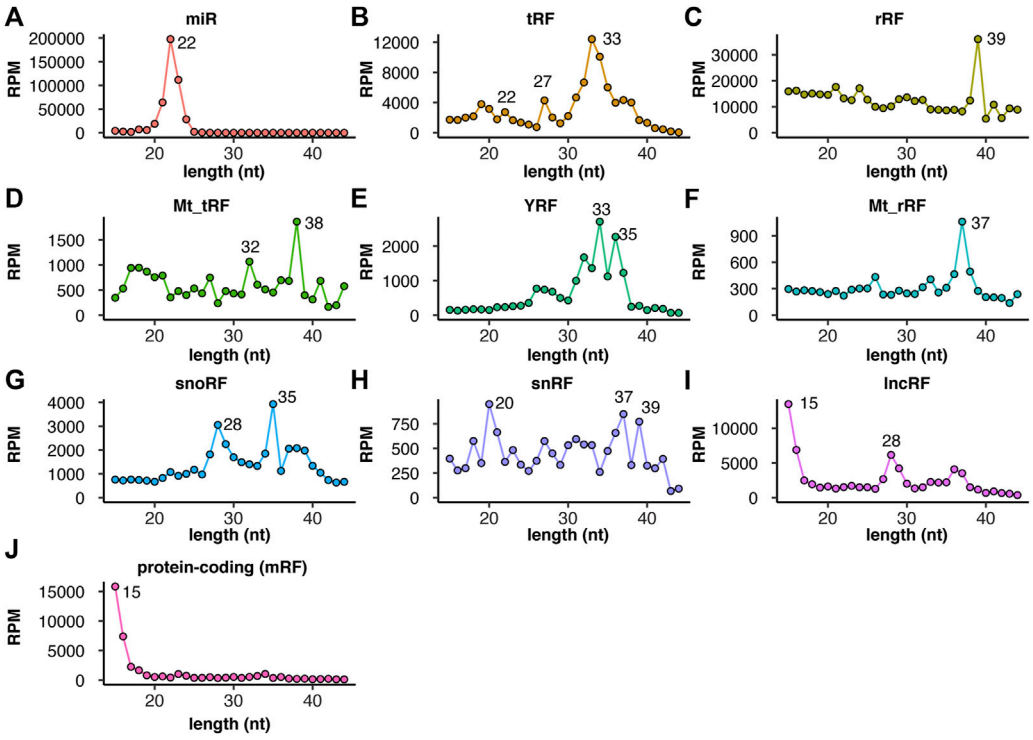

FIGURE 2
microRNAs and non-microRNA small RNAs show distinct size distribution. Size distribution (*X*-axis in nucleotides, *Y*-axis in reads per million mapped reads) of each subtype of small RNAs including **(A)** microRNAs, **(B)** tRFs, **(C)** rRFs, **(D)** mitochondrial tRFs, **(E)** YRFs, **(F)** mitochondrial rRFs, **(G)** snoRFs, **(H)** snRFs, **(I)** lncRFs and **(J)** mRFs. Major peaks in length are labeled for each small RNA subtype. RPM values are averaged from 12 samples (individual samples plotted in Supplementary Figure S2).

that in some patients (patients 2, 5, 6, 8 and 12), rRF read counts were nearly equal to or more than microRNAs. Interestingly, relative read distribution among different small RNA subgroups was quite variable for different patients (Figure 1C).

microRNAs and nmsRNAs (non-microRNA-small RNAs) show distinct size distribution

To further understand the characteristics of the nmsRNAs, we checked the length distribution of each subtype. As expected, microRNAs have a specific size of 22 nucleotides (average from 12 samples shown in Figure 2A, individual patient samples shown in Supplementary Figure S2). Meanwhile, the other small RNAs showed distinct size distributions that were different from microRNAs. For example, tRFs (Figure 2B), rRFs (Figure 2C), mitochondrial tRFs (Figure 2D), YRFs (Figure 2E), mitochondrial rRFs (Figure 2F) and snoRFs (Figure 2G) all have a longer size range than microRNAs. snRFs have a peak at 20 nucleotides and additional peaks at longer size of 37 and 39 nucleotides (Figure 2H). This also suggests these longer nmsRNAs were missed or underrepresented if a library was size selected around 22 nucleotides.

Similar to what we found before (Kumar et al., 2014), tRFs display specific peaks in length at 33, 27, 22 and 18 nucleotides (Figure 2B), which will be further discussed in the next section. Intriguingly, mitochondrial tRFs display additional peaks at 38 and 32 nucleotides (Figure 2D). In addition, both genomic and mitochondrial rRFs are represented by a very specific peak (39 and 37 nucleotides) (Figure 2C and Figure 2F). YRFs have peaks of 33, 35 and 31 nucleotides (Figure 2E), whereas snoRFs have peaks of 35 and 28 nucleotides (Figure 2G). On the other hand, lncRFs and mRFs have predominantly shorter reads of 15 nucleotides, (Figures 2I–J) which is the size cut-off for our bioinformatics analysis (we discarded reads shorter than 15 nucleotides to avoid ambiguous mapping). This may suggest more non-specific cleavage on lncRNA and mRNAs than the other RNAs. In general, the pre-dominant size for each small RNA subtype was consistently observed across 12 tumor samples, which shows distinct pattern between different RNA subtypes (Supplementary Figure S2). Below we describe specific nmsRNA subtypes in more details.

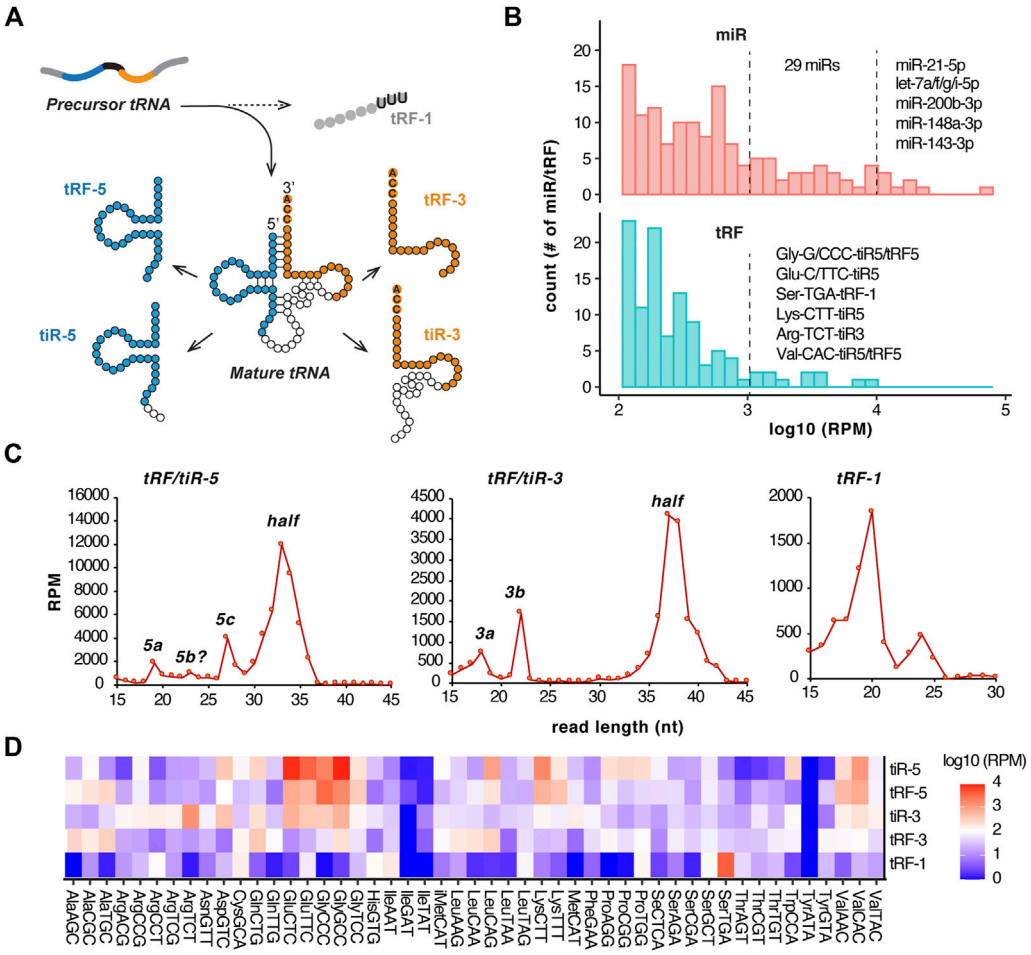

FIGURE 3
Abundant tRFs show distinct size distribution. **(A)** Major subtypes of tRFs. **(B)** Comparison of relative abundance of microRNAs and tRFs by histogram (*X*-axis: log 10 scale of reads per million). Top expressed miRs and tRFs (RPM >1,000) are labeled. tRF is grouped by each of the five types in **(A)** and further by anticodon. **(C)** Size distribution (*X*-axis in nucleotides, *Y*-axis in reads per million mapped reads) of each tRF subtype. **(D)** tRF abundance shown as a heatmap grouped by tRF types and anticodons. RPM values are averaged from 12 samples (individual samples plotted in Supplementary Figure S3).

TGIRT-seq detects tRNA halves and tRFs in the microRNA-size range at an abundance comparable to microRNAs

tRFs are grouped by their start and end positions on parental tRNAs, including 5′ fragments and 3′ fragments from mature tRNAs and tRF-1s from precursor tRNA trailers (Figure 3A). Both 5′ and 3′ fragments can be further divided into longer fragments (or called tRNA halves, tiRs) and shorter tRFs. Generally, expression levels for microRNAs are higher than that of tRFs (Figure 3B, one-sided Kolmogorov-Smirnov test, p = 1E-5). The most abundant microRNAs detected by TGIRT-seq include miR-21-5p, let-7-5p, miR-200b-3p, miR-148a-3p and miR-143-3p (each more than 10,000 reads per million). When compared with these highly abundant microRNAs, specific tRFs are also expressed at high levels, including 5′ halves/fragments from $tRNA^{Gly}$, $tRNA^{Glu}$, $tRNA^{Lys}$, $tRNA^{Val}$, 3’ half from $tRNA^{Arg}$ and tRF-1 from $tRNA^{Ser}$, all of which exceed 1,000 reads per million averaged from 12 samples (Figure 3B). The abundance (1,000-10,000 RPM) of these five tRFs is comparable to that of 29 unique microRNAs (let-7b-5p, let-7e-5p, miR-100-5p, miR-101-3p, miR-103a-3p, miR-10a-5p, miR-10b-5p, miR-125a-5p, miR-126-3p, miR-148b-3p, miR-151a-3p, miR-191-5p, miR-199a-3p, miR-200a-3p, miR-200c-3p, miR-203a-3p, miR-205-5p, miR-23a-3p, miR-23b-3p, miR-25-3p, miR-26a-5p, miR-26b-5p, miR-27a-3p, miR-27b-3p, miR-30d-5p, miR-378a-3p, miR-92a-3p, miR-98-5p, miR-99b-5p).

Both 5′ and 3′ fragments have a major peak corresponding to the tRNA halves that are cleaved in the anticodon loop,

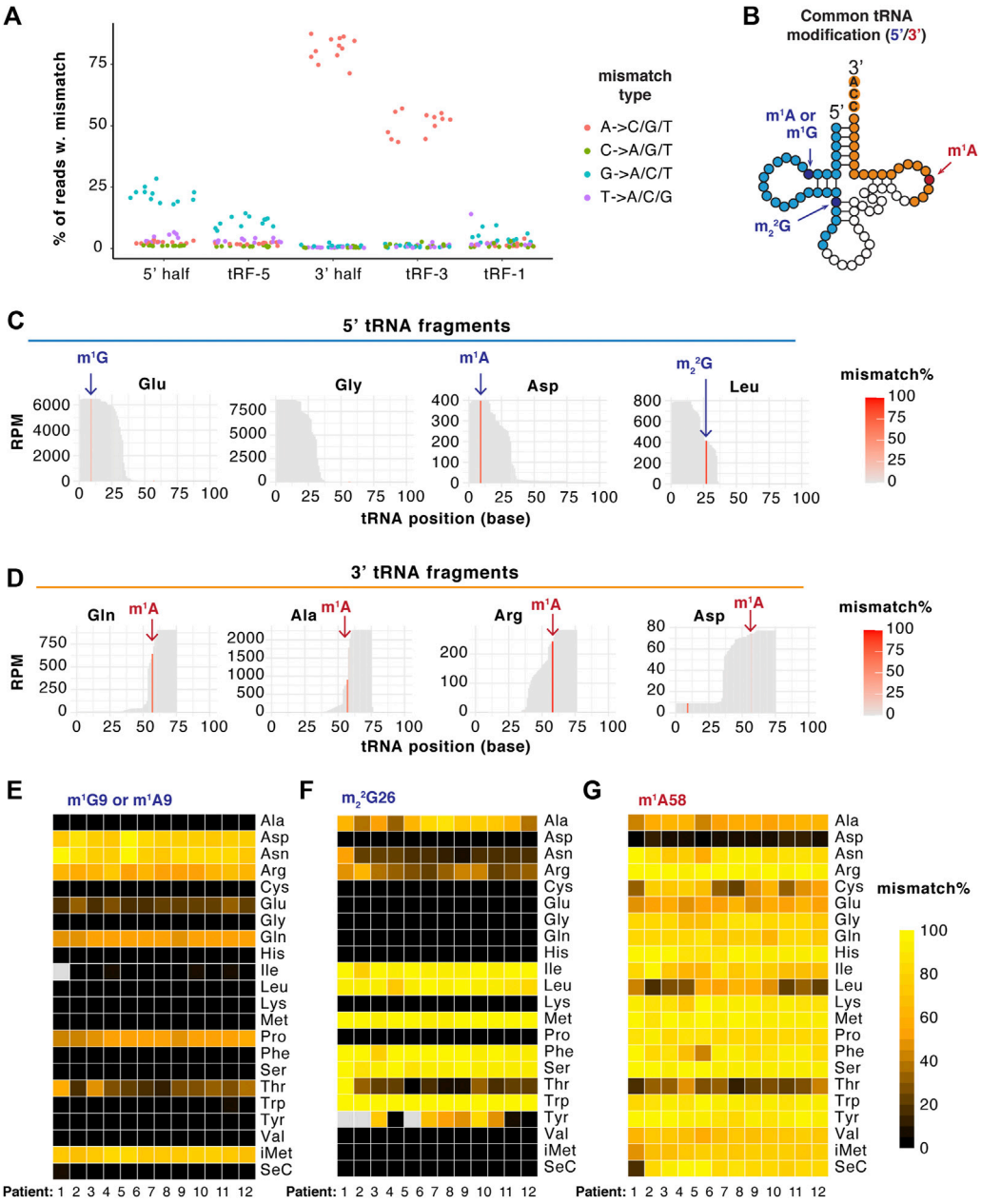

FIGURE 4
TGIRT-seq captures mismatch at specific positions corresponding to RNA modification sites. **(A)** A- and G-type mismatch is abundantly detected in tRFs by TGIRT-seq. In particular, A-type mismatch is enriched in 3′ fragments while G-type mismatch is enriched in 5′ fragments. Each dot represents one patient sample (n = 12), separated by mismatch types (by color) and tRF types (X-axis). Y axis represents the percentage of reads that contain specific type of mismatch. **(B)** Scheme of known common tRNA modifications that are detected on tRFs by TGIRT. **(C,D)** Example coverage plot of 5′ **(C)** and 3′ **(D)** tRNA fragments with mismatch positions highlighted at each position (patient #1 shown as example). **(E–G)** Heatmap of tRF mismatch index (percentage) at specific positions representing m^1G/A9 **(E)**, m_2^2G26 **(F)** and m^1A58 **(G)**. All tRF reads are combined and clustered on the length of parental tRNAs. Each column represents one tumor sample (n = 12). Grey squares represent no read coverage at that site.

with other minor peaks representing shorter isoforms (average from 12 samples shown in Figure 3C, individual patient samples shown in Supplementary Figure S3). 5′ fragments have dominant size of 32–34 nt (5′ halves), 27 nt (tRF-5c) and 19 nt (tRF-5a). 3′ fragments have dominant size of 37–38 nt (3’ halves), 22 nt (tRF-3b) and 18 nt (tRF-3a). tRF-1s are generally shorter than 25 nt with a major peak at 20 nt (Figure 3C). Again, the size distribution pattern is

overall consistent among 12 samples (Supplementary Figure 3).

tRF reads are derived from different tRNA genes (Figure 3D). tRF-1 expression shows the lowest correlation with the other tRF types, with the highest tRF-1 expression from tRNA-Ser-TGA (tRF-1001). The most abundant fragments are tiR-5, tRF-5 and tiR-3 from tRNA-Glu-C/TTC and tRNA-Gly-C/GCC. tRF-3s have highest expression from $tRNA^{Gln}$, $tRNA^{Leu}$ and $tRNA^{Ala}$.

TGIRT-seq captures mismatch at specific positions corresponding to RNA m^1G, m_2^2G and m^1A modification sites

Allowing one nucleotide mismatch increased tRF mapping (Supplementary Figure S1), suggesting tRFs likely bear mismatch-inducing RNA modifications. We checked what type of mismatch was captured in the TGIRT library and found around 15% of tRF reads contain A- > C/G/T mismatch and 15% contain G- > A/C/T mismatch, both of which are much higher than the percentage seen in microRNA reads (Supplementary Figure S4). This is consistent with the fact that tRNAs bear an array of RNA modifications, including modified adenosines and guanosines (Clark et al., 2016; Behrens et al., 2021). Specifically, the G-type mismatch mainly happens on the 5′ fragments, whereas the A-type mismatch is strongly enriched in 3′ fragments (Figure 4A). Common guanosine or adenosine modification on tRNAs (Figure 4B) include m^1G, m^2G and m_2^2G on the 5' half of tRNA or anticodon loop, and m^1A on the T-loop or on the ninth position of specific tRNAs. The presence and relative abundance of these modifications on tRFs have not been extensively investigated, especially in bladder cancer.

High mismatch rate was detected by TGIRT-seq at specific positions on specific tRFs (patient #1 shown as example in Figures 4C,D). For example, G-type mismatch was detected at the ninth position on the highly abundant 5′ fragment from $tRNA^{Glu}$ (Figure 4C), consistent with the known m^1G site on the parental tRNAs. Interestingly, another highly abundant 5' fragment, from $tRNA^{Gly}$, does not have high mismatch rate detected, despite having guanosine at its ninth position. Across 12 tumor samples, the mismatch pattern at ninth position (Figure 4E) corresponds very well with previous measurements of mismatch on mature tRNAs: high mismatch rate on tRF^{Asn}, tRF^{Arg}, tRF^{Gln}, tRF^{Pro} and tRF^{iMet}, moderate mismatch rate on tRF^{Glu} and tRF^{Thr}.

A-type mismatch at the ninth position was also detected on tRF^{Asp} (Figure 4C), corresponding to the reported m^1A modification on $tRNA^{Asp}$. Similarly, we detected G-type mismatch frequently at the 26th position on specific 5′ fragments across 12 samples (Figure 4F): high mismatch rate on tRF^{Ile}, tRF^{Leu}, tRF^{Met}, tRF^{Phe}, tRF^{Ser} and tRF^{Trp}, moderate mismatch rate on tRF^{Ala}, tRF^{Asn}, tRF^{Arg} and tRF^{Tyr}. Lastly, TGIRT detects overall high mismatch rate at m^1A58 position on 3' tRNA fragments across 12 samples with slightly lower rate on tRF^{Ala}, tRF^{Cys}, tRF^{Glu}, tRF^{Leu} and tRF^{Thr} (Figure 4G) and very low mismatch on tRF^{Asp} (Figures 4D, G). Overall TGIRT-seq captures mismatch at specific positions on tRFs, with a mismatch pattern similar to that expected from the mismatch pattern of the corresponding tRNAs. This suggests modifications like m^1G, m_2^2G and m^1A are highly prevalent on tRFs.

TGIRT-seq detects abundant rRFs with overall low mismatch rate but high mismatch at specific positions

Another group of abundant nmsRNAs is rRFs (Figure 1). The rRF reads are mapped to all four mature rRNA sequences, 18, 28, 5.8 and 5S. rRFs are highly abundant with comparable RPMs to abundant miRs or tRFs. The rRF coverage along the length of rRNAs is not evenly distributed, as would be expected if they were random degradation products, but interestingly concentrated at discrete regions (Figure 5A, patient #2 shown as an example, all 12 samples shown in Supplementary Figure S5). Consistent with the dominant peak at 39 nt of all rRFs (Figure 2C), these discrete regions show up as peaks of around 39 nt at various sites on the rRNAs (Figure 5A). The rRFs from 18S RNA have the two highest peaks at 0, 1200 bases along the length or the RNA, and this general pattern is seen across 12 patients, with new rRF source sites towards 3' end seen in patient #6 (Supplementary Figure S5). We do not know the explanation for the different pattern in individuals, but there may be interesting biological differences in the tumor accounting for the difference. Similar analysis was done for rRFs from 5.8S (Supplementary Figure S6), 5S (Supplementary Figure S7) and 28S (Supplementary Figure S8), which shows generally conserved patterns across 12 patients.

Unlike tRFs, rRFs are not associated with high mismatch reads on an overall view (Figure 5). However, mismatch is observed at specific position, for example position 1322 on fragments from 28S rRNA (Figure 5B). This position is known to bear m^1A but has not been reported on the rRFs. We were able to detect high mismatch at position 4530 of 28S rRF (Figure 5C) corresponding to known m^3U modification and position 1248 of 18S rRF (Figure 5D) corresponding to $m^1acp^3\Psi$. All these modifications are known to disrupt base pairing therefore induce mismatch during reverse transcription. We didn't observe high mismatch (>10%) at positions consistent in multiple patients from 5.8S to 5S rRFs (Supplementary Figures S6, 7). Lastly, these three rRF mismatch sites are consistently detected among 12 patients with overall very high mismatch rate (Figure 5E). This suggests specific rRFs could harbor

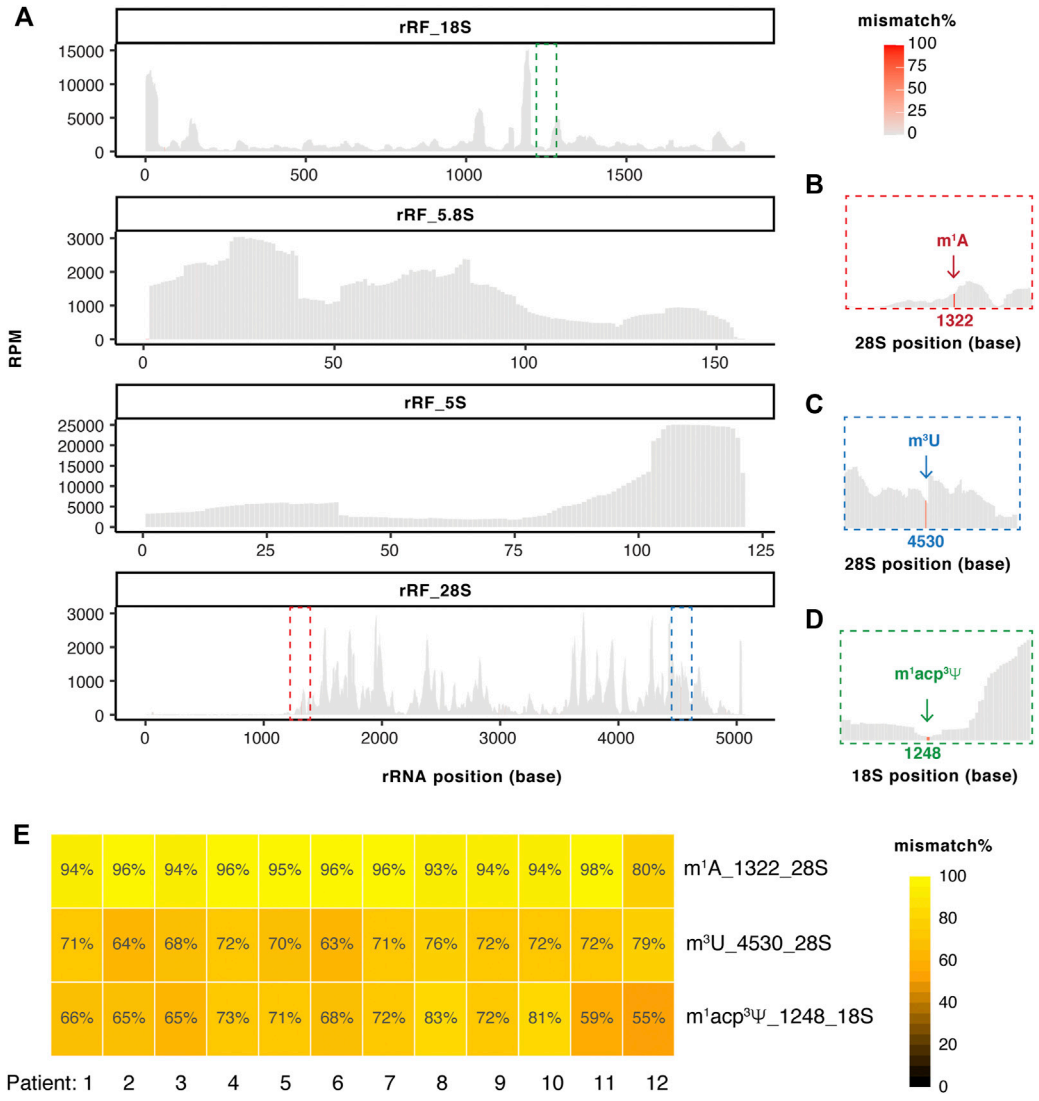

FIGURE 5
TGIRT-seq detects abundant rRFs with overall low mismatch rate and high mismatch at specific positions. **(A)** Example coverage plot of rRFs mapped on each rRNA sequences with mismatch highlighted at each position (patient #2 shown as example). Coverage plots for all 12 samples are shown in Supplementary Figures S5–8. Squared boxes are further zoomed in panel **(B)** to show high mismatch positions. **(B–D)** High mismatch at **(B)** position 1322 on 28S rRNA **(C)** position 4530 on 28SrRNA and **(D)** position 1248 on 18S rRNA are highlighted. **(E)** Patient-to-Patient variation of the mismatch% at the three high mismatch positions on rRFs **(B–D)**.

modifications from the parental rRNAs, which will require further future investigation.

Specific and abundant YRNA fragments with overall low mismatch rate

In addition to tRFs and rRFs, we also detected abundant YRNA fragments (YRF) from all four YRNAs, RNY1, RNY3, RNY4 and RNY5 (Figure 6A, patient #1 shown as an example, all 12 patient samples shown in Supplementary Figure S9). The most abundant YRF is 3′ fragment from RNY5 (~10,000 RPM), which is close to the most abundant microRNA level (Figure 3B). Interestingly, the fragmentation pattern is very specific and generates 5′ and 3′ molecules similar in length to the tRNA halves, although they are not themselves exactly half of a YRNA (Figure 6B). YRNAs share conserved secondary structure with a ~20 bp stem formed by annealing of the 5′ and 3’ ends, which is adjacent to a loop (preterminal loop) (Figure 6B). The YRF cleavage occurs at single-stranded region of YRNAs, especially within the preterminal loop of RNY1, 4 and 5 (Figure 6B). This cleavage pattern is highly consistent among 12 patient samples

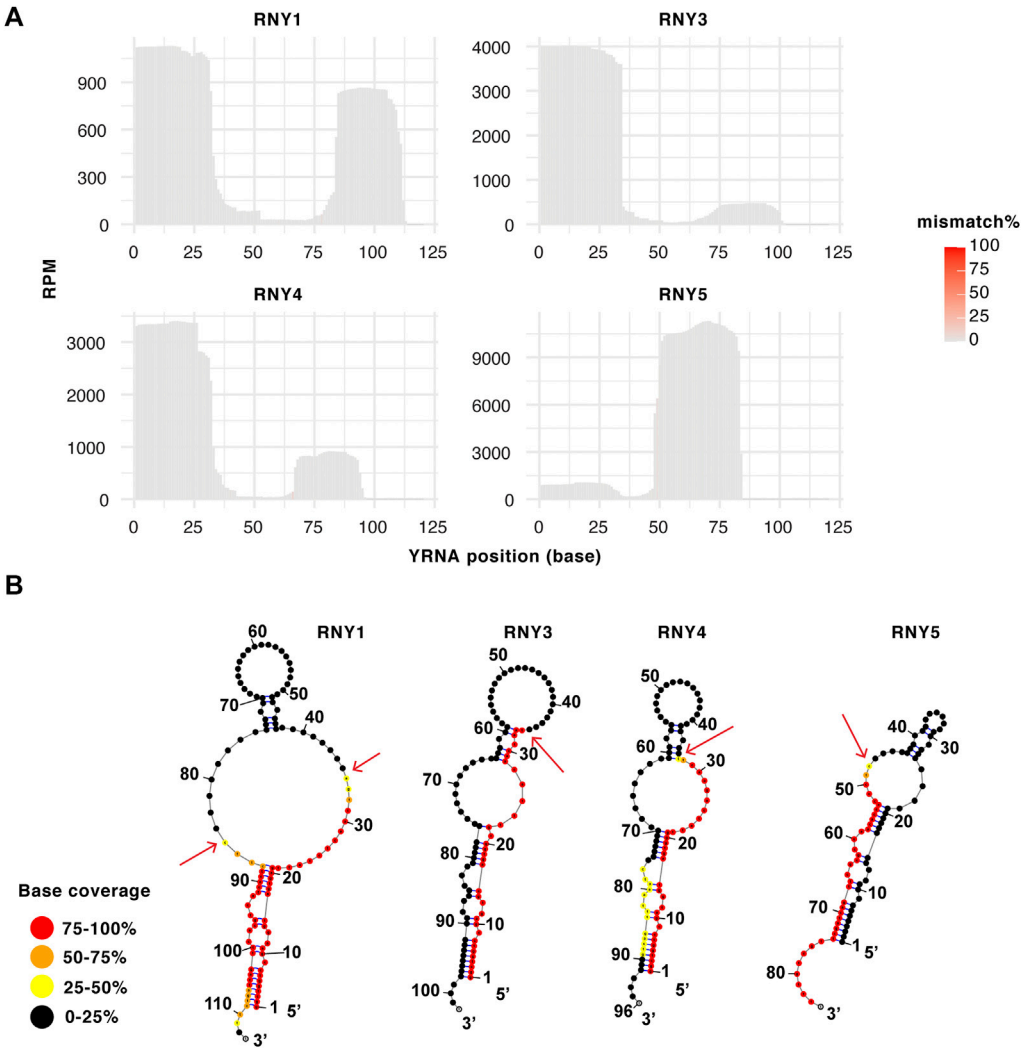

FIGURE 6
Specific Y-RNA fragments with overall low mismatch rate. **(A)** Example coverage plot of YRFs mapped on each Y-RNA sequences with mismatch highlighted at each position (patient #1 shown as example). Coverage plots for all 12 samples are shown in Supplementary Figure S9. **(B)** YRF base coverage shown with Y-RNA secondary structures. Base coverage is color coded with red showing highest coverage and black showing lowest coverage. YRF cleavage site as indicated by the coverage drop is indicated by arrow.

with some patient-to-patient variation in abundance (Supplementary Figure S9), suggesting specific cleavage. Overall, YRFs are not associated with high mismatch reads (Figure 6A).

NmsRNAs in the 18–24 base range, that may enter argonaute complexes

Given the emerging reports of tRF involvement in Argonaute-mediated gene silencing activity (Maute et al., 2013; Kuscu et al., 2018; Ren et al., 2019), it is important to determine how many and which nmsRNAs are likely to enter Argonaute and potentially affect gene expression. We used the following criteria: 1) 18–24 base long and so expected to enter Argonaute complexes, 2) consistently detected in at least 10 out of the 12 samples, 3) present at an abundance comparable to that of microRNAs. As listed in Supplementary Table S1, 12 unique nmsRNA sequences in this size range were seen at an abundance of 500–15,000 RPM, an abundance at which we see 96 unique microRNA sequences (isomiRs were not combined due to sequence variations). These include tRF-1001, tRF-3001a, tRF-5027b and tRF-5004a (3 nt shorter than annotated sequence). All have been detected in AGO PAR-CLIP (photoactivatable ribonucleoside-enhanced crosslinking and immunoprecipitation) except tRF-1001 (Kumar et al., 2014;

Kumar et al., 2015). The identities of nmsRNAs that have the potential to enter productively into Argonaute complexes by virtue of their length, and are present at an abundance comparable to that of microRNAs, is listed in Supplementary Table S1. Various rRFs have been detected associated with AGO (Guan and Grigoriev, 2021). However, the abundant rRFs that we have identified in this paper have not been reported in association with AGO, but this could either be because these rRFs are not sufficiently abundant in the cell lines where the AGO PAR-CLIP experiments were done, or because there is a mechanism that keeps these fragments away from being loaded into AGO. This analysis suggests that tRF-3001a, tRF-5027b and tRF-5004a should be studied further in BLCA for their microRNA-like activity, and the other nmsRNAs in Supplementary Table S1 may also emerge as being important for BLCA biology through mechanisms waiting to be elucidated.

Discussion

We utilized TGIRT-seq of small RNAs that were size-selected to include RNAs that are usually discarded during microRNA profiling. The results identified a large array of non-microRNA-small RNAs (nmsRNAs) and associated modifications in bladder cancer tumor samples. nmsRNAs are as abundant as the well-studied microRNAs (Figure 1). nmsRNAs display different size distribution than microRNAs of 22 nucleotides, with a significant portion with a longer length (Figure 2). General abundance, cleavage patterns and potential modification sites were reported for nmsRNAs, including tRNA-derived fragments (tRFs), rRNA-derived fragments (rRFs) and YRNA-derived fragments (YRFs) (Figures 3–6). Overall, this highlights the usefulness of TGIRT-seq to profile both abundance and RNA modifications on small RNAs from clinical samples.

Emerging evidence suggests technical biases in small RNA-seq leads to under-representation of certain RNAs. The great abundance of nmsRNAs of length greater than 22 nucleotides (Figure 2) indicates they are often excluded by the size selection that is used during microRNA profiling. Furthermore, both internal RNA modifications that interfere with reverse transcription and terminal modifications that interfere with ligation could lead to under-cloning (Shi et al., 2021). Here we utilized TGIRT, a thermostable group-II intron reverse transcriptase based on bacterial retrotransposons, that has been developed into a powerful research tool (Belfort and Lambowitz, 2019). TGIRT can mitigate the RT-stalling problem caused by certain internal modifications, but RNAs with other modifications may still be under-cloned. Newer techniques to tackle this gap in true short RNA representation are needed (Alfonzo et al., 2021).

The most abundant nmsRNAs are tRFs and rRFs (Figures 3–5), both with sequences present at similar abundance as the most abundant microRNAs (500-15,000 RPM). Diverse biological functions of tRFs have been reported in cancers (Su et al., 2020b). The highly abundant tRFs detected in BLCA samples by this study include 19-nt tRF-1001 from $tRNA^{Ser}$ (Figure 3 and Supplementary Table S1) that was initially reported in cancer cell lines and associated with cell proliferation (Lee et al., 2009). Another abundant tRF reported here is 18-nt tRF-3001a from $tRNA^{Leu}$, which has been shown to enter Argonaute complexes (Kumar et al., 2014) and is capable of repressing target gene expression in a seed sequence match manner (Kuscu et al., 2018). In addition, both 5′ and 3′ tRNA halves from $tRNA^{Glu}$, $tRNA^{Gly}$, $tRNA^{Lys}$ and $tRNA^{Val}$ appear to be very abundant in BLCA samples (Figure 3). Despite their high abundance, the functions of these tRNA halves have not been extensively studied in cancers. tRNA halves can be induced by various stress conditions but can also be detected at endogenous non-stress condition. While 5′ tRNA halves have been associated with translational repression (Ivanov et al., 2011), non-coding RNA levels and histone levels (Boskovic et al., 2020) and more recently tRNA transcription (Chen et al., 2021), much less work has been done on 3’ tRNA halves. So far, correlational studies based on tRF expression in BLCA patients suggests tRFs very likely play a role in BLCA gene regulation (Telonis et al., 2019; Papadimitriou et al., 2020), however future investigation in a refined experimental system is required to establish a direct association.

In addition to tRFs, we also detected abundant rRFs and YRFs in BLCA samples (Figures 5, 6). Biological significance and functions are still awaiting investigation for rRFs and YRFs, as recent evidence suggests they are not random degradation products. Profiling of rRFs (<34 nt) in 1000 Genome Project revealed sex- and population-dependent patterns (Cherlin et al., 2020). Furthermore, rRFs ~20 nt are identified associated with Argonaute and paired with cellular transcripts with enriched motifs that are different from microRNA rules (Guan and Grigoriev, 2021). Intriguingly, the abundant rRFs detected in this study were not identified in the Argonaute association studies. Similarly, YRFs ~31 nt could be regulated by stress and were not found associated with Ago, as recently reviewed (Guglas et al., 2020). This could be either because these nmsRNAs are not abundant in the cell lines where the association studies were performed or have been under-cloned due to RT-stalling modifications, or more intriguingly, have other Ago-independent functions. Further investigation is needed to shed light on these abundant nmsRNAs, both the Ago-compatible species and the longer species. Interestingly, relative distribution among different RNA sub-groups is quite variable from sample to sample, with some samples having higher percentage of nmsRNAs than others (Figure 1). In the future, it will be worthwhile to survey potential causes for such difference in a more systematic analysis. Such causes could be technical (sample handling or contamination) or biological (dysregulation of small RNA homeostasis or correlation with certain clinical features).

We also tested whether TGIRT-mediated mismatches identify known modification sites (m^1G, m^1A and m_2^2G) on tRFs and rRFs (Figure 4 and Figure 5). In general, the mismatch pattern on tRFs corresponds very well with the sites of modification detected previously on mature tRNAs (Clark et al., 2016; Behrens et al., 2021). The very low m^1A mismatch on tRF^{Asp} (Figures 4D,G) is consistent with the very low m^1A58 on $tRNA^{Asp}$. Similarly, the A1322 position is known to bear m^1A on large ribosomal subunit RNA across species and is catalyzed by nucleomethylin (also known as RRP8) in humans (Waku et al., 2016; Sharma et al., 2018). The U1248 position of 18S is known to be $m^1acp^3\Psi$ modified and is located within the ribosome decoding region (Meyer et al., 2011). The U4530 position of 28S is known to be m^3U modified (Tan et al., 2021). These three rRF modification sites were detected with high mismatch by TGIRT (Figure 5). Interestingly, 18S:1248 ($m^1acp^3\Psi$) was suggested to have a lower modification level based on mismatch pattern from long RNA-seq in TCGA tumors, especially READ, UCEC and COAD (Tan et al., 2021). Surprisingly, although rRNA modifications on human ribosomes have very recently been visualized by Cryo-EM (Natchiar et al., 2017), a lot of the rRNA modification enzymatic processes are not well elucidated in humans. The mismatch profile may also be used to identify unannotated modification sites in the parental RNAs in the future but will need to be verified with orthogonal methods. How could these modifications alter in disease conditions and whether they have any impact on ncRNA functions will be an interesting prospective research topic. Recently we reported m^1A impedes tRF-3 gene-silencing activity and is over-expressed in BLCA tumor, coinciding with over-expression of the writer enzyme proteins TRMT6/61A and dysregulation of the tRF-3 targetome (Su et al., 2022). In addition to bladder cancer, TRMT6/61A is also over-expressed in liver cancer and glioma. This is particularly important for cancer since disruption of many RNA modification enzymes has been linked to cancer (Janin et al., 2020; Chujo and Tomizawa, 2021).

Alterations in urinary RNA modification levels hold potential to serve as a non-invasive way to diagnose patients with BLCA and moreover as a monitoring tool to detect disease recurrence. Several studies have reported elevated levels of modified nucleosides detected in urine from BLCA patients, including m^1A (Kvist et al., 1993; Zhang et al., 2014; Sun et al., 2015). The significance of miRNA in BLCA carcinogenesis and as urine cancer biomarkers has been well studied (Yoshino et al., 2013; Hammouz et al., 2021). However, the role of nmsRNAs in BLCA pathogenesis, or as clinically relevant biomarkers, is only beginning to emerge. Interestingly, urine was one of the biofluids with the highest proportion of tRFs detected in healthy donors (Yeri et al., 2017; El-Mogy et al., 2018; Godoy et al., 2018). Both YRNAs and YRFs are recognized as biomarkers in various malignancies as reviewed (Guglas et al., 2020). They are generally downregulated in BLCA and a low expression of RNY1, 3 and 4 is associated with muscle invasiveness, lymph node metastases, advanced stage, and an unfavorable prognosis (Tolkach et al., 2017). Our observed specific YRNA cleavage pattern taken together with the previous knowledge of YRNA in BLCA suggests a potential regulatory role in the pathogenesis. Yet, whether YRNAs or YRFs are useful urine biomarkers require further investigation.

Data availability statement

The data analyzed in this study is subject to the following licenses/restrictions: The raw sequencing data for small RNA TGIRT-seq in BLCA patients are protected by European and national regulations regarding data privacy laws but will be available upon request. Requests should be directed to Rune Ougland (runoug@vestreviken.no) and will be forwarded to the Data Protection Officer and the Ethics Committee for legal- and ethical evaluation. The data will be available for 10 years after publication and if the requesting institution has implemented the European GDPR, or is able to sign the Standard Contractual Clauses for international transfers, the process will take <6 weeks. Otherwise, inter-institutional negotiation is necessary which may prolong the wait time. Meanwhile, we provide the gene counts as Supplementary Data.

Ethics statement

The studies involving human participants were reviewed and approved by the Vestre Viken Hospital Trust and The Regional Ethics Committee South-Eastern Norway Regional Health Authority. The patients/participants provided their written informed consent to participate in this study.

Author contributions

Conceptualization, ZS, RO, and AD; Methodology and Investigation, ZS and IM; Data Curation and Visualization, ZS; Resources, IM, AK, and RO; Writing, ZS, IM, RO, and AD; Funding Acquisition and Supervision, AD and RO.

Funding

The study was supported by the NIH grant AR067712 (to AD), K99 CA259526 (to ZS), and research grants from Vestre Viken Hospital Trust (25C003, to IM) and the Norwegian Cancer Society (216,115, to RO).

Conflict of interest

The authors declare that the research was conducted in the absence of any commercial or financial relationships that could be construed as a potential conflict of interest.

Publisher's note

All claims expressed in this article are solely those of the authors and do not necessarily represent those of their affiliated organizations, or those of the publisher, the editors and the reviewers. Any product that may be evaluated in this article, or claim that may be made by its manufacturer, is not guaranteed or endorsed by the publisher.

Acknowledgments

We appreciate the invaluable help provided by the clinicians at the Vestre Viken Hospital Trust in enrollment of patients and harvesting surgical specimens. The study was supported by the NIH grant AR067712 (to A.D.), K99 CA259526 (to Z.S.), and research grants from Vestre Viken Hospital Trust (25C003, to I.M.) and the Norwegian Cancer Society (216115, to R.O.).

Supplementary material

The Supplementary Material for this article can be found online at: https://www.frontiersin.org/articles/10.3389/fmolb.2022.887686/full#supplementary-material

References

Alfonzo, J. D., Brown, J. A., Byers, P. H., Cheung, V. G., Maraia, R. J., and Ross, R. L. (2021). A call for direct sequencing of full-length RNAs to identify all modifications. *Nat. Genet.* 53 (8), 1113–1116. doi:10.1038/s41588-021-00903-1

Armstrong, D. A., Green, B. B., Seigne, J. D., Schned, A. R., and Marsit, C. J. (2015). MicroRNA molecular profiling from matched tumor and bio-fluids in bladder cancer. *Mol. Cancer* 14, 194. doi:10.1186/s12943-015-0466-2

Behrens, A., Rodschinka, G., and Nedialkova, D. D. (2021). High-resolution quantitative profiling of tRNA abundance and modification status in eukaryotes by mim-tRNAseq. *Mol. Cell.* 81 (8), 1802–1815. doi:10.1016/j.molcel.2021.01.028

Belfort, M., and Lambowitz, A. M. (2019). Group II intron RNPs and reverse transcriptases: from retroelements to research tools. *Cold Spring Harb. Perspect. Biol.* 11 (4), a032375. doi:10.1101/cshperspect.a032375

Boegemann, M., and Krabbe, L.-M. (2020). Prognostic implications of immunohistochemical biomarkers in non-muscle-invasive blad cancer and muscle-invasive bladder cancer. *Mrmc* 20 (12), 1133–1152. doi:10.2174/1389557516666160512151202

Borkowska, E. M., Konecki, T., Pietrusiński, M., Borowiec, M., and Jabłonowski, Z. (2019). MicroRNAs which can prognosticate aggressiveness of bladder cancer. *Cancers* 11 (10), 1551. doi:10.3390/cancers11101551

Boskovic, A., Bing, X. Y., Kaymak, E., and Rando, O. J. (2020). Control of noncoding RNA production and histone levels by a 5′ tRNA fragment. *Genes Dev.* 34 (1-2), 118–131. doi:10.1101/gad.332783.119

Bray, F., Ferlay, J., Soerjomataram, I., Siegel, R. L., Torre, L. A., and Jemal, A. (2018). Global cancer statistics 2018: GLOBOCAN estimates of incidence and mortality worldwide for 36 cancers in 185 countries. *CA A Cancer J. Clin.* 68 (6), 394–424. doi:10.3322/caac.21492

Burger, M., Catto, J. W. F., Dalbagni, G., Grossman, H. B., Herr, H., Karakiewicz, P., et al. (2013). Epidemiology and risk factors of urothelial bladder cancer. *Eur. Urol.* 63 (2), 234–241. doi:10.1016/j.eururo.2012.07.033

Cancer Genome Atlas Research (2014). Comprehensive molecular characterization of urothelial bladder carcinoma. *Nature* 507 (7492), 315–322. doi:10.1038/nature12965

Chan, P. P., and Lowe, T. M. (2016). GtRNAdb 2.0: an expanded database of transfer RNA genes identified in complete and draft genomes. *Nucleic Acids Res.* 44 (D1), D184–D189. doi:10.1093/nar/gkv1309

Chen, L., Xu, W., Liu, K., Jiang, Z., Han, Y., Jin, H., et al. (2021). 5′ Half of specific tRNAs feeds back to promote corresponding tRNA gene transcription in vertebrate embryos. *Sci. Adv.* 7 (47), eabh0494. doi:10.1126/sciadv.abh0494

Cherlin, T., Magee, R., Jing, Y., Pliatsika, V., Loher, P., and Rigoutsos, I. (2020). Ribosomal RNA fragmentation into short RNAs (rRFs) is modulated in a sex- and population of origin-specific manner. *BMC Biol.* 18 (1), 38. doi:10.1186/s12915-020-0763-0

Chujo, T., and Tomizawa, K. (2021). Human transfer RNA modopathies: diseases caused by aberrations in transfer RNA modifications. *FEBS J.* 288 (24), 7096–7122. doi:10.1111/febs.15736

Clark, W. C., Evans, M. E., Dominissini, D., Zheng, G., and Pan, T. (2016). tRNA base methylation identification and quantification via high-throughput sequencing. *RNA* 22 (11), 1771–1784. doi:10.1261/rna.056531.116

El-Mogy, M., Lam, B., Haj-Ahmad, T. A., McGowan, S., Yu, D., Nosal, L., et al. (2018). Diversity and signature of small RNA in different bodily fluids using next generation sequencing. *BMC Genomics* 19 (1), 408. doi:10.1186/s12864-018-4785-8

Fang, Z., Dai, W., Wang, X., Chen, W., Shen, C., Ye, G., et al. (2016). Circulating miR-205: a promising biomarker for the detection and prognosis evaluation of bladder cancer. *Tumor Biol.* 37 (6), 8075–8082. doi:10.1007/s13277-015-4698-y

Gebert, D., Hewel, C., and Rosenkranz, D. (2017). Unitas: the universal tool for annotation of small RNAs. *BMC Genomics* 18 (1), 644. doi:10.1186/s12864-017-4031-9

Godoy, P. M., Bhakta, N. R., Barczak, A. J., Cakmak, H., Fisher, S., MacKenzie, T. C., et al. (2018). Large differences in small RNA composition between human biofluids. *Cell. Rep.* 25 (5), 1346–1358. doi:10.1016/j.celrep.2018.10.014

Guan, L., and Grigoriev, A. (2021). Computational meta-analysis of ribosomal RNA fragments: Potential targets and interaction mechanisms. *Nucleic Acids Res.* 49 (7), 4085–4103. doi:10.1093/nar/gkab190

Guglas, K., Kołodziejczak, I., Kolenda, T., Kopczyńska, M., Teresiak, A., Sobocińska, J., et al. (2020). YRNAs and YRNA-derived fragments as new players in cancer research and their potential role in diagnostics. *Ijms* 21 (16), 5682. doi:10.3390/ijms21165682

Hammouz, R. Y., Kołat, D., Kałuzińska, Ż., Płuciennik, E., and Bednarek, A. K. (2021). MicroRNAs: their role in metastasis, angiogenesis, and the potential for biomarker utility in bladder carcinomas. *Cancers* 13 (4), 891. doi:10.3390/cancers13040891

Ivanov, P., Villen, J., Gygi, S. P., Anderson, P., and Anderson, P. (2011). Angiogenin-induced tRNA fragments inhibit translation initiation. *Mol. Cell.* 43 (4), 613–623. doi:10.1016/j.molcel.2011.06.022

James, A. C., and Gore, J. L. (2013). The costs of non-muscle invasive bladder cancer. *Urologic Clin. N. Am.* 40 (2), 261–269. doi:10.1016/j.ucl.2013.01.004

Janin, M., Coll-SanMartin, L., and Esteller, M. (2020). Disruption of the RNA modifications that target the ribosome translation machinery in human cancer. *Mol. Cancer* 19 (1), 70. doi:10.1186/s12943-020-01192-8

Jiang, H., and Wong, W. H. (2008). SeqMap: mapping massive amount of oligonucleotides to the genome. *Bioinformatics* 24 (20), 2395–2396. doi:10.1093/bioinformatics/btn429

Kirkali, Z., Chan, T., Manoharan, M., Algaba, F., Busch, C., Cheng, L., et al. (2005). Bladder cancer: epidemiology, staging and grading, and diagnosis. *Urology* 66 (6 Suppl. 1), 4–34. doi:10.1016/j.urology.2005.07.062

Kozomara, A., Birgaoanu, M., and Griffiths-Jones, S. (2019). miRBase: from microRNA sequences to function. *Nucleic Acids Res.* 47 (D1), D155–D162. doi:10.1093/nar/gky1141

Kumar, P., Anaya, J., Mudunuri, S. B., and Dutta, A. (2014). Meta-analysis of tRNA derived RNA fragments reveals that they are evolutionarily conserved and

associate with AGO proteins to recognize specific RNA targets. *BMC Biol.* 12, 78. doi:10.1186/s12915-014-0078-0

Kumar, P., Mudunuri, S. B., Anaya, J., and Dutta, A. (2015). tRFdb: a database for transfer RNA fragments. *Nucleic Acids Res.* 43, D141–D145. doi:10.1093/nar/gku1138

Kuscu, C., Kumar, P., Kiran, M., Su, Z., Malik, A., and Dutta, A. (2018). tRNA fragments (tRFs) guide Ago to regulate gene expression post-transcriptionally in a Dicer-independent manner. *RNA* 24 (8), 1093–1105. doi:10.1261/rna.066126.118

Kvist, E., Sjølin, K.-E., Iversen, J., and Nyholm, K. (1993). Urinary excretion patterns of pseudouridine and β-aminoisobutyric acid in patients with tumours of the urinary bladder. *Scand. J. Urology Nephrol.* 27 (1), 45–53. doi:10.3109/00365599309180413

Lee, J.-Y., Ryu, D.-S., Kim, W.-J., and Kim, S.-J. (2016). Aberrantly expressed microRNAs in the context of bladder tumorigenesis. *Investig. Clin. Urol.* 57 (Suppl. 1), S52–S59. doi:10.4111/icu.2016.57.S1.S52

Lee, Y. S., Shibata, Y., Malhotra, A., and Dutta, A. (2009). A novel class of small RNAs: tRNA-derived RNA fragments (tRFs). *Genes Dev.* 23 (22), 2639–2649. doi:10.1101/gad.1837609

Li, X., Chen, J., Hu, X., Huang, Y., Li, Z., Zhou, L., et al. (2011). Comparative mRNA and microRNA expression profiling of three genitourinary cancers reveals common hallmarks and cancer-specific molecular events. *PLoS One* 6 (7), e22570. doi:10.1371/journal.pone.0022570

Li, X., Peng, J., and Yi, C. (2021). The epitranscriptome of small non-coding RNAs. *Non-coding RNA Res.* 6 (4), 167–173. doi:10.1016/j.ncrna.2021.10.002

Li, X., Xiong, X., Zhang, M., Wang, K., Chen, Y., Zhou, J., et al. (2017). Base-Resolution mapping reveals distinct m^1 a methylome in nuclear- and mitochondrial-encoded transcripts. *Mol. Cell.* 68 (5), 993–1005. doi:10.1016/j.molcel.2017.10.019

Li, Y., Li, G., Guo, X., Yao, H., Wang, G., and Li, C. (2020). Non-coding RNA in bladder cancer. *Cancer Lett.* 485, 38–44. doi:10.1016/j.canlet.2020.04.023

Magee, R., and Rigoutsos, I. (2020). On the expanding roles of tRNA fragments in modulating cell behavior. *Nucleic Acids Res.* 48 (17), 9433–9448. doi:10.1093/nar/gkaa657

Martin, M. (2011). Cutadapt removes adapter sequences from high-throughput sequencing reads. *EMBnet J.* 17, 10–12. doi:10.14806/ej.17.1.200

Maute, R. L., Schneider, C., Sumazin, P., Holmes, A., Califano, A., Basso, K., et al. (2013). tRNA-derived microRNA modulates proliferation and the DNA damage response and is down-regulated in B cell lymphoma. *Proc. Natl. Acad. Sci. U.S.A.* 110 (4), 1404–1409. doi:10.1073/pnas.1206761110

Meyer, B., Wurm, J. P., Kötter, P., Leisegang, M. S., Schilling, V., Buchhaupt, M., et al. (2011). The Bowen-Conradi syndrome protein Nep1 (Emg1) has a dual role in eukaryotic ribosome biogenesis, as an essential assembly factor and in the methylation of Ψ1191 in yeast 18S rRNA. *Nucleic Acids Res.* 39 (4), 1526–1537. doi:10.1093/nar/gkq931

Morais, D. R., Reis, S. T., Viana, N., Piantino, C. B., Massoco, C., Moura, C., et al. (2014). The involvement of miR-100 in bladder urothelial carcinogenesis changing the expression levels of mRNA and proteins of genes related to cell proliferation, survival, apoptosis and chromosomal stability. *Cancer Cell. Int.* 14 (1), 119. doi:10.1186/s12935-014-0119-3

Natchiar, S. K., Myasnikov, A. G., Kratzat, H., Hazemann, I., and Klaholz, B. P. (2017). Visualization of chemical modifications in the human 80S ribosome structure. *Nature* 551 (7681), 472–477. doi:10.1038/nature24482

Papadimitriou, M.-A., Avgeris, M., Levis, P., Papasotiriou, E. C., Kotronopoulos, G., Stravodimos, K., et al. (2020). tRNA-derived fragments (tRFs) in bladder cancer: increased 5′-tRF-LysCTT results in disease early progression and patients' poor treatment outcome. *Cancers* 12 (12), 3661. doi:10.3390/cancers12123661

Ren, B., Wang, X., Duan, J., and Ma, J. (2019). Rhizobial tRNA-derived small RNAs are signal molecules regulating plant nodulation. *Science* 365 (6456), 919–922. doi:10.1126/science.aav8907

Sanli, O., Dobruch, J., Knowles, M. A., Burger, M., Alemozaffar, M., Nielsen, M. E., et al. (2017). Bladder cancer. *Nat. Rev. Dis. Prim.* 3, 17022. doi:10.1038/nrdp.2017.22

Schrier, B. P., Hollander, M. P., van Rhijn, B. W. G., Kiemeney, L. A. L. M., and Alfred Witjes, J. (2004). Prognosis of muscle-invasive bladder cancer: difference between primary and progressive tumours and implications for therapy. *Eur. Urol.* 45 (3), 292–296. doi:10.1016/j.eururo.2003.10.006

Sharma, S., Hartmann, J. D., Watzinger, P., Klepper, A., Peifer, C., Kötter, P., et al. (2018). A single N^1- methyladenosine on the large ribosomal subunit rRNA impacts locally its structure and the translation of key metabolic enzymes. *Sci. Rep.* 8 (1), 11904. doi:10.1038/s41598-018-30383-z

Shi, J., Zhang, Y., Tan, D., Zhang, X., Yan, M., Zhang, Y., et al. (2021). PANDORA-seq expands the repertoire of regulatory small RNAs by overcoming RNA modifications. *Nat. Cell. Biol.* 23 (4), 424–436. doi:10.1038/s41556-021-00652-7

Slack, F. J., and Chinnaiyan, A. M. (2019). The role of non-coding RNAs in oncology. *Cell.* 179 (5), 1033–1055. doi:10.1016/j.cell.2019.10.017

Su, Z., Frost, E. L., Lammert, C. R., Przanowska, R. K., Lukens, J. R., and Dutta, A. (2020a). tRNA-derived fragments and microRNAs in the maternal-fetal interface of a mouse maternal-immune-activation autism model. *RNA Biol.* 17 (8), 1183–1195. doi:10.1080/15476286.2020.1721047

Su, Z., Kuscu, C., Malik, A., Shibata, E., and Dutta, A. (2019). Angiogenin generates specific stress-induced tRNA halves and is not involved in tRF-3-mediated gene silencing. *J. Biol. Chem.* 294 (45), 16930–16941. doi:10.1074/jbc.RA119.009272

Su, Z., Monshaugen, I., Wilson, B., Wang, F., Klungland, A., Ougland, R., et al. (2022). TRMT6/61A-dependent base methylation of tRNA-derived fragments regulates gene-silencing activity and the unfolded protein response in bladder cancer. *Nat. Commun.* 13 (1), 2165. doi:10.1038/s41467-022-29790-8

Su, Z., Wilson, B., Kumar, P., and Dutta, A. (2020b). Noncanonical roles of tRNAs: tRNA fragments and beyond. *Annu. Rev. Genet.* 54, 47–69. doi:10.1146/annurev-genet-022620-101840

Sun, X., Wei, P., Shen, C., Yang, Y., Wang, Y., Li, Y., et al. (2015). Prognostic value of the IASLC/ATS/ERS classification and IMP3 expression in lung adenocarcinoma of Chinese cases. *Am. J. Cancer Res.* 5 (7), 2266

Tan, K.-T., Ding, L.-W., Wu, C.-S., Tenen, D. G., and Yang, H. (2021). Repurposing RNA sequencing for discovery of RNA modifications in clinical cohorts. *Sci. Adv.* 7 (32), eabd2605. doi:10.1126/sciadv.abd2605

Telonis, A. G., Loher, P., Magee, R., Pliatsika, V., Londin, E., Kirino, Y., et al. (2019). tRNA fragments show intertwining with mRNAs of specific repeat content and have links to disparities. *Cancer Res.* 79 (12), 3034–3049. doi:10.1158/0008-5472.CAN-19-0789

Tolkach, Y., Stahl, A. F., Niehoff, E.-M., Zhao, C., Kristiansen, G., Müller, S. C., et al. (2017). YRNA expression predicts survival in bladder cancer patients. *BMC Cancer* 17 (1), 749. doi:10.1186/s12885-017-3746-y

van Rhijn, B. W. G., Burger, M., Lotan, Y., Solsona, E., Stief, C. G., Sylvester, R. J., et al. (2009). Recurrence and progression of disease in non-muscle-invasive bladder cancer: from epidemiology to treatment strategy. *Eur. Urol.* 56 (3), 430–442. doi:10.1016/j.eururo.2009.06.028

Waku, T., Nakajima, Y., Yokoyama, W., Nomura, N., Kako, K., Kobayashi, A., et al. (2016). NML-mediated rRNA base methylation links ribosomal subunit formation to cell proliferation in a p53-dependent manner. *J. Cell. Sci.* 129 (12), 2382–2393. doi:10.1242/jcs.183723

Wang, H., Zhang, W., Zuo, Y., Ding, M., Ke, C., Yan, R., et al. (2015). miR-9 promotes cell proliferation and inhibits apoptosis by targeting LASS2 in bladder cancer. *Tumor Biol.* 36 (12), 9631–9640. doi:10.1007/s13277-015-3713-7

Yeri, A., Courtright, A., Reiman, R., Carlson, E., Beecroft, T., Janss, A., et al. (2017). Total extracellular small RNA profiles from plasma, saliva, and urine of healthy subjects. *Sci. Rep.* 7, 44061. doi:10.1038/srep44061

Yin, X.-H., Jin, Y.-H., Cao, Y., Wong, Y., Weng, H., Sun, C., et al. (2019). Development of a 21-miRNA signature associated with the prognosis of patients with bladder cancer. *Front. Oncol.* 9, 729. doi:10.3389/fonc.2019.00729

Yoshino, H., Seki, N., Itesako, T., Chiyomaru, T., Nakagawa, M., and Enokida, H. (2013). Aberrant expression of microRNAs in bladder cancer. *Nat. Rev. Urol.* 10 (7), 396–404. doi:10.1038/nrurol.2013.113

Yun, S. J., Jeong, P., Kim, W.-T., Kim, T. H., Lee, Y.-S., Song, P. H., et al. (2012). Cell-free microRNAs in urine as diagnostic and prognostic biomarkers of bladder cancer. *Int. J. Oncol.* 41 (5), 1871–1878. doi:10.3892/ijo.2012.1622

Zhang, X., Cozen, A. E., Liu, Y., Chen, Q., and Lowe, T. M. (2016). Small RNA modifications: integral to function and disease. *Trends Mol. Med.* 22 (12), 1025–1034. doi:10.1016/j.molmed.2016.10.009

Zhang, Y. R., Shi, L., Wu, H., Tang, D. D., Wang, S. M., Liu, H. M., et al. (2014). Urinary modified nucleosides as novel biomarkers for diagnosis and prognostic monitoring of urothelial bladder cancer. *Tumori* 100 (6), 660–666. doi:10.1700/1778.19274

frontiers | Frontiers in Molecular Biosciences

TYPE Original Research
PUBLISHED 08 September 2022
DOI 10.3389/fmolb.2022.931354

OPEN ACCESS

EDITED BY
Inhan Lee,
Other, United States

REVIEWED BY
Stokes Peebles,
Vanderbilt University Medical Center, United States
Terri J Harford,
Cleveland Clinic, United States

*CORRESPONDENCE
Antonella Casola,
ancasola@utmb.edu

SPECIALTY SECTION
This article was submitted to Molecular Diagnostics and Therapeutics, a section of the journal Frontiers in Molecular Biosciences

RECEIVED 28 April 2022
ACCEPTED 03 August 2022
PUBLISHED 08 September 2022

CITATION
Corsello T, Kudlicki AS, Liu T and Casola A (2022), Respiratory syncytial virus infection changes the piwi-interacting RNA content of airway epithelial cells.
Front. Mol. Biosci. 9:931354.
doi: 10.3389/fmolb.2022.931354

Respiratory syncytial virus infection changes the piwi-interacting RNA content of airway epithelial cells

Tiziana Corsello[1], Andrzej S Kudlicki[2,3], Tianshuang Liu[1] and Antonella Casola[1,2,4]*

[1]Department of Pediatrics, The University of Texas Medical Branch at Galveston (UTMB), Galveston, TX, United States, [2]Institute for Translational Sciences, The University of Texas Medical Branch at Galveston (UTMB), Galveston, TX, United States, [3]Department of Biochemistry and Molecular Biology, The University of Texas Medical Branch at Galveston (UTMB), Galveston, TX, United States, [4]Department of Microbiology and Immunology, The University of Texas Medical Branch at Galveston (UTMB), Galveston, TX, United States

Piwi-interacting RNAs (piRNAs) are small non-coding RNAs (sncRNAs) of about 26–32 nucleotides in length and represent the largest class of sncRNA molecules expressed in animal cells. piRNAs have been shown to play a crucial role to safeguard the genome, maintaining genome complexity and integrity, as they suppress the insertional mutations caused by transposable elements. However, there is growing evidence for the role of piRNAs in controlling gene expression in somatic cells as well. Little is known about changes in piRNA expression and possible function occurring in response to viral infections. In this study, we investigated the piRNA expression profile, using a human piRNA microarray, in human small airway epithelial (SAE) cells infected with respiratory syncytial virus (RSV), a leading cause of acute respiratory tract infections in children. We found a time-dependent increase in piRNAs differentially expressed in RSV-infected SAE cells. We validated the top piRNAs upregulated and downregulated at 24 h post-infection by RT-qPCR and identified potential targets. We then used Gene Ontology (GO) tool to predict the biological processes of the predicted targets of the most represented piRNAs in infected cells over the time course of RSV infection. We found that the most significant groups of targets of regulated piRNAs are related to cytoskeletal or Golgi organization and nucleic acid/nucleotide binding at 15 and 24 h p.i. To identify common patterns of time-dependent responses to infection, we clustered the significantly regulated expression profiles. Each of the clusters of temporal profiles have a distinct set of potential targets of the piRNAs in the cluster Understanding changes in piRNA expression in RSV-infected airway epithelial cells will increase our knowledge of the piRNA role in viral infection and might identify novel therapeutic targets for viral lung-mediated diseases.

KEYWORDS

piwi-interacting RNA, viral infection, airways, RSV, epithelial cells

Introduction

Respiratory syncytial virus (RSV) is a single-stranded RNA virus that belongs to the family of Pneumoviridae (Rima et al., 2017) and is the leading cause of acute lower respiratory tract infections in children worldwide, and it also results in severe respiratory infections in the elderly and immunocompromised patients (Shi et al., 2017; Shi et al., 2020). An effective treatment or vaccine is not currently available for RSV infection, and many molecular mechanisms regarding RSV-induced lung disease are still unknown (Mazur et al., 2015; Domachowske et al., 2021). Piwi-interacting RNAs (piRNAs) are a novel class of small non-coding RNAs (sncRNAs) which are between 26 and 32 nucleotides in length and have a 2′-O-methylated residue on their 3′ terminal base (Kirino and Mourelatos, 2007 (Fu and Wang, 2014). piRNAs can be grouped into four classes according to their origin: 1) transposon—derived piRNAs, coming from RNA transcripts of active transposable element copies; 2) piRNAs originated from the three untranslated regions (UTRs) of messenger RNAs (mRNAs); 3) non-coding RNAs derived piRNAs and 4) Caenorhabditis piRNAs found in worms with unique properties (Han and Zamore, 2014; Yang et al., 2016; Ernst et al., 2017), although their biogenesis is still not fully understood. piRNAs interact with the P-element Induced Wimpy Testis (PIWI) proteins, forming RNA-protein complexes known as piwi-interacting RNA complex (piRC). The piRC are involved in multiple cellular functions as gene regulation, chromatin modifications and transposon silencing in different organisms (Iwasaki et al., 2016; Monga and Banerjee, 2019). piRNAs were originally discovered in germ cells, maintaining the genome integrity and repressing mutations via transposable elements (Weick and Miska, 2014). Recently, they have been characterized in multiple organs and somatic cells (Zamore, 2010; Théron et al., 2014), and their unique expression profile is associated with the development of several diseases, including cancer, diabetes, cardiovascular and neurodegenerative disorders (Moyano and Stefani, 2015; Wakisaka and Imai, 2019; Wu et al., 2020; Rayford et al., 2021; Zeng et al., 2021). However, little is known about changes in piRNA expression and possible function occurring in response to viral infections. In our previous published work, we identified piRNAs among the sncRNAs present in extracellular vesicles altered by infection of airway epithelial cells with RSV (Chahar et al., 2018). In this study, we examined the changes in piRNA profile in primary small airway epithelial (SAE) cells infected with RSV, using a human piRNA microarray. We found that RSV infection of SAE cells was associated with a time-dependent increase in differentially expressed piRNAs, when compared to uninfected cells. Among the detected piRNAs, we validated six of the top ten upregulated at 24 h p. i. By RT-qPCR method. We used Gene Ontology (GO) analysis to predict the biological processes, molecular function and cell components of the most represented predicted targets of piRNAs over the three time points and we performed cluster analysis of the expression profiles. Identification of human piRNAs and their targets in airway epithelial cells will help to uncover new roles of this class of sncRNAs following viral infections, and to identify possible biomarkers and/or novel therapeutic targets for viral-mediated lung diseases.

Materials and methods

Small airway epithelial (SAE) culture and Respiratory syncytial virus infection

SAE cells (Lonza Inc., San Diego, CA), derived from terminal bronchioli of two different cadaveric donors (25- and 38-years old donors), were grown in growth medium, containing 7.5 mg/ml bovine pituitary extract (BPE), 0.5 mg/ml hydrocortisone, 0.5 μg/ml hEGF, 0.5 mg/ml epinephrine, 10 mg/ml transferrin, 5 mg/ml insulin, 0.1 μg/ml retinoic acid, 0.5 μg/ml triiodothyronine, 50 mg/ml gentamicin and 50 mg/ml bovine serum albumin. For preparation of RSV stocks, RSV Long strain was grown in Hep-2 cells and purified by centrifugation on discontinuous sucrose gradient as described previously (Ueba, 1978). SAE cells were switched to basal media (not supplements added) prior to RSV infection. At 90%–95% confluence, cell monolayers were infected with RSV at multiplicity of infection (MOI) of 3. An equivalent amount of 30% sucrose solution was added to uninfected SAE cells as a control (mock cells). Cells were collected at 6, 15 and 24 h RSV post-infection (p.i.) for the next analysis. We used two different donors and three replicates per time point.

Total RNA extraction and Piwi-interacting RNAs microarray

Total RNA was extracted using ToTALLY RNA kit from Ambion (Life Technologies). piRNA microarray analysis was performed by Go Beyond RNA Company (Arraystar Inc., Rockville, MD). RNA samples were quantified using a Nanodrop Spectrophotometer (Nanodrop Technologies) and integrity was assessed using standard denaturing agarose gel electrophoresis. The Arraystar HG19 piRNA array was designed for profiling of piRNAs in human cells. Human piRNAs were downloaded from the NCBI database and mapped to the HG19 genome sequence using UCSC Blat. DQ (accession ID) was used to search exact piRNA in the GenBank sequences, NCBI database (Wang et al., 2019). piRNAs with good match were selected, and on this array, probes of about 23,000 piRNAs were designed successfully using a duplex method. piRNA sample labeling was performed using an RNA ligase method. Briefly, 1 μg of each sample was 3′-end-labeled with Cy3 fluorescent label, using T4 RNA ligase using the following procedure: RNA in 2.0 μl of water was combined with 1.0 μl of CIP buffer and CIP (Exiqon). The mixture was incubated for 30 min (min) at 37°C, and was terminated by incubation for 5 min at 95°C. Then 3.0 μl of labeling buffer, 1.5 μl of fluorescent label (Cy3), 2.0 μl of DMSO,

2.0 µl of labeling enzyme were added into the mixture. The labeling reaction was incubated for 1 h at 16°C, and terminated by incubation for 15 min at 65°C. After stopping the labeling procedure, the Cy3-labeled samples were hybridized on the Arraystar Human piRNA Array. Hybridization was performed at 65°C for 18 h in Agilent's SureHyb Hybridization Chambers. After being washed in an ozone-free environment, the slides were fixed and scanned using the Agilent DNA Microarray Scanner.

Data analysis of the Piwi-interacting RNAs microarray

Agilent Feature Extraction software (version 11.0.1.1) was used to analyze the acquired array images. Quantile normalization and subsequent data processing were performed using the GeneSpring GX v12.1 software package (Agilent Technologies). After quantile normalization of the raw data, piRNAs with Present or Marginal calls (microarray quality control flags) for at least four out of the 24 samples (six replicates for four time points) were chosen for further data analysis. Consistency between the two groups of three replicates at each time point was confirmed by visual inspection of the corresponding scatterplot. Differentially expressed piRNAs were identified through Fold Change filtering, combined with paired *t*-test across the six replicates. The *t*-test analysis was performed on log-transformed expression values. The use of logarithmic transformation is justified based on the skewness test (mean skewness of log transformed data $k_3 = -0.3$, which signifies only moderate deviation from normal distribution). Differentially expressed piRNAs between two groups were defined through a cut-off fold ratio, and significance, equivalent to Volcano Plot filtering. The resulting data were listed as fold ratios and *p*-values.

Predicted targets of Piwi-interacting RNAs and functional analysis

Prediction of potential targets of the piRNAs was performed by combining piRNA alignments with lists of genomic features, using the bedtools package. To annotate the potential targets of the identified piRNAs, we used the genomic coordinates of the piRNAs, as available from the piRNAQuest resource, http://bicresources.jcbose.ac.in/zhumur/pirnaquest/, (Ghosh et al., 2022). We used the UCSC liftOver tool (Hinrichs et al., 2006) and BEDTools (Quinlan and Hall, 2010) to identify overlaps of piRNA sequences with genomic features, as in the piRNAdb database. We verified the implementation by comparing selected results against piRNAdb. We used Panther version 17.0 to analyze the Gene Ontology (GO) annotations and enrichments within the significant predicted target genes for the differentially active piRNAs between each two timepoints (*p* value <0.01 for differential expression). The cutoff for calling enrichments in Panther was set as FDR <0.05 for Fisher exact test. We examined the three primary GO categories: biological process, molecular function, and cell component. Relative frequencies were calculated against the entire human genome as background.

TABLE 1 Top 10 highly up- (≥2 fold) and down-regulated (≤2 fold) piRNAs by RSV 6 h p.i ($p \leq 0.01$). DQ is the accession number of piRNA in the NCBI database.

Name	Accession number	Fold change (Log2)
piR-61505	DQ595393	2.29
piR-38587	DQ600521	1.61
piR-47139	DQ579027	1.51
piR-36425	DQ598359	1.48
piR-30033	DQ569921	1.42
piR-30123	DQ570011	1.38
piR-55301	DQ588189	1.28
piR-44781	DQ576669	1.25
piR-36222	DQ598156	1.24
piR-43294	DQ575182	1.22
piR-45856	DQ577744	−2.74
piR-45855	DQ577743	−2.45
piR-45854	DQ577742	−2.29
piR-45512	DQ577400	−2.19
piR-32882	DQ582770	−2.13
piR-56993	DQ589881	−2.11
piR-31311	DQ571199	−2.08
piR-30049	DQ569937	−2.01
piR-47273	DQ579161	−2.00
piR-32318	DQ582206	−1.99

Reverse transcription quantitative PCR (RT-qPCR)

Briefly, 600 ng total RNA containing the piRNA was reversed transcribed into cDNA in 1X RT buffer, 50 nM RT primers (Table 1), 250 nM dNTPs, 0.6 U RNase Inhibitor, and 3 U M-MuLV Reverse Transcriptase in a 20 µl reaction volume. The reaction was incubated at 16°C for 30°min, 42°C for 40°min, and 85°C for 5 min 20°µl of the synthesized cDNA was diluted in 100 µL water. The 2 µl cDNA dilution was mixed with 5 µl Arraystar SYBR® Green Real-time qPCR Master Mix and 0.5 µl of 10 µM Forward and Reverse PCR primers (Table 2) in a 10 µL reaction volume. The qPCR was carried out in QuantStudio5 Real-time PCR System (Applied Biosystems) by one cycle of (95°C for 10 min) and 40 cycles of (95°C for 10°s, 60°C for 1°min, optical reading). U6 RNA was used as the housekeeping gene reference. ΔΔCt method was used to calculate the differential expression. Reverse transcription was performed using the First Strand cDNA Synthesis Kit (Arraystar). Quantitative PCR was conducted using the SYBR Green qPCR Master Mix (Arraystar), according to the manufacturer's instructions. Primer sequences are available upon request. For the viral replication quantification, RSV N

TABLE 2 Top 10 highly up- (≥4 fold) and down-regulated (≤4 fold) piRNAs by RSV 15 h p.i. ($p \leq 0.01$). DQ is the accession number of piRNA in the NCBI database.

Name	Accession number	Fold change (Log2)
piR-38587	DQ600521	8.26
piR-61505	DQ595393	7.95
piR-47139	DQ579027	7.06
piR-61160	DQ595048	6.61
piR-37886	DQ599820	5.86
piR-32372	DQ582260	5.76
piR-45936	DQ583610	5.51
piR-50722	DQ577824	5.37
piR-32201	DQ582089	5.32
piR-54651	DQ587539	4.98
piR-38945	DQ600879	−2.26
piR-56993	DQ589881	−2.17
piR-32318	DQ582206	−2.12
piR-32882	DQ582770	−2.10
piR-45856	DQ577744	−2.06
piR-37981	DQ599915	−2.03
piR-45512	DQ577400	−2.00
piR-45855	DQ577743	−1.96
piR-30049	DQ569937	−1.84
piR-46025	DQ577913	−1.77

gene was amplified using specific primers, as previously described (Li et al., 2015).

Statistical analysis

The statistical analysis of the piRNA microarray was run using the PDL:Stats and Statistics:PointEstimation modules from CPAN. Differentially expressed piRNAs were identified for every pair of timepoints (6 h versus mock, 15 h versus mock, 24 h versus mock). Fold change of the differentially expressed piRNA by microarray were calculated as linear average or Log2 average ratio. Fold change of RT-qPCR experiments was calculated by $2^{-\Delta\Delta Ct}$ method and represent mean ± SEM using GraphPad Prism v4 (GraphPad 160 Software). p value <0.05 or 0.01 was considered statistically significant.

Results

RSV infection induces changes in piRNAs profile expression

To investigate the impact of infection on the piRNA expression profile in primary airway epithelial cells, we analyzed piRNAs changes in human SAE cells infected with RSV for 6, 15 and 24 h p. i., using the Arraystar HG19 piRNA array, which probes for 23,677 different piRNAs. Total RNA from each sample was extracted and assessed for quality control. We measured viral repliation by detecting RSV N gene as shown in Supplementary Figure 1. Samples were labeled and hybridized to perform the piRNA microarray according to the company's protocol. After quantile normalization and subsequent data processing, we detected 548 (6 h p.i.), 897 (15 h p.i.) and 1,644 (24 h p.i.) differentially expressed piRNAs in RSV-infected cells compared to mock (uninfected) cells. A total of 120, 321 and 772 piRNAs were significantly upregulated at 6, 15 and 24 h p. i., respectively. Interestingly, there was a higher number of downregulated piRNAs in response to viral infection, with 428, 576 and 872 differentially expressed piRNAs at 6, 15 and 24 h p. i., respectively (Figure 1). Among the differentially expressed piRNAs, 244 were shared between the time points of 6 and 15 h p.i.; 221 between 6 and 24 h p.i. And 515 between 15 and 24 h p.i., with 157 piRNAs commonly detected over all time points, as represented in the intersecting Venn diagram (Figure 2). The top ten piRNAs upregulated and downregulated (≤2 Fold) for each time point p. i. Are shown in Table 1 (6 h), Table 2 (15 h) and Table 3 (24 h). The complete list of piRNAs whose expression in SAE cells was changed in a time-dependent manner after RSV infection is shown in Supplementary files 1, two and 3.

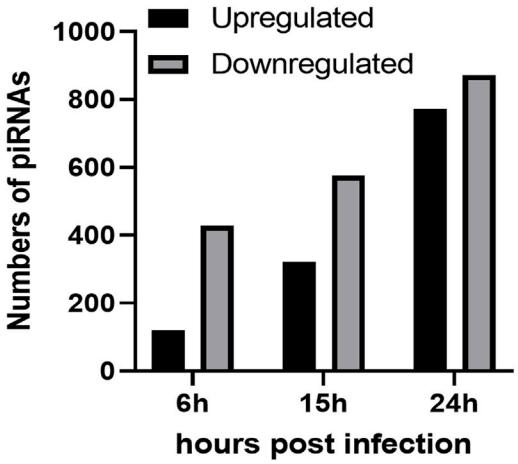

FIGURE 1
Numbers of upregulated (black bars) and downregulated (grey bars) piRNAs in RSV infected SAE cells at 6, 15 and 24 h p. i. Compared to the mock (uninfected) SAE cells. Data is representative of six replicates for each time point with $p < 0.01$.

We then validated the expression of six or eight of the top ten upregulated or downregulated piRNAs at 24 h p.i. Listed in Table 3. Total RNA was isolated from SAE mock or RSV infected cells at 24 h p.i. And subjected to RT-qPCR. We found that piR-54651 (DQ587539), piR-32372 (DQ582260)

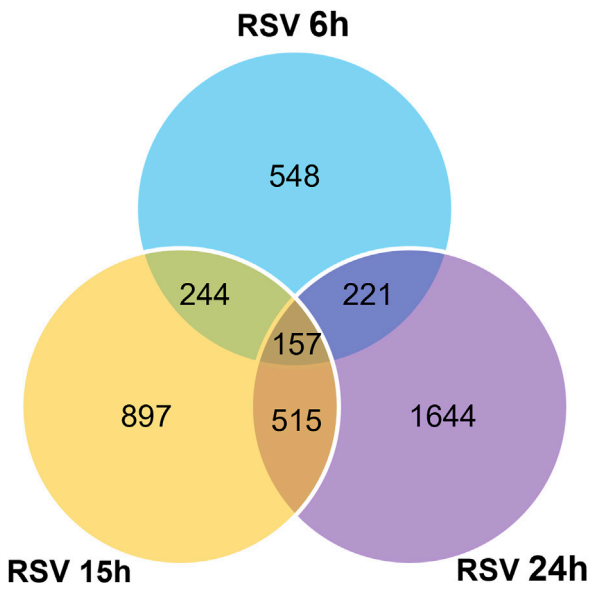

FIGURE 2
Intersecting Venn diagram showing the numbers of up- and down-regulated piRNAs differentially expressed at the three different time points (6, 15 and 24 h) RSV p. i. Compared to the mock (uninfected) SAE cells. The numbers in overlapping area(s) represent the differential regulated number of piRNAs shared among all the time points. Data is representative of six replicates for each time point with $p < 0.01$.

TABLE 3 Top 10 highly up- (≥4 fold) and down-regulated (≤4 fold) piRNAs by RSV 24 h p.i. ($p \leq 0.01$). DQ is the accession number of piRNA in the NCBI database.

Name	Accession number	Fold change (Log2)
piR-38587	DQ600521	9.97
piR-61505	DQ595393	9.41
piR-37886	DQ599820	8.67
piR-47139	DQ579027	8.57
piR-61160	DQ595048	8.24
piR-32372	DQ582260	8.03
piR-50722	DQ583610	7.33
piR-54651	DQ587539	7.26
piR-32201	DQ582089	7.08
piR-45936	DQ577824	6.92
piR-37981	DQ599915	−3.42
piR-42627	DQ574515	−2.85
piR-46025	DQ577913	−2.73
piR-30049	DQ569937	−2.72
piR-41627	DQ573515	−2.66
piR-38945	DQ600879	−2.64
piR-32318	DQ582206	−2.64
piR-53794	DQ586682	−2.51
piR-50660	DQ583548	−2.45
piR-60132	DQ594020	−2.31

and piR-61160 (DQ595048) levels increased more than threefold, and the other three piRNAs, piR-61505 (DQ595393), piR-37886 (DQ599820) and piR-50722 (DQ583610) increased one and half fold in viral-infected cells compared to mock (uninfected) cells, as shown in Figure 3A. We observed more than two fold decreased levels of piR-46025 (DQ577913) and piR-38945 (DQ600879), and the other two piRNAs, piR-41627 (DQ573515) and piR-30049 (DQ5699370) showed more than one and half fold of decreased levels in viral-infected cells compared to mock (uninfected) cells Figure 3B. In general, fold change values of piRNAs analyzed by microarray were at least two times higher than the fold change of the same piRNAs validated by RT-qPCR.

Potential targets and Gene Ontology prediction of the viral-induced up- and down-regulated piRNAs

To characterize potential targets of piRNAs identified in RSV-infected SAE cells for each time point, we combined the piRNA alignments with lists of genomic features, using the bedtools package, and verified the approach by comparing selected results against the piRNAdb database (Piuco and Galante, 2021). At the stricter threshold for piRNA regulation at $p < 0.01$, we identified a total of 629, 1,044 and 2,750 targets, including 519, 874, and 2,118 targets of down-regulated piRNAs, and 153, 245 and 886 targets of up-regulated piRNAs, all respectively at 6, 15 and 24 h p. i. With RSV. Using the inclusive approach, we found a total of 2,874, 2,341, and 6,967 potential targets of regulated piRNAs at 6, 15 and 24 h p. i. Compared to mock (uninfected cells) with a p value <0.05, respectively. Of these, 1961, 1978, and 5,778 are targets of down-regulated piRNAs, and 1,313, 568, and 2,684 are targets of up-regulated piRNAs at 6, 15 and 24 h p. i. We found that most of the piRNAs had multiple target genes and that several piRNAs shared common gene targets. Potential targets of selected upregulated piRNAs following RSV infection are listed in Table 4. Most of the predicted targets belong to the class of long noncoding RNAs (lncRNAs), including long intergenic non-coding RNAs (lincRNAs) such as LINC01297, LINC01087 and LINC01087. LincRNAs are autonomously transcribed RNAs of more than 200 nucleotides in length that do not overlap protein-coding genes (Ransohoff et al., 2018). Other identified targets of the upregulated piRNAs were the endosome protein Pleckstrin Homology Domain Containing B2 (PLEKHB2), and the cytoplasm proteins the Adaptor Related Protein Complex five Subunit Zeta 1 (AP5Z1), the Probable ATP-dependent RNA helicase (DDX4), and the Signal transducer and activator of transcription 2 (STAT2). PLEKHB2 is involved in retrograde transport of recycling endosomes.

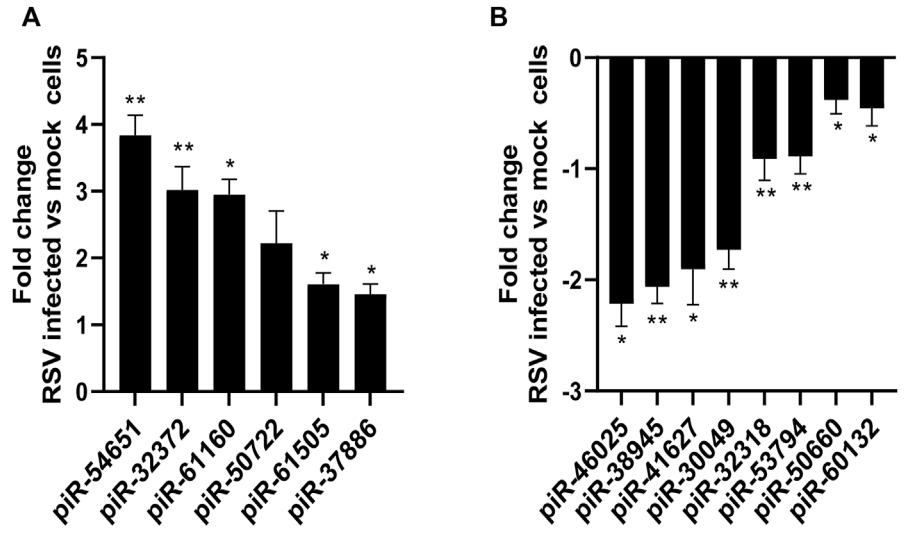

FIGURE 3
Validation of up **(A)** or down **(B)** regulated piRNAs expression in SAE cells infected with RSV at 24 h p. i. RNA extracted from SAE mock (uninfected) and RSV infected cells (24 h) was subjected to piRNAs analysis by RT-qPCR. Fold changes in piRNA expression were determined by $2^{-\Delta\Delta CT}$ method and represent mean ± SEM normalized to a small nuclear RNA, U6. * and ** indicates a statistical difference comparing RSV infected versus mock cells (*p value <0.05; **p value <0.01). Data is representative of three independent experiments.

AP5Z1 belongs to the family of Clathrin adaptor proteins, known also as adaptin proteins (APs), and participates in the processes of homologous recombination DNA double-strand break repair (HR-DSBR). DDX4, highly expressed in the ovary and testis, has been involved in the production of piRNAs in fetal male germ cells through a ping-pong amplification cycle, and in the secondary piRNAs metabolic process (Li et al., 2010). STAT2 protein is critical to the biological response of type I interferons (IFNs) with a DNA-binding transcription factor activity (Park et al., 2000). The complete lists of the potential target genes for each time point of RSV infection are presented in Supplementary files 1 (6 h p.i.), 2 (15 h p.i.) and 3 (24 h p.i.).

To characterize the prevalent functions of the predicted targets of the differentially expressed piRNAs we use the Gene Ontology (GO) functional classification (biological process, cellular component, and molecular function). We found that the most significant groups of targets of regulated piRNAs are related to cytoskeletal or Golgi organization and nucleic acid/nucleotide binding at 15 and 24 h p.i. ($p < 0.01$). A summary of the GO biological process of the predict targets of piRNAs upregulated at 24 h RSV p.i ($p < 0.05$) is listed in Table 5. The most enriched biological processes at 24 h p.i. included endosomal, intracellular and nitrogen compound transports with regulation of vesicles-mediated transport. The GO analysis also showed Golgi organelle and cytoskeleton organizations and interestingly immune response mediated by cells involved in somatic diversification process (immunological memory). Complete GO analysis of biological process, cellular component, and molecular function (BP, CC and MF) for all three time points is provided as supplementary files 4, 5 and 6 (6 h p.i.), files 7, 8 and 9 (15 h p. i.), and files 10, 11 and 12 (24 h p.i.).

Clustering of piRNA expression profiles

To identify common patterns of time-dependent responses to infection, we clustered the significantly regulated expression profiles. Specifically, we used the piRNAs with a significant change at $p < 0.01$ in at least one of the time points, p.i., compared to control. The expression profiles were converted to the log2 scale, averaged over the six replicates, and normalized to levels in uninfected cells and root mean square deviation (rmsd) was equal to 1, rmsd = 1. The preprocessed data were clustered using an in-house implementation of the Hartigan-Wong k-Means algorithm. After conducting an elbow test as shown in Figure 4, we assessed that the most informative clustering was either into three or five groups of temporal profiles. The results of the clustering into five groups are shown in Figure 5. The five basic types of behavior are early (6 h) upregulation, followed by remaining in the upregulated, or uninfected-base level (cluster 0), early downregulation, remaining downregulated (cluster 1), steady downregulation (cluster 2), steady upregulation (cluster 3), and early upregulation, followed by strong downregulation (cluster 4). The complete list of

TABLE 4 Predicted target genes of selected upregulated piRNAs during the course of RSV infection.

piRNAs	Target gene
piR-38587	FOXK1, AP5Z1
piR-54651	PLEKHB2
piR-32372	LINC01087
piR-61160 and piR-50722	ANKRD18A and RP11-146D12.2
piR-50722	FAR2P1, LINC01297
piR-49367	SUCLG1
piR-36763	RP11-20I23.6, PDPK1, AC141586.5, PDPK2P
piR-39104	CTD-2210P24.1
piR-42026	AC093627.9
piR-53025	CAND2
piR-48109	MRPL45P1
piR-54343	RP11-753D20.1
piR-57616	NBPF11 NBPF12
piR-55323	RNF219-AS1
piR-33637	PDXDC1
piR-54439	RP11-386M24.3
piR-51361	TBC1D3P4, USP6 TBC1D3P3
piR-54546	RP1-63G5.5
piR-59040	LINC00837
piR-36425	RP11-17M15.2
piR-30123	TXNRD1
piR-55301	RP11-403P17.5, TK2
piR-44781	RP11-386M24.9
piR-36222	TRIM14
piR-43294	SQSTM1, C5orf45
piR-48124	LRIG2, RLIMP2
piR-51401	NOD2
piR-40148	TRAP1
piR-57640	STAT2
piR-49095	DDX4

piRNAs for both type of clustering, three or five groups, is included in the supplementary files 13 and 14 named "clustered_list_3. xlsx, and clustered_list_5. xlsx".

Each of the clusters of temporal profiles have a distinct set of potential targets of the piRNAs in the cluster. Moreover, the targets are associated with enrichment of different functional categories that can be expressed in terms of Gene Ontology biological process enrichments. For example, the early upregulated cluster 0 is enriched with targets with a role in protein transport and localization. The targets of early downregulated piRNAs (cluster 1) are enriched in organelle organization, including Golgi, cytoplasm, and membranes, but depleted in genes coding for regulatory proteins. The piRNAs steadily upregulated (Cluster 3) have potential targets enriched in regulatory genes and inter-cellular signaling.

TABLE 5 Gene Ontology (GO), biological processes (BP) analysis for the top gene targets of piRNAs (time point, RSV 24 h p.i) with *p* values <0.01 or <0.05

Biological process (BP)	Fold enrichment
Golgi organization (GO:0007030)	3.29
activation of GTPase activity (GO:0090630)	2.94
endosomal transport (GO:0016197)	2.11
regulation of small GTPase mediated signal transduction (GO:0051056)	1.93
localization within membrane (GO:0051668)	1.84
protein localization to membrane (GO:0072657)	1.83
regulation of vesicle-mediated transport (GO:0060627)	1.69
intracellular protein transport (GO:0006886)	1.65
cytoskeleton organization (GO:0007010)	1.62
establishment of protein localization (GO:0045184)	1.59
protein transport (GO:0015031)	1.59
protein localization (GO:0008104)	1.56
cellular protein localization (GO:0034613)	1.48
cellular macromolecule localization (GO:0070727)	1.48
macromolecule localization (GO:0033036)	1.48
intracellular transport (GO:0046907)	1.46
establishment of localization in cell (GO:0051649)	1.43
nitrogen compound transport (GO:0071705)	1.43
organelle organization (GO:0006996)	1.42
cellular localization (GO:0051641)	1.39
organic substance transport (GO:0071702)	1.35
cellular component assembly (GO:0022607)	1.29
transport (GO:0006810)	1.28
establishment of localization (GO:0051234)	1.27
cellular component organization (GO:0016043)	1.26
regulation of signaling (GO:0023051)	1.25
cellular component organization or biogenesis (GO:0071840)	1.25
regulation of cell communication (GO:0010646)	1.24
localization (GO:0051179)	1.24
regulation of biological quality (GO:0065008)	1.24
cellular process (GO:0009987)	1.07
biological process (GO:0008150)	1.05
Unclassified (UNCLASSIFIED)	0.71
immune response (GO:0006955)	0.67
G protein-coupled receptor signaling pathway (GO:0007186)	0.5
adaptive immune response (GO:0002250)	0.4

The full lists of the significantly enriched/depleted GO biological process categories for the five clusters are included in the supplementary file 15. We analyzed if specific clusters shown in Figure 5 correlate with subsets of GO categories. The overlaps, for GO BP categories significant at *p* value <0.01 are listed in Table 6. We found that the early (cluster 0) and the steadily upregulated (cluster 3) piRNAs, for

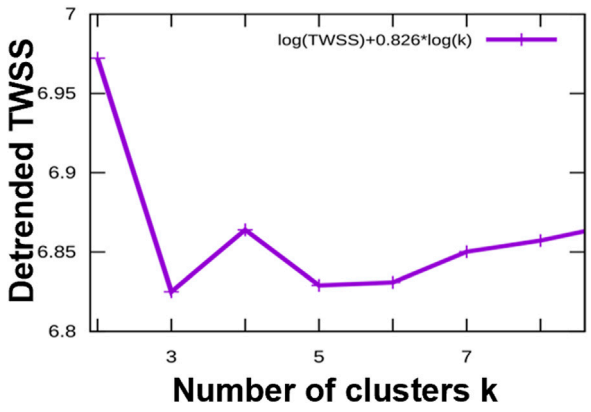

FIGURE 4
The elbow test indicates that the most informative representations of the categories of temporal profiles of the differentially regulated piRNAs are classifications into three clusters or into five clusters. *X*-axis: number of clusters, *Y*-axis: detrended (residual) *Total Within Sum of Squares*, a measure of structure unexplained by the clustering.

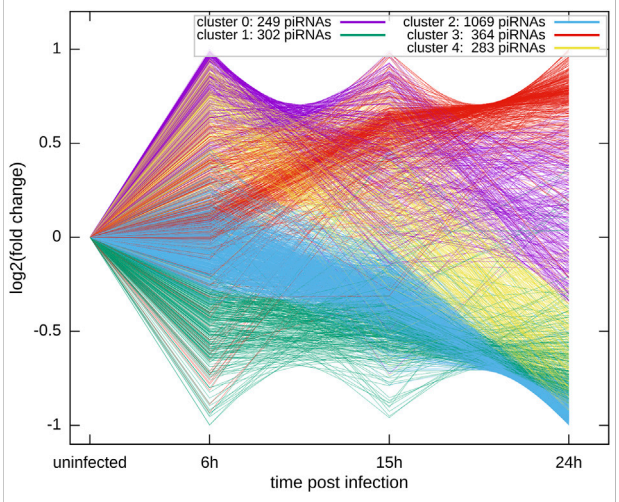

FIGURE 5
The k-means clustering of the temporal profiles of *X*-axis: time post-infection with RSV (cluster zero represents uninfected cells). *Y*-axis: normalized expression profile, averaged over the replicates, and shown in the $\log_2$ scale.

example, were linked to GO subcategories regulating the mediated signal transduction of small GTPase, typically involved in the viral immune response. Many cellular functions such as protein transport, intracellular or membrane protein localization, etc. GO subsets were highly associated with targets of piRNAs from the steady downregulated level (cluster 2), which was also associated with adaptive immune response subset. The piRNA targets from the steadily downregulated or upregulated clusters (2 and three respectively) were interestingly connected to GO subcategories involved in the regulation of cellular signaling or biological quality.

Discussion

The present study is the first to report changes in piRNAs expression in response to RSV infection of human primary airway epithelial cells. piRNAs are the largest class of sncRNA molecules expressed in animal cells and they can be derived from multiple sources, including transposons, mRNAs, and ncRNAs, such as lncRNAs, snoRNAs and tRFs. Among these piRNAs, only the function of transposon-derived piRNAs in gonadal cells has been relatively well studied (Weick and Miska, 2014). piRNAs have been shown to play a crucial role to safeguard genome, maintaining the genome complexity and integrity, as they suppress the insertional mutations caused by transposable elements, however, there is growing evidence of their role in controlling gene expression in somatic cells as well. The biogenesis and function of piRNAs is associated with three different proteins, namely PIWI, Argonaute-3 (AGO3), and Aubergine (AUB). PIWI proteins are found both in somatic cells and germ cells, while AGO3 and AUB are observed primarily in germ cells. Precursors of piRNAs are exported from the nucleus into the cytoplasm to be further processed into smaller sequences and reach their partners to form piRNA-PIWI complexes. These complexes can migrate back to the nucleus to block the transcription of target genes. There are several mechanisms underlying piRNA-mediated gene regulation. The better characterized one relates to epigenetic changes, including DNA methylation and histone modifications, whereas piRNA–PIWI complex can bind to the promoter region of a gene and favors recruitment of methylation factors, enabling transcriptional silencing. Some examples of this mode of gene regulation in somatic cells are the silencing of killer immunoglobulin-like receptor, the immune receptor CD1A and the antioxidant enzyme glutathione-S-transferase (Zhang et al., 2016; Zhang et al., 2020). In addition, piRNAs can also regulate gene expression at the post-transcriptional level, as in the case of piRNA-30840 which binds to IL-4 pre-mRNA, leading to its degradation (Zhong et al., 2015), and piR-FTH1, a piRNA found in breast cancer cells, which downregulates ferritin heavy chain mRNA (Balaratnam et al., 2018). One last mechanism by which piRNAs regulate gene expression has been recently identified and it related to the interaction with the cellular RNA methylation machinery, leading to changes in mRNA m6A methylation, a post-transcriptional

TABLE 6 Correlation of Gene Ontology (GO) biological processes (BP) subset categories with the clustering of the temporal profiles of *X*-axis.

Overlaps of GO BP categories at 6 h RSV p.i		
GO:0007030	clusters: 1 2 4	Golgi organization
GO:0010256	clusters: 1 2 4	endomembrane system organization
GO:0006996	clusters: 1 2	organelle organization
Overlaps of GO BP categories at 15 h RSV p.i		
GO:0007030	clusters: 1 2 4	Golgi organization
GO:0007186	clusters: 1 2	G protein-coupled receptor signaling pathway
Overlaps of GO BP categories at 24 h RSV p.i		
GO:0007030	clusters: 1 2 4	Golgi organization
GO:0090630	clusters: 2 4	activation of GTPase activity
GO:0016197	cluster: 2	endosomal transport
GO:0051056	clusters: 0 3	regulation of small GTPase mediated signal transduction
GO:0051668	clusters: 0 2	localization within membrane
GO:0072657	clusters: 0 2	protein localization to membrane
GO:0060627	clusters: 0 2	regulation of vesicle-mediated transport
GO:0006886	clusters: 0 2	intracellular protein transport
GO:0007010	clusters: 2	cytoskeleton organization
GO:0045184	clusters: 0 2	establishment of protein localization
GO:0015031	clusters: 0 2	protein transport
GO:0008104	clusters: 0 2	protein localization
GO:0034613	clusters: 0 2	cellular protein localization
GO:0070727	clusters: 0 2	cellular macromolecule localization
GO:0033036	clusters: 0 2	macromolecule localization
GO:0046907	clusters: 0 2	intracellular transport
GO:0051649	clusters: 0 2	establishment of localization in cell
GO:0071705	clusters: 0 2	nitrogen compound transport
GO:0006996	clusters: 1 2	organelle organization
GO:0051641	clusters: 0 2	cellular localization
GO:0071702	clusters: 0 2	organic substance transport
GO:0022607	clusters: 0 2	cellular component assembly
GO:0006810	cluster: 2	transport
GO:0051234	cluster: 2	establishment of localization
GO:0016043	cluster: 2	cellular component organization
GO:0023051	clusters: 2 3	regulation of signaling
GO:0071840	cluster: 2	cellular component organization or biogenesis
GO:0010646	clusters: 2 3	regulation of cell communication
GO:0051179	cluster: 2	localization
GO:0065008	clusters: 2 3	regulation of biological quality
GO:0009987	cluster: 2	cellular process
GO:0008150	cluster: 2	BP
GO:0006955	clusters: 2 4	immune response
GO:0007186	clusters: 1 2	G protein-coupled receptor signaling pathway
GO:0002250	cluster: 2	adaptive immune response
GO:0050906	cluster: 2	detection of stimulus involved in sensory perception
GO:0009593	clusters: 1 2	detection of chemical stimulus
GO:0007606	cluster: 2	sensory perception of chemical stimulus
GO:0007608	cluster: 2	sensory perception of smell
GO:0050907	cluster: 2	detection of chemical stimulus involved in sensory perception
GO:0050911	cluster: 2	detection of chemical stimulus involved in sensory perception of smell

modification of mRNAs in mammals that plays a fundamental role in RNA stability and translation (Gao et al., 2020).

Although the role of piRNAs was initially confined to gonad development, recent studies have identified specific expression profile of piRNAs from multiple organs and cell types. Currently, piRNA-disease association data are available for several diseases, including various types of cancers, cardiovascular diseases, autoimmune and neurodegenerative disorders (Muhammad et al., 2019). Surprisingly, almost nothing is known regarding piRNA generation/function and PIWI proteins in the context of viral infections. In our recent published study, analysis of RNA content of exosomes isolated from RSV-infected airway epithelial cells identified piRNAs as an important component of the exosomal cargo (Chahar et al., 2018) Next-generation sequencing analysis revealed that 52 piRNAs were commonly present in both mock and RSV exosomes, with 28 upregulated and 24 downregulated piRNAs in RSV exosomes, with 3 and 19 piRNAs that uniquely present in mock and RSV exosomes, suggesting a biological function for this class of sncRNAs during infection. In the current study, we show for the first time that RSV infection can lead to significant changes in piRNAs in infected SAE cells in a time-dependent manner. Our piRNA microarray analysis revealed an enrichment in numbers of up- and down-regulated piRNAs in airway epithelial cells upon RSV infection compared to mock cells, with the highest numbers of differentially expressed piRNAs detected at 24 h p. i. With RSV. Significant changes in the expression profiles of piRNAs was recently reported for Coxsackievirus B3 (CVB3) infection in human HeLa cells using high-throughput sequencing. Similar to RSV, CVB3 infection was associated with time-dependent changes in piRNAs numbers, although the highest number of differentially expressed piRNAs was observed at the early time points post-infection (Yao et al., 2020). In an animal model of ducks infected with avian influenza virus, piRNAs represented the highest class of sncRNAs expressed after infection compared to other snRNA classes, such as microRNAs (miRNAs) and small nucleolar RNAs (snoRNAs) (Samir et al., 2020). There were major organ-specific differences in sncRNA populations at baseline and substantial reprogramming of all sncRNA classes throughout infection.

Target prediction analysis suggested that piR-38587 could possibly target AP5Z1, the adaptin proteins 5 (AP5). Very little is known on AP5 because it is the most recently identified adaptin complex. Although AP5 has not been investigated in the context of viral infection, AP2, another type of AP complex has been shown to function as a target of ocular infection upon human adenovirus species D type 37 (HAdV-D37) infection (Lee et al., 2020) or be involved in the entry process of human enterovirus 71 (HEV71) (Hussain et al., 2011). Similarly, piR-4095 target includes DDX4 which is an RNA helicases enzyme. Different DDX enzymes, as DDX1, DDX3X, and DDX5, have been known to play important roles in the replication cycle of coronaviruses (Taschuk and Cherry, 2020). piR-57640 could target STAT2 which is involved in RSV infection. It is known that RSV is a potent inducer of type I interferon release from infected airway epithelial cells (Garofalo et al., 1996), and the virus specifically downregulates human STAT2 protein expression, thus enabling RSV to evade the host type I interferon response (Elliott et al., 2007). The Gene Ontology functional classification found that the most significant groups of targets of regulated piRNAs are related to long noncoding RNA, DNA- and protein-binding, transcriptional and post-transcriptional regulation.

Although piRNA function in response to an infection in mammalian cells has not been explored yet, murine neural stem cells (NSCs) were recently shown to release piRNA-containing exosomes/microvesicles with antiviral immunity (Ikhlas et al., 2022). When NSCs were exposed to RNA fragments of SARSCoV-2 genome, the derived extracellular vesicles displayed enhanced antiviral activity. The increased antiviral effect of these vesicles was associated with increased expression of piRNA species some of which were predicted to target SARS-CoV-2 genome. Knockout of piRNA-interacting protein PIWIL2 in NSCs led to a reduction in the induced antiviral effect, suggesting that the PIWI-piRNA system is important for these antiviral actions (Ikhlas et al., 2022). A recent study of bacterial pneumonia using a knockout mouse for MIWI2, the mouse homologue of human PIWIL4, revealed an important role of this piwi protein in lung innate immune response. MIWI2 was expressed by a subpopulation of multiciliated airway epithelial cells, and its expression was increased following infection with *S. pneumoniae* (Wasserman et al., 2017). RNA sequencing found that MIWI2-positive cells expressed a significantly different transcriptome compared with neighboring cells that did not express MIWI2, and MIWI2 −/− was associated with enhanced innate immune responses and faster bacterial clearance (Wasserman et al., 2017).

In conclusion, our study provides insights into changes of the expression profile of piRNAs during RSV infection and highlight the need for more detailed investigations of the piRNA/PIWI protein pathway in the context of viral infection to establish their potential role in regulation of cellular responses. A better understanding of this pathway could potentially identify novel therapeutic targets for future piRNA-mediated strategies to modulate RSV-associated lung disease, as well as potential biomarkers for disease diagnosis and prognosis.

Data availability statement

The original contributions presented in the study are included in the article/Supplementary Material, further inquiries can be directed to the corresponding author.

Author contributions

TC designed and performed the experiments, analyzed the data, wrote the manuscript; AK. contributed to piRNA data analysis and drafting of the manuscript; TL was the technical support of the cell culture. AC contributed to the conception of the manuscript, literature review, financial support, and final manuscript editing.

Funding

This research was funded by NIH grant AI062885, AI125434, AI142570. TC was supported in part by the Jeane B. Kempner Postdoctoral Scholar Award from UTMB.

Acknowledgments

The authors would like to thank Cynthia Tribble for assistance with submission of the manuscript.

Conflict of interest

The authors declare that the research was conducted in the absence of any commercial or financial relationships that could be construed as a potential conflict of interest.

Publisher's note

Supplementary material

The Supplementary Material for this article can be found online at: https://www.frontiersin.org/articles/10.3389/fmolb.2022.931354/full#supplementary-material

References

Balaratnam, S., West, N., and Basu, S. (2018). A piRNA utilizes HILI and HIWI2 mediated pathway to down-regulate ferritin heavy chain 1 mRNA in human somatic cells. *Nucleic Acids Res.* 46 (20), 10635–10648. 5068339[pii] [doi]. doi:10.1093/nar/gky728

Chahar, H. S., Corsello, T., Kudlicki, A. S., Komaravelli, N., and Casola, A. (2018). Respiratory syncytial virus infection changes cargo composition of exosome released from airway epithelial cells. *Sci. Rep.* 8 (1), 387. doi:10.1038/s41598-017-18672-5

Domachowske, J. B., Anderson, E. J., and Goldstein, M. (2021). The future of respiratory syncytial virus disease prevention and treatment. *Infect. Dis. Ther.* 10 (1), 47–60. doi:10.1007/s40121-020-00383-6

Elliott, J., Lynch, O. T., Suessmuth, Y., Qian, P., Boyd, C. R., Burrows, J. F., et al. (2007). Respiratory syncytial virus NS1 protein degrades STAT2 by using the Elongin-Cullin E3 ligase. *J. Virol.* 81 (7), 3428–3436. doi:10.1128/JVI.02303-06

Ernst, C., Odom, D. T., and Kutter, C. (2017). The emergence of piRNAs against transposon invasion to preserve mammalian genome integrity. *Nat. Commun.* 8 (1), 1411. doi:10.1038/s41467-017-01049-7

Fu, Q., and Wang, P. J. (2014). Mammalian piRNAs: Biogenesis, function, and mysteries. *Spermatogenesis* 4, e27889. doi:10.4161/spmg.27889

Gao, X. Q., Zhang, Y. H., Liu, F., Ponnusamy, M., Zhao, X. M., Zhou, L. Y., et al. (2020). The piRNA CHAPIR regulates cardiac hypertrophy by controlling METTL3-dependent N(6)-methyladenosine methylation of Parp10 mRNA. *Nat. Cell Biol.* 22 (11), 1319–1331. doi:10.1038/s41556-020-0576-y

Garofalo, R., Mei, F., Espejo, R., Ye, G., Haeberle, H., Baron, S., et al. (1996). Respiratory syncytial virus infection of human respiratory epithelial cells up-regulates class I MHC expression through the induction of IFN-beta and IL-1 alpha. *J. Immunol.* 157 (6), 2506–2513.

Ghosh, B., Sarkar, A., Mondal, S., Bhattacharya, N., Khatua, S., and Ghosh, Z. (2022). piRNAQuest V.2: an updated resource for searching through the piRNAome of multiple species. *RNA Biol.* 19 (1), 12–25. doi:10.1080/15476286.2021.2010960

Han, B. W., and Zamore, P. D. (2014). piRNAs. *Curr. Biol.* 24 (16), R730–R733. doi:10.1016/j.cub.2014.07.037

Hinrichs, A. S., Karolchik, D., Baertsch, R., Barber, G. P., Bejerano, G., Clawson, H., et al. (2006). The UCSC genome browser database: Update 2006. *Nucleic Acids Res.* 34, D590–D598. doi:10.1093/nar/gkj144

Hussain, K. M., Leong, K. L., Ng, M. M., and Chu, J. J. (2011). The essential role of clathrin-mediated endocytosis in the infectious entry of human enterovirus 71. *J. Biol. Chem.*. 286 (1), 309–321. doi:10.1074/jbc.M110.168468

Ikhlas, S., Usman, A., Kim, D., and Cai, D. (2022). Exosomes/microvesicles target SARS-CoV-2 via innate and RNA-induced immunity with PIWI-piRNA system. *Life Sci. Alliance* 5 (3), e202101240. doi:10.26508/lsa.202101240

Iwasaki, Y. W., Murano, K., Ishizu, H., Shibuya, A., Iyoda, Y., Siomi, M. C., et al. (2016). Piwi modulates chromatin accessibility by regulating multiple factors including histone H1 to repress transposons. *Mol. Cell.* 63 (3), 408–419. doi:10.1016/j.molcel.2016.06.008

Lee, J. S., Mukherjee, S., Lee, J. Y., Saha, A., Chodosh, J., Painter, D. F., et al. (2020). Entry of epidemic keratoconjunctivitis-associated human adenovirus type 37 in human corneal epithelial cells. *Invest. Ophthalmol. Vis. Sci.*. 61 (10), 50. doi:10.1167/iovs.61.10.50

Li, H. J., Yu, N., Zhang, X. Y., Jin, W., and Li, H. Z. (2010). Spermatozoal protein profiles in male infertility with asthenozoospermia. *Chin. Med. J.* 123 (20), 2879–2882.

Li, H., Ma, Y., Escaffre, O., Ivanciuc, T., Komaravelli, N., Kelley, J. P., et al. (2015). Role of hydrogen sulfide in paramyxovirus infections. *J. Virol.* 89 (10), 5557–5568. doi:10.1128/JVI.00264-15

Mazur, N. I., Martinón-Torres, F., Baraldi, E., Fauroux, B., Greenough, A., Heikkinen, T., et al. (2015). Lower respiratory tract infection caused by respiratory syncytial virus: current management and new therapeutics. *Lancet Respir. Med.* 3 (11), 888–900. doi:10.1016/s2213-2600(15)00255-6

Monga, I., and Banerjee, I. (2019). Computational identification of piRNAs using features based on RNA sequence, structure, thermodynamic and physicochemical properties. *Curr. Genomics.* 20 (7), 508–518. doi:10.2174/1389202920666191129112705

Moyano, M., and Stefani, G. (2015). piRNA involvement in genome stability and human cancer. *J. Hematol. Oncol.* 8 38. doi:10.1186/s13045-015-0133-5

Muhammad, A., Waheed, R., Khan, N. A., Jiang, H., and Song, X. (2019). piRDisease v1.0: a manually curated database for piRNA associated diseases. *Database. (Oxford)* 2019, baz052. doi:10.1093/database/baz052

Park, C., Li, S., Cha, E., and Schindler, C. (2000). Immune response in Stat2 knockout mice. *Immunity* 13 (6), 795–804. doi:10.1016/s1074-7613(00)00077-7

Piuco, R., and Galante, P. A. F. (2021). piRNAdb: A piwi-interacting RNA database. *bioRxiv*. 2021.2009.2021.461238. doi:10.1101/2021.09.21.461238

Quinlan, A. R., and Hall, I. M. (2010). BEDTools: a flexible suite of utilities for comparing genomic features. *Bioinformatics* 26 (6), 841–842. btq033 [pii][doi]. doi:10.1093/bioinformatics/btq033

Ransohoff, J. D., Wei, Y., and Khavari, P. A. (2018). The functions and unique features of long intergenic non-coding RNA. *Nat. Rev. Mol. Cell Biol.* 19 (3), 143–157. doi:10.1038/nrm.2017.104

Rima, B., Collins, P., Easton, A., Fouchier, R., Kurath, G., Lamb, R. A., et al. (2017). ICTV Virus Taxonomy Profile: Pneumoviridae. *J. Gen. Virol.* 98 (12), 2912–2913. doi:10.1099/jgv.0.000959

Rayford, K. J., Cooley, A., Rumph, J. T., Arun, A., Rachakonda, G., Villalta, F., et al. (2021). piRNAs as modulators of disease pathogenesis. *Int. J. Mol. sci.*. 22 (5), 2373. doi:10.3390/ijms22052373

Samir, M., Vidal, R. O., Abdallah, F., Capece, V., Seehusen, F., Geffers, R., et al. (2020). Organ-specific small non-coding RNA responses in domestic (Sudani) ducks experimentally infected with highly pathogenic avian influenza virus (H5N1). *RNA Biol.*. 17 (1), 112 –124. doi:10.1080/15476286.2019.1669879

Shi, T., Denouelt, A., Tietjen, A. K., Campbell, I., Moran, E., Li, X., et al. (2020). Global Disease Burden Estimates of Respiratory Syncytial Virus-Associated Acute Respiratory Infection in Older Adults in 2015: A Systematic Review and Meta-Analysis. *J. Infect. Dis.* 222 (Suppl 7), S577–S583. doi:10.1093/infdis/jiz059

Shi, T., McAllister, D. A., O'Brien, K. L., Simoes, E. A. F., Madhi, S. A., Gessner, B. D., et al. (2017). Global, regional, and national disease burden estimates of acute lower respiratory infections due to respiratory syncytial virus in young children in 2015: A systematic review and modelling study. *Lancet*. 390 (10098), 946–958. doi:10.1016/s0140-6736(17)30938-8

Taschuk, F., and Cherry, S. (2020). DEAD-box helicases: Sensors, regulators, and effectors for antiviral defense. *Viruses* 12 (2), 181. doi:10.3390/v12020181

Théron, E., Dennis, C., Brasset, E., and Vaury, C. (2014). Distinct features of the piRNA pathway in somatic and germ cells: From piRNA cluster transcription to piRNA processing and amplification. *Mob. DNA*. 5 (1), 28. doi:10.1186/s13100-014-0028-y

Ueba, O. (1978). Respiratory syncytial virus. I. Concentration and purification of the infectious virus. *Acta Med. Okayama.* 32 (4), 265–272.

Wakisaka, K. T., and Imai, Y. (2019). The dawn of pirna research in various neuronal disorders. *Front. Biosci. (Landmark Ed.)*. 24 1440–1451. doi:10.2741/4789

Wang, J., Zhang, P., Lu, Y., Li, Y., Zheng, Y., Kan, Y., et al. (2019). piRBase: A comprehensive database of piRNA sequences. *Nucleic. Acids Res.* 47 (D1), D175–D180. doi:10.1093/nar/gky1043

Wasserman, G. A., Szymaniak, A. D., Hinds, A. C., Yamamoto, K., Kamata, H., Smith, N. M., et al. (2017). Expression of Piwi protein MIWI2 defines a distinct population of multiciliated cells. *J. Clin. Invest.* 127 (10), 3866–3876. doi:10.1172/JCI94639

Weick, E. M., and Miska, E. A. (2014). piRNAs: from biogenesis to function. *Development* 141 (18), 3458–3471. doi:10.1242/dev.094037

Wu, X., Pan, Y., Fang, Y., Zhang, J., Xie, M., Yang, F., et al. (2020). The Biogenesis and Functions of piRNAs in Human Diseases. *Mol. Ther. Nucleic. Acids*. 21 108–120. doi:10.3390/ijms22052373

Yang, J. X., Rastetter, R. H., and Wilhelm, D. (2016). Non-coding RNAs: An Introduction. *Adv. Exp. Med. Biol.* 886, 13–32. doi:10.1007/978-94-017-7417-8_2

Yao, H., Wang, X., Song, J., Wang, J., Song, Q., and Han, J. (2020). Coxsackievirus B3 infection induces changes in the expression of numerous piRNAs. *Arch. Virol.*. 165 (1), 105–114. doi:10.1007/s00705-019-04451-2

Zamore, P. D. (2010). Somatic piRNA biogenesis. *The EMBO J.* 29 (19), 3219–3221. doi:10.1038/emboj.2010.232

Zeng, Q., Cai, J., Wan, H., Zhao, S., Tan, Y., Zhang, C., et al. (2021). PIWI-interacting RNAs and PIWI proteins in diabetes and cardiovascular disease: Molecular pathogenesis and role as biomarkers. *Clin. Chim. Acta.*. 518, 33–37. doi:10.1016/j.cca.2021.03.011

Zhang, L., Meng, X., Pan, C., Qu, F., Gan, W., Xiang, Z., et al. (2020). piR-31470 epigenetically suppresses the expression of glutathione S-transferase pi 1 in prostate cancer via DNA methylation. *Cell. Signal.* 67, 109501. doi:10.1016/j.cellsig.2019.109501

Zhang, X., He, X., Liu, C., Liu, J., Hu, Q., Pan, T., et al. (2016). IL-4 inhibits the biogenesis of an epigenetically suppressive PIWI-interacting RNA to upregulate CD1a molecules on monocytes/dendritic cells. *J. Immunol.* 196 (4), 1591–1603. doi:10.4049/jimmunol.1500805

Zhong, F., Zhou, N., Wu, K., Guo, Y., Tan, W., Zhang, H., et al. (2015). A SnoRNA-derived piRNA interacts with human interleukin-4 pre-mRNA and induces its decay in nuclear exosomes. *Nucleic Acids Res.* 43 (21), 10474–10491. doi:10.1093/nar/gkv954

Frontiers in
Molecular Biosciences

Explores biological processes in living organisms on a molecular scale

Focuses on the molecular mechanisms underpinning and regulating biological processes in organisms across all branches of life.

Discover the latest Research Topics

See more →

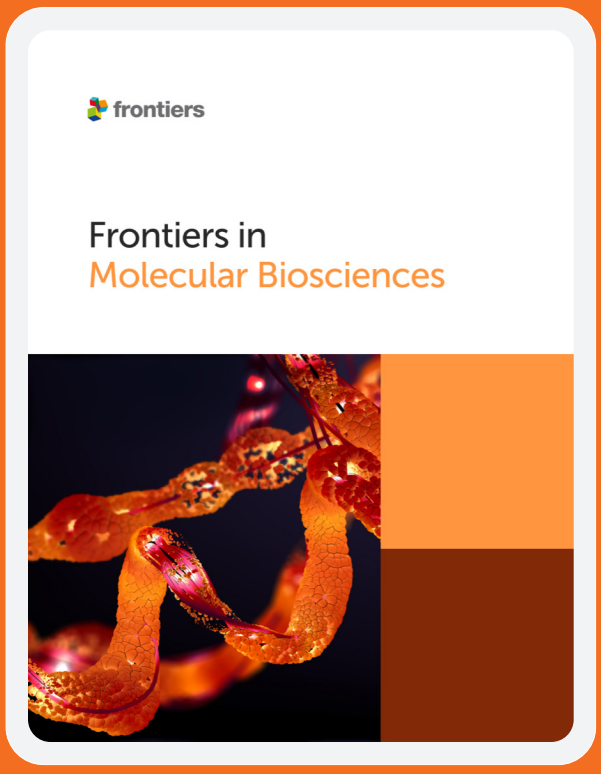

Frontiers

Avenue du Tribunal-Fédéral 34
1005 Lausanne, Switzerland
frontiersin.org

Contact us

+41 (0)21 510 17 00
frontiersin.org/about/contact